CRC Press
Taylor & Francis Group

Deep Eutectic Solvents in Liquid–Liquid Extraction

Correlation and Molecular Dynamics Simulation

Papu Kumar Naik, Nikhil Kumar, Nabendu Paul, and Tamal Banerjee

Deep Eutectic Solvents in Liquid–Liquid Extraction

Deep eutectic solvents (DESs) are a new class of green solvents that open a whole new world of opportunities for separation challenges. This book comprehensively provides a detailed discussion of their application as an extractive solvent in separation processes, adopting molecular dynamics (MD) simulations for atomistic insight into the solute transfer across biphasic systems. Furthermore, it explains ternary and quaternary mixtures, including MD simulation of relevant DES systems.

Features in this volume include the following:

- Applications of DESs in the extraction of aromatics and polyaromatics from fuel oil by liquid–liquid extraction
- Eutectic behavior with respect to hydrocarbon and aqueous solutions
- MD insights on extraction using DESs
- Possible industrial applicability of potential DESs
- Results from Gaussian, NAMD, and PACKMOL software packages

This book is aimed at researchers and graduate students working in the field of fuels and petrochemicals, separation science, chromatography, and chemical processing and design.

Deep Eutectic Solvents in Liquid–Liquid Extraction

Correlation and Molecular Dynamics Simulation

Papu Kumar Naik, Nikhil Kumar,
Nabendu Paul, and Tamal Banerjee

CRC Press
Taylor & Francis Group
Boca Raton London New York

CRC Press is an imprint of the
Taylor & Francis Group, an **informa** business

Designed cover image: © Shutterstock

First edition published 2023
by CRC Press
6000 Broken Sound Parkway NW, Suite 300, Boca Raton, FL 33487–2742

and by CRC Press
4 Park Square, Milton Park, Abingdon, Oxon, OX14 4RN

CRC Press is an imprint of Taylor & Francis Group, LLC

ISBN: 978-1-032-13856-5 (hbk)
ISBN: 978-1-032-13858-9 (pbk)
ISBN: 978-1-003-23115-8 (ebk)

DOI: 10.1201/9781003231158

Typeset in Times New Roman
by Apex CoVantage, LLC

Contents

About the Authors

Dr. Papu Kumar Naik works as Research Associate at the Department of Chemical Engineering, Indian Institute of Technology Guwahati. He earned his PhD from the Centre for the Environment, Indian Institute of Technology Guwahati, Assam in 2020. He completed his master's degree from Sambalpur University, Odisha in 2015. He was the first-rank holder and awarded with the University Gold medal in Environmental Science. He received the prestigious INSPIRE Fellowship from the Department of Science and Technology, Government of India in 2015. His work focuses on the extraction study of polyaromatic hydrocarbon from fuel oil using deep eutectic solvents. His work also emphasizes molecular modeling, thermodynamic study, and the synthesis of deep eutectic solvents along with its application on liquid–liquid extraction process. He is the author of 12 internationally acclaimed peer reviewed articles.

Mr. Nikhil Kumar is currently pursuing his PhD (2017–present) in chemical engineering from the Indian Institute of Technology Guwahati. His research work is dedicated to the development of novel deep eutectic solvents for the extraction of aromatic compounds from petroleum fuels. He uses both quantum chemical and molecular dynamics simulation studies for the extraction of aromatics from hydrocarbon phase. He has been published in three peer-reviewed international publications in reputed journals and has presented five papers in international and national conferences.

Mr. Nabendu Paul is pursuing his PhD (2017–present) from Department of Chemical Engineering at Indian Institute of Technology Guwahati. He completed both his master's and Bachelor of Technology in Chemical Engineering from National Institute of Technology, Agartala in 2015 and 2013, respectively. His work of interest is in the experimental and molecular modeling studies on the extraction and recovery of pharmaceuticals and biomolecules from an aqueous environment using deep eutectic solvents.

Prof. Banerjee is currently a professor in the Department of Chemical Engineering, Indian Institute of Technology Guwahati since 2017. His group uses both quantum chemical and molecular dynamics (MD) methods to predict thermodynamic and transport properties of ionic liquids (ILs) and deep eutectic solvents (DESs). His interests lie in Conductor-like Screening Model–based methods and molecular modeling techniques, which includes both classical MD and reactive force-field simulations.

Application areas include both renewable (alcohols) and nonrenewable (coal and chemical hydrides) energy sources. He has also authored two books (published by CRC and Elsevier) and more than 130 publications. His group has to date contributed about 900 data points related to the thermodynamic data points for IL and DES mixtures and is now available in National Institute of Standards and Technology (NIST). Overall, he has guided 15 PhD and 22 master's students, many of whom are involved in applying green solvents to energy and environmental domain. He is currently the Fellow of both Royal Society of Chemistry and Indian Chemical Society. He also serves in the editorial board of *Fluid Phase Equilibria*.

Preface

Green chemistry researchers have been looking for alternatives to volatile organic compounds (VOCs) as solvents for the last 20 years. VOCs have indeed raised severe safety and environmental issues, particularly in light of achieving sustainable development, in light of several of their properties, such as flammability, volatility, and the fact that they are petroleum-derived. Significant interest has been shown in deep eutectic solvents (DESs) and ionic liquids in this context as prospective media that may replace VOCs in various applications. Since they are more ecologically friendlier than their predecessors, they are becoming more important in the development of green processes. Energy, separation, metal plating, electrochemistry, biotechnology, materials, and catalysis are among the fields in which DESs have been used. Hence, DESs have developed as a major class of fluids. The melting point of a "deep eutectic" is arbitrary, although the common view is that the melting point is lower than what would be anticipated from perfect ideal behavior.

An advantage of DES over ordinary organic solvents is that they are easy to prepare, have low volatility, and are very inexpensive when compared to ionic liquids. Due to the large number of possible hydrogen bond donor/acceptor combinations that could form a DES, it quickly became clear that a fundamental understanding of the physical and chemical properties of DESs was required to develop new materials with characteristics tailored to specific applications. Most recently, efforts have focused on the DES media's non–fossil fuel precursor characteristics to show off its inherent and unique characteristics.

In the current book, DESs are described in detail in the first chapter, with the second chapter focusing on extracting aromatic chemicals using these solvents using a mix of liquid–liquid equilibrium data and continuum solvation models. The next two chapters examine the extraction of aromatic and pesticide components from hydrocarbon and aqueous streams using quantum chemistry and molecular dynamic methods, respectively. These chapters shall provide an in-depth understanding of computational methods and a way of recognizing different structural details like the spatial distribution function, coordination number, and radial distribution function. With each year, researchers are discovering more and more complex DES structures as they gain a better grasp of their physical chemistry. In the concluding chapter, a brief introduction to possible industrial applications is highlighted. At the conclusion of the Appendix, script files for the NAMD package are provided.

Papu Kumar Naik

Nikhil Kumar

Nabendu Paul

Tamal Banerjee

January 2022

Acknowledgments

The authors of this book, **Mr. Nabendu Paul** and **Dr. Tamal Banerjee**, would like to acknowledge the **Scheme for Promotion of Academic and Research Collaboration (SPARC), (Project Code: P848)** under Ministry of Human Resource Development (MHRD), Government of India for sanctioning the financial grant in the project titled **"Hydrophobic Deep Eutectic Solvent for Remediation of Antifungal and Antibiotics in Waste Water"** in accomplishing the works associated with extracting pesticides and pharmaceuticals from an aqueous environment and the studies on the stability of hydrophobic deep eutectic solvents (DESs) that are included in the Chapters 3 and 4 of this book. The molecular dynamic (MD) studies focused on the extraction of nitenpyram from a water environment and the stability of menthol-based, as well as ammonium-based, DESs in aqueous surroundings are the outputs of this project.

The authors also would like to acknowledge **Prof. Isabel Maria Marrucho** and her laboratory from Instituto Superior Técnico under Universidade de Lisboa for providing support to Mr. Nabendu Paul when visiting her laboratory in Instituto Superior Técnico, Lisbon to carry out a portion of the experimental work. Her valuable knowledge and insights on the eutectic systems and their application in the extraction field were incredibly useful in carrying out the experiments.

The authors also would like to acknowledge **Dr. Partho Sarathi Gooh Pattader** from the Indian Institute of Technology Guwahati, India and **Dr. Bernardo Dias Ribeiro** from Universidade Federal Do Rio De Janeiro, Brazil for being an indispensable part of the project. Their knowledge and involvement have immensely enriched the whole work.

Furthermore, the authors would like to acknowledge **Param-Ishan supercomputing facility, IIT Guwahati** for providing the enormous computational requirement to carry out the simulation and computational works.

1 Deep Eutectic Solvents

1.1 INTRODUCTION

Over the last few decades, many eutectic systems have been predicted and explored. Most research has concentrated on three forms of eutectics: eutectic metals, eutectic salts, and deep eutectic solvents. On the other hand, they are all eutectic systems with the same eutectic principle. The term *eutectic* derives from the field of metallurgy. Since the 2000s, many eutectics have become prevalent, and now they are used in different industries mainly electronics and semiconductor, chemical, removal and separation technology, and others [1–3]. Various research, however, considers eutectics to have importance to the physicochemical professionals and that it is not interesting enough to ordinary chemistry readers. Even though there have been several assessments of eutectics, most of them have been negative. Eutectics also have the ability to extend the scope of traditional conventional solvents (when operating under specific temperature and pressure conditions).

Eutectic systems have a wide range of properties and applications. Although eutectic metals are extensively studied in electronics, we are unaware of any research on dissolution and separation in this domain. Furthermore, a number of papers on eutectic salts as an energy storage medium are found, but not in environmental research [4, 5]. Deep eutectic solvents (DESs) have demonstrated tremendous potential in the disciplines of environmental research and separation science [6, 7]. These eutectics have crosslinked uses in several disciplines, and exploring DESs will help further multidisciplinary studies in domains including chemistry, materials, and the environment.

Most of the scientific publications with respect to DESs has emerged since 2012. There is a rapid growth of research activities due to its versatile usability. DESs are sustainable and cheap alternatives to the far more cumbersome solvents used today. A DES often contains two inexpensive solid/liquid components that can be combined by hydrogen bond interactions to form a eutectic mixture with a melting temperature much lower than that of the individual chemicals. It's because of the formation of hydrogen bonds between the salt's hydrogen bond donor (HBD) and hydrogen bond acceptor (HBA), usually a halide anion that liquid molten salts form at normal temperature. DESs have a significantly lower freezing point and are therefore liquid at room temperature. Some researchers also named them low-transition-temperature mixtures (LTTMs). The mixture's lower freezing point is the result of halide ion—hydrogen bond donor supramolecular complex development, with alteration in the solid phase's free energy in comparison to the liquid phase [8, 9].

In most cases, a DES is obtained by mixing an HBD that has the ability to form a complex with the halide anion of the quaternary ammonium or phosphonium salt [10]. Figure 1.1 summarizes the different quaternary salts that are widely used in combination with various HBDs in the formation of DESs. The earliest definition of

DOI: 10.1201/9781003231158-1

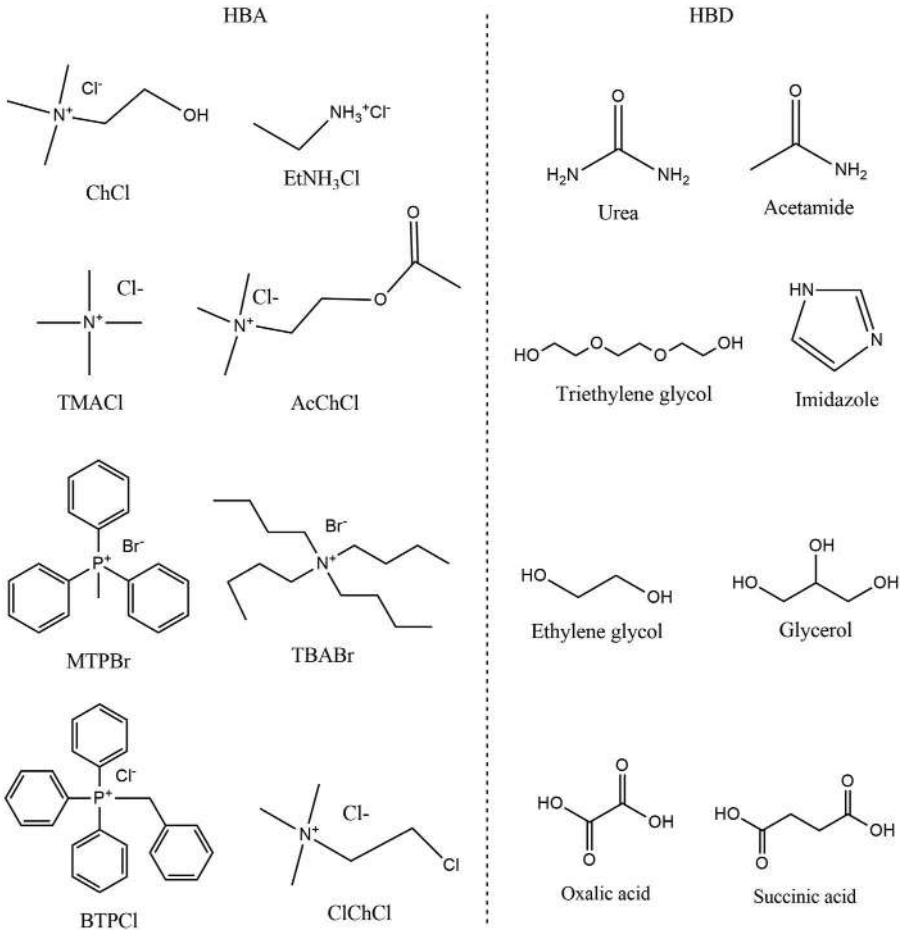

FIGURE 1.1 Structures of the hydrogen bond acceptors and donors used for DES synthesis.

DES was given by Abbott et al. [11]. In their research, a DES was obtained by mixing urea and substituted quaternary ammonium salts such as hydroxyethyltrimethylammonium (choline) chloride. When the finished result was tested, it was discovered to be a liquid.

DESs are generating considerable scientific and technological attention at the moment as low-cost substitutes for traditional and unusual solvents, such as ionic liquids (ILs). Because they share many features and behaviors with ILs, DESs are now commonly recognized as a novel family of IL analogues. DESs are systems that are constituted by a eutectic mixing of the anions and/or cations that are subsets of Lewis or Bronsted acids and bases, whereas ILs are composed mostly of a specific kind of anion and cation.

DES preparation can be seen as a strategic method for overcoming some IL drawbacks, such as high melting temperatures, expensive prices, and high toxicity. DESs have several solvent characteristics that are appealing for ILs, such as low volatility,

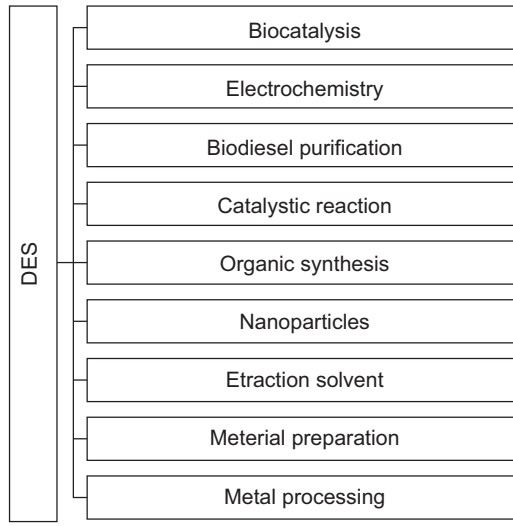

FIGURE 1.2 Application of DESs in different research fields.

high thermal conductivity and stability, a wide range of liquids, and strong solvation power. DESs have other noteworthy benefits over ILs in addition to these. They can be synthesized easily and just require the stirring of the two components with gentle heating as no additional purification of the components is required. Because of the cheap price of beginning materials, they have minimal production costs. Some exciting features of the synthesized DESs are biodegradability, biocompatibility, and nontoxicity. Figure 1.2 shows different types of applications for DESs.

1.2 HYDROPHOBIC AND HYDROPHILIC DESs

The HBDs and HBAs combine to produce DES mixes, which, when mixing, form liquids with melting points considerably lower than the individual components' melting points [12] The depression in melting point occurs because of strong hydrogen bonds formation between the HBA and the HBD. DESs tend to be hydrophilic, meaning they dissolve easily in water, owing to their hydrogen bonding capabilities. Recent advances in the domain of DESs, however, have opened a lot of possibilities in finding a class of DESs in which the water-miscibility of the solvent is considerably low.

Based on the miscibility of the deep eutectic solvents with water, it can be classified into two types: (1) hydrophilic and (2) hydrophobic DES. Deep Eutectic solvents that are miscible in water or interact with an aqueous environment and disintegrate after a certain period are termed hydrophilic DES. One or both of the DES-forming components are hydrophilic, resulting in DES leaching into the water phase and vice versa. If both the components are hydrophobic and the DES as a whole repels water, forming a distinct phase with a well-formed interface with water, then it can be termed hydrophobic DES (HDES). The degree of hydrophobicity depends on the amount of moisture present in the solvent. The relative interactions among the

components and water contribute to the relative stability of an HDES in an aqueous environment. The relative stability factor proposed in recent work in this field illustrated the relation between the nonbonded interaction energies of the components and their effect on the overall stability of HDES [13, 14]. Because no solvent is fully hydrophobic in nature, there will be little moisture present in the system. The DES-forming components are not fully devoid of water affinity. The number of publications regarding HDESs has increased in the past few years, as shown in Figure 1.3.

HDESs may be divided into two categories. The first kind of HDES that has received the most attention comprises quaternary ammonium salts containing long alkyl chains. For example, decanoic acid was selected as HBD and six quaternary ammonium salts with varied carbon numbers (tetraoctylammonium bromide, methyl-trioctylammonium bromide, tetraheptylammonium chloride, methyltrioctylammonium chloride, tetraoctylammonium chloride, tetrabutylammonium chloride) were chosen as HBAs to produce the first-ever HDES that has been reported

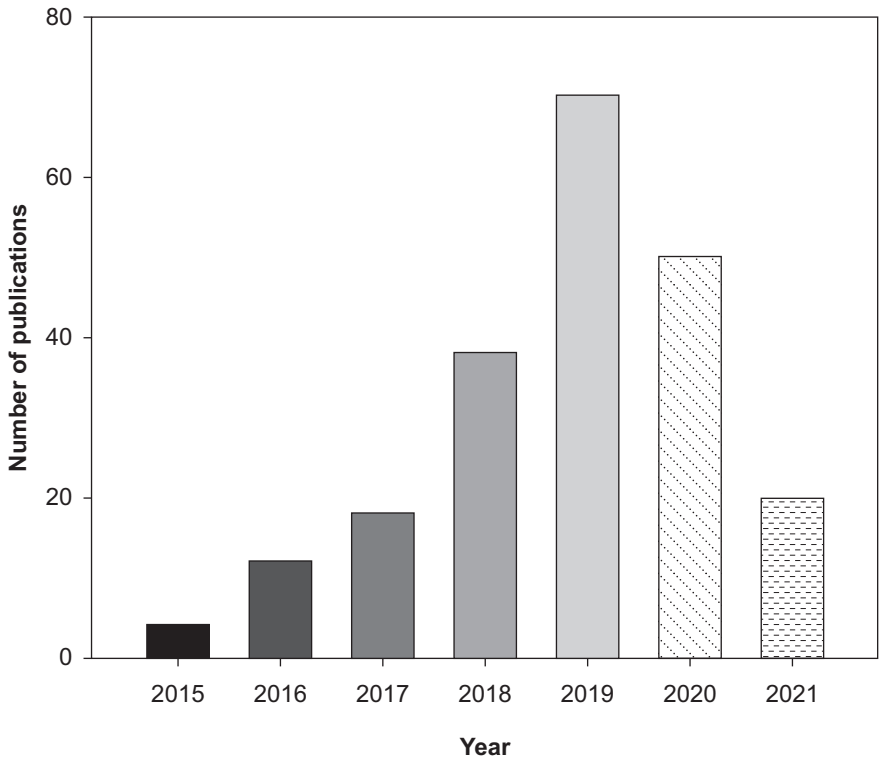

FIGURE 1.3 Number of publications on hydrophobic DESs over 2015–early February 2021 as reported in the Web of Knowledge.

Source: Reprinted from *Journal of Industrial and Engineering Chemistry*, 97, Zainal-Abidin, M.H., M. Hayyan, and W.F. Wong, Hydrophobic deep eutectic solvents: Current progress and future directions, 142–162, Copyright (2021), with permission from Elsevier [14]

[15]. The second kind is a combination of two neutral chemicals, namely, hydrophobic compounds of natural formation that function as HBAs with certain hydrophobic HBDs. The first-ever reported example of this kind is DL-menthol as the HBA and carboxylic acids (acetic, pyruvic, lactic, and lauric acid) as the HBD [16]. Other neutral compounds, such as thymol, L-menthol, and others, in combination with carboxylic acid and alcohols with long chains have also been utilized to form different HDES [17–19]. Combining two fatty acids has also been reported where the fatty acids can act as both HBAs and HBDs. Some examples of such DESs include HBA and HBD such as lauric acid, octanoic acid, lauric acid, nonanoic acid, lauric acid, decanoic acid, respectively and others [20].

1.3 AN OVERVIEW OF EUTECTICS

A eutectic mixture of choline chloride and urea with a particular molar ratio of 1:2 is the first synthesized DES. The melting point of this deep eutectic mixture is 13°C, while the melting points of individual choline chloride and urea are too high. These DESs may be tuned to meet particular needs by varying the molar ratio of either the HBA or the HBD. An aqueous solution of dimethyl sulfoxide with a freezing temperature of less than −130°C was designed as a sodium–ion battery electrolyte with an ultra-low operating temperature, for example.

Eutectic is a term that means "easy to melt", which is interpreted as "reducing the melting point after mixing". Single components in many of the eutectic systems described in the following are solid at specific temperatures and pressures, while eutectic mixtures are liquid. The majority of substances are made up of atoms, ions, or molecules in general. Table 1.1 shows the basic formula for classifying DESs, and Table 1.2 shows the many types of binary mixtures that may be developed.

Eutectic metals may be thought of as eutectic atom mixtures because metals are atomic in nature. Metal may also be conceived of as a collection of fixed nuclei and free electrons; hence, eutectic metals are made up of cations and electrons (Figure 1.4). Anions and cations are found in both salts and eutectic salts, albeit the latter contains a wider diversity of ions than the former. Similarly, eutectic molecular liquids have a simple composition. The term *DES* refers to a group of ion–molecule pairings.

TABLE 1.1
General formula for the classification of DESs. Reprinted with permission from American Chemical Society, Copyright (2014), (https://pubs.acs.org/doi/10.1021/cr300162p, further permissions related to the material excerpted should be directed to the ACS) [9].

Type	General formula	Terms
Type I	$Cat^+X^-zMCl_x$	M = Zn [21–23], Sn [24], Fe, Al [25], Ga [26], In [27]
Type II	$Cat^+X^-zMCl_x.yH2O$	M = Cr [28], Co, Cu, Ni, Fe
Type III	Cat^+X^-zRZ	Z = $CONH_2$ [29], COOH [12], OH [30]
Type IV	$MCl_x{}^+RZ = MCl_{x-1}{}^+.RZ + MCl_{x+1}$	M = Al, Zn and Z = $CONH_2$, OH

TABLE 1.2
Different Categories of Eutectic Systems Composed of Atoms, Ions, and Molecules

Category	Example	Reference
Metal + metal (atomic) (Eutectic metal)	Pb—Sn	[31]
Salt + salt (ions) (Eutectic salt)	LiCl—KCl	[32]
Compound + compound (Eutectic molecular mixture)	Benzophenone—diphenylamine	[33]
Salt (ions) + molecules (Deep eutectic mixture)	ChCl—urea	[34]
Metal (atoms) + salt (ions) (Eutectic mixture: atomic and ionic)	Bi—$BiCl_3$	[35]

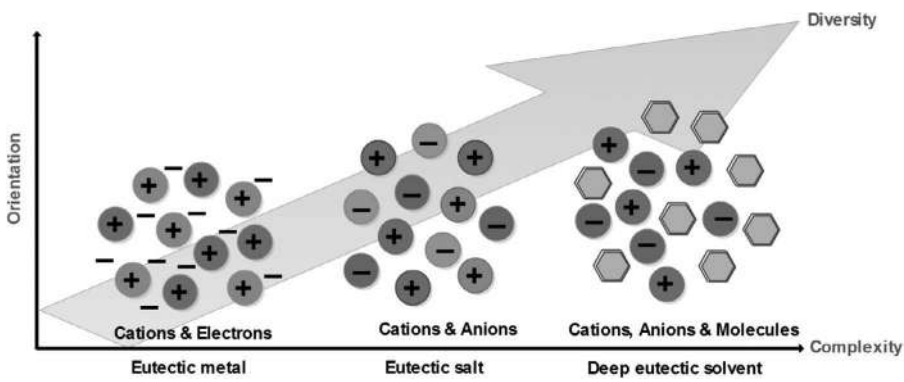

FIGURE 1.4 Evolution of eutectics systems in terms of comparison of three different eutectics.

Different eutectics compositions can be utilized to infer their properties. Electronic conductivity exists in a system with free electrons, whereas ionic conductivity exists in a system with ions. Regardless of composition changes, the eutectic principle stays the same. In the next sections, we look at how eutectics are created in-depth.

1.4 EUTECTIC BEHAVIOR OF DESs

A DES is generally composed of two or three cheap and safe components capable of associating with each other through hydrogen bond interactions to form a eutectic mixture. Melting points lower than that for each element characterizes the resulting DES. DESs usually have very significant freezing point depression and are liquid below 150°C temperature. Please note that most are in a liquid state at room temperatures up to 70°C. A DES is mostly derived by the combination of quaternary

ammonium salt with metal salts, or an HBA, with which the halide anion of quaternary ammonium salt can develop a complex.

The eutectic process is depicted in a binary phase diagram as a three-phase change that happens at a specific temperature and pressure. During the solid–liquid phase transition, pressure has a minor impact. It is possible to establish a connection between state functions and temperature.

In Figure 1.5, the appearance of "deep" depression of the individual component melting temperature of the DES at the mixture composition and temperature. The melting point is Tm. The solid line indicates the melting point temperature in accordance with the mixture composition, while the dashed lines indicate the eutectic mixture temperature and composition. Note that, the eutectic composition is a singular point in the phase diagram with the lowest melting temperature. DESs have one of the most significant and distinctive recognized features of lower melting points in comparison to their salt (HBAs) and HBDs. This signifies the clear definition of the word *deep* in DES, which shows that the DES deviates from its ideal behavior.

Apart from Coulombic interactions between ions, hydrogen bonding, which is a noncovalent interaction, is the most crucial interaction in DESs. Because of its inherent properties, DES works effectively to dissolve polar polymers like cellulose. Eutectic molecular liquids (EMLs) were suggested by Mu et al. [36], which are made up of two molecular compounds that interact noncovalently. From component to interaction, Figure 1.6 depicts the distinctions between a DES and an EML. An EML is made up of two molecular compounds, whereas a DES (binary) is made up of an ionic component and a molecule compound. Furthermore, by merely combining two molecular components with noncovalent bonding, a huge number of EMLs may be deliberately created and produced. Hydrogen bonding, π–π stacking, and s-hole (halogen, chalcogen, pnicogen, tetrel bonds), p-hole, k-hole, and m-hole bonding interactions are all examples of these interactions. The eutectic liquid systems can be significantly enhanced in this way. Nonionic eutectics were also

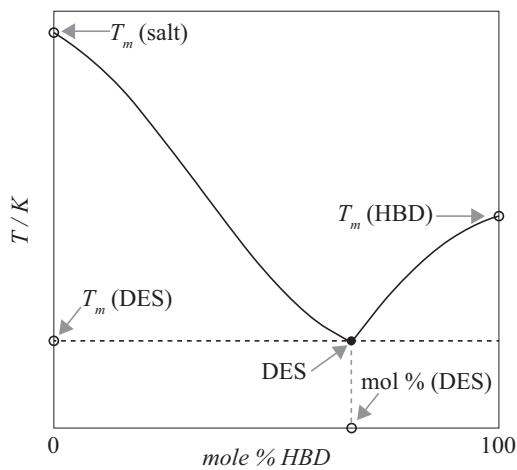

FIGURE 1.5 Solid–liquid schematic phase diagram for a binary mixture of a salt and an HBD.

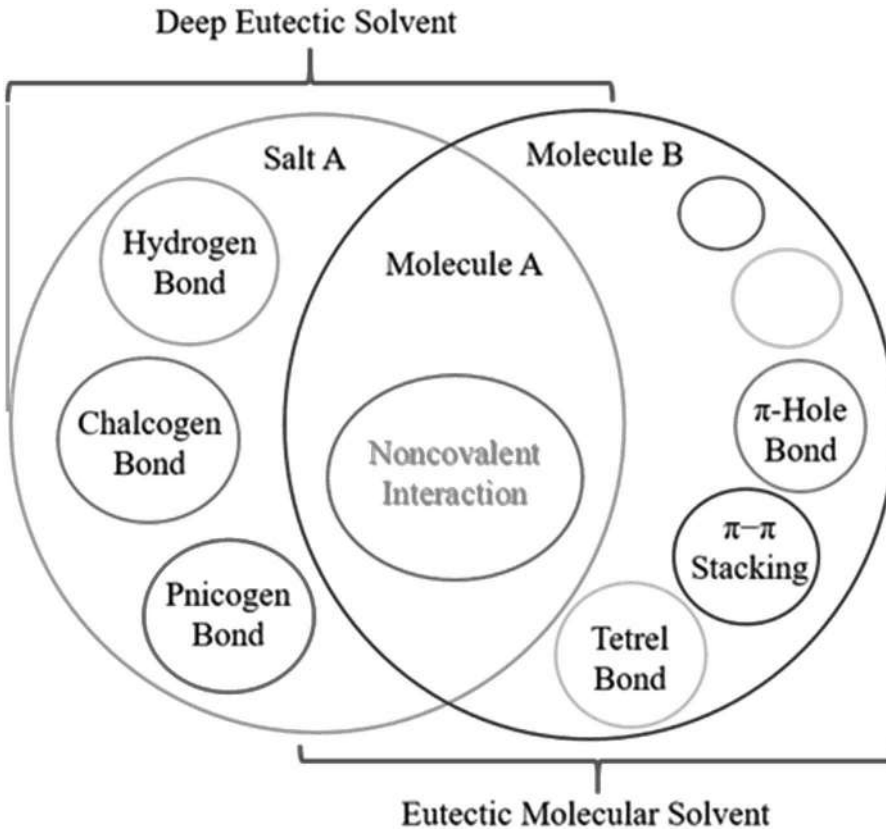

FIGURE 1.6 Composition and noncovalent interaction of components in DESs and EMLs.

discovered by Coutinho and his colleagues. In their latest research, they combined molecular components (such as thymol and menthol) to create a variety of eutectics [37]. A significant molecular connection was discovered in the thymol–menthol system. The huge acidity difference between phenolic group and hydroxyl groups with aliphatic part was thought to be the cause of eutectic formation. According to a review paper, this contact is actually a hydrogen bonding interaction [38]. As a result, they dubbed these nonionic eutectics "the type V DESs". Despite the fact that the nomenclature is not the same as EML, it is fundamentally a eutectic system created by two molecular molecules. This also highlights the importance of proposing EMLs from the other side.

According to the latest published literature, the formation of a deep eutectic mixture is caused by strong hydrogen bonding interactions between the HBA and the HBD [12]. The strong hydrogen bond existing between the HBD and the HBA is considered as main driving force that prevents the entire system from crystallizing. When the nature of hydrogen bonds between HBDs and HBAs is strengthened, the negative charge from the anion seems to diffuse more toward the organic molecules, but the positive charge appears to concentrate more around cations. However,

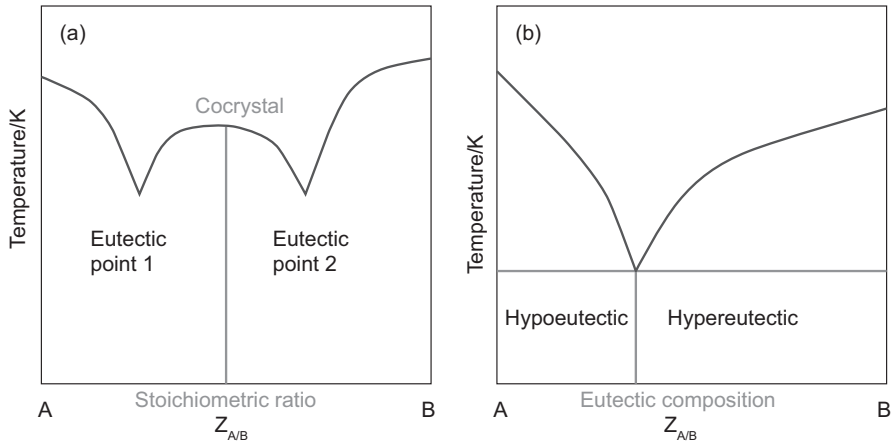

FIGURE 1.7 Two eutectic points are shown in binary-phase diagram. (a) The cocrystal is located within the two eutectic points and has a stoichiometric ratio of components A and B. (b) Both sides of the eutectic composition have hypoeutectic and hypereutectic regions.

Mollenhauer's research revealed that in choline chloride urea combinations, the negative charge shifted from chloride to urea was insignificant [39].

The terms *hypoeutectic* and *hypereutectic* have extremely specific meanings. These terms are used to elaborate the difference between a solid component and the eutectic component in a basic eutectic mixture (typically with one eutectic point). The region to the left of the eutectic composition will create a hypoeutectic point, meaning the component A content, is less than that of eutectic components (Figure 1.7). Hypereutectic is defined as the component A content being higher than the eutectic ratio. Despite the fact that these solids are mixed crystals, their strength varies depending on the composition [40]. It's worth noting that the distinction between hypoeutectic and hypereutectic is made based on the relative positions of substances A and B in a phase diagram, which is typically established by convention.

Ab initio molecular dynamics simulations of reline (choline chloride:urea = 1:2) in Zahn's study indicate hydrogen bonding interactions of a similar nature in the spatial distribution function analysis across both components [40]. Furthermore, the oxygen atoms of urea and chloride anions have a comparable spatial arrangement around the cationic part of choline. The low melting point of reline is due to undetected cluster movement caused by numerous identical contacts and rapid hydrogen bonding aided by the hydrogen atoms. Anions and cations combine in a pure material (salt); in DES, this combination is disrupted by the molecular form; that is, anions compete with cations and hydrogen. The rise in entropy is regarded as another key change in the combined system, in addition to the development of hydrogen bonding interactions.

1.5 ENTROPY CHANGE

The degree of disorder in a system is measured in terms of entropy. Two distinct solids are combined to produce a liquid at a constant temperature and pressure.

During the simple mixing process, the entropy of the system grows for all eutectic mixtures.

The entropy rise process is straightforward and easy to grasp, and it may be used to explain melting point depression. A change in Gibbs energy, ΔG = 0, is when a phase change occurs at the eutectic point. The following equation may be derived using Gibb's equation:

$$T_m = \frac{\Delta H^*_{fus}}{\Delta S^*_{fus}}, \tag{1.1}$$

where T_m represents the melting point of a pure material, while ΔH^*_{fus} and ΔS^*_{fus} are the enthalpy and entropy changes of melting point, respectively. If a eutectic system exists, Equation 1.1 can be written as follows:

$$T_m = \frac{\Delta H_e}{\Delta S_e}. \tag{1.2}$$

The physical amount of the eutectic system is denoted by the subscript *e*. In the solid phase, the components in the solid form have a restricted range of motion; there is a minimum entropy difference between pure and impure substances. As a result, the species in impure liquid are more disorganized, resulting in a more dramatic entropy differential between pure and impure liquid [41]. The change in entropy is considerably higher than the change in enthalpy in most eutectic systems. As a consequence, if an impure solid merges into an impure fluid, the entropy changes will be larger than a pure solid melting into a pure liquid.

The melting point of the eutectic mixture is lower than the melting point of individual components. The melting temperature of crystals is relatively high due to a substantial enthalpy shift. Increasing entropy change while decreasing enthalpy change might be considered a technique for lowering the melting point (or glass transition temperature) of the desired combination of HBAs and HBDs. Besides Coulombic interactions, hydrogen bonding, as well as coordination interactions, is thought to affect enthalpy and entropy variations significantly. The interaction intensity influences the extent to which enthalpy and entropy vary throughout the transition of phase. Figure 1.7(b) depicts the corresponding connection. The preceding interpretations and inferences are superficial and serve only to assist readers to grasp the thermodynamic concepts underlying eutectics systems.

1.6 ILs VERSUS DESs

ILs were originally thought to be pure salts or eutectic salts in a molten state. ILs have increasingly developed into various types as research has expanded (Figure 1.8) [42]. The missing connection between aqueous/organic solutions and molten salts at high temperatures is considered room temperature ionic liquids (RTILs) [43]. They are ideal choices for engineering and physical and analytical chemistry, as well as electrochemistry and biochemistry, because of their great temperature stability and large electrochemical windows [44]. Many characteristics of ILs may be

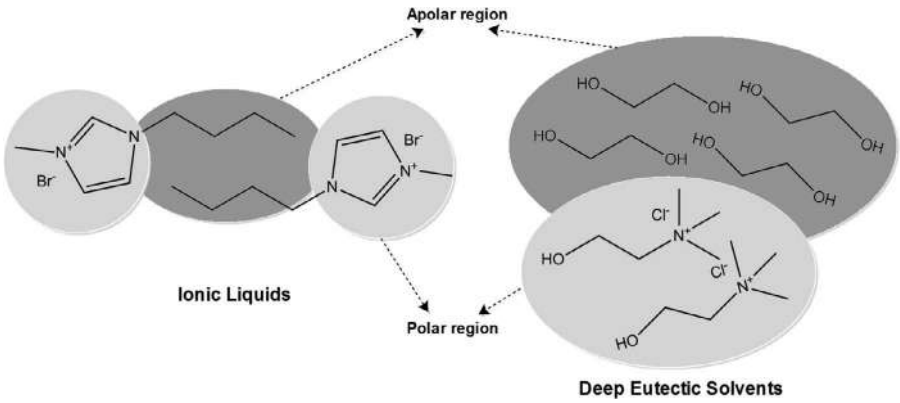

FIGURE 1.8 Comparison of ionic liquid and DES.

modified by altering the anions and cations in the mix, depending on the application. Furthermore, modifying ions (typically cations) chemically increases their effectiveness as task-specific solvents. The melting point of a cation is thought to be lowered by having a longer alkyl chain. ILs with long side chains have a bicontinuous shape, with a polar moiety in one area and apolar, alkyl tails in the other (Figure 1.8) [45]. In the nanoscale, DESs, like RTILs, have a polar and nonpolar domain. In several fields, studies have demonstrated that the applications of DESs virtually completely cover those of the ILs. Furthermore, the preparation of DESs is considerably more manageable than the preparation of ILs. As a result, DESs can be considered a step forward in the creation of eutectic salts.

1.7 DES PREPARATION

DESs are made by combining the two components (an HBA and an HBD) in a flat-bottom flask containing a jacketed perimeter with a stirring speed of 300–500 rpm generated by a mechanical stirrer and a temperature above the melting points of the separate components until a homogeneous liquid emerges. The HBA and HBD molar ratio must be accurately maintained to obtain the perfect eutectic mixture at the eutectic point, the lowest point in the melting point curve between two specific components. It is recommended to dry the HBA and the HBDs in a high vacuum oven at 35–40°C for three to four days before mixing them together to minimize and avoid the presence of moisture in the DES forming components. This process ensures a higher purity of the DESs. As mentioned earlier, the compounds with specific molar ratios of HBA and HBD were first inserted in a flat-bottom flask and heated to 343.15 K or over their individual melting point. A reflux condenser was fitted to the flask in order to prevent any solvent loss due to vaporization. This was then put through to heating and stirring for 12–24 hours to obtain a homogeneous solution. It was then cooled at a particular rate only to offer sufficient time for the appearance of the solid or crystal phase and continued heating was provided till the disappearance of the last solid. The phase transition point between the solid and liquid phases can be located

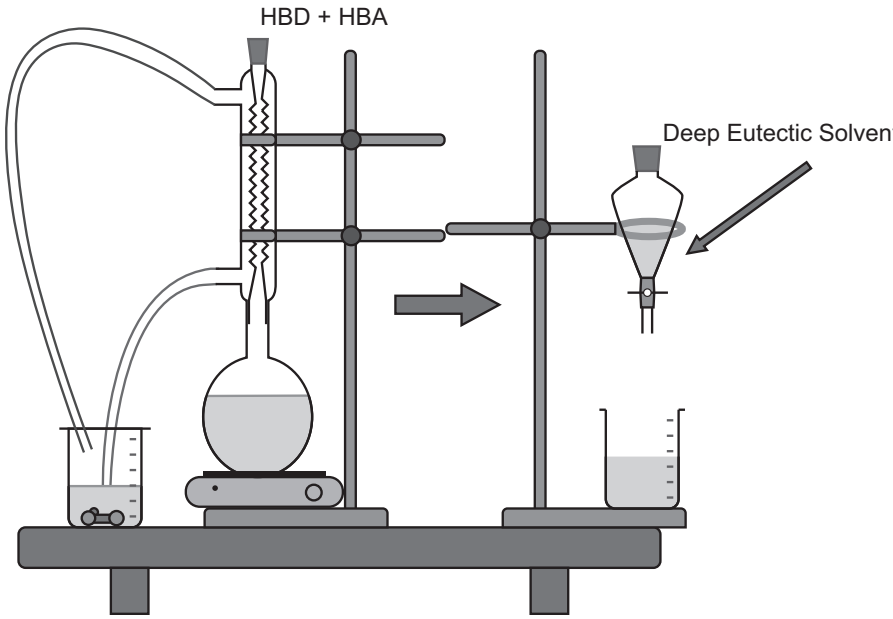

FIGURE 1.9 Preparation of a DES.

precisely by this method. After getting a clear liquid, the mixture was kept at room temperature (298.15 K) overnight in order to observe any solidification event. A typical synthetic preparation setup of DES is shown in Figure 1.9.

When two components with higher melting points are mixed in a defined molar ratio, the resulting melting point is called eutectic point, which is less than the melting point of the individual component. Abott et al. [46] attributed the first DES to a choline chloride and urea combination in 2003. Choline chloride (ChCl) has a melting point of 302°C, while urea has the same at 133°C. Their combined melting point is 120°C, which is lower than the melting points of urea and ChCl. The molar ratio can also be predicted by COSMO-RS model [47, 48], where a solid–liquid equilibria (SLE) prediction can be made prior to experimentation. Nuclear magnetic resonance (NMR) spectroscopy (^{1}H NMR) can be carried out to ensure the composition of the DES.

1.8 PROPERTIES OF DESs

The variability of DESs is explored in this section, which may be useful in determining the inherent process behind their remarkable solubility characteristics. The complicated hydrogen bonding arrangements in DESs have been investigated using sophisticated neutron scattering technologies and molecular dynamics modeling. In general, determining the physical characteristics of DESs, such as density and viscosity, is the foundation of the industrial application [49]. Also covered are thermodynamic characteristics such as entropy change, enthalpy change, and melting point. Because thermal behavior defines the maximum working temperature for DESs, it is an important

feature. Some known thermal stability rules are described, and a new test technique for DES thermal stability during long-term heating is also provided. The chemical and physical characteristics, such as melting point prediction using given algorithm and machine learning, are available in addition to measurement and testing.

The implementation of DESs in a variety of applications necessitates a detailed understanding of their different physicochemical characteristics. Different applications need different kinds of solvents, necessitating the specification of particular DES properties. The following section addresses the density, viscosity, solubility, and thermal stability of DESs in water. Additional study is necessary to ascertain the other physicochemical characteristics of DESs.

1.8.1 Density

HDESs, in contrast to hydrophilic DESs, have densities that are similar to but lower than water, ranging between 0.89–0.974 depending on the constituents. Some DESs, such as DL-menthol- salol (1:1) (1.070 g/cm^3) and thymol:coumarin (2:1) (1.050 g/cm^3), have a density greater than 1, whereas a large number of DESs have densities quite lower than that of water. Density declines with increasing alkyl chain length for all hydrophobic DES families, whether on the HBD or the HBA. For example, fatty acid–based DESs comprise following order of densities: dodecanoic acid:octanoic acid (3:1; 0.901 g/cm^3) > dodecanoic acid:nonanoic acid (3:1; 0.897 g/cm^3) > dodecanoic acid:decanoic acid (2:1; 0.894 g/cm^3). Furthermore, DESs using sodium salt as an HBA instead of its corresponding fatty acid show a substantial impact, resulting in a considerable rise in density values. The greater the density difference between DES and water, the better it is for extraction and separation studies. A greater density difference results in a well-formed interface, allowing for better phase separation and, over time, more solvent recovery. Table 1.3 represents the density of the well-known DESs. However, further study and investigations are necessary in this area before we can fully grasp the density of DESs.

1.8.2 Viscosity

Hydrogen bonding interactions between the precursor components are known to cause DES formation. These interactions might affect the mobility of the DES component molecules and result in higher viscosity of the solvent. Although the viscosity of DESs changes with the type of components selected to form the eutectic solvents, the chemical composition such as molar ratio and the temperature and the moisture content present in the solvent are important factors in viscosity variation. As the HDESs comprise a wide range of viscosities, they allow relatively easy tuning ability for specific requirements for the application in various fields. Both electrostatic and van der Waals interactions occur in DESs. The extent of both interactions determines the overall viscosity of DES along with cohesive forces present within the molecules. The extensive hydrogen bond network present in ammonium-based DESs increases the viscosity of the solvent to a great extent [50].

The temperature is another factor that influences the viscosity of the DESs. For both the hydrophilic and hydrophobic DESs, the viscosity–temperature relation

TABLE 1.3
Properties of some previously reported DESs at 298.15 K

DES		Molar ratio (HBA:HBD)	Density (g/cm³)	Viscosity (mPa.s)	Reference
HBA	HBD				
DL-menthol	Acetic acid	1:1	0.931	8.7	[16]
	Salol	1:1	1.070	–	[51]
	Pyruvic acid	1:2	0.995	30.0	[16]
	Lactic acid	1:2	1.033	218.9	[16]
	Levulinic acid	1:1	0.985	–	[52]
	Lidocaine	2:1	0.939	–	[53]
	Octanoic acid	1:1	0.901	–	[51]
	Decanoic acid	2:1	0.896	–	[54]
	Lauric acid	2:1	0.894	24.4	[16]
	Oleic acid	2:1	0.901		[51]
Thymol	Camphor	1:1	0.967	20.8	[55]
	10-undecylenic acid	7:3	0.960	–	[56]
	Decanoic acid	1:1	0.944	12.2	[57]
	Coumarin	2:1	1.050	–	[53]
	Menthol	1:1	0.937	180	[58]
Dodecanoic acid	Octanoic acid	3:1	0.901	7.1	[20]
	Nonanoic acid	3:1	0.897	8.6	[20]
	Decanoic acid	2:1	0.894	10.8	[20]
Tetrabutyl ammonium chloride	Decanoic acid	1:2	0.917	265.3	[15]
Tetrabutyl ammonium bromide	Octanoic acid	1:1	0.974	–	[59]
	Decanoic acid	1:2	0.957	–	[59]
	Oleic acid	1:2	0.959	–	[59]
Methyltrioctyl ammonium chloride	Decanoic acid	1:2	0.896	783.4	[15]
	Hydroquinone	1:1	0.952	–	[60]
	4-phenylphenol	1:1	0.937	–	[60]
	4-cyanophenol	2:1	0.919	–	[60]
Methyltrioctyl ammonium bromide	Decanoic acid	1:2	0.942	576.5	[15]
Tetraoctyl ammonium bromide	Decanoic acid	1:2	0.930	636.4	[15]
Methyltrioctyl-ammonium bromide	Decanoic acid	1:2	0.942	576.5	[15]
Methyltrioctyl-ammonium chloride	Decanoic acid	1:2	0.896	783.4	[15]
L-menthol	Octanoic acid	1.5 : 1	0.900	15.3	[57]
	Decanoic acid	1 : 1	0.896	22.0	[61]
	Dodecanoic acid	3 : 1	0.893	28.1	[57]

follows a similar trend for any liquid. The viscosity decreases with an increase in the temperature mainly due to the disruption of the electrostatic interactions among the components as a higher temperature imparts higher energy to the molecules, which increases the motion of the molecules. The neutral-based DESs comprise low viscosity, an attractive characteristic for various applications, mainly in extraction, separation, and purification processes. The hydrophobic DESs' viscosity is reduced by the increase in ammonium salts' alkyl chain length (Table 1.3). The viscosity of the hydrophobic DESs decreases with an increase in the alkyl chain length largely due to increased van der Waals interaction.

1.8.3 Solubility of DESs in Water

The hydrophilic DESs are readily miscible with water. After mixing with water, the DES forming components get separated. They tend to interact with the water molecules based on their relative affinity toward the aqueous phase and solubility in water. The DES structure gets disrupted by the breakage of hydrogen bonds initially formed within the DES and new hydrogen bonds appear in the presence of water. However, it is very important for a hydrophobic DES (HDES) not to interact with water used in the applications such as extraction and separation processes. The DES structure needs to be intact upon mixing with water with minimum loss of DES components, creating a stable formation to incorporate effective extraction of valuable compounds from water. The hydrophobicity of HDES depends on the solubility of the individual components in an aqueous phase. The lower the solubility of the precursor compounds in water, the greater the DES's hydrophobicity.

Van Osch et al. [15] demonstrated the hydrophobic property of DESs produced from different combinations of decanoic acid (HBD) and a list of quaternary ammonium salts for the first time. They observed a very low degree of leaching from DES components (~1.9 wt%) and the presence of a small amount of water (~1.8 wt%) when mixed with water. Additionally, it was discovered that as the carbon chain length increased, DES components' water content and leaching decreased. In other work, Florindo et al. [62] observed the water-miscibility of various DESs considering DL-menthol and tetrabutylammonium chloride as HBAs and changing the HBD with varying carbon chain lengths. The selected HBDs range from C_1 to C_{12} of carboxylic acids (acetic acid, butyric acid, hexanoic acid, octanoic acid, decanoic acid, dodecanoic acid, etc.). Interestingly, they noticed that the leaching tendency of the HBD decreases with an increase in the carbon chain length. Paul et al. [13] investigated the same systems by molecular dynamics simulation to highlight the molecular-level scenario and obtained similar results. Remarkably, they obtained a relation between the nonbonded interaction energy among the different components present in the system to propose a new term, "relative stability factor", which gave a qualitative analysis of the hydrophobicity and relative stability of HDES with a quantitative approach. Shishov et al. [63] proposed these unstable HDESs to be called "quasi-hydrophobic" DESs. A metal-containing HDES derived from dodecanoate sodium salt and decanoic acid produced a supramolecular hydrogel when it came into contact with water [64]. The sodium ion's presence has a substantial impact on supramolecular hydrogel formation.

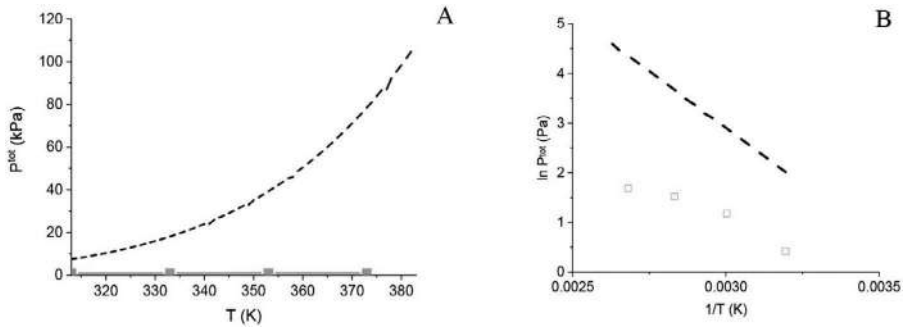

FIGURE 1.10 (A) Total vapor pressure of the DES menthol:decanoic acid (1:1) (orange squares) and the vapor pressure of toluene (black line) at different temperatures. (B) Linearized with reciprocal temperature.

Source: Reprinted (adapted) with permission from Dietz, C.H., et al., Determination of the total vapor pressure of hydrophobic deep eutectic solvents: experiments and perturbed-chain statistical associating fluid theory modeling. ACS Sustainable Chemistry & Engineering, 2019, 7(4): p. 4047–4057 Copyright 2019 American Chemical Society [61]

1.8.4 Thermal Stability

One of the key advantages of DESs, including HDESs, is their excellent heat stability, which ensures they remain in a liquid form. To utilize the DES in a wide variety of applications, one needs to obtain a relatively higher thermally stable DES. The thermal stability of a DES largely depends on the individual component's thermal stability which ensures that the DES does not degrade chemically or physically till a certain temperature and pressure. The principles of green chemistry and engineering require that HDESs with the lowest feasible vaporization levels be screened before they are used [65]. High temperatures may cause the volatilization of DESs owing to the deterioration of their separate components (HBA and HBD) that weakens the hydrogen bonding connections, according to one study [66]. Various studies projected that the hydrophilic DESs are more thermally stable than the hydrophobic DESs due to the lower order of hydrogen bonding in the latter. Figure 1.10 illustrates that when compared to toluene, the DES menthol:decanoic acid (1:1) has a much lower vapor pressure at temperature 320–380 K with 150–1000-fold volatility difference [61]. Apparently, because the volatility of DESs has received little attention, further research is necessary in the future to collect additional data on the volatility of HDESs.

1.9 ENVIRONMENTAL ASPECTS OF DESs

ILs, mostly due to their low vapor pressure, have been termed "green solvents". Their toxicity was, however, examined and shown not to be intrinsically "green". DESs may be considered a "greener" option to many traditional ILs, but they are not "green" by definition either. Some DESs are made of benign components that are intrinsically nontoxic. Some metal salts containing eutectics are found to have

toxicity. On the other hand, the phosphonium and ammonium halide salt and polyols such as glycerol and ethylene glycol have low inherent toxicity. As both components of the DESs are environmentally safe and both may easily be biologically degraded with the resulting DES, the liquid based on ethylene glycol was not environmentally damaging compared to most ILs. Furthermore, the DESs have lower vapor pressures than other molecular solvents, which reduces emissions into the atmosphere. They nonetheless are somewhat miscible with water. A recycling mechanism has to be determined for DESs to be genuinely "green".

Although DES components can be non-toxic and of a low environmental effect, the mixes of these components are not always "green" or nontoxic. The DESs have specific features that neither component has. Methyltriphenylphosphonium bromide and tetrabutylammonium bromide having slightly acute oral, skin, and inhalation toxicity. In the field of green chemistry, DESs are the most promising findings of the last several years. DES not only makes the design of safe processes possible but also allows straightforward access over the current solvent to new substances and materials. Clerk et al. [67] studied the criteria for green solvents in terms of life cycle assessment on the basis of their solvency, ease of use, reusability, health and safety, environmental impact, and economic cost that is best suited for a DES. In recent years, research on solvents has increased dramatically because of the intriguing features of DES, namely, its minimal ecological imprint and its appealing pricing. The outcome will be improved in the near future in new (not present) laboratory and industrial applications. Figure 1.4 shows the various properties of DES.

DESs are a class of ecologically acceptable solvents that are made up of an ionic compound such a quaternary ammonium salt and molecular compounds like a polyol. They have been used in a variety of areas since Abbott et al. introduced them in 2003 [34]. When the DESs constituents are primary metabolites, the synthesized DESs are referred to as NADESs (meaning natural DESs). NADESs' flexibility is similar to

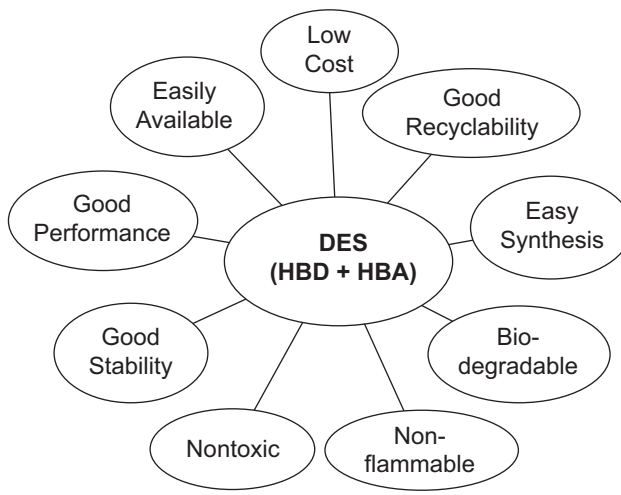

FIGURE 1.11 Different properties of DESs as a green solvent.

that of ionic liquids, with the major differences being their considerably cheaper cost and excellent sustainability [68]. As a result, NADESs are known as the solvents of the 21st century. Smith et al. redefined four kinds of DESs in 2014 [9] (Table 1.1). Among all types of DESs due to their great characteristics and variety, the third kind is the most popular. In addition, a significant variety of DESs have been developed for various purposes. It is essential to investigate their characteristics.

Advantage of DESs

1. *Availability:* The raw material of most of DESs are mostly available easily on a large scale, such as urea and common halide salt.
2. *Price:* Most constituents of DESs are cheap and economically viable, and the cost will be less during times of sustainability for the chemical process. Some of them are obtained naturally.
3. *Recyclability:* Solvent DESs are fully recyclable in the extraction process without contamination or loss [69].
4. *Synthesis:* The preparation of DESs is an easy and energy-saving process, with the synthetic reaction being highly atom-efficient.
5. *Toxicity:* Most DESs have minimal toxicity, which decreases the danger to persons and wildlife.
6. *Biodegradability:* DESs being green solvents, they do not produce any toxic metabolites and are biodegradable [70].
7. *Performance:* In comparison to the contemporary solvents, most of the DESs show similar and even superior performances in terms of their application like extraction capacity.
8. *Stability:* During a chemical process, most DESs are thermally and chemically stable up to high temperatures [71].
9. *Flammability:* These green solvents are nonflammable and are safe to manipulate.
10. *Storage:* The storage of DESs is easy and safe because they stable and self-stainable in nature.

1.10 SUMMARY

DES can be prepared with little effort and has chemical properties directly related to the HBA and HBD interaction, as well as the temperature. Nevertheless, by altering the characteristics of the HBA and the HBD, the physicochemical properties of DESs can be fine-tuned. DESs have advantages, such as their straightforward preparation, which is highly economical, low price, low toxicity, and higher biocompatibility, for which they are considered superior compared to the ILs. With all these advantages, DESs have the potential to come to the fore in a variety of industrial applications. The use of naturally occurring substances as DES-forming components that are neutral has opened a new class of DESs that are easily synthesized and have higher stability in different task-specific conditions. A new class of HDESs is emerging that has started to prove its worth in the separation and extraction of valuable compounds from a water-based medium. The ability to tune DESs by adjusting the HBA and the HBD has granted the flexibility to use them in various

applications such as liquid–liquid extraction, removing contaminants, metal extraction, carbon dioxide capture, therapeutic applications, and others. DESs have a reactive component, but their association with a hydrogen bond limits their reactivity, and as a result, they can be safely applied in many research areas, some of which are discussed in the following chapters. However, although DESs have been applied in various research fields since last decade, the physico-chemical properties are yet to be extensively studied. There is still much to learn about DESs' fundamental characteristics and behavior, both physically and chemically. The nonbonded interaction between the HBA and the HBD, the extent of electrostatic and van der Waals forces, and the alteration in the interaction due to presence of any third molecular group or such environment, among others, are quite eminent subjects that need extensive research. Both experimental, as well as modeling and simulation works in this field can enrich our knowledge to attain a thorough understanding of the fundamental properties of the DESs. Thermodynamic studies combined with validation with experimental findings are quite feasible to extract valuable insights into the matter. Along with numerous advantages of the DESs, there are some disadvantages as well. The HBA–HBD interaction is weaker than the ionic interaction between the IL-forming components. In general, the thermal stability of the DESs is lower than the ILs, meaning that the DESs cannot withstand severe operating conditions. Moreover, most of the DES-based applications are conducted at a lab scale; consequently, it will be challenging to develop a full-scale industrial pilot plant based on the lab-scale information. All these aspects are addressed and discussed quite elaborately in the following chapters.

REFERENCES

1. Matsuhisa, N., et al., *Materials and structural designs of stretchable conductors*. Chemical Society Reviews, 2019. **48**(11): p. 2946–2966.
2. Daeneke, T., et al., *Liquid metals: Fundamentals and applications in chemistry*. Chemical Society Reviews, 2018. **47**(11): p. 4073–4111.
3. García, G., et al., *Deep eutectic solvents: Physicochemical properties and gas separation applications*. Energy & Fuels, 2015. **29**(4): p. 2616–2644.
4. Qu, Y., et al., *Superelastic multimaterial electronic and photonic fibers and devices via thermal drawing*. Advanced Materials, 2018. **30**(27): p. 1707251.
5. Lin, X., et al., *High temperature electrical energy storage: Advances, challenges, and frontiers*. Chemical Society Reviews, 2016. **45**(21): p. 5848–5887.
6. Vuoti, S., K. Narasimha, and K. Reinikainen, *Green wastewater treatment flocculants and fixatives prepared from cellulose using high-consistency processing and deep eutectic solvents*. Journal of Water Process Engineering, 2018. **26**: p. 83–91.
7. Alli, R.D., I.M. AlNashef, and M.C. Kroon, *Removal of 2-and 3-methylthiophene from their mixtures with n-heptane using tetrahexylammonium bromide-based deep eutectic solvents as extractive desulfurization agents*. The Journal of Chemical Thermodynamics, 2018. **125**: p. 172–179.
8. Abbott, A.P., et al., *Preparation of novel, moisture-stable, Lewis-acidic ionic liquids containing quaternary ammonium salts with functional side chainsElectronic supplementary information (ESI) available: Plot of conductivity vs. temperature for the ionic liquid formed from zinc chloride and choline chloride (2: 1)*. Chemical Communications, 2001. (19): p. 2010–2011.

9. Smith, E.L., A.P. Abbott, and K.S. Ryder, *Deep eutectic solvents (DESs) and their applications*. Chemical Reviews, 2014. **114**(21): p. 11060–11082.
10. Zhang, Q., et al., *Deep eutectic solvents: Syntheses, properties and applications*. Chem Soc Rev, 2012. **41**(21): p. 7108–7146.
11. Abbott, A.P., et al., *Novel solvent properties of choline chloride/urea mixtures Electronic supplementary information (ESI) available: Spectroscopic data*. Chemical Communications, 2003. (1): p. 70–71.
12. Abbott, A.P., et al., *Deep eutectic solvents formed between choline chloride and carboxylic acids: Versatile alternatives to ionic liquids*. Journal of the American Chemical Society, 2004. **126**(29): p. 9142–9147.
13. Paul, N., et al., *Molecular Dynamics Insights and Water Stability of Hydrophobic Deep Eutectic Solvents Aided Extraction of Nitenpyram from an Aqueous Environment*. The Journal of Physical Chemistry B, 2020. **124**(34): p. 7405–7420.
14. Zainal-Abidin, M.H., M. Hayyan, and W.F. Wong, *Hydrophobic deep eutectic solvents: Current progress and future directions*. Journal of Industrial and Engineering Chemistry, 2021. **97**: p. 142–162.
15. van Osch, D.J., et al., *Hydrophobic deep eutectic solvents as water-immiscible extractants*. Green Chemistry, 2015. **17**(9): p. 4518–4521.
16. Ribeiro, B.D., et al., *Menthol-based eutectic mixtures: Hydrophobic low viscosity solvents*. ACS Sustainable Chemistry & Engineering, 2015. **3**(10): p. 2469–2477.
17. Schaeffer, N., et al., *Sustainable hydrophobic terpene-based eutectic solvents for the extraction and separation of metals*. Chemical Communications, 2018. **54**(58): p. 8104–8107.
18. van Osch, D.J., et al., *Removal of alkali and transition metal ions from water with hydrophobic deep eutectic solvents*. Chemical Communications, 2016. **52**(80): p. 11987–11990.
19. Santana-Mayor, Á., et al., *Quality assessment of environmental water by a simple and fast non-ionic hydrophobic natural deep eutectic solvent-based extraction procedure combined with liquid chromatography tandem mass spectrometry for the determination of plastic migrants*. Analytical and Bioanalytical Chemistry, 2021. **413**(7): p. 1967–1981.
20. Florindo, C., et al., *From phase change materials to green solvents: Hydrophobic low viscous fatty acid—based deep eutectic solvents*. ACS Sustainable Chemistry & Engineering, 2018. **6**(3): p. 3888–3895.
21. Abbott, A.P., et al., *Preparation of novel, moisture-stable, Lewis-acidic ionic liquids containing quaternary ammonium salts with functional side chains Electronic Supplementary Information (ESI) available: Plot of conductivity vs. temperature for the ionic liquid formed from zinc chloride and choline chloride (2: 1). See www. rsc. org/suppdata/cc/b1/b106357j*. Chemical Communications, 2001. (19): p. 2010–2011.
22. Hsiu, S.-I., et al., *Lewis acidity dependency of the electrochemical window of zinc chloride—1-ethyl-3-methylimidazolium chloride ionic liquids*. Electrochimica Acta, 2002. **47**(27): p. 4367–4372.
23. Lin, Y.-F. and I.-W. Sun, *Electrodeposition of zinc from a Lewis acidic zinc chloride-1-ethyl-3-methylimidazolium chloride molten salt*. Electrochimica Acta, 1999. **44**(16): p. 2771–2777.
24. Abbott, A.P., et al., *Ionic liquids based upon metal halide/substituted quaternary ammonium salt mixtures*. Inorganic Chemistry, 2004. **43**(11): p. 3447–3452.
25. Hurley, F.H. and T.P. Wier Jr, *Electrodeposition of metals from fused quaternary ammonium salts*. Journal of The Electrochemical Society, 1951. **98**(5): p. 203.
26. Xu, W.G., et al., *Studies on the thermodynamic properties of the ionic liquid BMIGaCl4*. Chinese Journal of Chemistry, 2006. **24**(3): p. 331–335.
27. Yang, J.-Z., et al., *Studies on room temperature ionic liquid InCl3—EMIC*. Fluid Phase Equilibria, 2003. **204**(2): p. 295–302.

28. Abbott, A.P., et al., *Ionic liquid analogues formed from hydrated metal salts*. Chemistry—A European Journal, 2004. **10**(15): p. 3769–3774.
29. Abbott, A.P., G. Capper, and D.L. Davies, *Rasheed; RK; Tambyrajah, V.* Chem. Commun, 2003: p. 70–71.
30. Abbott, A., et al., *Electropolishing of stainless steel in an ionic liquid*. Transactions of the IMF, 2005. **83**(1): p. 51–53.
31. Islam, R., et al., *Investigations on microhardness of Sn—Zn based lead-free solder alloys as replacement of Sn—Pb solder*. Journal of Alloys and Compounds, 2005. **392**(1–2): p. 149–158.
32. Richards, T.W. and W.B. Meldrum, *The melting points of the chlorides of lithium, rubidium andcaesium, and the freezing points of binary and ternary mixtures of these salts, including also potassium and sodium chloride*. Journal of the American Chemical Society, 1917. **39**(9): p. 1816–1828.
33. Chadwick, K., R. Davey, and W. Cross, *How does grinding produce co-crystals? Insights from the case of benzophenone and diphenylamine*. CrystEngComm, 2007. **9**(9): p. 732–734.
34. Abbott, A.P., et al., *Novel solvent properties of choline chloride/urea mixtures*. Chemical Communications, 2003. (1): p. 70–71.
35. Cubicciotti, D., *Solutions of metals in molten salts*. 1960: ACS Publications.
36. Yu, D. and T. Mu, *Strategy to form eutectic molecular liquids based on noncovalent interactions*. The Journal of Physical Chemistry B, 2019. **123**(23): p. 4958–4966.
37. Abranches, D.O., et al., *Phenolic hydrogen bond donors in the formation of non-ionic deep eutectic solvents: The quest for type V DES*. Chemical Communications, 2019. **55**(69): p. 10253–10256.
38. van der Lubbe, S.C. and C. Fonseca Guerra, *The nature of hydrogen bonds: A delineation of the role of different energy components on hydrogen bond strengths and lengths*. Chemistry—An Asian Journal, 2019. **14**(16): p. 2760–2769.
39. Zahn, S., B. Kirchner, and D. Mollenhauer, *Charge spreading in deep eutectic solvents*. ChemPhysChem, 2016. **17**(21): p. 3354–3358.
40. Jorstad, J. and D. Apelian, *Hypereutectic Al-Si alloys: Practical casting considerations*. International Journal of Metalcasting, 2009. **3**(3): p. 13–36.
41. Yu, D., Z. Xue, and T. Mu, *Eutectics: Formation, properties, and applications*. Chemical Society Reviews, 2021.
42. Angell, C.A., Y. Ansari, and Z. Zhao, *Ionic liquids: Past, present and future*. Faraday Discussions, 2012. **154**: p. 9–27.
43. Zein El Abedin, S. and F. Endres, *Ionic liquids: The link to high-temperature molten salts?* Accounts of Chemical Research, 2007. **40**(11): p. 1106–1113.
44. Wang, B., et al., *Are ionic liquids chemically stable?* Chemical Reviews, 2017. **117**(10): p. 7113–7131.
45. Bhargava, B.L., et al., *Nanoscale organization in room temperature ionic liquids: A coarse grained molecular dynamics simulation study*. Soft Matter, 2007. **3**(11): p. 1395–1400.
46. Abbott, A.P., et al., *Novel solvent properties of choline chloride/urea mixtures*. Chem. Commun., 2003. **1**: p. 70.
47. Klamt, A., F. Eckert, and W. Arlt, *COSMO-RS: An alternative to simulation for calculating thermodynamic properties of liquid mixtures*. Annual Review of Chemical and Biomolecular Engineering, 2010. **1**: p. 101–122.
48. Kundu, D., P.S. Rao, and T. Banerjee, *First Principle Prediction of Kamlet-Taft Solvatochromic Parameters of Deep Eutectic Solvent Using COSMO-RS Model*. Industrial & Engineering Chemistry Research, 2020. **59**(24): p. 11329–11339.
49. Shahbaz, K., et al., *Prediction of deep eutectic solvents densities at different temperatures*. Thermochimica Acta, 2011. **515**(1–2): p. 67–72.

50. Stefanovic, R., et al., *Nanostructure, hydrogen bonding and rheology in choline chloride deep eutectic solvents as a function of the hydrogen bond donor.* Physical Chemistry Chemical Physics, 2017. **19**(4): p. 3297–3306.
51. Křížek, T., et al., *Menthol-based hydrophobic deep eutectic solvents: Towards greener and efficient extraction of phytocannabinoids*. Journal of Cleaner Production, 2018. **193**: p. 391–396.
52. Bezold, F. and M. Minceva, *A water-free solvent system containing an L-menthol-based deep eutectic solvent for centrifugal partition chromatography applications*. Journal of Chromatography A, 2019. **1587**: p. 166–171.
53. Van Osch, D., et al., *A search for natural hydrophobic deep eutectic solvents based on natural components.* ACS Sustainable Chemistry & Engineering, 2019. **7**: p. 2933–2942.
54. Verma, R., et al., *Operational strategies and comprehensive evaluation of menthol based deep eutectic solvent for the extraction of lower alcohols from aqueous media*. ACS Sustainable Chemistry & Engineering, 2018. **6**(12): p. 16920–16932.
55. Martins, M.A., et al., *Greener terpene—terpene eutectic mixtures as hydrophobic solvents.* ACS Sustainable Chemistry & Engineering, 2019. **7**(20): p. 17414–17423.
56. Makoś, P., A. Przyjazny, and G. Boczkaj, *Hydrophobic deep eutectic solvents as "green" extraction media for polycyclic aromatic hydrocarbons in aqueous samples*. Journal of Chromatography A, 2018. **1570**: p. 28–37.
57. Martins, M.A., et al., *Tunable hydrophobic eutectic solvents based on terpenes and monocarboxylic acids*. ACS Sustainable Chemistry & Engineering, 2018. **6**(7): p. 8836–8846.
58. Hussin, S.A.M., et al., *Synthesis and characterization of green menthol-based low transition temperature mixture with tunable thermophysical properties as hydrophobic low viscosity solvent*. Journal of Molecular Liquids, 2020. **308**: p. 113015.
59. Yousefi, S.M., F. Shemirani, and S.A. Ghorbanian, *Hydrophobic deep eutectic solvents in developing microextraction methods based on solidification of floating drop: Application to the trace HPLC/FLD determination of PAHs*. Chromatographia, 2018. **81**(8): p. 1201–1211.
60. Zhang, K., et al., *A hydrophobic deep eutectic solvent based vortex-assisted liquid-liquid microextraction for the determination of formaldehyde from biological and indoor air samples by high performance liquid chromatography.* Journal of Chromatography A, 2019. **1589**: p. 39–46.
61. Dietz, C.H., et al., *Determination of the total vapor pressure of hydrophobic deep eutectic solvents: Experiments and perturbed-chain statistical associating fluid theory modeling.* ACS Sustainable Chemistry & Engineering, 2019. **7**(4): p. 4047–4057.
62. Florindo, C., L. Branco, and I. Marrucho, *Development of hydrophobic deep eutectic solvents for extraction of pesticides from aqueous environments*. Fluid Phase Equilibria, 2017. **448**: p. 135–142.
63. Shishov, A., et al., *Deep eutectic solvents are not only effective extractants*. TrAC Trends in Analytical Chemistry, 2020. **129**: p. 115956.
64. Florindo, C., et al., *Supramolecular hydrogel based on a sodium deep eutectic solvent*. Chemical Communications, 2018. **54**(54): p. 7527–7530.
65. Dietz, C.H., et al., *Selective separation of furfural and hydroxymethylfurfural from an aqueous solution using a supported hydrophobic deep eutectic solvent liquid membrane*. Faraday Discussions, 2017. **206**: p. 77–92.
66. Chen, Y., et al., *Volatility of deep eutectic solvent choline chloride: N-methylacetamide at ambient temperature and pressure*. Industrial & Engineering Chemistry Research, 2019. **58**(17): p. 7308–7317.
67. Clark, J.H. and S.J. Tavener, *Alternative solvents: Shades of green*. Organic Process Research & Development, 2007. **11**(1): p. 149–155.

68. Paiva, A., et al., *Natural deep eutectic solvents—solvents for the 21st century.* ACS Sustainable Chemistry & Engineering, 2014. **2**(5): p. 1063–1071.
69. Jeong, K.M., et al., *Tailoring and recycling of deep eutectic solvents as sustainable and efficient extraction media*. Journal of Chromatography A, 2015. **1424**: p. 10–17.
70. Juneidi, I., M. Hayyan, and M.A. Hashim, *Evaluation of toxicity and biodegradability for cholinium-based deep eutectic solvents.* RSC Advances, 2015. **5**(102): p. 83636–83647.
71. Delgado-Mellado, N., et al., *Thermal stability of choline chloride deep eutectic solvents by TGA/FTIR-ATR analysis.* Journal of Molecular Liquids, 2018. **260**: p. 37–43.

2 Thermodynamic Insights and Phase Equilibria Measurements on Aromatic Systems

2.1 AROMATIC AND POLYAROMATIC HYDROCARBONS

Aromatic and polyaromatic hydrocarbons (PAHs) impurities are the most perilous compounds found in fuel oil. These are gaining importance for being removed from fuel oil due to the strict limits set by government agencies. These are very difficult to remove completely [1]. Furthermore, these PAHs are the major source of pollution as it releases SO_x and NO_x into the atmosphere. This emission causes harmful effects on the environment and contributes to air pollution, the greenhouse effect, and acid rain [2]. Thus, it becomes invariably necessary to extract sulfur- and nitrogen-containing PAH species from fuel oil by using physical methods in ambient conditions. Nowadays, the maximum nitrogen content is also limited to <0.1 ppm. The nitrogen-based PAH compounds are more reactive, forming pollutants in the combustion process. The nitrogen molecules are also known to influence the formation of coke at specified and/or moderate operating conditions [2]. They sometimes inhibit the sulfur removal process. Thus, these PAH molecules point out to a hazardous threat due to their emission into the atmosphere. The toxic effects are mainly due to the carcinogenic products released in the environment as a result of combustion [3]. This makes the removal of aromatic and PAHs from the fuel oil an essential step before utilization.

Industrially, the separation of aromatic ring compounds from straight-chain aliphatic compounds occurs using traditional methods with solvents such as sulfolane, ethylene glycol, tetraethylene glycol, N-methylpyrrolidone, and glycols. The industrial operation uses conventional solvents as an extracting agent with a liquid–liquid extraction (LLE) process, accompanied by extractive distillation for solvent recovery [4]. However, they are not an effective separation method for mixtures with an aromatic content of less than 20 wt% due to the high-energy expenditure required for solvent recovery. Therefore, in fuels such as diesel and kerosene, where the desired aromatic content is lower, the separation of aromatics from aliphatic compounds is carried out using LLE. However, if the issue of solvent recovery is solved, the extraction could be achieved at the starting of the naphtha cracking. Thus, the energy requirements would be decreased during the entire cracking process due to the decrease in the flows to be heated in the columns [5, 6].

DOI: 10.1201/9781003231158-2

Among the physical methods, the solvent extraction process is an imminent operation for removing PAHs in moderate conditions [7]. Conventional solvents like sulfolane and n-methyl pyrrolidone (NMP) have some limitations for removing sulfur and nitrogen contents [7–10]. The efficiency of liquid–liquid extraction process depends on its solvent. In recent times, various solvents have been discovered as substitutes for the conventional sulfolane process. Thus, new-generation green solvents are being explored so as to replace the conventional solvents. It has been stated that ionic liquids (ILs) [11] might be used in application as extracting agents for aromatic decantation from aliphatic compounds [12, 13]. Some ILs show similar values of solute distribution coefficient and selectivity as compared to sulfolane. Furthermore, the negligible vapor pressure of ILs eases the recovery cost as compared to the sulfolane process. These are extensively reported in the literature [14–19]. However, high-purity ILs are difficult to synthesize and some of them degrade at temperatures well below 100°C, inhibiting its use in extraction even though it is highly selective toward PAHs. Due to their complicated synthesis, the high price of ILs is a major drawback for implementation in large-scale industrial applications. The new-generation green solvents such as deep eutectic solvents (DESs) have been used for extraction of PAH and has hence gained enormous importance [20]. DESs, which are analogous to ILs, now used as an alternative to traditional solvent for extraction of aromatic from naphthalene [20]. Due to the advantage of DESs over ILs, DESs can be better used as extraction media for removing PAH from fuel oil. The details on DESs were described in Chapter 1. In this chapter, LLE experiments for multicomponent mixtures are discussed for fuel oil.

Liquid–liquid separation of aromatics with ILs is well known [21–23], but the application of DESs for aromatic separation is limited [24, 25]. Kareem et al. [24] reported that phosphonium-based DESs have a greater extraction capacity of aromatics from fuel oil compared to conventional solvents and ILs. Mohammad et al. [26] also demonstrated the physicochemical character of DESs in achieving superior denitrogenation performance. Recently, Hizaddin et al. applied the Conductor-like Screening Model for Real Solvents (COSMO-RS) model for denitrification of fuel in DES-based solvents [27].

DESs are formed by combining a salt and a hydrogen bond donor (HBD) [28, 29]. DESs are easy to synthesize, possess a high purity, and, most important, are economically applicable [30]. Studies involving DESs for LLE of aromatics and hydrocarbons mixtures are scarce [31–33]. The phosphonium-based salt, being a constituent of DES, is more stable than the ammonium counterpart as it forms strong interaction with HBD such as ethylene glycol and glycerol [34, 35]. Methyltriphenyl phosphonium bromide (MTPB)-ethylene glycol (1:4) and MTPB-glycerol (1:4) have been used for the extraction of an aromatic (benzene, toluene) and PAH (indoline, quinoline) from a hydrocarbon at ambient condition. Along with the LLE experimental data, the distribution coefficient (β) and selectivity (S) were also computed for both the systems. Again, the fuel oil in the hydrocarbon stream having both aromatic and PAH simultaneously along with other aliphatic. Therefore, it is a necessary need to study the simultaneous extraction of both toluene and quinoline component within the hydrocarbon stream. Hence again, quaternary LLE data are discussed for the separation of quinoline and indoline from toluene—heptane mixture. Gibb's free

energy models, such as nonrandom two liquid (NRTL) and universal quasi-chemical (UNIQUAC), were then used to correlate the experimental data. The equations are provided in Table A.1 of the appendix. Furthermore, the continuum solvation model is employed to predict the phase behavior of studied systems.

2.2 FORMULATION OF EUTECTIC SOLVENTS

2.2.1 Preparation

MTPB and ethylene glycol were mixed in a molar ratio of 1:4 to produce DES1. In a similar fashion, MTPB and glycerol (1:4) were used for synthesizing DES2. The details are provided in Chapter 1 and described in detail by Kareem et al. [36]. Here, MTPB is taken as a salt, that is, the hydrogen bond acceptor (HBA), and ethylene glycol or glycerol as the HBD. The respective proportion of chemicals was weighted by digital weight balance (Denver Instrument, Model SI-234) and mixed inside a flat-bottom flask which was fitted with a reflux condenser. The total mixture was mixed by magnetic stirring at a temperature of 60°C with a rotational speed of 800 rpm. This was further mixed for 24 hours, after which a clear liquid of DES was observed after overnight settling. The densities of the synthesized DES were then measured at atmospheric pressure with a digital densitometer (Anton Paar DMA 4500) having an uncertainty of ±0.001g/cm^3. The viscosity of DES was measured in a rheometer (make: Anton Paar (Austria), model: Physica MCR 301) employing a parallel plate geometry at 25°C with a shear rate of $u = 1\ s^{-1}$. Karl Fisher Titrator (Model No.: 787 KF; Make: M/s Metrohm, Switzerland) was used for the measurement of water content in DES. The water content measured in DES was 0.001 wt%. Later, the vacuum-dried DES was characterized for purity with ^{1}H NMR spectra through a composition analysis by recording the NMR spectra (600 MHz NMR, Bruker, Germany).

2.2.2 Extraction Studies

A single-stage LLE phase equilibrium experiment for each tie line was conducted. This was performed by preparing an adequate mixture of the solvent and feed components in a 15 mL stoppered vial such that they form a heterogeneous mixture. For generating the tie lines, the feed composition was varied with respect to the quantity of the solute, which ranged from 0.1–0.8 mole fraction. The compositions were chosen in such a way that they cover the concentration of aromatic content lower than 20 wt%. The corresponding feed volumes were computed according to the densities, molecular weight, and proportion of the individual compounds. The total volume of the DES was kept at 10 ml. Thereafter, the desired volume of components was transferred into a 15 ml culture bottle for mixing. All the bottles were properly covered with parafilm tape to prevent loss of the compound to the atmosphere due to evaporation. The bottles were then kept inside an incubator shaker (Daihan Lab Tech, China), which was capable of controlling both shaking speed and temperature. The shaker was set to 298.15 K at 200 rpm for 6 hours. The uncertainty in temperature was within ±0.01 K. The mixture was then kept overnight (12 hours) for settling at the same temperature so as to ensure a clear and stable separation of layers.

2.2.3 Measurement of Extract and Raffinate Phase

LLE data for the ternary system were analyzed by ^{1}H NMR spectra analysis (ACD NMR software). In recent times, ^{1}H NMR spectra are used to determine the composition of phases at equilibrium [37–41] successfully. Both the phases, namely, extract and raffinate, were analyzed using a 600-MHz NMR spectrometer (Bruker). The measured values were within an uncertainty of ±0.001 in the mole fraction. Throughout the LLE experiment, the DES was treated as a single pseudo-compound as it is referred to as a binary eutectic mixture with a unique eutectic point. The term *pseudo* has been introduced to indicate that the DES was treated as a *pseudo*-pure species instead of a mixture of HBA and HBD. The composition of pure DES was justified experimentally using ^{1}H NMR.

The proton peak areas of each component were located in order to obtain the molar phase concentration of each compound. A small amount (0.1 ml) of each phase was dissolved in a 0.5 ml deuterated solvent in two different NMR (thrift grade) tubes, after which they were sealed properly. The deuterated solvent used was $CdCl_3$ and DMSO for DES1 and DES2, respectively. This was required as DES2 was not found to be miscible in $CdCl_3$. The caps of the NMR tubes were then closed with parafilm tape to prevent loss. The tubes were then placed in an NMR spectrometer for proton analysis. The reference peak for $CdCl_3$ and DMSO were found to lie at 7.27 and 2.5, respectively. The peaks with respect to individual components were identified and then integrated into the NMR spectra. From the integral area, the compositional mole fraction is calculated as

$$x_i = \frac{H_i}{\sum_{i=1}^{3} H_i}. \tag{2.1}$$

Here, H_i and x_i represent the peak area and mole fraction for single hydrogen of i^{th} component in the mixture. ^{1}H NMR spectra of DES1 and DES2 are shown in Figure 2.1 and Figure 2.2, respectively. In the spectrum, the total area of all hydrogen is normalized. Only one prominent resonance peak is chosen for the respective component to quantify the corresponding mole fraction in the respective phase. As discussed earlier, the number of hydrogens of the corresponding moiety is determined by calculating the area under the resonance and dividing the area (Equation 2.1) with the total hydrogen atom of that moiety to calculate a single hydrogen atom area. The detailed calculation steps can be found in our previous literature [42].

In the case of DES1, MTPB has a triphenyl ($-(C_6H_5)_3-$) group peak at about 7.66–7.54 ppm, which is the region for the aromatic ring. The methyl group ($-CH_3$) shows a peak at about 2.89 ppm. Similarly, the –OH and $-CH_2-$ group of ethylene glycol depicts a peak at about 4.26 ppm and 3.41 ppm, respectively. For DES2, the triphenyl ($-(C_6H_5)_3-$) and methyl group ($-CH_3$) were obtained at about 7.88–7.75 and 3.18 ppm, respectively. Glycerol, having three hydroxyl (–OH) groups, is evident at approximately 4.53–4.46 ppm, while the $-CH_2-$ presence is confirmed at about 3.45–3.31 ppm. However, as stated earlier concentrations of about <1% mole fraction may not be well detected by proton NMR as the peaks are lost or diminished in the baseline of the spectrum.

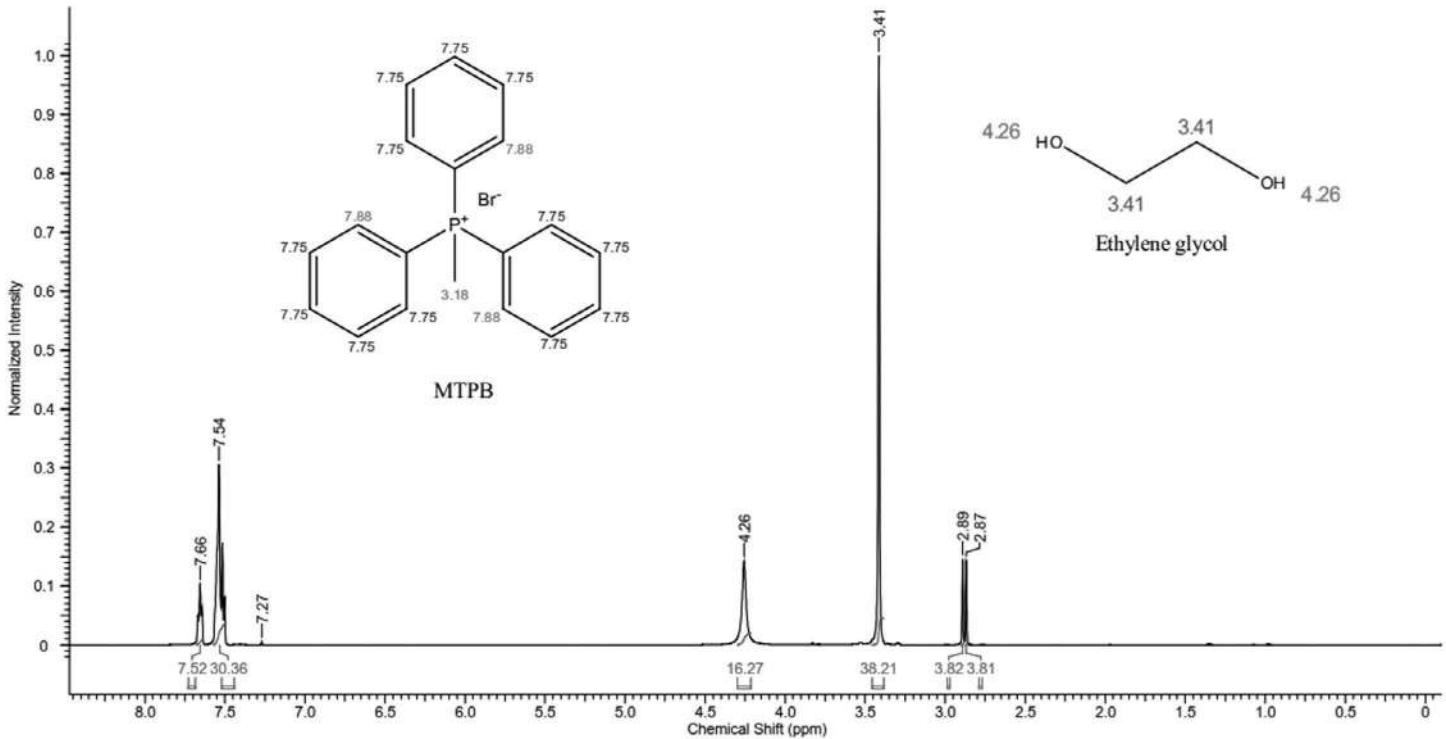

FIGURE 2.1 ^{1}H NMR spectra of DES1.

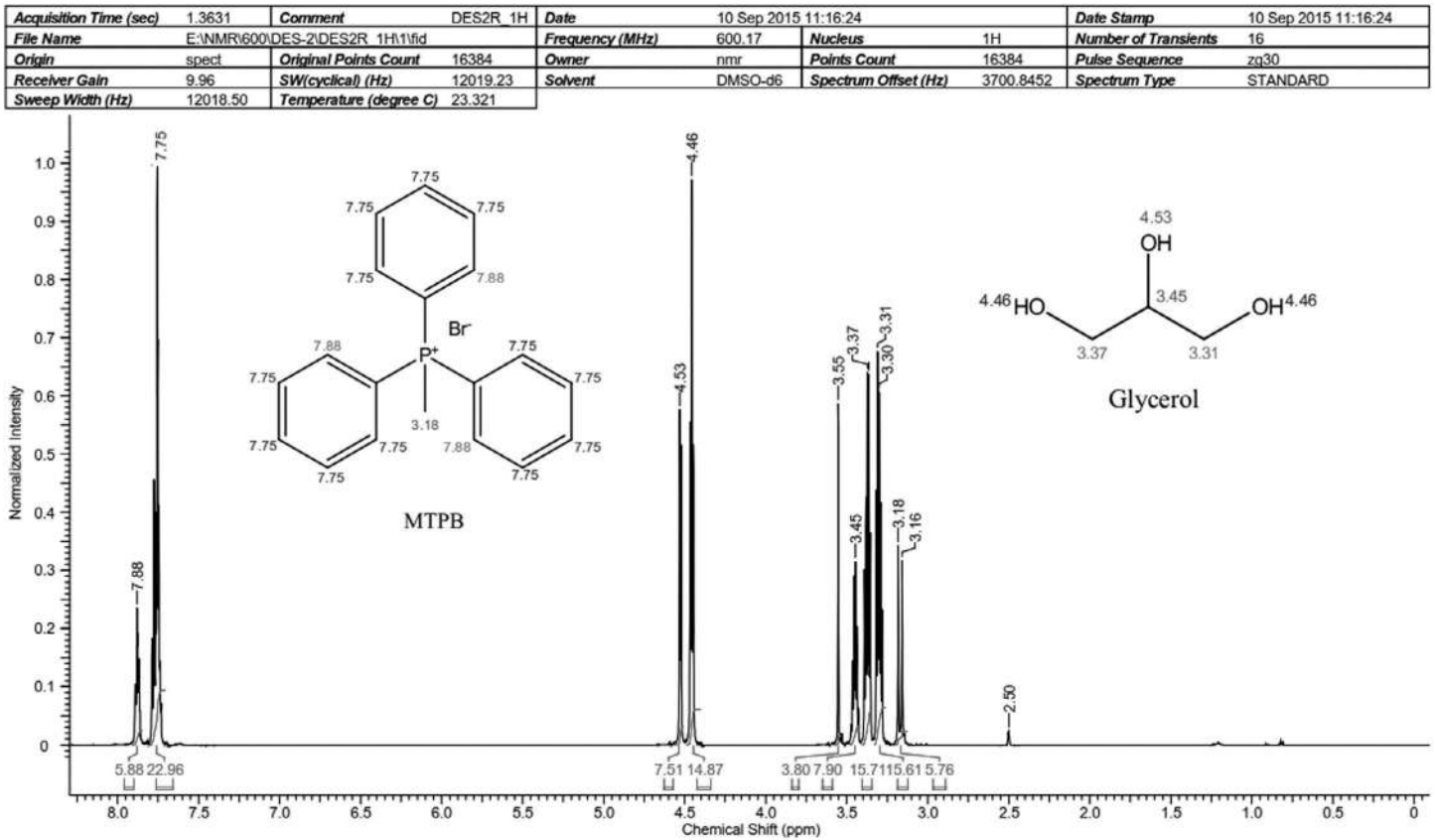

FIGURE 2.2 ^{1}H NMR spectra of DES2.

2.3 EXTRACTION OF AROMATICS AND POLYAROMATIC HYDROCARBON FROM FUEL

2.3.1 Ternary Systems of DES–Aromatic–Aliphatic

The LLE experimental data for DES1 + toluene + heptane, DES2 + toluene + heptane, DES1 + quinoline + heptane, DES2 + quinoline + heptane, DES1 + indoline + heptane, DES1 + benzene + decane, DES1 + benzene + dodecane, and DES1 + benzene + hexadecane were studied. The ternary LLE data are available in Tables 2.1–2.8, respectively. The extraction capacity of a solvent is usually expressed by parameters such as distribution ratio (β) and selectivity (S). These are in turn computed from experimental mole fractions. The degree of affinity of the solute with extract and raffinate phases is calculated by the distribution ratio (β). A considerable value of the distribution ratio implies a lower amount of solvent is required with respect to the feed. Selectivity (S) is the ratio of the distribution ratio of solute-rich phase to the model's diesel component–rich phases. The mathematical forms are given as follow:

$$\beta = \frac{x_i^{Extract}}{x_i^{Raffinate}} \tag{2.2}$$

$$S = \frac{x_i^{Extract}}{x_i^{Raffinate}} \Big/ \frac{x_j^{Extract}}{x_j^{Raffinate}} \tag{2.3}$$

$$\%EE = \left[\frac{x_{i(initial)} - x_{i(final)}}{x_{i(initial)}} \right] \tag{2.4}$$

Here, $x_i^{Extract}$ and $x_i^{Raffinate}$ represent the mole fractions of ith component, that is, aromatic, and $x_j^{Extract}$ and $x_j^{Raffinate}$ represent the mole fractions of the j^{th} component, that is, hydrocarbon representative compound in the extract and raffinate phase, respectively. In extraction efficiency, (EE) $x_{i(initial)}$ refers to the initial mole fraction of aromatic in the feed, and $x_{i(final)}$ is the final mole fraction of aromatic in the hydrocarbon-rich phase after extraction.

In both the extract and raffinate phases, the peak due to the phenyl group of MTPB (~7.7) has been used for the quantification of DES1 and DES2. In other words, the $(–C_6H_5–)_3$ peak at about 7.7 ppm consisting of 15 hydrogen atoms was taken for the calculation. Similarly, the aromatic peak of approximately 7.2 was used for the quantification of toluene in the extract phases of both systems. Continuing with the same trend, the methyl peak ($–CH_3–$) consisting of 3Hydrogen atoms at about 2.47 ppm in DES + toluene + heptane was considered for toluene in raffinate phases. Heptane shows peaks at different domains, namely, at about 0.9 ppm for the $(–CH_3–)_2$ group and about 1.2 ppm for the $(–CH_2–)_5$ group. In this case, we consider $(–CH_3–)_2$ consisting of 6 hydrogen atoms for the quantification of heptane in both phases of DES1. In the case of DES + quinoline + heptane, due to the overlap of the peak with quinoline, we consider the $–CH_3–$ peak (~3 ppm) consisting of 3 hydrogen atoms of MTPB for DES. For quinoline, the peak at approximately 8.7 ppm due to the single H atom

was considered for quantification. Like the previous system, $(–CH_3–)_2$ consisting of 6 hydrogen atoms was used for the quantification of heptane. This was necessitated as the glycerol–OH peak is not a stable one for quantification. A sample calculation of the mole fraction from NMR spectra is also given in the Appendix. In all cases, it is clear that the concentration of DES is zero in the raffinate phase, which indicates that DES acts as a solvent, and it nearly eliminates the necessity of a solvent recovery step. The reproducibility of the NMR-derived mole fractions was checked on known mixtures of toluene–DES1 and quinoline–DES1, and it was found that the mole fractions lie within the uncertainty range of ±0.001. However, it is generally acknowledged that concentrations of about 1–2% mole fraction may not be well detected by proton NMR as the peaks are lost or diminished in the baseline of the spectrum. Therefore, some small amounts of the solvent might be continuously lost in a real extraction unit in an industrial process if no attempts were made to recover the solvent from the raffinate stream.

Figures 2.3 and 2.4 show the comparison of β and S values with respect to the solute mole fraction in the aromatic feed composition. When compared with the selectivity values, we may need to tune the selection of a solvent based on its concentration

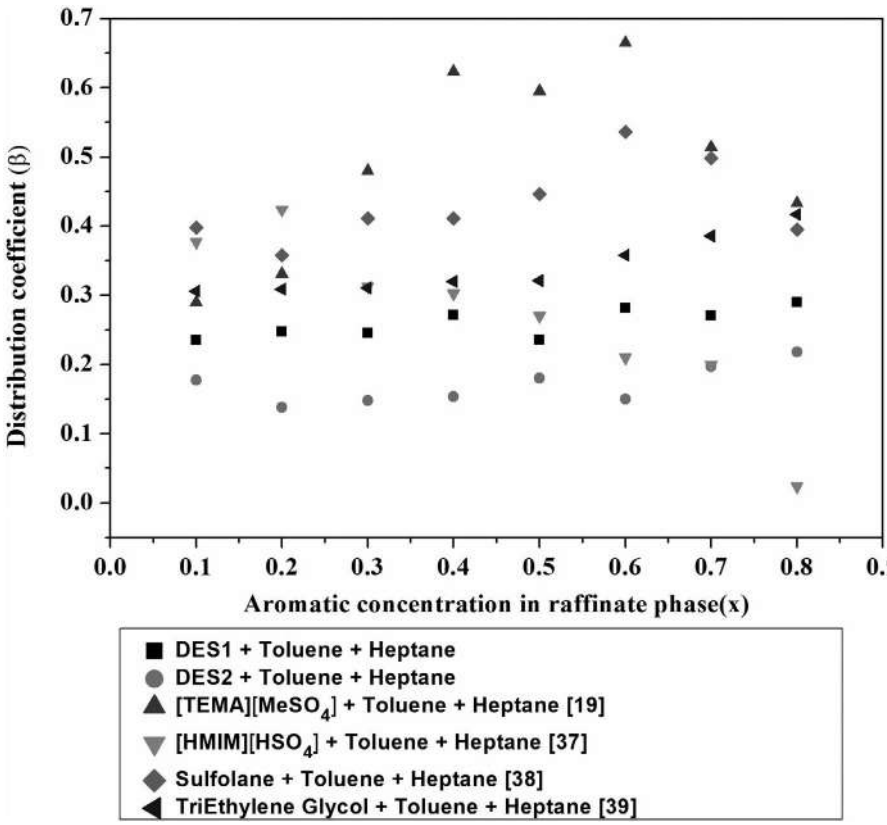

FIGURE 2.3 Distribution coefficient and comparison with existing solvents.

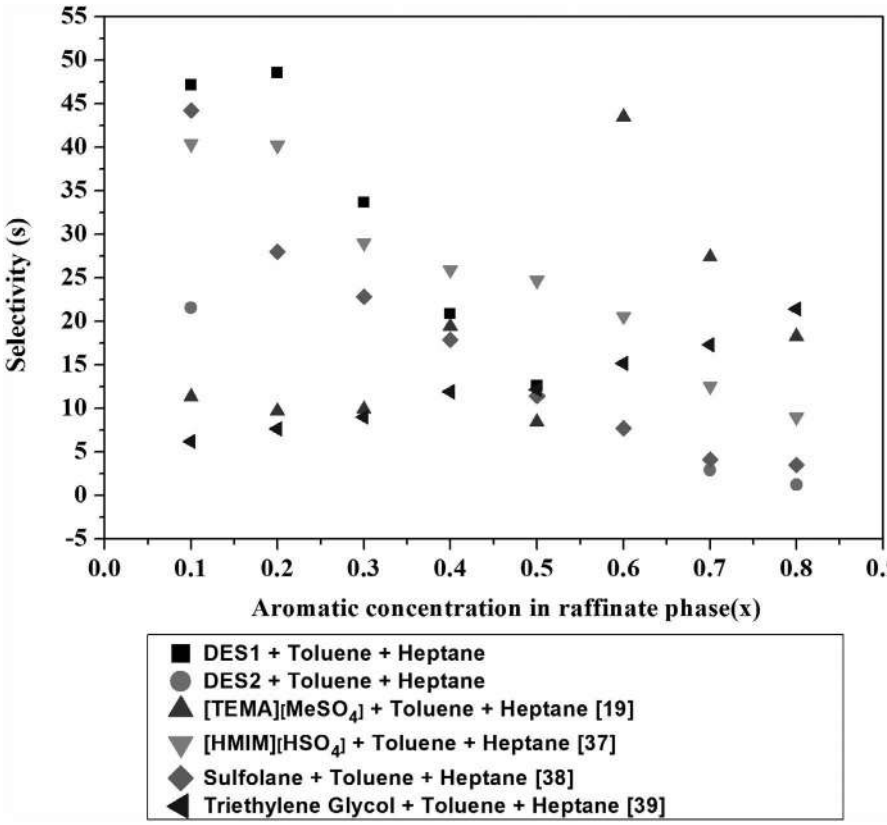

FIGURE 2.4 Selectivity and comparison with existing solvents.

in the raffinate phase. For example, at a lower concentration of toluene, DES1 may be preferred, while DES2 emerges as the recommended solvent at a high concentration. Due to an absence of LLE data for quinoline, a similar comparison could not be performed. For DES1 + toluene + heptane (Table 2.1), the solubility of heptane in DES1 is negligible. The solute distribution coefficient (β) values are less than unity and increase gradually. The DES concentration here is nearly zero in the upper raffinate layer or the hydrocarbon rich phase. The distribution coefficient and selectivity values were found to range from 0.23–0.29, and selectivity from 48.5–12.6, respectively. Thus, with an increase in the concentration of toluene in the feed, the deviation in β and S are contrary in nature. Similarly, for DES2 + toluene + heptane (Table 2.2), β value ranges from 0.14–0.22, and the selectivity tends to decrease with toluene concentration. It is interesting to observe that among the reported ILs and sulfolane, both the DES possess a lower distribution coefficient (Figure 2.3). This fact is vindicated in the conventional process where sulfolane (developed by Shell and Universal Oil Products (UOP)) is the most employed technology to extract aromatics at an industrial scale. However, the recovery cost of the sulfolane process is quite

high. This is inherently due to two reasons: a high boiling point of sulfolane (280°C) and the high solubility of sulfolane in the raffinate stream. Hence, DES may be recommended for the recovery of toluene albeit with a lower selectivity (Figure 2.4). This also follows a similar trend as observed by previous authors [43–46], where β and S were found to decrease with an increase in aromatic feed concentration.

TABLE 2.1
Experimental tie-line data with selectivity (S) and distribution ratio (β) for DES1 + toluene + heptane at T = 308.15 K and atmospheric pressure[a]

Extract phase			Raffinate phase				Selectivity
x_{DES}	x_{tol}	x_{hep}	x_{DES}	x_{tol}	x_{hep}	β_{tol}	(S)
0.996	0.000	0.004	0.000	0.000	1.000	∞	∞
0.962	0.034	0.004	0.000	0.143	0.857	0.23	47.1
0.931	0.065	0.004	0.000	0.264	0.736	0.25	48.5
0.899	0.097	0.004	0.000	0.394	0.606	0.24	33.6
0.851	0.143	0.006	0.000	0.526	0.474	0.27	20.8
0.845	0.148	0.007	0.000	0.628	0.372	0.24	12.6
0.802	0.198	0.000	0.000	0.703	0.297	0.28	∞
0.786	0.214	0.000	0.000	0.792	0.208	0.27	∞
0.747	0.253	0.000	0.000	0.875	0.125	0.29	∞
0.654	0.346	0.000	0.000	1.000	0.000	∞	∞

[a] Standard uncertainties u are u(T) = 0.01 K, u(x) = 0.001.

TABLE 2.2
Experimental tie-line data with selectivity (S) and distribution ratio (β) for DES2 + toluene + heptane at T = 308.15 K and atmospheric pressure[a]

Extract phase			Raffinate phase				Selectivity
x_{DES}	x_{tol}	x_{hep}	x_{DES}	x_{tol}	x_{hep}	β_{tol}	(S)
0.998	0.000	0.002	0.000	0.000	1.000	∞	∞
0.968	0.025	0.007	0.000	0.142	0.858	0.18	21.6
0.960	0.040	0.000	0.000	0.293	0.708	0.14	∞
0.940	0.060	0.000	0.000	0.407	0.593	0.15	∞
0.919	0.081	0.000	0.000	0.530	0.470	0.15	∞
0.884	0.116	0.000	0.000	0.644	0.356	0.18	∞
0.890	0.110	0.000	0.000	0.729	0.271	0.15	∞
0.828	0.159	0.013	0.000	0.806	0.194	0.19	2.9
0.786	0.192	0.021	0.000	0.883	0.117	0.22	1.2
0.745	0.255	0.000	0.000	1.000	0.000	∞	∞

[a] Standard uncertainties u are u(T) = 0.01 K, u(x) = 0.001.

TABLE 2.3
Experimental Tie-Line Data with Selectivity (*S*) and Distribution Ratio (β) for DES1 + Quinoline + Heptane at *T* = 308.15 K and Atmospheric Pressure[a]

Extract phase			Raffinate phase				Selectivity
x_{DES}	x_{qui}	x_{hep}	x_{DES}	x_{qui}	x_{hep}	β_{qui}	(*S*)
0.996	0.000	0.004	0.000	0.000	1.000	∞	∞
0.808	0.170	0.022	0.000	0.005	0.995	35.27	1592.3
0.698	0.295	0.007	0.000	0.013	0.987	23.13	3204.7
0.561	0.434	0.005	0.000	0.024	0.976	17.95	3344.2
0.446	0.542	0.012	0.000	0.035	0.965	15.63	1260.3
0.354	0.638	0.008	0.000	0.062	0.938	10.32	1298.2
0.290	0.699	0.011	0.000	0.097	0.903	7.22	583.2
0.184	0.797	0.019	0.000	0.123	0.877	6.46	293.5
0.115	0.850	0.036	0.000	0.144	0.856	5.92	142.4

[a] Standard uncertainties *u* are *u*(T) = 0.01 K, *u*(x) = 0.001.

TABLE 2.4
Experimental Tie-Line Data with Selectivity (*S*) and Distribution Ratio (β) for DES2 + Quinoline + Heptane at *T* =308.15 K and Atmospheric Pressure[a]

Extract phase			Raffinate phase				Selectivity
x_{DES}	x_{qui}	x_{hep}	x_{DES}	x_{qui}	x_{hep}	β_{qui}	(*S*)
0.998	0.000	0.002	0.000	0.000	1.000	∞	∞
0.868	0.132	0.000	0.000	0.008	0.992	16.66	∞
0.690	0.311	0.000	0.000	0.019	0.981	16.48	∞
0.547	0.453	0.000	0.000	0.038	0.962	11.83	∞
0.433	0.568	0.000	0.000	0.041	0.959	13.91	∞
0.331	0.664	0.005	0.000	0.056	0.944	11.89	2246.5
0.253	0.744	0.004	0.000	0.068	0.932	10.90	2539.2
0.166	0.827	0.007	0.000	0.090	0.910	9.23	1201.1
0.106	0.879	0.015	0.000	0.112	0.888	7.83	463.5

[a] Standard uncertainties *u* are *u*(T) = 0.01K, *u*(x) = 0.001.

It is interesting to note that both the toluene systems (Figures 2.5–2.6) form a negative slope of the tie lines, which implies that toluene preferentially adheres to the raffinate phase or, in other words, depicts a low toluene extraction capacity. This agrees with the earlier work of Manohar et al. [47] in which they used an IL-based on a phosphonium cation, namely, tributyl methyl phosphonium methyl sulfate for the extraction of toluene. In their work, the distribution coefficient (β) values were

TABLE 2.5
Experimental Tie-Line Data with Selectivity (*S*) and Distribution Ratio (β) for DES1 + Indoline + Heptane at T = 308.15 K and Atmospheric Pressure[a]

Extract phase			Raffinate phase				Selectivity
x_{DES}	x_{ind}	x_{hep}	x_{DES}	X_{ind}	x_{hep}	β_{ind}	(*S*)
0.998	0.000	0.002	0.000	0.000	1.000	∞	∞
0.860	0.134	0.006	0.000	0.009	0.991	14.89	2459.15
0.698	0.296	0.006	0.000	0.016	0.984	18.50	3034.00
0.594	0.398	0.008	0.000	0.017	0.983	23.41	2876.72
0.476	0.514	0.010	0.000	0.024	0.976	21.42	2090.27
0.352	0.635	0.013	0.000	0.045	0.955	14.11	1036.62
0.270	0.712	0.018	0.000	0.067	0.933	10.63	550.83
0.197	0.777	0.026	0.000	0.096	0.904	8.09	281.41
0.128	0.829	0.043	0.000	0.143	0.857	5.80	115.54

[a] Standard uncertainties are u(T) = 0.01 K, u(x) = 0.001.

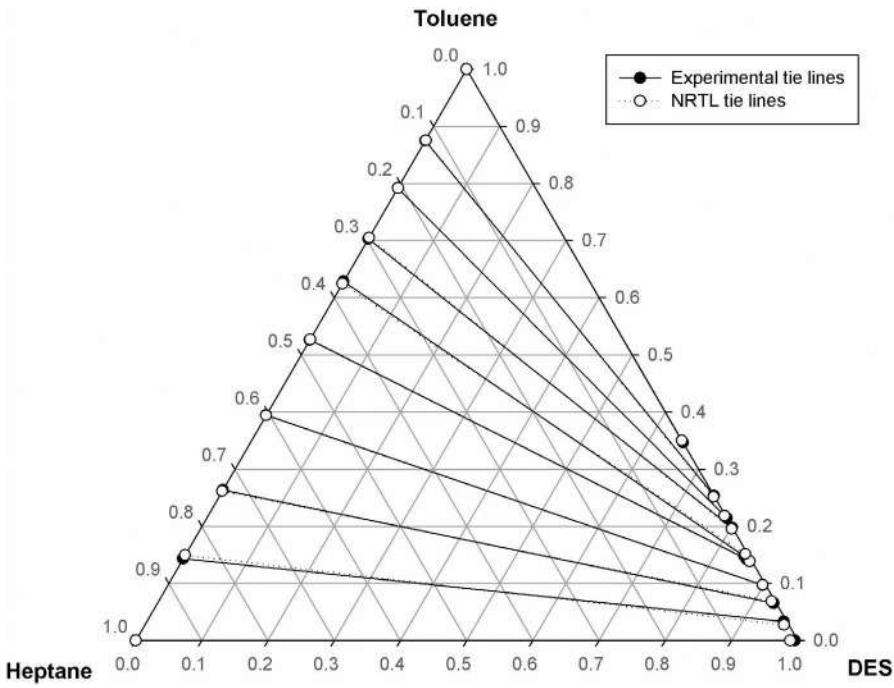

FIGURE 2.5 Experimental and NRTL tie lines for DES1 + toluene + heptane at T = 308.15 K and p = 1 bar.

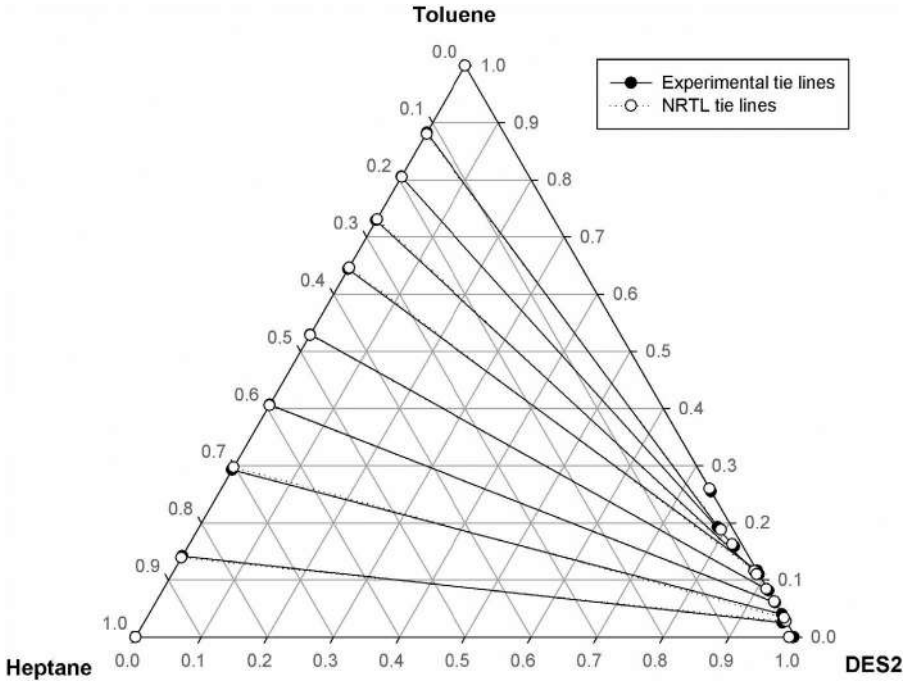

FIGURE 2.6 Experimental and NRTL tie lines for DES2 + toluene + heptane at $T = 308.15$ K and $p = 1$ bar.

found to be less than unity. Figures 2.7 and 2.8 represent the LLE for the removal of quinoline, a potential carcinogenic compound from DES1 and DES2, respectively. The distribution ratios for DES1 + quinoline + heptane (Table 2.3 and Figure 2.7) range from 35.27–9.92 and decrease with an increase in quinoline concentration in raffinate phase. A pretty large selectivity of 3344.2 is observed for a 30% concentration of quinoline. The selectivity values are also high for a low concentration of aromatic feed and decrease with an increase in quinoline concentration. In a similar trend for DES2 + quinoline + heptane (Table 2.4 and Figure 2.8), β values decrease from 16.66–7.83. The selectivity values were found to be much higher than those of toluene (Figures 2.5 and 2.6). It is also very evident that the slope of the tie lines for toluene and quinoline are opposite in nature. While toluene has a preferential solubility in the hydrocarbon phase, quinoline appears to diffuse in the extract (DES)-phase rich. Hence, the selectivity of the toluene + heptane system (Tables 2.1–2.2) is lower than in the quinoline + heptane system (Tables 2.3–2.4). From the phase equilibrium data, it is clear that the extraction of quinoline is much easy and effectively done as compared to toluene using phosphonium-based DES. Further, the β values are less than unity in toluene, implying a higher amount of DES.

Figures 2.5–2.9 corresponds to a type two diagram [48]. For example, in Figure 2.5, the binary, namely, heptane–DES1, exhibits immiscibility while the

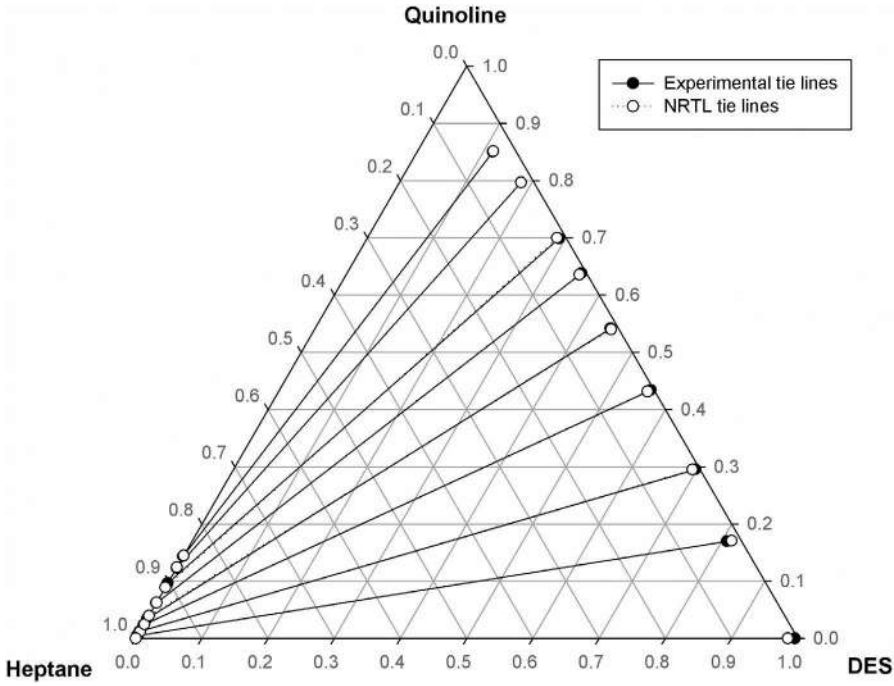

FIGURE 2.7 Experimental and NRTL tie lines for DES1 + quinoline + heptane at $T = 308.15$ K and $p = 1$ bar.

binary system such as heptane–quinoline and quinoline–DES1 are completely miscible. The binary solubility of heptane–DES1 is further confirmed from the LLE plot as evident in Table 2.1. We did not observe any plait point, and the tie lines near the edge of the graph are nearly parallel with the sides of the triangle. Finally, the ternary system DES1 + indoline + heptane also gave large values of the distribution coefficient (23.41–5.8) and selectivity (3034.0–115.54; Table 2.5 and Figure 2.9). These obtained values were very close to DES1 + quinoline + heptane system.

The variation of the HBD, namely, glycerol and ethylene glycol, did not alter the selectivity by a large magnitude. However, from Tables 2.3–2.4, it is clear that the distribution coefficient and selectivity value are higher for DES1 compared to DES2. Thus, it is evident that it is the inorganic salt that controls the extraction. In order to study the effect of the phosphonium salt, we have performed the LLE experiments using ethylene glycol as the solvent for the extraction of both toluene and quinoline. The choice of ethylene glycol is due to the fact that DES1 (Table 2.3) has proved to be better a solvent in terms of selectivity as compared to DES2 (Table 2.4). In order to compare the predictions with DES1, four aromatic feed points with compositions of 10%, 30%, 50%, and 70% (of toluene or quinolone) were prepared. LLE data for the two systems, namely, heptane + toluene + ethylene glycol and heptane + quinoline + ethylene glycol, were reported in Tables 2.6 and 2.7, respectively. Both the systems

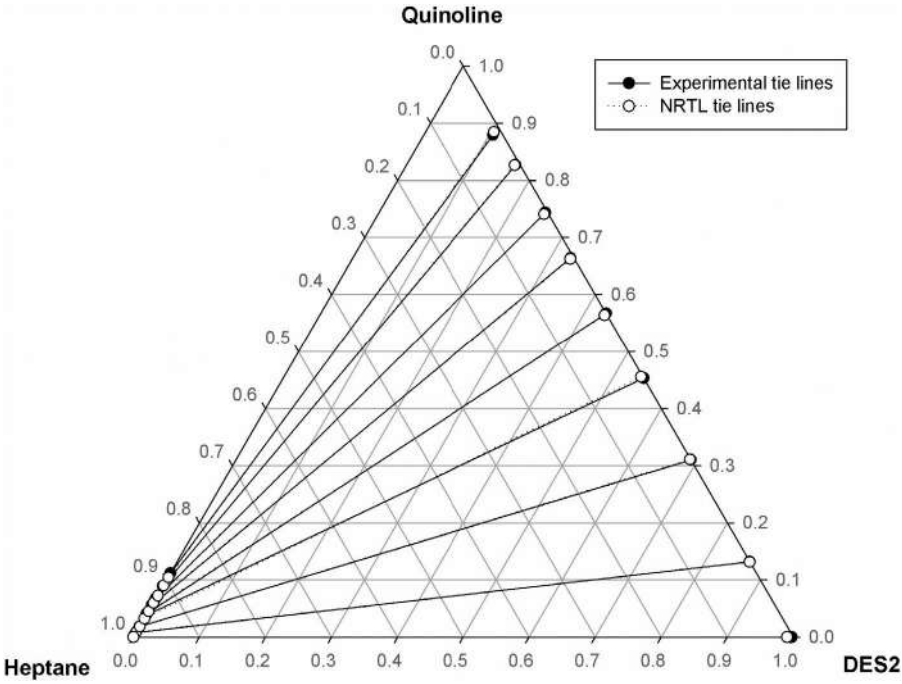

FIGURE 2.8 Experimental and NRTL tie lines for DES2 + quinoline + heptane at $T = 308.15$ K and $p = 1$ bar.

were found to have lower selectivity with ethylene glycol compared to DES. The increase in selectivity is more pronounced for quinoline (Table 2.6). In both cases, it is seen that the distribution coefficients are lower than that of pure DES (Table 2.7). The ternary diagrams are also plotted in Figures 2.10 and 2.11, respectively. Overall, the presence of bromide salt in the mixture influences the extraction procedure due to its phenyl ring. Hence the direct utilization of the mixture of the solvent namely ethylene glycol with the bromide salt is justified and can provide pathways for several other solvent formulations. In such a scenario, the quantum chemical–based COSMO-RS model or molecular dynamics simulations may provide further insights into this phenomenon.

Nevertheless, DES1, with lower number of –OH groups (ethylene glycol), reduces the intramolecular hydrogen bonding between the DES1 molecules compared to glycerol. This is due to the fact that the hydrogen bond allows the incoming quinoline molecules to be entrapped. This is possible as the interaction of DES with quinoline molecule is strong when compared to toluene. Due to this reason, the extraction with DES1 or DES2 is more preferential toward quinoline. An important observation lies in the fact that, unlike the traditional solvent sulfolane, DES is totally immiscible with the heptane-rich layer. Thus, for the separation of aromatic and aliphatic hydrocarbon, DES is a recommended solvent. Thus, in summary, we did not observe

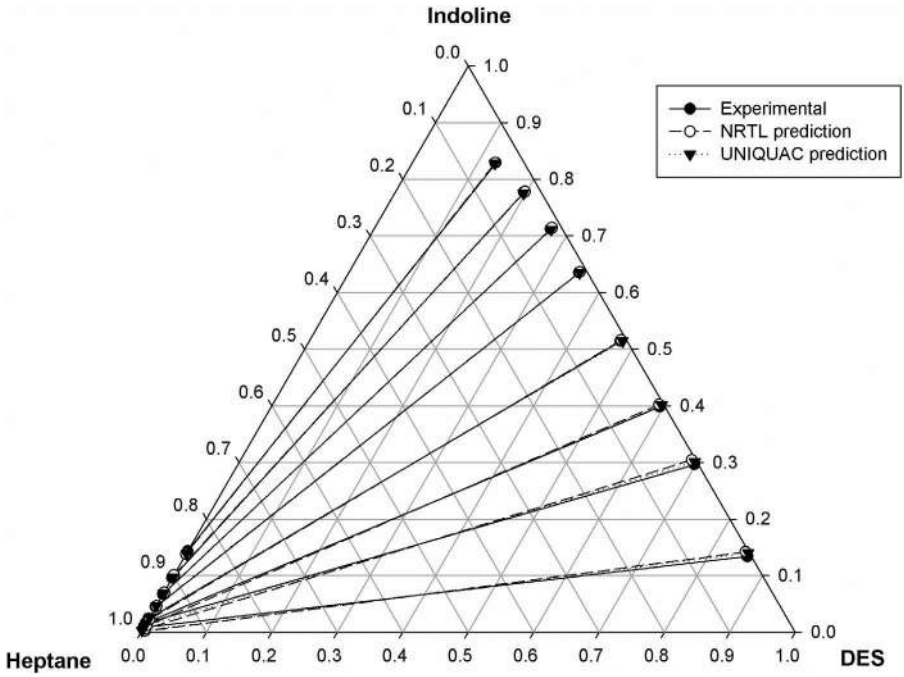

FIGURE 2.9 Experimental tie lines with NRTL and UNIQUAC model predictions for DES1 + indoline + heptane at $T = 308.15$ K and $p = 1$ bar.

TABLE 2.6
Experimental Tie Lines with Selectivity (S) and Distribution Ratio (β) for Ethylene Glycol + Toluene + Heptane at $T = 308.15$ K and Atmospheric Pressure[a]

Extract phase			Raffinate phase				Selectivity	Selectivity
x_{eg}	x_{tol}	x_{hep}	x_{eg}	x_{tol}	x_{hep}	β_{tol}	(S_{eg})	(S_{DES})
0.995	0.000	0.005	0.000	0.000	1.000	–	–	–
0.982	0.015	0.003	0.000	0.176	0.824	0.080	23.4	47.1
0.979	0.019	0.002	0.000	0.447	0.553	0.043	11.8	33.6
0.977	0.022	0.001	0.000	0.648	0.352	0.034	11.9	12.6
0.962	0.037	0.001	0.000	0.855	0.145	0.043	6.3	∞
0.945	0.055	0.000	0.000	1.000	0.000	–	–	–

[a] Standard uncertainties u are $u(T) = 0.01$ K, $u(x) = 0.001$.

any solvent loss as we did not notice any prominent peak resembling DES solvent in the raffinate phase. After the ternary LLE measurements, we shall now provide its effect on the simultaneous removal, namely, of indoline and quinoline from the heptane-rich phase using the same set of DES. This is attempted in the next section.

TABLE 2.7
Experimental Tie Lines with Selectivity (*S*) and Distribution Ratio (β) for Ethylene Glycol + Quinoline + Heptane at *T* = 308.15 K and Atmospheric Pressure[a]

Extract phase			Raffinate phase				Selectivity	Selectivity
x_{eg}	x_{qui}	x_{hep}	x_{eg}	x_{tol}	x_{hep}	β_{tol}	(S_{eg})	(S_{DES})
0.997	0.000	0.003	0.000	0.000	1.000	–	–	–
0.845	0.151	0.004	0.000	0.030	0.970	5.040	1100.5	1592.3
0.588	0.388	0.024	0.000	0.066	0.934	5.848	230.3	3344.2
0.355	0.578	0.067	0.000	0.112	0.888	5.171	68.39	1298.2
0.178	0.704	0.119	0.000	0.150	0.850	4.703	33.73	293.5

[a] Standard uncertainties *u* are *u*(T) = 0.01 K, *u*(x) = 0.001.

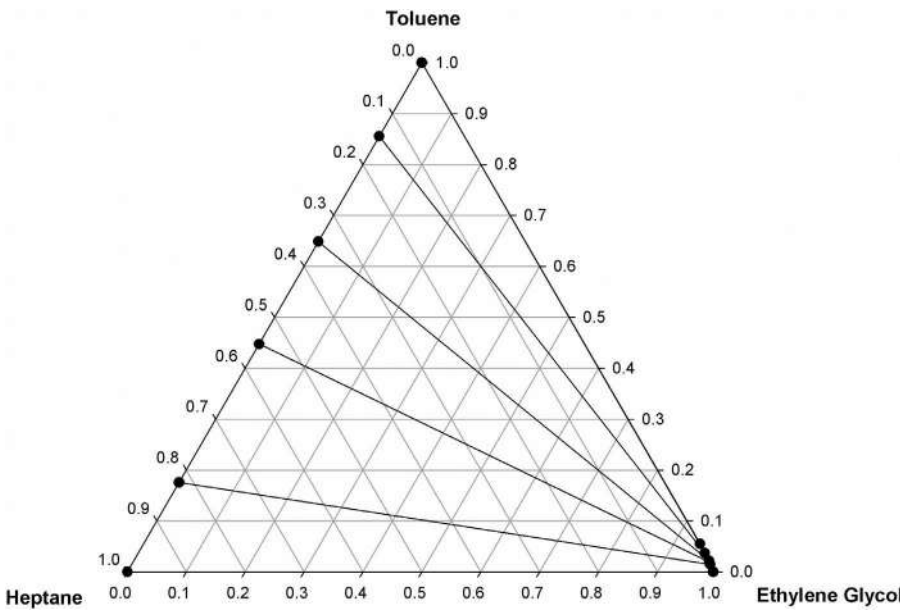

FIGURE 2.10 Experimental tie lines for ethylene glycol + toluene + heptane at *T* = 308.15 K and *p* = 1 bar.

Again, LLE data of three experimental systems consisting of DES1 + benzene + decane, DES1 + benzene + dodecane, and DES1 + benzene + hexadecane were studied at 298.15 K and 0.1 MPa. The experimental LLE data are plotted through a triangular phase diagram for each system in Figures 2.12–2.14. The numerical values of experimentally obtained tie-lines data of the equilibrium composition are given in Tables 2.8–2.10 for the solvent-to-feed ratios of 1:1. Based on the calculated LLE composition data, it is found that the concentrations of decane, dodecane, and

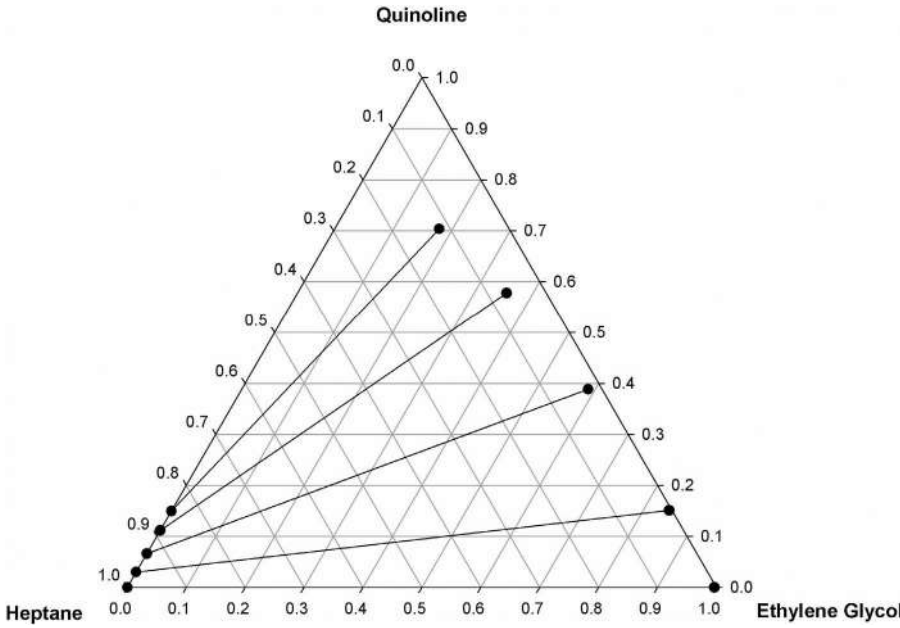

FIGURE 2.11 Experimental tie lines for ethylene glycol + quinoline + heptane at $T = 308.15$ K and $p = 1$ bar.

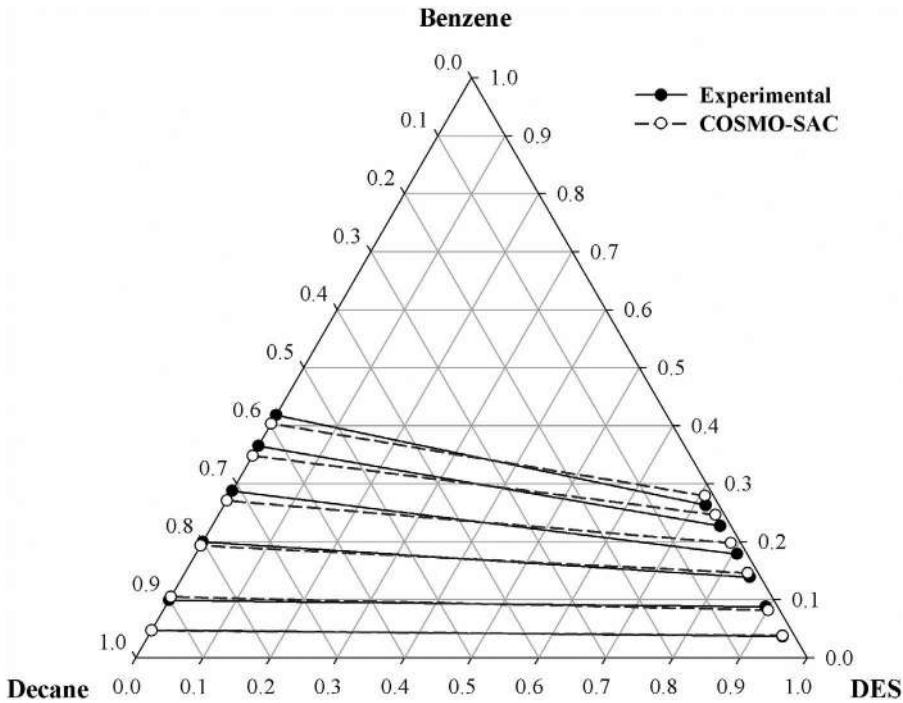

FIGURE 2.12 Experimental tie lines and COSMO-SAC model predictions for DES1 + benzene + decane at $T = 298.15$ K and $p = 1$ bar.

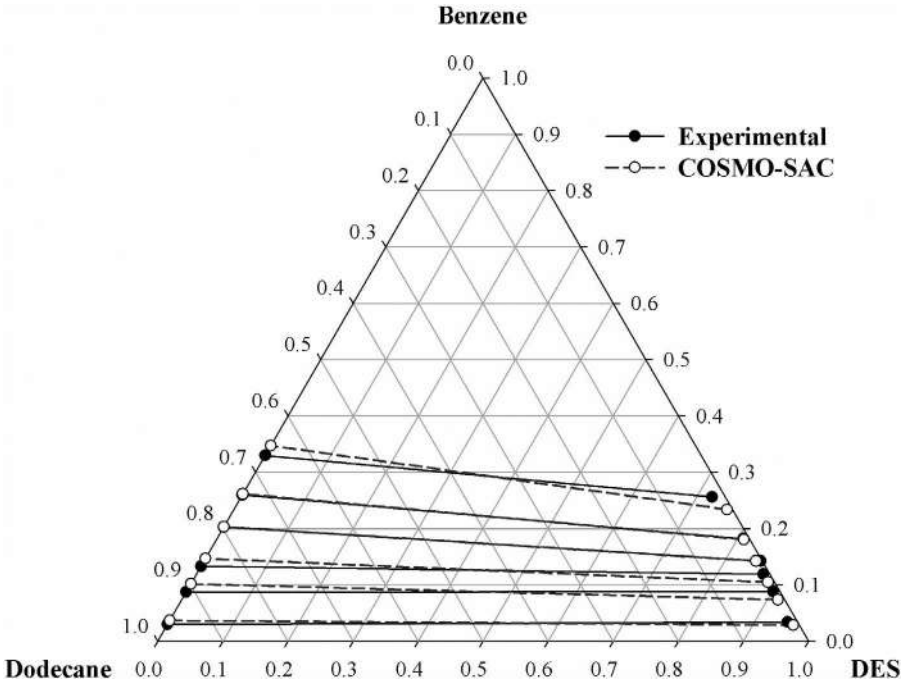

FIGURE 2.13 Experimental tie lines and COSMO-SAC model predictions for DES1 + benzene + dodecane at $T = 298.15$ K and $p = 1$ bar.

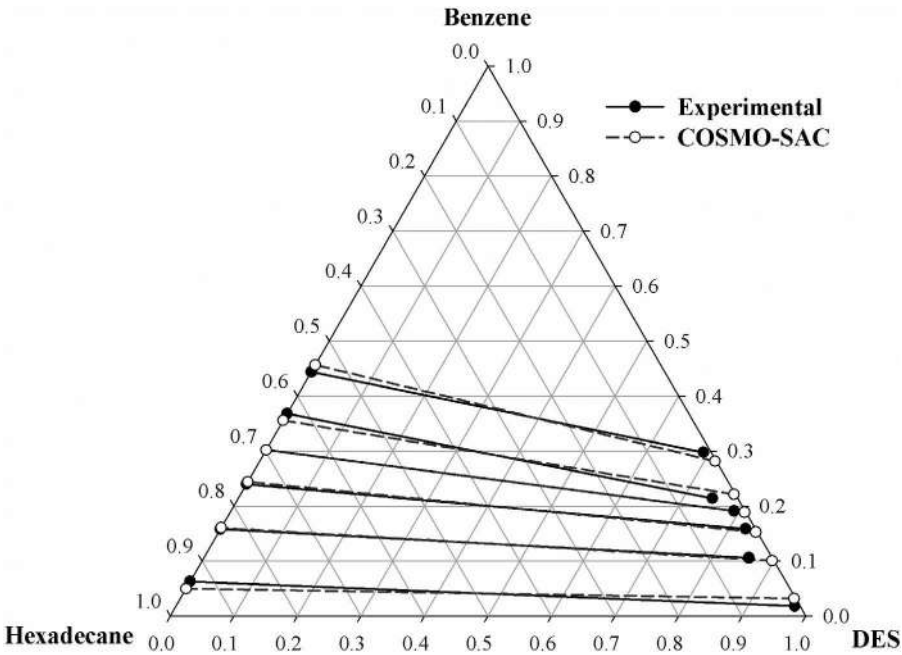

FIGURE 2.14 Experimental tie lines and COSMO-SAC model predictions for DES1 + benzene + hexadecane at $T = 298.15$ K and $p = 1$ bar.

TABLE 2.8
Experimental Tie Lines with Selectivity (*S*) and Distribution Ratio (β) for DES1 + Benzene + Decane at *T* = 298.15 K and Atmospheric Pressure[a]

Extract phase			Raffinate phase				Selectivity
x_{DES}	x_{ben}	x_{dec}	x_{DES}	x_{ben}	x_{dec}	β_{ben}	(*S*)
0.944	0.053	0.008	0.000	0.048	0.953	1.12	129.9
0.891	0.099	0.010	0.000	0.099	0.901	1.00	94.0
0.845	0.139	0.016	0.000	0.180	0.821	0.77	39.7
0.806	0.179	0.015	0.000	0.288	0.713	0.62	29.8
0.757	0.227	0.016	0.000	0.365	0.635	0.62	25.0
0.718	0.263	0.019	0.000	0.418	0.582	0.63	18.8

[a] Standard uncertainties *u* are *u*(T) = 0.01 K, *u*(x) = 0.001.

TABLE 2.9
Experimental Tie Lines with Selectivity (*S*) and Distribution Ratio (β) for DES1 + Benzene + Dodecane at *T* = 298.15 K and Atmospheric Pressure[a]

Extract phase			Raffinate phase				Selectivity
x_{DES}	x_{ben}	x_{dodec}	x_{DES}	x_{ben}	x_{dodec}	β_{ben}	(*S*)
0.961	0.034	0.005	0.000	0.030	0.970	1.23	218.47
0.901	0.089	0.010	0.000	0.087	0.913	1.02	91.00
0.861	0.119	0.020	0.000	0.133	0.867	0.89	38.92
0.835	0.142	0.022	0.000	0.203	0.797	0.70	25.08
0.789	0.182	0.029	0.000	0.260	0.740	0.70	18.01
0.724	0.256	0.020	0.000	0.330	0.670	0.78	26.11

[a] Standard uncertainties *u* are *u*(T) = 0.01 K, *u*(x) = 0.001.

hexadecane in the extract phase for all three ternary systems are less. It gave an insignificant amount of *model diesel compounds* in the extract phases and the non-appearance of DES1 compound in the raffinate phases, which specify negligible cross-contamination between the extract and raffinate phases [49]. This is highly favorable for solvent recovery using the LLE process. It should be mentioned that the results obtained from ^{1}H NMR showed a distinctive peak for each impurity in both the DES-rich phase and *n*-alkane-rich phase, and no new peaks were detected.

It can be recognized that the usage of DES for benzene extraction is reasonable for model diesel fuel as it requires a smaller amount of solvent-to-feed ratio, which, in turn, gives higher values for selectivity and distribution coefficients. The main reason for a significant extraction was the higher solubility of benzene in DES as compared to aliphatic hydrocarbons. Higher solubility behavior can be explained by

TABLE 2.10
Experimental Tie Lines with Selectivity (*S*) and Distribution Ratio (β) for DES1 + Benzene + Hexadecane at T = 298.15 K and Atmospheric Pressure[a]

Extract phase			Raffinate phase				Selectivity
x_{DES}	x_{ben}	$x_{hexadec}$	x_{DES}	x_{ben}	$x_{hexadec}$	β_{ben}	(*S*)
0.921	0.071	0.008	0.000	0.033	0.967	2.16	261.16
0.848	0.141	0.011	0.000	0.108	0.892	1.30	105.72
0.811	0.169	0.020	0.000	0.240	0.760	0.70	26.70
0.778	0.191	0.031	0.000	0.302	0.698	0.63	14.23
0.735	0.231	0.034	0.000	0.368	0.632	0.63	11.76
0.690	0.272	0.038	0.000	0.424	0.576	0.64	9.73

[a] Standard uncertainties u are u(T) = 0.01K, u(x) = 0.001.

considering the π-electron cloud around the benzene (due to the molecule's aromatic nature), due to which a strong electrostatic field is generated around the molecule. The presence of a strong π-electron cloud of benzene molecules induces the interactions within the phenyl and hydroxyl group of DES and, as a result, provides higher extraction efficiency.

On the other hand, no such π-electron cloud is available around the aliphatic hydrocarbon molecule; consequently, the aliphatic hydrocarbon–DES interactions are weaker than the benzene–DES interactions. It can be observed that increasing the initial concentration gradually decreases the extraction efficiency of benzene. For a single-stage extraction, the highest efficiencies were found for hexadecane followed by dodecane and decane. For all three benzene + DES1 systems, extraction efficiencies for the single stage were found to be in the range of 60–72%. It also shows DES as an effective extractant that follows the order of hexadecane > dodecane > decane for benzene extraction from model diesel components.

It can be observed that the selectivities of the DES1 + benzene system follow the order of hexadecane > dodecane > decane, and distribution coefficients were also found highest for the DES1 + benzene + hexadecane system. Both the distribution coefficients and selectivity values are higher when compared to ammonium-based DES and the conventional solvent, namely, sulfolane [50, 51]. Overall, the higher values of distribution coefficients and selectivity values of the DES1 can also be explained by strong noncovalent interaction through the COSMO-SAC model.

2.3.2 Quaternary Mixtures Involving DES–Aromatic (1)–Aromatic (2)–Aliphatic

The need for the study is due to the fact that a simultaneous recovery of both PAH (indoline or quinoline) and aromatic components (toluene) are desired from the fuel oil. Our earlier section reports the selection of DES1 [methyltriphenylphosphonium

bromide + ethylene glycol (1:4)] for the extraction of quinolone, indoline, benzene, and toluene from model fuel oil. The LLE of the three quaternary systems namely, DES + quinoline + indoline + heptane, DES + quinoline + toluene + heptane, and DES + indoline + toluene + heptane were studied at 308.15 K. The respective mole fractions along with their distribution coefficient (β) and selectivity (S) for quaternary systems are given in Tables 2.11–2.13. Table 2.14 summarizes the individual selection parameters (S and β) of the corresponding quaternary system. The corresponding pseudo-ternary plots for the quaternary system are represented in Figures 2.15–2.17.

TABLE 2.11
Experimental Tie-Line Data with Corresponding Distribution Coefficient (β) and Selectivity (S) for DES1 + Quinoline + Indoline + Heptane System at T = 308.15 K and Atmospheric Pressure

Sl No.	DES-rich phase					Heptane-rich phase					β	S
	x_1^I	x_2^I	x_3^I	x_4^I	x_{23}^I	x_1^{II}	x_2^{II}	x_3^{II}	x_4^{II}	x_{23}^{II}		
1	0.819	0.088	0.088	0.005	0.175	0.000	0.003	0.002	0.994	0.006	29.17	5798.33
2	0.748	0.119	0.125	0.008	0.244	0.000	0.006	0.005	0.989	0.011	22.18	2742.23
3	0.644	0.169	0.182	0.006	0.351	0.000	0.006	0.006	0.987	0.013	27.00	4441.50
4	0.578	0.201	0.214	0.007	0.415	0.000	0.008	0.009	0.983	0.017	24.41	3428.11
5	0.502	0.238	0.252	0.009	0.490	0.000	0.011	0.013	0.976	0.024	20.42	2214.07
6	0.428	0.272	0.288	0.012	0.560	0.000	0.020	0.022	0.957	0.043	13.02	1038.60
7	0.403	0.280	0.306	0.012	0.586	0.000	0.016	0.019	0.966	0.034	17.24	1387.44
8	0.371	0.296	0.321	0.013	0.617	0.000	0.019	0.022	0.959	0.041	15.05	1110.14

TABLE 2.12
Experimental Tie-Line Data with Corresponding Distribution Coefficient (β) and Selectivity (S) for DES1 + Quinoline + Toluene + Heptane System at T = 308.15 K and Atmospheric Pressure

Sl No.	DES-rich phase					Heptane-rich phase					β	S
	x_1^I	x_2^I	x_3^I	x_4^I	x_{23}^I	x_1^{II}	x_2^{II}	x_3^{II}	x_4^{II}	x_{23}^{II}		
1	0.927	0.062	0.006	0.005	0.068	0.000	0.005	0.028	0.967	0.033	2.06	398.52
2	0.858	0.120	0.015	0.007	0.135	0.000	0.003	0.047	0.950	0.050	2.70	366.43
3	0.755	0.207	0.030	0.008	0.237	0.000	0.006	0.087	0.907	0.093	2.55	288.92
4	0.720	0.242	0.034	0.004	0.277	0.000	0.014	0.129	0.857	0.143	1.94	415.02
5	0.647	0.297	0.052	0.004	0.349	0.000	0.016	0.169	0.815	0.185	1.89	384.37
6	0.579	0.347	0.070	0.004	0.416	0.000	0.030	0.231	0.739	0.261	1.59	294.47
7	0.611	0.333	0.052	0.004	0.385	0.000	0.028	0.197	0.775	0.225	1.71	331.53
8	0.549	0.379	0.067	0.005	0.446	0.000	0.040	0.249	0.711	0.289	1.54	219.45

TABLE 2.13
Experimental Tie-Line Data with Corresponding Distribution Coefficient (β) and Selectivity (S) for DES1 + Indoline + Toluene + Heptane System at T = 308.15 K and Atmospheric Pressure

Sl No.	DES-rich phase					Heptane-rich phase					β	S
	x_1^I	x_2^I	x_3^I	x_4^I	x_{23}^I	x_1^{II}	x_2^{II}	x_3^{II}	x_4^{II}	x_{23}^{II}		
1	0.904	0.078	0.012	0.007	0.090	0.000	0.003	0.026	0.971	0.029	3.10	430.49
2	0.844	0.127	0.021	0.007	0.148	0.000	0.007	0.045	0.948	0.052	2.85	385.45
3	0.747	0.210	0.037	0.006	0.247	0.000	0.011	0.090	0.899	0.101	2.45	366.42
4	0.671	0.269	0.053	0.007	0.322	0.000	0.015	0.136	0.849	0.151	2.13	258.64
5	0.623	0.309	0.061	0.007	0.370	0.000	0.024	0.162	0.815	0.185	2.00	232.86
6	0.592	0.330	0.071	0.006	0.401	0.000	0.028	0.186	0.786	0.214	1.87	245.47
7	0.558	0.356	0.081	0.005	0.437	0.000	0.036	0.218	0.746	0.254	1.72	256.69
8	0.519	0.381	0.094	0.006	0.475	0.000	0.035	0.255	0.710	0.290	1.64	193.82

TABLE 2.14
Individual Selection Parameters for All Three Quaternary LLE Systems

System-1*				System-2**				System-3***			
β_{qui}	β_{ind}	S_{qui}	S_{ind}	β_{qui}	β_{tol}	S_{qui}	S_{tol}	β_{ind}	β_{tol}	S_{ind}	S_{tol}
29.33	44.00	5831.47	8747.20	12.40	0.21	2398.16	41.44	26.00	0.46	3606.57	64.02
19.83	25.00	2451.90	3090.63	40.00	0.32	5428.57	43.31	18.14	0.47	2457.06	63.20
28.17	30.33	4633.42	4989.83	34.50	0.34	3911.44	39.09	19.09	0.41	2860.45	61.60
25.13	23.78	3528.27	3339.08	17.29	0.26	3703.46	56.47	17.93	0.39	2175.06	47.27
21.64	19.38	2346.34	2102.15	18.56	0.31	3782.11	62.69	12.88	0.38	1499.02	43.84
13.60	13.09	1084.60	1044.00	11.57	0.30	2136.94	55.98	11.79	0.38	1543.93	50.01
17.50	16.11	1408.75	1296.47	11.89	0.26	2304.24	51.14	9.89	0.37	1475.42	55.44
15.58	14.59	1149.25	1076.36	9.48	0.27	1347.35	38.26	10.89	0.37	1288.14	43.62

* DES1 + quinoline + indoline + heptane.
** DES1 + quinoline + toluene + heptane.
*** DES1 + indoline + toluene + heptane.

Figure 2.15–2.17 presents the correlation between experimental tie-lines data and local thermodynamic models (NRTL and UNIQUAC). For all the investigated systems, the concentration of heptane in the extract phase is almost negligible. It is also noteworthy to observe that the concentration of DES in the raffinate phase is zero. Therefore, it results in a favorable environment for the simultaneous extraction of PAHs since the interaction between DES and heptane are negligible. Hence, this phenomenon will make easier solvent recovery without additional heat. It was also

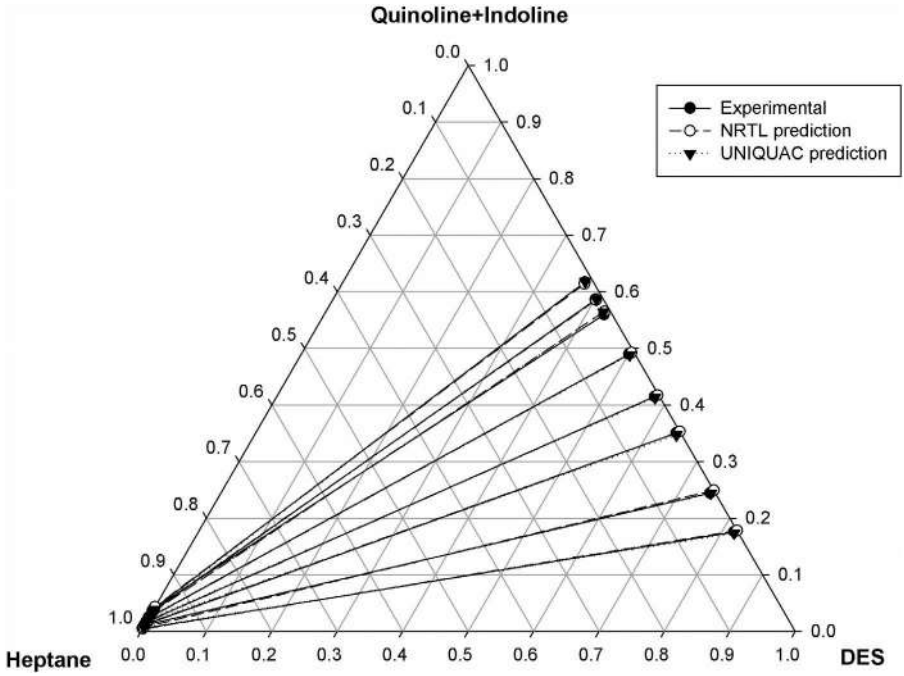

FIGURE 2.15 Pseudo-ternary LLE tie lines with NRTL and UNIQUAC model predictions for DES1 + quinoline + indoline + heptane at $T = 308.15$ K and atmospheric pressure.

confirmed from the NMR spectroscopy, where no trace amount of DES (absence of peaks) was present in the raffinate phase. The pseudo-ternary diagram indicates that the system exhibited type 2–phase behavior, implying that the DES is able to extract PAH very effectively from heptane.

The values of β and S are greater than unity for all LLE systems. The value of β decreases with an increase in the mole fraction of PAH in the raffinate phase. From Table 2.11, it is clearly showing the distribution coefficient of quinoline and indoline was seen to be decreased with increase in the solute concentration. It was also noticed that the pseudo component (PAH + toluene) has higher selectivity (Table 2.12–2.13) when compared to individuals. Similarly, the selectivity of the pure PAH (quinoline or indoline) was higher than that of a mixture of toluene and PAH. Therefore, the presence of toluene in a mixture leads to a decrease in the PAH extraction efficiency. On the other hand, the selectivity was much higher at a lower concentration of the PAH feed composition, which was beneficial as the amount of PAH in fuel oil is usually lower.

From the previous section, the slopes of tie lines were opposite in nature for quinoline and toluene in the case of ternary systems. But here, all the tie lines are positively sloped toward DES, which implies that the mixture of PAHs is efficiently and selectively extracted when compared to heptane or toluene. For higher values

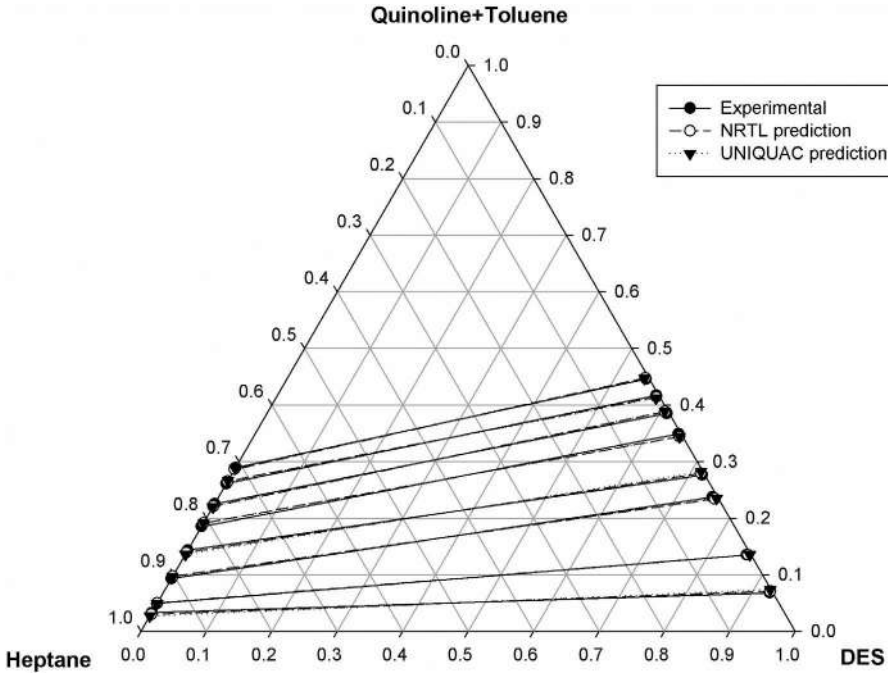

FIGURE 2.16 Pseudo-ternary LLE tie lines with NRTL and UNIQUAC model predictions for DES1 + quinoline + toluene + heptane at $T = 308.15$ K and atmospheric pressure.

of β (>1), lower amounts of DES were required. The PAH molecules were known to interact preferentially with DES molecules by π–π interaction [19]. From Tables 2.11–2.13, it was noticed that an increase in PAH concentration leads to decrease in the distribution coefficient and selectively. This is due to the fact that the cation has phenyl groups that are able to accommodate a smaller number of PAH molecules due to steric hindrance [20]. Further, the PAH molecule consists of an extra lone pair of electrons on the nitrogen, which makes the quinoline or indoline more electronegative and exerts a greater affinity toward DES cation. Thus, this results in higher hydrogen bonding interaction with the methyl group of the HBA and incoming PAH molecule. This is contrary to toluene, where due to the unavailability of the lone pair, the interaction decreases. Hence, the selection of the cationic species or HBA is critical in such an extraction. The ternary diagram shows a longer tie-line length in the immiscible region. This suggests that DES1 has a higher affinity for PAHs than does heptane or toluene.

The quaternary system of DES1 + quinoline + indoline + heptane (Table 2.11 and Figure 2.15) exhibited the highest value of distribution coefficient and selectivity among all the systems. The distribution coefficient was found in the range between 29.17 to 13.02 and selectivity from 5798.33 to 1038.6, respectively. Both values were found to decrease with increase in PAH concentration. For the system

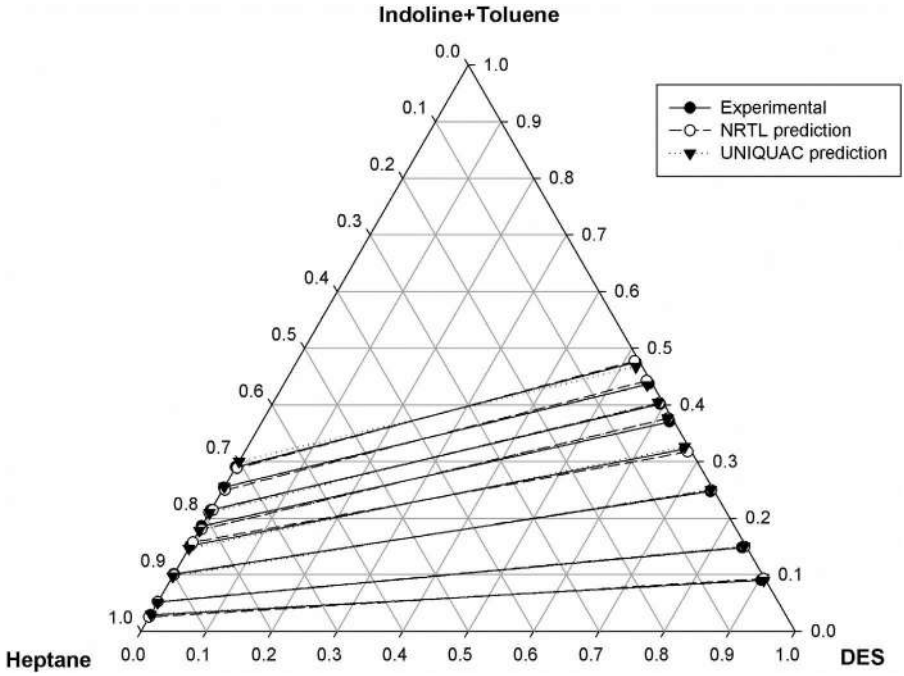

FIGURE 2.17 Pseudo-ternary LLE tie lines with NRTL and UNIQUAC model predictions for DES1 + indoline + toluene + heptane at $T = 308.15$ K and atmospheric pressure.

DES1 + quinoline + toluene + heptane (Table 2.12 and Figure 2.16), the distribution coefficient and selectivity were significantly lower than in other systems, here selectivity values ranging from 415.02 to 219.45 and distribution ratio values from 2.7 to 1.54. Similarly, the distribution coefficient for DES1 + indoline + toluene + heptane (Table 2.13 and Figure 2.17) ranges from 3.1 to 1.64, which was decreasing gradually with PAH concentration.

For comparing the efficiency of the DES, the selectivity (Figure 2.18) and distribution coefficients (Figure 2.19) of all the LLE systems were compared at 30% aromatic concentration as this is the limit where we obtain the highest selectivity. It was observed that the selectivity of quinoline and indoline in a simultaneous mode is much higher than that of toluene or heptane. Individually, both quinoline and indoline gave a higher selectivity than toluene. However, it may be noticed that irrespective of simultaneous or individual mode, the selectivity remains the same for both quinoline and indoline. With respect to the distribution coefficient, which is an indicator for solvent requirement, we observe a lower ratio for a simultaneous recovery.

2.4 THERMODYNAMICS MODELING

Even though DES is a mixture of two components, still it behaves as a single pseudo-solvent for LLE. This is consistent with the ratio of 1:4 (HBD:HBA) as

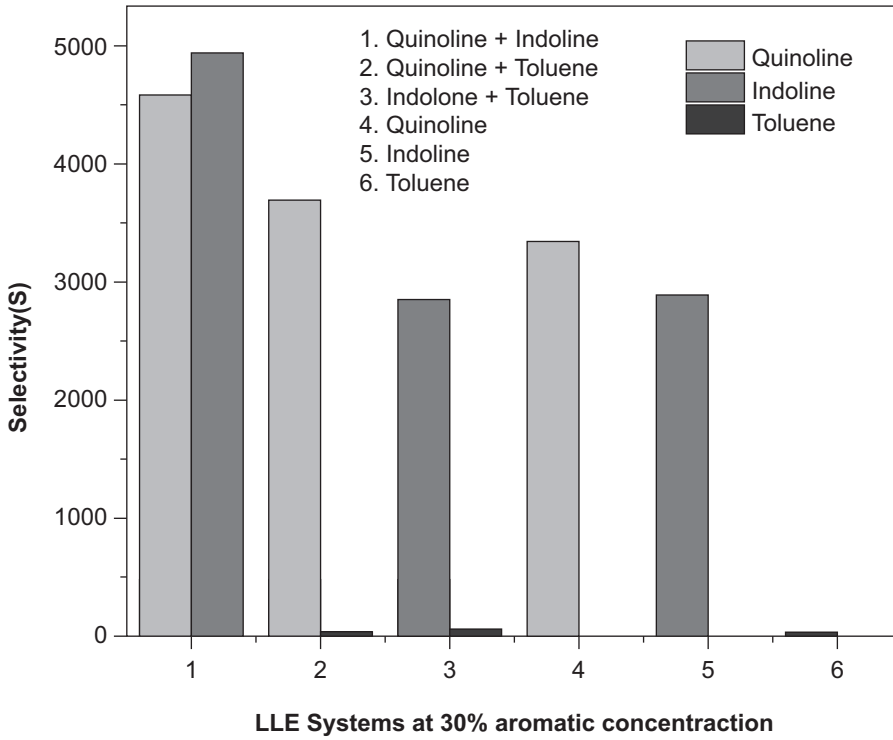

FIGURE 2.18 Selectivity (*S*) of all LLE system at 30 % aromatic concentration.

validated from the NMR spectra. One can observed a similar ratio in both the DES- and hydrocarbon-rich phases of the studied systems. Hence, DES is considered as a single pseudo-solvent in regression studies. The compositions in Tables 2.1–2.14 will merely change the mole fractions of MTBP and ethylene glycol or glycerol in the ratio of 1:4. This assumption is also in line with many authors [24, 52] who have studied DES for aromatic extraction where DES is considered as a single solvent in the NRTL [53] and UNIQUAC [54] models. The NRTL and UNIQUAC model regressions are usually performed using GA as they are highly nonlinear [55].

The nonideal mixture of liquids is quantified by the activity coefficient (γ) of the component. The results are then analyzed in terms of root mean square deviation (RMSD) value between experimental and model predictions. For the UNIQUAC model, the structural parameters r and q are predicted using the polarizable continuum model (PCM) via GEPOL algorithm [55]. The final output of the PCM calculation contains the cavity surface area (A^{pcm}) and the cavity volume (V^{pcm}) of the DES.

$$r = \frac{(V^{pcm}\text{Å}^3)(10^{-8}\,cm)^3 N_{av}}{V_{ws}} \tag{2 5}$$

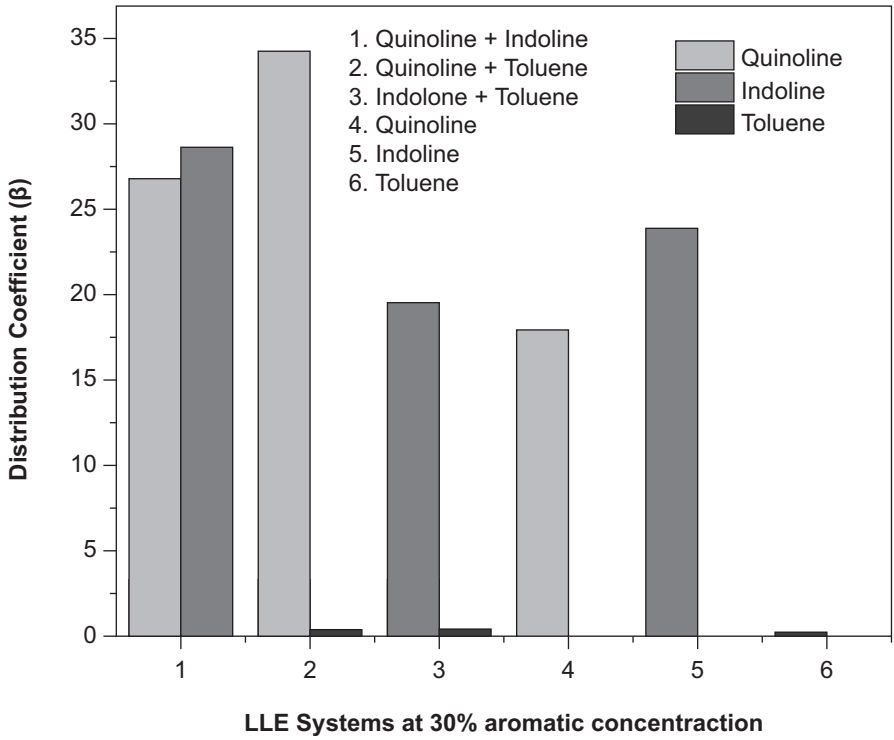

FIGURE 2.19 Distribution coefficient (β) of all LLE system at 30% aromatic concentration.

$$q = \frac{(A^{pcm}\mathring{A}^3)(10^{-8}cm)^2 N_{av}}{A_{ws}} \tag{2 6}$$

Here N_{av} is the Avogadro's number; V_{ws}, the standard segment volume (15.17 cm^3/mol); and A_{ws}, the standard segment area (2.5×10^9 cm^2/mol). The r and q values of DES1 and DES2 are calculated by Equations 2.5 and 2.6 respectively, by adding values of each component (salt and HBD) of DES.

To ascertain the validity of the tie lines, excess Gibb's free energy models such as NRTL and UNIQUAC models are applied to obtain the binary interaction parameters. These models are used to correlate the experimental LLE data of ternary and quaternary systems. The equation, being nonlinear in nature, needs to be regressed by a suitable optimization routine. The details of such as a calculation are given elsewhere [56]. The binary interaction parameter (τ_{ij}) is calculated from experimental data by minimizing the objective function (F) by using Genetic Algorithm (GA) program [56] which is given as

$$F_{\left(\begin{array}{c}\text{with respect to Aij}\\ \text{where } i,j=1,2,3\\ \text{and } j\neq i\end{array}\right)} = -\sum_{k=1}^{m}\sum_{l=I}^{II}\sum_{i=1}^{c}\left(x_{ik}^{l}-\hat{x}_{ik}^{l}\right)^2. \tag{2.7}$$

This is in fact a minimization even due to the presence of negative sign. This was necessitated due to the fact that the MATLAB GA toolbox tends to maximize a function. The population size, *npop* =100 and number of generations, *ngen* = 200 were used for the minimization of the total error in Equation 2.7 for the genetic algorithm (GA) program [43]. The compositions of the extract and raffinate phases are calculated using the standard Modified Rashford-Rice algorithm [57]. Here we have used $\alpha = 0.2$ as a nonrandomness factor for NRTL model.

The correlation between the experimental data with NRTL and UNIQUAC model tie-line data was measured with root mean square deviation (RMSD) as the possible fitness of the data, which is defined as

$$RMSD(in\%) = \left(-\frac{F}{2mc} \right)^{1/2} = \left[\sum_{k=1}^{m} \sum_{l=I}^{II} \sum_{i=1}^{c} \frac{\left(x_{ik}^{l} - \hat{x}_{ik}^{l} \right)^2}{2mc} \right]^{1/2} \times 100, \tag{2.8}$$

where m = number of tie lines and c = number of components. Here, x_{ik}^{l} and $\hat{x}_{ik}^{l}$ are experimental and predicted values of the mole fraction composition. The calculated binary interaction parameters of these NRTL and UNIQUAC models for various systems are given in Tables 2.15–2.16 along with their RMSD values. The deviation between experimental and model predictions as given in RMSD range from 0.28–0.31% and 0.22–0.73% for the NRTL and UNIQUAC models, respectively, for ternary systems. Similarly, the RMSD value of quaternary systems varies from 0.27–0.31% for NRTL and 0.19–0.35% for UNIQUAC model. The RMSD value, which is less than 1%, indicates that the thermodynamic models gave an excellent agreement between them. This can be visualized in Figures 2.5–2.17 where the tie lines are seen to overlap with each other. The lower and upper bounds for estimation of interaction parameters for all the systems were set in such a way that all parameters are lies within the same range.

2.5 CONTINUUM SOLVATION MODELS FOR SOLUTES IN PHASES

The extraction efficiency of DES can be described by comparing the σ-profiles interaction between benzene and aliphatic compounds with respect to the σ-profiles given by the COSMO-RS (Conductor-like Screening Model for Realistic Solvents) model as described in detail by Klamt [58]. Using updated COSMO-SAC (Segment Activity Coefficient)–based σ-profiles [59], the extraction mechanism for aromatic using DES from model diesel components can be explained and then corroborated to its high extraction efficiency. σ-profiles are the probability distribution of the screening charges in a specified compound. The prediction of the LLE tie lines from the experimental data was performed using the COSMO-SAC model. With Gaussian view [60], the chemical structures of HBA, HBD, and aromatic and aliphatic compounds were drawn. The molecular structure optimization of the compounds was then performed using the B3LYP level of theory and 6–31* basis set within Gaussian 09 [61]. After the optimization of geometry, the COSMO file was generated at the PBVP86 level of density functional theory[62] using the triple zeta valence potential

TABLE 2.15
NRTL Interaction Parameter for Ternary and Quaternary Systems

i-j	NRTL model parameters			
	τ_{ij}	τ_{ji}	*F**	*RMSD***
		DES1 + toluene + heptane		
1–2	19.52	19.811		
1–3	3.927	11.097	-3.76×10^{-4}	0.28
2–3	5.829	8.001		
		DES2 + toluene + heptane		
1–2	19.609	1.064		
1–3	17.678	15.926	-4.86×10^{-4}	0.31
2–3	6.309	5.531		
		DES1 + quinoline + heptane		
1–2	−1.590	1.811		
1–3	2.504	5.031	-4.51×10^{-4}	0.30
2–3	18.182	1.55		
		DES2 + quinoline + heptane		
1–2	5.024	3.971		
1–3	9.815	7.386	-4.3×10^{-4}	0.29
2–3	−2.594	0.678		
		DES1 + indoline + heptane		
1–2	−2.85	2.03		
1–3	3.69	3.40	-6.66×10^{-4}	0.37
2–3	15.71	1.38		
		DES1 + quinoline + indoline + heptane		
1–2	64.45	−78.66		
1–3	−9.29	8.86		
1–4	0.58	36.69	-4.8×10^{-4}	0.27
2–3	97.34	−72.09		
2–4	−7.84	3.55		
3–4	54.55	−3.88		
		DES1 + quinoline + toluene + heptane		
1–2	−35.81	16.31		
1–3	−34.56	−34.13		
1–4	28.91	38.29	-4.66×10^{-4}	0.27
2–3	11.37	7.01		
2–4	−66.93	−4.79		
3–4	3.39	99.38		
		DES1 + indoline + toluene + heptane		
1–2	−63.73	−60.68		
1–3	−51.89	−99.19		
1–4	25.26	83.96	-6.35×10^{-4}	0.31
2–3	−71.81	−39.42		
2–4	−89.16	−75.04		
3–4	3.65	−33.45		

* Equation 2.7
** Equation 2.8

TABLE 2.16
UNIQUAC Interaction Parameter for Ternary and Quaternary Systems

i-j	UNIQUAC model parameters			
	A_{ij}	A_{ji}	*F**	*RMSD***
		DES1 + toluene + heptane		
1–2	113.96	413.04		
1–3	391.99	−26.467	-1.02×10^{-3}	0.46
2–3	95.493	−229.66		
		DES2 + toluene + heptane		
1–2	200.51	−277.42		
1–3	238.68	243.43	-2.62×10^{-3}	0.73
2–3	−21.036	761.25		
		DES1 + quinoline + heptane		
1–2	−292.94	325.95		
1–3	341.37	−12.31	-1.27×10^{-3}	0.51
2–3	511.06	−52.266		
		DES2 + quinoline + heptane		
1–2	−225.48	279.73		
1–3	889.07	−72.157	-2.42×10^{-4}	0.22
2–3	323.25	2.6017		
		DES1 + indoline + heptane		
1–2	75.74	29.89		
1–3	503.16	8.75	-3.7×10^{-4}	0.28
2–3	−150.63	154.33		
		DES1 + quinoline + indoline + heptane		
1–2	−65.68	997.86		
1–3	−134.33	992.28		
1–4	384.97	144.91	-2.3×10^{-4}	0.19
2–3	666.53	−6.407		
2–4	70.99	131.98		
3–4	936.37	285.08		
		DES1 + quinoline + toluene + heptane		
1–2	−961.09	−211.45		
1–3	−112.19	−772.89		
1–4	437.3	843.97	-6.79×10^{-4}	0.32
2–3	−164.86	102.1		
2–4	−489.6	−754.59		
3–4	−62.33	−889.26		
		DES1 + indoline + toluene + heptane		
1–2	−10.91	500.02		
1–3	423.32	250.87		
1–4	421.74	765.38	-7.96×10^{-4}	0.35
2–3	915.99	34.71		
2–4	−17.92	579.91		
3–4	44.38	195.22		

*Equation 2.7
**Equation 2.8

(TZVP) basis set with the DGA1 [63] density fitting. COSMO calculation generates the sigma profiles, which comprise the surface screening charges of molecules. The screening charge (σ) for the molecules gives the sigma profile, which, in turn, computes the individual segment activity coefficient [64, 65]. The summation of the entire segment activity coefficient gives us the component activity coefficient in either phase. The details of the calculation and methodology are not discussed here as it is given the literature [55, 56].

For the sigma profile calculation of DES, a suitable feed ratio was inserted for both the HBD and HBA molecules. The charge distribution for such a DES was the algebraic sum of all the sigma profiles calculated separately [66]. It takes the form

$$p_{DES}(\sigma) = p_{HBA}(\sigma) + p_{HBD}(\sigma) = f_{HBA}\,p_{HBA}(\sigma) + f_{HBD}\,p_{HBD}(\sigma). \tag{2.9}$$

Here $p_{HBA}(\sigma)$ and $p_{HBD}(\sigma)$ are the sigma profiles of the constituent of DES. f_{HBA} and f_{HBD} are the mole ratios that have been adopted in the experimental work (i.e., 1:4). The σ-profiles of HBA and HBD are then normalized to obtain the sigma profile of the solvent. COSMO-SAC-predicted pseudo-ternary tie lines of LLE are estimated and matched with experimental calculated tie lines [67] with a modified Rachford Rice algorithm [57]. The equations and methodology can be obtained from the literature [68–70] and COSMO-SAC implementation [71]. COSMO-SAC data and experimental data of pseudo-ternary tie lines of LLE were compared [72] using RMSD given in Equation 2.8, in the previous section.

The first step of the COSMO calculation is to generate the sigma profiles of investigated compounds and is presented in Figure 2.23. The hydrogen-bonding contribution [64] is nonzero only if one segment has a negative charge density less than the cutoff value −0.0084 e/Å^2 and the other side has a positive charge density greater than 0.0084 e/Å^2. In this way, hydrogen bonding is limited to segment pairs of opposite charge and larger magnitudes. From Figure 2.23, it is clear that the σ-profile of the DES possesses a large fraction of peak toward the positive region indicating the possibility of hydrogen bonding with MTPB cation. Quinoline and indoline both display a symmetrical profile and have a higher fraction of charge both in the hydrogen bonding acceptor and donor region. This enables them to initiate hydrogen bonding with DES molecules. Furthermore, the complementary profiles [64, 65] of DES and PAH do indeed refer to excellent miscibility, which is magnified in the experimental tie-line data (Tables 2.15–2.17). It is interesting to note that toluene has a lower fraction of charge in the HBA or HBD region. Thus, toluene was less extracted as compared to PAH. Heptane being nonpolar in nature is resistant to hydrogen bonding due to its nonavailability of acceptor or donor groups.

Similarly, Figure 2.21 shows the σ-profiles of benzene and representative diesel components with DES used in this work. Model diesel components as decane, dodecane, and hexadecane σ-profiles are nonpolar but vary in magnitude because of the extra carbon atoms or methyl groups. The σ-profiles of DES and benzene overlap each other in the nonpolar region. The regions of the donor and acceptor are explained from the value of $\pm\sigma_{hb}$ = 0.0084 e/Å^2 as stated previously. The solubility of benzene is relatively much higher than n-alkane, which results in higher extraction efficiency of DES. This

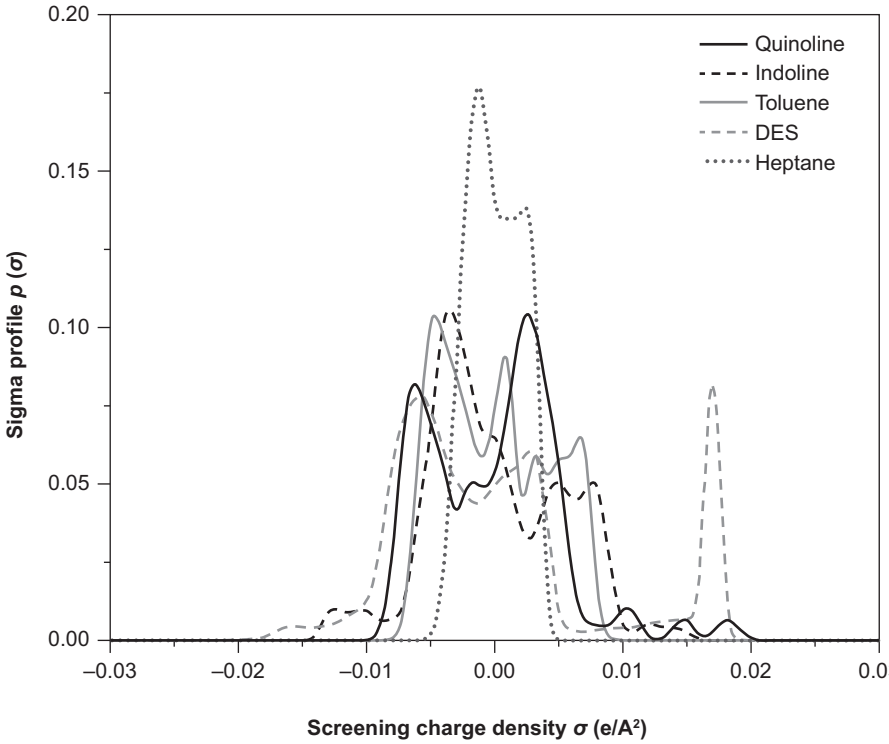

FIGURE 2.20 Normalized sigma profile comparison for different compounds

could be attributed to the presence of π-electrons around the benzene component, which is absent in the n-alkane compound. As a consequence, the DES has more ability as an HBA than an HBD. The σ-profiles also confirm this effect where a noncovalent interaction between DES and benzene ring is established by the overlapping sigma profiles (Figure 2.21). This also results in the enhancement of the electron-withdrawing potential of benzene, leading to an improvement in the density of the benzene ring electron and its associated electron density of the hydrogen nucleus. Therefore, it can be concluded that the noncovalent interaction formed between MTPB/EG and the π-electron cloud of benzene mainly accounts for the greater efficiency of benzene extraction.

Figures 2.22–2.24 show the pseudo-ternary diagram of the three quaternary systems validated with the COSMO-RS prediction along experimental tie lines along with their RMSD values. In the quinoline + indoline PAH mixture (Figure 2.20), the deviation between the COSMO-RS tie lines and experimental tie lines was shown to be higher. For other systems, the deviation was lower and had better agreement with experimental data. As evident from experimental data, the COSMO-RS model also predicts a negligible DES fraction in the raffinate phase. These values of RMSD indicate that COSMO-RS model is indeed consistent and can be used for the prediction of phase equilibria predictions. The detail equations for COSMO calculations are provided in Table A.2 of the appendix.

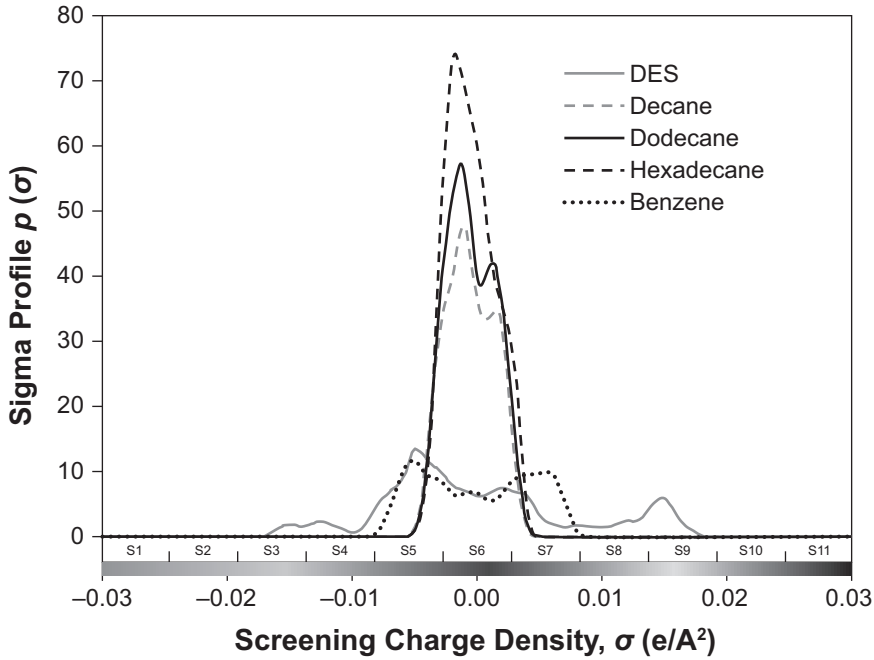

FIGURE 2.21 σ-profiles of DES and model diesel compounds using COSMO-SAC model.

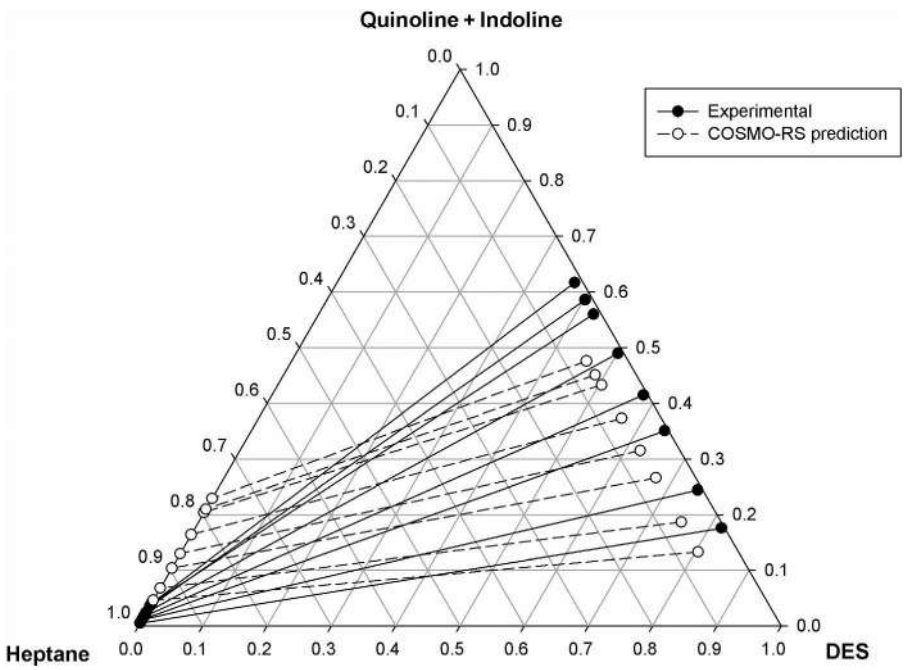

FIGURE 2.22 Pseudo-ternary LLE tie lines with COSMO-RS prediction for DES + quinoline + indoline + heptane at T = 308.15 K and atmospheric pressure.

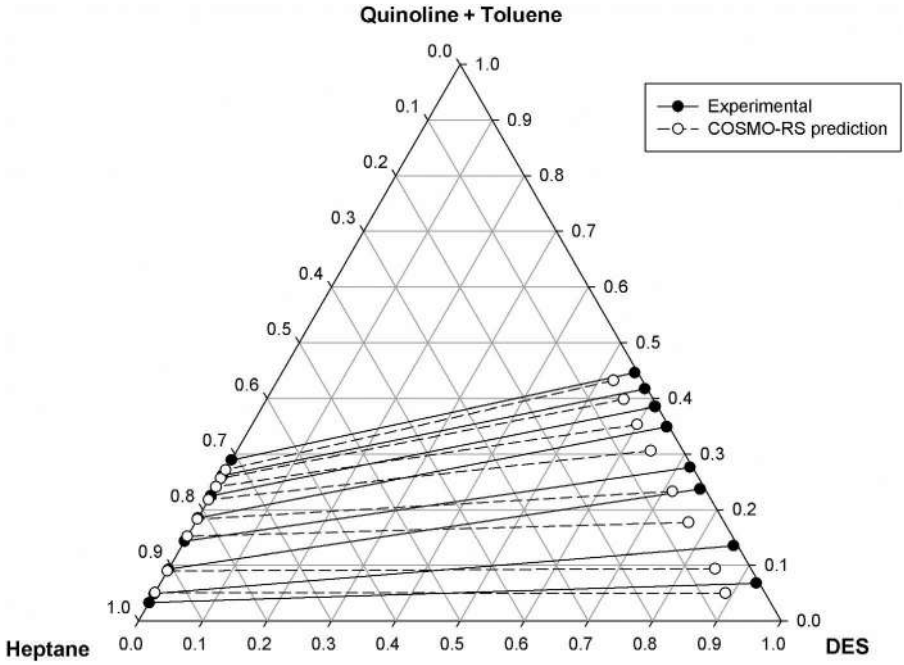

FIGURE 2.23 Pseudo-ternary LLE tie lines with COSMO-RS prediction for DES + quinoline + toluene + heptane at $T = 308.15$ K and atmospheric pressure.

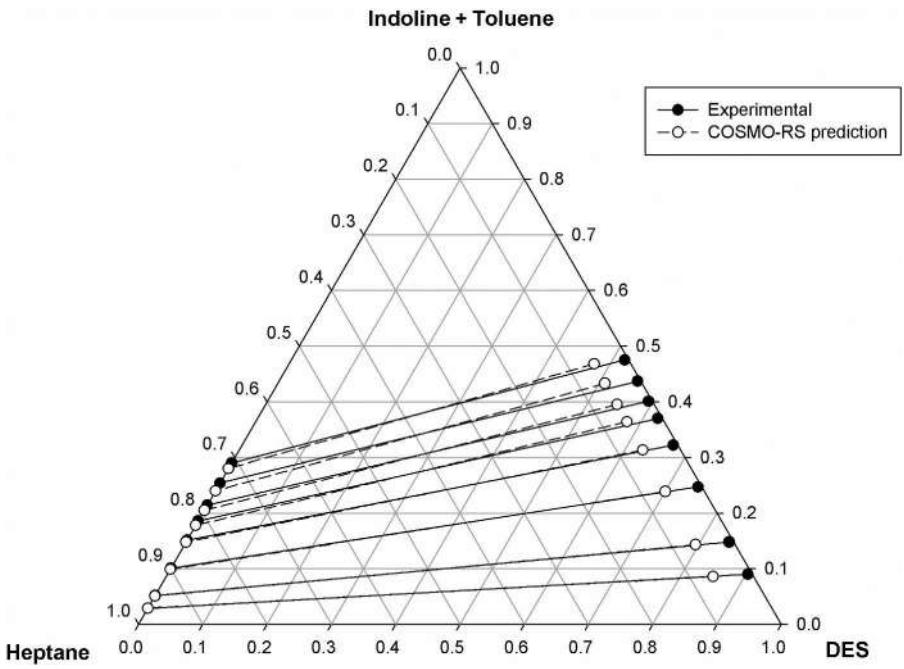

FIGURE 2.24 Pseudo-ternary LLE tie lines with COSMO-RS prediction for DES + indoline + indoline + heptane at $T = 308.15$ K and atmospheric pressure.

2.6 SUMMARY

Deep eutectic solvents with common salt (MTPB) along with hydrogen bond donors, namely, glycerol and ethylene glycol, were synthesized. LLE experiments were performed for the extraction of toluene and quinoline from heptane by employing DES as solvents at ambient conditions. The distribution coefficient and selectivity were found to be much higher for quinoline/indoline as compared to benzene/toluene. The selectivity and distribution coefficient values were found to be higher at a low concentration of the aromatic feed. NMR analysis shows absence of DES concentration in the raffinate phase. This indicates that the DES does not contaminate the hydrocarbon phase, thereby enabling the ease of solvent recycling. It was also observed that the concentration of DES in raffinate phase was zero. This will imply a smaller number of processing units or unit operations for solvent recovery. The experimental tie-line data were correlated with the three thermodynamic models (NRTL, UNIQUAC, COSMO) gave RMSD values less than unity, thereby giving an excellent agreement with the experimental data. The study reveals that the phosphonium-based DES can be used as a potential solvent for the selective removal of PAH from diesel oil.

REFERENCES

1. Jayaraman, A., F.H. Yang, and R.T. Yang, *Effects of nitrogen compounds and polyaromatic hydrocarbons on desulfurization of liquid fuels by adsorption via π-complexation with Cu (I) Y zeolite*. Energy & Fuels, 2006. **20**(3): p. 909–914.
2. Yongtan, Y., *Determination of nitrogen compounds in catalytic diesel oil using gas chromatography*. Chinese Journal of Chromatography, 2008. **26**(4): p. 478–483.
3. Macaud, M., et al., *Novel methodology toward deep desulfurization of diesel feed based on the selective elimination of nitrogen compounds*. Industrial & Engineering Chemistry Research, 2004. **43**(24): p. 7843–7849.
4. Meindersma, G.W. and A.B. De Haan, *Cyano-containing ionic liquids for the extraction of aromatic hydrocarbons from an aromatic/aliphatic mixture*. Science China Chemistry, 2012. **55**(8): p. 1488–1499.

5. Meindersma, G.W. and A.B. de Haan, *Conceptual process design for aromatic/aliphatic separation with ionic liquids*. Chemical Engineering Research and Design, 2008. **86**(7): p. 745–752.
6. Orr, W.L., *Sulfur in heavy oils, oil sands and oil shales*. Oil Sand and Oil Shale Chemistry, 1978: p. 223–243.
7. Zhang, S., Q. Zhang, and Z.C. Zhang, *Extractive desulfurization and denitrogenation of fuels using ionic liquids*. Industrial & Engineering Chemistry Research, 2004. **43**(2): p. 614–622.
8. Ali, S.H., et al., *Extraction of aromatics from naphtha reformate using propylene carbonate*. Fluid Phase Equilibria, 2003. **214**(1): p. 25–38.
9. González, E.J., et al., *(Liquid+ liquid) equilibria for ternary mixtures of (alkane+ benzene+ [EMpy][ESO 4]) at several temperatures and atmospheric pressure*. The Journal of Chemical Thermodynamics, 2009. **41**(11): p. 1215–1221.
10. Zhang, J., et al., *Extraction of aromatic hydrocarbons from aromatic/aliphatic mixtures using chloroaluminate room-temperature ionic liquids as extractants*. Energy & Fuels, 2007. **21**(3): p. 1724–1730.
11. Ghandi, K., *A review of ionic liquids, their limits and applications*. Green and sustainable chemistry, 2014. **2014**.
12. Hossain, M.A., et al., *Ionic liquids as benign solvents for the extraction of aromatics*. Bulletin of the Korean Chemical Society, 2012. **33**(10): p. 3241–3247.
13. Domínguez, I., E.J. Gonzalez, and Á. Domínguez, *Liquid extraction of aromatic/cyclic aliphatic hydrocarbon mixtures using ionic liquids as solvent: Literature review and new experimental LLE data*. Fuel Processing Technology, 2014. **125**: p. 207–216.
14. Varma, N.R., A. Ramalingam, and T. Banerjee, *Experiments, correlations and COSMO-RS predictions for the extraction of benzothiophene from n-hexane using imidazolium-based ionic liquids*. Chemical Engineering Journal, 2011. **166**(1): p. 30–39.
15. Kumar, L., T. Banerjee, and K. Mohanty, *Prediction of selective extraction of cresols from aqueous solutions by ionic liquids using theoretical approach*. Separation Science and Technology, 2011. **46**(13): p. 2075–2087.
16. Pilli, S.R., T. Banerjee, and K. Mohanty, *Ionic liquids as green solvents for the extraction of endosulfan from aqueous solution: A quantum chemical approach*. Chemical Product and Process Modeling, 2013. **8**(1): p. 1–14.
17. González, E.J., et al., *(Liquid+liquid) equilibrium data for the ternary systems (cycloalkane+ethylbenzene+1-ethyl-3-methylimidazolim ethylsulfate) at T=298.15K and atmospheric pressure*. The Journal of Chemical Thermodynamics, 2011. **43**(5): p. 725–730.
18. Calvar, N., et al., *Evaluation of ionic liquids as solvent for aromatic extraction: Experimental, correlation and COSMO-RS predictions*. The Journal of Chemical Thermodynamics, 2013. **67**: p. 5–12.
19. Marciniak, A. and M. Wlazło, *Ternary (liquid+liquid) equilibria of {trifluorotris (perfluoroethyl)phosphate based ionic liquids+thiophene+heptane}: Part 2*. The Journal of Chemical Thermodynamics, 2015. **86**: p. 196–201.
20. Hou, Y., et al., *Novel binary eutectic mixtures based on imidazole*. Journal of Molecular Liquids, 2008. **143**(2): p. 154–159.
21. Cassol, C.C., et al., *On the extraction of aromatic compounds from hydrocarbons by imidazolium ionic liquids*. International Journal of Molecular Sciences, 2007. **8**(7): p. 593–605.
22. Ravilla, U.K. and T. Banerjee, *Liquid liquid equilibria of imidazolium based ionic liquid+ pyridine+ hydrocarbon at 298.15 K: Experiments and correlations*. Fluid Phase Equilibria, 2012. **324**: p. 17–27.
23. Shah, M.R., et al., *Quaternary (liquid+ liquid) equilibria for systems of imidazolium based ionic liquid+ thiophene+ pyridine+ cyclohexane at 298.15 K: Experiments and*

quantum chemical predictions. The Journal of Chemical Thermodynamics, 2013. **62**: p. 142–150.
24. Kareem, M.A., et al., *Phase equilibria of toluene/heptane with deep eutectic solvents based on ethyltriphenylphosphonium iodide for the potential use in the separation of aromatics from naphtha*. The Journal of Chemical Thermodynamics, 2013. **65**: p. 138–149.
25. Oliveira, F.S., et al., *Deep eutectic solvents as extraction media for azeotropic mixtures*. Green Chemistry, 2013. **15**(5): p. 1326–1330.
26. Ali, M.C., et al., *Efficient removal of both basic and non-basic nitrogen compounds from fuels by deep eutectic solvents*. Green Chemistry, 2016. **18**(1): p. 157–164.
27. Hizaddin, H.F., et al., *Evaluating the performance of deep eutectic solvents for use in extractive denitrification of liquid fuels by the conductor-like screening model for real solvents*. Journal of Chemical & Engineering Data, 2014. **59**(11): p. 3470–3487.
28. Shahbaz, K., et al., *Densities of ammonium and phosphonium based deep eutectic solvents: Prediction using artificial intelligence and group contribution techniques*. Thermochimica Acta, 2012. **527**: p. 59–66.
29. Helalat-Nezhad, Z., K. Ghanemi, and M. Fallah-Mehrjardi, *Dissolution of biological samples in deep eutectic solvents: An approach for extraction of polycyclic aromatic hydrocarbons followed by liquid chromatography-fluorescence detection*. J Chromatogr A, 2015. **1394**: p. 46–53.
30. Shahbaz, K., et al., *Prediction of the surface tension of deep eutectic solvents*. Fluid Phase Equilibria, 2012. **319**: p. 48–54.
31. Shahbaz, K., et al., *Using Deep Eutectic Solvents Based on Methyl Triphenyl Phosphunium Bromide for the Removal of Glycerol from Palm-Oil-Based Biodiesel*. Energy & Fuels, 2011. **25**(6): p. 2671–2678.
32. Lu, H., et al., *Deep catalytic oxidative desulfurization (ODS) of dibenzothiophene (DBT) with oxalate-based deep eutectic solvents (DESs).* Chem Commun (Camb), 2015. **51**(53): p. 10703–10706.
33. Pena-Pereira, F. and J. Namiesnik, *Ionic liquids and deep eutectic mixtures: Sustainable solvents for extraction processes*. ChemSusChem, 2014. **7**(7): p. 1784–1800.
34. Chowdhury, S., R.S. Mohan, and J.L. Scott, *Reactivity of ionic liquids*. Tetrahedron, 2007. **63**(11): p. 2363–2389.
35. Fraser, K.J. and D.R. MacFarlane, *Phosphonium-based ionic liquids: An overview*. Australian Journal of Chemistry, 2009. **62**(4): p. 309–321.
36. Kareem, M.A., et al., Phosphonium-based ionic liquids analogues and their physical properties. Journal of Chemical & Engineering Data, 2010. 55(11): p. 4632–4637.
37. Alonso, L., et al., (Liquid+ liquid) equilibria of [C 8 mim][NTf 2] ionic liquid with a sulfur-component and hydrocarbons. The Journal of Chemical Thermodynamics, 2008. 40(2): p. 265–270.
38. García, S., et al., *Separation of toluene from n-heptane by liquid—liquid extraction using binary mixtures of [bpy][BF4] and [4bmpy][Tf2N] ionic liquids as solvent*. The Journal of Chemical Thermodynamics, 2012. **53**: p. 119–124.
39. Ramalingam, A. and S. Kanniayan, *Phase equilibria upon denitrification of liquid fuels using imidazolium-based ionic liquids: Experiment and quantum chemical calculations*. Industrial & Engineering Chemistry Research, 2015. **54**(51): p. 12948–12959.
40. Potdar, S., R. Anantharaj, and T. Banerjee, *Aromatic extraction using mixed ionic liquids: Experiments and COSMO-RS predictions.* Journal of Chemical & Engineering Data, 2012. **57**(4): p. 1026–1035.
41. Anantharaj, R. and T. Banerjee, *Liquid—liquid equilibria for quaternary systems of imidazolium based ionic liquid+ thiophene+ pyridine+ iso-octane at 298.15 K: Experiments and quantum chemical predictions*. Fluid Phase Equilibria, 2011. **312**: p. 20–30.

42. Bharti, A., et al., *Phase equilibria in ionic liquid facilitated liquid-liquid extractions*. 2017: CRC Press.
43. Dukhande, V.A., et al., *Separation of toluene from n-heptane using monocationic and dicationic ionic liquids*. Fluid Phase Equilibria, 2013. **342**: p. 75–81.
44. Tripathi, R.P., A.R. Ram, and P.B. Rao, *Liquid-liquid equilibriums in ternary system toluene-n-heptane-sulfolane*. Journal of Chemical and Engineering Data, 1975. **20**(3): p. 261–264.
45. Hughes, M.A. and Y. Haoran, *Liquid-liquid equilibria for separation of toluene from heptane by benzyl alcohol tri (ethylene glycol) mixtures*. Journal of Chemical and Engineering Data, 1990. **35**(4): p. 467–471.
46. Manohar, C., et al., *Liquid—liquid equilibria studies on ammonium and phosphonium based ionic liquid—aromatic—aliphatic component at T= 298.15 K and p= 1 bar: Correlations and a-priori predictions*. Fluid Phase Equilibria, 2013. **360**: p. 392–400.
47. Manohar, C., et al., *Liquid—liquid equilibria studies on ammonium and phosphonium based ionic liquid—aromatic—aliphatic component at T= 298.15 K and p= 1bar: Correlations and a-priori predictions*. Fluid Phase Equilibria, 2013. **360**: p. 392–400.
48. Sørensen, J.M., et al., *Liquid-liquid equilibrium data: Their retrieval, correlation and prediction part I: Retrieval*. Fluid Phase Equilibria, 1979. **2**(4): p. 297–309.
49. Alli, R.D. and M.C. Kroon, *Extraction of benzothiazole and thiophene from their mixtures with n-heptane using tetrahexylammonium bromide-based deep eutectic solvents as extractive denitrogenation and desulfurization agents*. Fluid Phase Equilibria, 2018. **477**: p. 1–11.
50. Rodriguez, N.R., P.F. Requejo, and M.C. Kroon, *Aliphatic—aromatic separation using deep eutectic solvents as extracting agents*. Industrial & Engineering Chemistry Research, 2015. **54**(45): p. 11404–11412.
51. Mulyono, S., et al., *Separation of BTEX aromatics from n-octane using a (tetrabutylammonium bromide+ sulfolane) deep eutectic solvent—experiments and COSMO-RS prediction*. RSC Advances, 2014. **4**(34): p. 17597–17606.
52. Kareem, M.A., et al., *Liquid—liquid equilibria for the ternary system (phosphonium based deep eutectic solvent—benzene—hexane) at different temperatures: A new solvent introduced*. Fluid Phase Equilibria, 2012. **314**: p. 52–59.
53. Renon, H. and J.M. Prausnitz, *Local compositions in thermodynamic excess functions for liquid mixtures*. AIChE Journal, 1968. **14**(1): p. 135–144.
54. Abrams, D.S. and J.M. Prausnitz, *Statistical thermodynamics of liquid mixtures: A new expression for the excess Gibbs energy of partly or completely miscible systems*. AIChE Journal, 1975. **21**(1): p. 116–128.
55. Banerjee, T., et al., *Volume, surface and UNIQUAC interaction parameters for imidazolium based ionic liquids via polarizable continuum model*. Fluid Phase Equilibria, 2005. **234**(1–2): p. 64–76.
56. Singh, M.K., T. Banerjee, and A. Khanna, *Genetic algorithm to estimate interaction parameters of multicomponent systems for liquid—liquid equilibria*. Computers & Chemical Engineering, 2005. **29**(8): p. 1712–1719.
57. Seader, J. and E. Henley, *Separation process principles*. John Wiley & Sons. Inc., 1998.
58. Klamt, A., *COSMO-RS: From quantum chemistry to fluid phase thermodynamics and drug design*. 2005: Elsevier.
59. Xiong, R., S.I. Sandler, and R.I. Burnett, *An improvement to COSMO-SAC for predicting thermodynamic properties.* Industrial & Engineering Chemistry Research, 2014. **53**(19): p. 8265–8278.
60. Dennington, R., T. Keith, and J. Millam, *GaussView, version 5*. 2009.
61. Frisch, M., et al., *Gaussian 09, Revision d. 01*. 2009: Gaussian. Inc., **201**.
62. Perdew, J.P., *Density-functional approximation for the correlation energy of the inhomogeneous electron gas*. Physical Review B, 1986. **33**(12): p. 8822.

63. Sosa, C., et al., *A local density functional study of the structure and vibrational frequencies of molecular transition-metal compounds*. The Journal of Physical Chemistry, 1992. **96**(16): p. 6630–6636.
64. Klamt, A. and G. Schüürmann, *COSMO: A new approach to dielectric screening in solvents with explicit expressions for the screening energy and its gradient*. Journal of the Chemical Society, Perkin Transactions 2, 1993. (5): p. 799–805.
65. Klamt, A., *Conductor-like screening model for real solvents: A new approach to the quantitative calculation of solvation phenomena*. The Journal of Physical Chemistry, 1995. **99**(7): p. 2224–2235.
66. Banerjee, T., K.K. Verma, and A. Khanna, *Liquid—liquid equilibrium for ionic liquid systems using COSMO-RS: Effect of cation and anion dissociation*. AIChE Journal, 2008. **54**(7): p. 1874–1885.
67. Kundu, D. and T. Banerjee, *Multicomponent vapor—liquid—liquid equilibrium prediction using an a priori segment based model*. Industrial & Engineering Chemistry Research, 2011. **50**(24): p. 14090–14096.
68. Banerjee, T., M.K. Singh, and A. Khanna, *Prediction of binary VLE for imidazolium based ionic liquid systems using COSMO-RS*. Industrial & Engineering Chemistry Research, 2006. **45**(9): p. 3207–3219.
69. Banerjee, T., et al., *Multicomponent liquid−liquid equilibria prediction for aromatic extraction systems using COSMO-RS*. Industrial & Engineering Chemistry Research, 2007. **46**(4): p. 1292–1304.
70. Banerjee, T. and A. Khanna, *Infinite dilution activity coefficients for trihexyltetradecyl phosphonium ionic liquids: Measurements and COSMO-RS prediction*. Journal of Chemical & Engineering Data, 2006. **51**(6): p. 2170–2177.
71. Lin, S.-T. and S.I. Sandler, *A priori phase equilibrium prediction from a segment contribution solvation model*. Industrial & Engineering Chemistry Research, 2002. **41**(5): p. 899–913.
72. Verma, R. and T. Banerjee, *Liquid—liquid extraction of lower alcohols using menthol-based hydrophobic deep eutectic solvent: Experiments and COSMO-SAC predictions*. Industrial & Engineering Chemistry Research, 2018. **57**(9): p. 3371–3381.
73. Naik, P.K., et al., *Evaluation of deep eutectic solvent for the selective extraction of toluene and quinoline at T= 308.15 K and p= 1 bar*. Fluid Phase Equilibria, 2016. **423**: p. 146–155.
74. Kumar, N. and T. Banerjee, *Dearomatization insights with phosphonium-based deep eutectic solvent: Liquid—liquid equilibria experiments and predictions*. Journal of Chemical & Engineering Data, 2021. **66**(9): p. 3432–3442.
75. Naik, P.K., S. Paul, and T. Banerjee, *Liquid liquid equilibria measurements for the extraction of poly aromatic nitrogen hydrocarbons with a low cost deep eutectic solvent: Experimental and theoretical insights*. Journal of Molecular Liquids, 2017. **243**: p. 542–552.

3 Molecular Dynamics Simulations for the Extraction of Aromatics and Pesticide

3.1 INTRODUCTION

As discussed in earlier chapters, extraction processes are reliable, cost-effective, and biocompatible as compared to hydrodenitrification process [1–3]. However, this depends on the efficiency of the solvent, its cost, its recyclability, and its environmental friendliness [4–8]. In our previous Chapter 2, we have mentioned that various deep eutectic solvents (DESs) consisting of phosphonium-based HBA salt and ethylene glycol (EG) can effectively remove benzene and quinoline from a hydrocarbon stream. We have also observed that the use of DES– methyltriphenyl phosphonium bromide (MTPB)–EG mixture in the extraction of PAH has shown higher values of selectivity and distribution coefficients as compared to the other conventional solvents. All the liquid–liquid equilibrium (LLE) experiments use a favorable solvent [2, 6, 9–11], where its success depends on its efficiency, recyclability, cost, and environmental friendliness. In order to compute an understanding of the extraction mechanism, simulation-based methods, such as molecular dynamics (MD) simulations, are an invaluable tool to derive the driving forces. There are few studies available with DES [12–15]. Very few research works have been devoted to the investigation of the mechanism by which the extraction process takes place by using computer simulation methods such as MD simulations. Classical MD simulation gives the fundamental molecular-level pathways and provides insights into the extraction process. Furthermore, classical MD simulations are also useful in carrying out the processes under extreme conditions that cannot be attained with conventional experimental techniques. Again, these computational methods also give us an opportunity to explore new solvent systems and the screening of many alternatives in an economical way [16–19]. Although theoretical studies are important to understand the mechanism, they are not expected to replace experiments but only to accompany them and enhance their use. For example, Stephenson et al. [20] carried out MD simulations for the extraction of ethanol from long-chain alcohols using classical MD simulations. Taha and Lee [21] observed the phase separation of organic solvents from water using a biological buffer as an external solvent. Celebi et al. [19] also reported the thermodynamic and transport properties of aqueous reline- and ethaline-based DESs. Dehury et al. [12] explored the phase behavior of butanol

DOI: 10.1201/9781003231158-3

in two different phases of ionic liquid (IL) and water by both LLE experiments and MD simulation studies. Perkins et al. [14] also investigated the experimental and computational study to get insight into the most common DES, that is, choline chloride–urea-based DES.

Real experiments are performed for a duration of the order of hours/minutes or seconds. In such an order, the atomic-scale simulation is not feasible due to computational restrictions. To make the system affordable, atomic-scale phenomena are generally recorded at nanosecond scale or in other words the velocities are computed after every 1 fs. Chemical phenomena such as disengagement at the atomic level occur at fractions of seconds that even digital instruments are even unable to detect. Therefore, theoretical calculations and simulations aim to capture this phenomenon through a statistical mechanical framework or ensemble theory. In such a scenario, the LLE simulation results defined in this chapter are one such result or trajectory. This inherently connects properties generated by chemical engineers, namely, the activity coefficient implicit for the computation of mole fractions using first principles. Hence, the role of molecular simulations in the LLE-based experiments is very important to understanding the behavior of different molecules and the mechanism involved in different ternary systems. In this chapter, we have compared MD simulation results with our previous experimental results from Chapter 2. A similar MD analysis was also performed for the DES–water–nitenpyram system in the concluding section where the extraction of nitenpyram from an aqueous environment with menthol-octanoic acid DES, was validated.

Most of the DESs that are synthesized till now are hydrophilic in nature. However, for water purification by solvent extraction and separation of toxic, as well as valuable products from water, the solvents need to be hydrophobic in nature. Researchers are currently working on the synthesis of various hydrophobic DESs from natural substances [22]. Six hydrophobic DESs were synthesized for the first time consisting of decanoic acid as hydrogen bond donors (HBDs) and a range of quaternary ammonium salts as hydrogen bond acceptors (HBAs) by van Osch et al. [22]. They studied the effect of the carbon chain length of the quaternary ammonium salts in the leaching of the HBA to the water phase and subsequently the overall hydrophobicity of the DESs. Hydrophobic DESs based on menthol, ammonium salt, organic acids, and terpenes are synthesized and applied in the separation of pesticides and pharmaceuticals from aqueous environments [23–25]. Four different pesticides were extracted from aqueous environments successfully by DL-menthol and carboxylic acid–based DESs. Furthermore, their water stability was investigated experimentally by Florindo et al. [23] for pesticides such as neonicotinoids, imidacloprid, acetamiprid, nitenpyram, and thiamethoxam from diluted aqueous solutions. Hydrophobic DESs consisting of various combinations of DL-menthol, long-chain carboxylic acids (C_8–C_{12}), and quaternary ammonium salt have been applied to extract ciprofloxacin from an aqueous solution by Florindo et al. [26]. They also studied the effect of various experimental conditions such as pH, stirring speed, contact time, and DES-to-water mass ratio. The extractability of the hydrophobic DESs hampered severely if the DES cannot stabilize in the presence of water. In other words, to maintain HBA–HBD integrity, the DES components need to be immiscible with water and should not

leach out in either phase. Most of the DESs were liquid at room temperature, which allowed studying the DES–water solubility and drugs extraction [27–29]. Recently, it was found that the menthol-based DES were the most promising for these types of studies because of its hydrophobicity and thermo-physical properties [30–34].

A proper understanding of various solvent properties of DESs, such as solubility and activity coefficient, could help us in selecting suitable solvents for specific applications. Sufficient and authentic experimental data combined with efficient and robust mathematical models related to such solvent properties can be very helpful in effectively selecting solvents. One such work is carried out by the research group of Verevkin et al. [35], where they have measured the activity coefficient at infinite dilution for 23 solutes in choline chloride– and EG-based DESs and validated the separation performances by perturbed chain statistical associating fluid theory (PC-SAFT) mathematical model for the first time for any DES system. Pontes et al. [36] studied the solid–liquid phase equilibrium of 15 DESs consisting of 3 quaternary ammonium salt and 5 carboxylic acids and then executed PC-SAFT equation of state to measure possible hydrogen bonding among the species. Dietz et al. [37] have incorporated density and vapor pressure data in the PC-SAFT model to successfully measure various thermodynamic properties of eight hydrophobic DESs and further investigated the extraction of 5-hydroxymethylfurfural (HMF) from sugars in an aqueous environment. They also analyzed the solubility of water and HMF in the DES phase. One major advantage of these models is that they are useful in identifying the eutectic composition of the DES, that is, the composition at which the DES becomes liquid [37]. All these studies suggest that a proper combination of experimental study along with simulation strategies can certainly help us in the proper understanding and address the complexity of the DES systems. This combined strategy can be considered the way forward for predicting the phase equilibria and the selection of suitable solvents. Overall, experiments and simulations can be carried out simultaneously to obtain a more efficient and precise pure component and phase equilibria data.

Therefore, this chapter also involves a molecular-level study to observe the validity of our simulation work and evaluate whether MD simulation can be useful for the extraction of pesticides from an aqueous environment, we carried out the simulation of a pesticide (nitenpyram) and compared the finding with the previous result. The composition of each system considered in the simulation work is kept identical to that of the experimental work of Florindo et al. [23]. The ensuing section starts with the computational details and thereafter discusses the evaluation of nonbonded interaction energies, including the relative stability factor. Further from the radial and combined distribution function, the hydrogen bond property between the different components of the DES, drug and water, spatial distribution function, mean square displacement (MSD), and self-diffusivity analysis were evaluated.

3.2 MD SIMULATION DETAILS

Initially, the structures of isolated ions of all DESs and other molecules were drawn separately in GaussView05 software with their geometries optimized by Gaussian09 [38] at B3LYP/6–31G* theory [39]. The partial charges for different atomic sites

of the isolated molecules were obtained by using the same level of theory, that is, B3LYP/6–31G*. The chemical structures of these species are shown in Figure 3.1 along with their atomic notations. The partial charges for different species (as obtained from the quantum calculations) were then fitted with the Restricted Electrostatic Potential (RESP) [40] module of AMBER12 [41]. All the force-field parameters (that are required for performing an MD simulation) were generated according to the Generalized Amber Force Field (GAFF) [42] functional form using the ANTECHAMBER [43] module of AMBER12 [41]. The detailed description on AMBER force fields are given in the Appendix. The generated force-field parameters were further validated by comparing the simulated density of DES at desired temperature (298.15, 308.15, and 318.15 K) and ambient pressure condition with

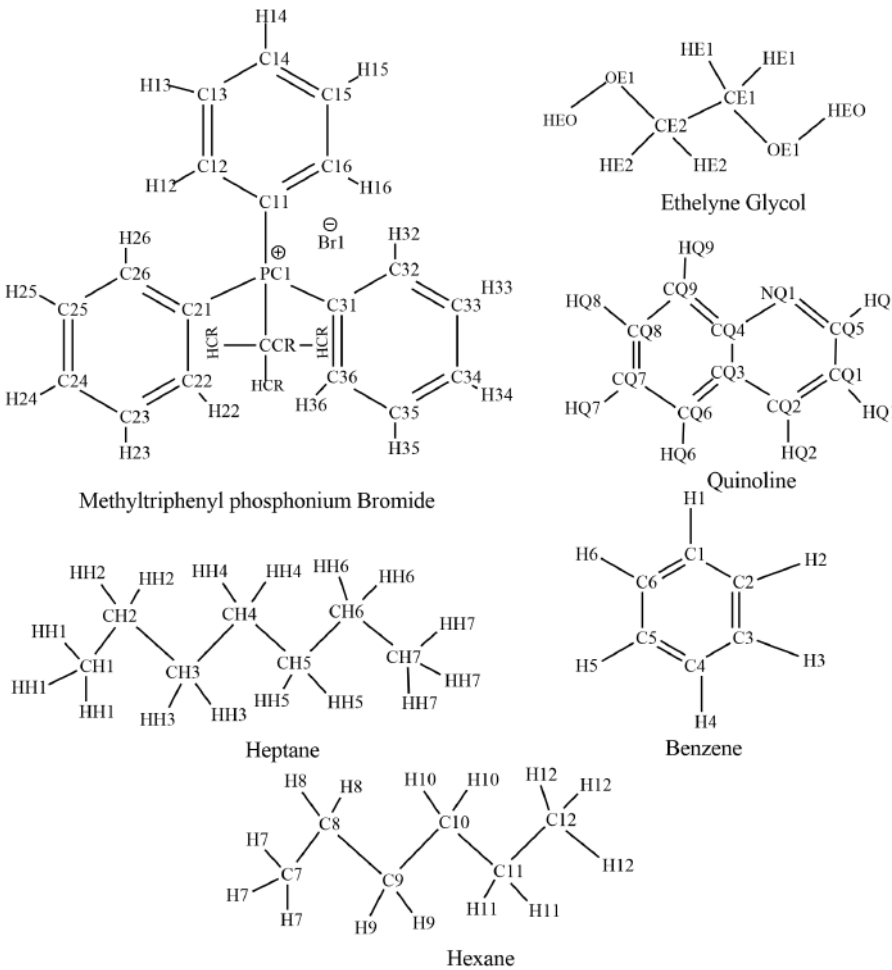

FIGURE 3.1 Structures with atom notations of different molecular species used aromatic extraction.

that of experimental density value at the same temperature and pressure condition. Classical MD simulations were then performed for two experimental LLE tie-line data points in order to understand their behavior and phase separations.

These ternary systems consisted of DES + quinoline + heptane and DES + benzene + hexane system. Due to the limitations and constraints, MD simulations were carried out for only a few tie-line data points. For DES + quinoline + heptane system tie-line-2 (system 1) and tie-line-5 (system 2), at their corresponding feed compositions were considered. These experimental tie-line data points were taken from previous reported literatures [44]. The number of molecules considered for different systems are presented in Table 3.1. The representation and molecular analysis of system 1 were carried out since it has a maximum value of distribution coefficient and selectivity. As can be seen from Table 3.1, 400 (S1: system 1) and 250 (S2: system 2) molecules of DES have been reported, which are considered for MD simulations. It should be noted that DES here is representing a solvent with the mixture of two components at a 1:4 molar ratio. Hence, for MD simulations 400 molecules of MTPB were mixed with 1600 molecules of EG for the S1 system. Similarly, 250 molecules of salt (MTPB) were mixed with 1000 molecules of EG for the S2 system. Similarly, three different experimental LLE tie-lines data points for the DES + benzene + hexane system was selected to understand the phase separation (S11–S13). These experimental tie data points were taken from a previously reported work [6]. MD simulations were then carried out for three such systems in which the number of molecules is given in Table 3.2. System S12 has been analyzed for a detailed MD insight. According to the molar ratios of HBA:HBD, the corresponding numbers of molecules were taken. Therefore, for MD simulations involving DES (1:4 molar ratio), 500 molecules of

TABLE 3.1
Experimental Composition and Considered Number of Molecules DES + Quinoline + Heptane System

System	Tie-line no.	Mole fraction				Number of molecules			
		DES	Quinoline	Heptane	Total	DES	Quinoline	Heptane	Total
S1	2	0.40	0.20	0.40	1	400	200	400	1000
S2	5	0.25	0.50	0.25	1	250	500	250	1000

TABLE 3.2
Number of Molecules in MD Simulations for DES + Benzene + Hexane System

System No	Mole fraction			Total	Number of molecules			Total
	DES	Benzene	Hexane		DES	Benzene	Hexane	
S11	0.5	0.025	0.475	1	500	25	475	1000
S12	0.5	0.105	0.395	1	500	105	395	1000
S13	0.5	0.205	0.295	1	500	205	295	1000

MTPB are mixed with 2000 molecules of EG for the S12 system. We have also performed the MD simulation by considering sulfolane as an extraction solvent to validate and benchmark the system. Here, the systems consist of sulfolane (500), benzene (105), and hexane (395) molecules. The simulation procedure thereafter remains the same as pursued for previous DES-based systems. Single-tie-line data was adopted from the literature [6] and was used to carried out the simulation study at 318.15 K.

For DES + nitenpyram + water system, the experimental compositions were used from an earlier work by Florindo et al. [23]. Here, the DES consists of DL-menthol and octanoic acid at a 1:1 molar ratio. The ternary system was prepared for the simulation study of pesticide extraction from the corresponding mole fraction in line with the respective molecules of the experiment. The exact mimicking of the experimental number of molecules was not possible due to the computational limit. As a result, the equal mass of DES and water for the simulated system with 5 molecules of nitenpyram in the aqueous phase has been considered initially. The chemical structures of these species are shown in Figure 3.2 and composition of the systems has been presented in Table 3.3. Nanoscale Molecular Dynamics (NAMD) was used for simulation. A sample NAMD configuration file is given in the Appendix. The Lennard–Jones (L-J) parameters used are reported in Table 3.4.

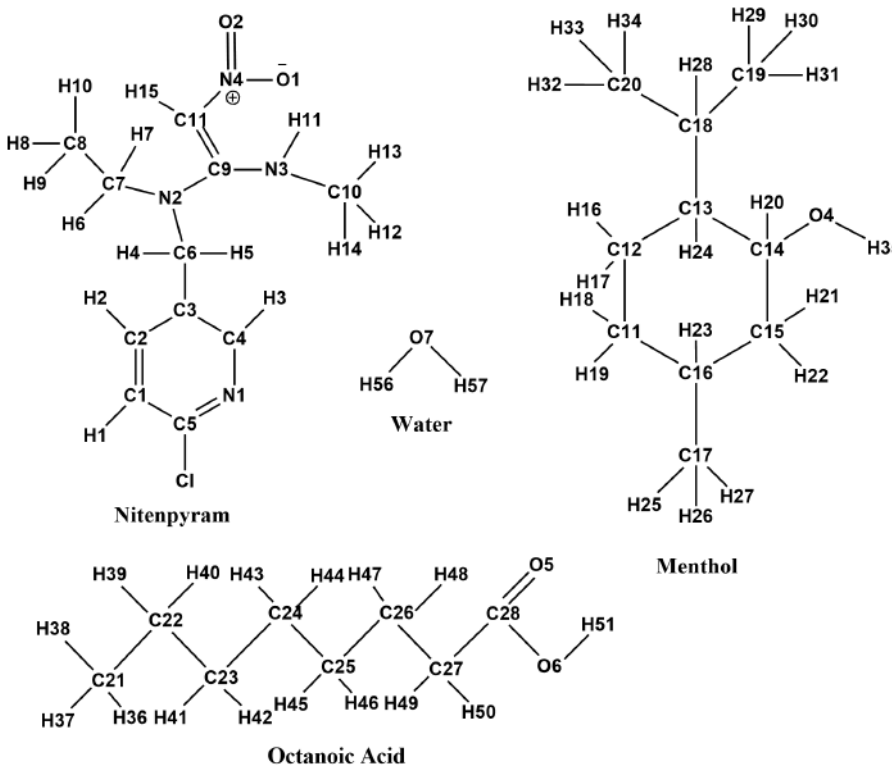

FIGURE 3.2 Structures of different components with atom notation used in the extraction of pesticide.

TABLE 3.3
Composition of the System Considering 1:1 Mass Ratio of DES and the Aqueous Solution of Nitenpyram and the Number of Molecules Considered for MD Simulation

Name of pesticide	DES		Number of molecules				
	HBA	HBD	HBA	HBD	Nitenpyram	Water	Total
Nitenpyram	DL-menthol	Octanoic acid	100	100	5	835	1040

TABLE 3.4
L-J Parameters Used for Different Atom Types

Atom Type	ε (kcal/mol)	R^* (Å)	Atom Type	ε (kcal/mol)	R^* (Å)
ca	0.0860	1.9080	h1	0.0157	1.3870
cg	1.9080	0.2100	h2	1.2870	0.0157
cd	1.9080	0.0860	h3	1.1870	0.0157
cc	1.9080	0.0860	h4	1.4090	0.0150
c	1.9080	0.0860	ha	0.0150	1.4590
c1	0.1094	1.9080	hc	0.0157	1.4870
c2	1.9080	0.0860	ho	0.0000	0.0000
c3	1.9080	0.1094	hn	0.6000	0.0157
oh	1.7210	0.2104	nh	1.8240	0.1700
o	1.6612	0.2100	nb	1.8240	0.1700
cl	1.9480	0.2650	n1	1.8240	0.1700
p5	0.2000	2.1000	br	0.320	2.2200

The initial configuration of different systems of molecules was generated using PACKMOL [45] and put in a definite rectangular box. Initially, DES molecules and hydrocarbon molecules were inserted into two separate boxes. After that, the boxes were made to come close to each other so as to create or mimic a two-phase system, that is, DES-rich and hydrocarbon-rich phase. Thereafter, the quinoline/benzene molecules were uniformly distributed in both phases. Therefore, the considered geometry was similar to the experimental condition. The experimental procedure was provided in Chapter 2, Section 2.2. All the MD simulations were run in NAMD 2.9 package [46] using Langevin thermostat and Nose–Hoover Langevin barostat [47, 48]. A time integration step of 1 fs was used for all simulations. Initially, the systems were energy minimized for 1 ns, and thereafter, each of the systems was gradually heated from 0 K to 308.15 K in 0.5 ns. After that, the systems were equilibrated for 8–10 ns in isothermal-isobaric (NPT) ensemble at 308.15 K temperature and 1 atm pressure. For maintaining the desired temperature Langevin dynamics method [49] with a collision frequency of 1 ps^{-1} was used. Nose-Hoover Langevin barostat was used for controlling the pressure with an oscillation period of 100 fs and damping factor of 50 fs [50]. Thereafter, the production runs lasted for 200 ns

for each of the systems with NVT ensemble. At every 5 ps, the trajectory data was saved for structural and transport analysis. SHAKE algorithm was used to restrain the bonds involving hydrogen atoms [51]. The particle mesh Ewald (PME) method was used to calculate the long-range intermolecular electrostatic interactions [52] and for treating short-ranged intermolecular interactions, a cutoff distance of 12 Å was used. To remove edge effect, periodic boundary conditions were applied in all three directions. In the current work, we have not used any charge scaling as, unlike the water model, the current system is devoid of any polarizability effect [53, 54]. At every 5 ps, the trajectory data were saved for analyzing the different structural and dynamical properties.

After successful completion of the production run, the trajectory file was obtained, which contains the trajectory of the molecules of the system. The parameter file and the trajectory files were then inserted in the VMD software package [55]. The non-bonded interaction energy, average hydrogen bonding, and radial distribution function on the specifications of the requisite criteria were obtained directly using the tools provided in VMD. TRAVIS package [56] was used to obtain the combined distribution function (CDF) and the spatial distribution function (SDF) where the final coordinate file was used as the input. Specific molecules and atoms, along with required criteria such as reference molecule and observed molecule, were selected to get the CDF datasheet SDF coordinate file. The data were then plotted on graph sheet. Proper isovalue was set to display the three-dimensional SDF. The MSD curve was obtained by solving Einstein's equation of self-diffusivity through VMD. The diffusion coefficient was obtained from the linear slope of the MSD curve.

3.3 EXTRACTION OF QUINOLINE AND BENZENE FROM THE ALIPHATIC PHASE

The available experimental results have shown that DES (MTPB: ETG) of molar ratio 1:4 gives the most promising result for the extraction of quinoline/benzene from heptane/hexane. We first compare the LLE experimental and MD simulated tie-line data for the system DES (1) + quinoline (2) + heptane (3) and DES (1) + benzene (2) + hexane (3) as shown in Table 3.5 and Table 3.6. Figure 3.3 depicts a tie line that is commonly used in the chemical engineering community for indicating the distribution of a component or solute in two phases, namely, the extract and raffinate phases for quinoline extraction. Here the two ends of the tie lines represent the composition in the extract and raffinate phases. The tie line will invariably pass through the initial feed mixture (Figure 3.3). To get a complete phase diagram we have to vary the solute concentration (i.e., quinoline/benzene) while keeping the other two components at the same volume ratio. In this way, the entire heterogeneity of the system is captured. Here, the LLE data show a type 2 behavior [57]. The respective numbers of molecules were calculated in each phase after 100 ns of MD simulation. After that, the corresponding mole fraction, distribution coefficient, and selectivity were estimated for the system.

A type II system exhibits a phase envelope that spans the composition space and connects two binary miscibility gaps. As shown in Figure 3.3 the binary system, namely, DES–quinoline shows miscibility while the other binaries, DES–heptane

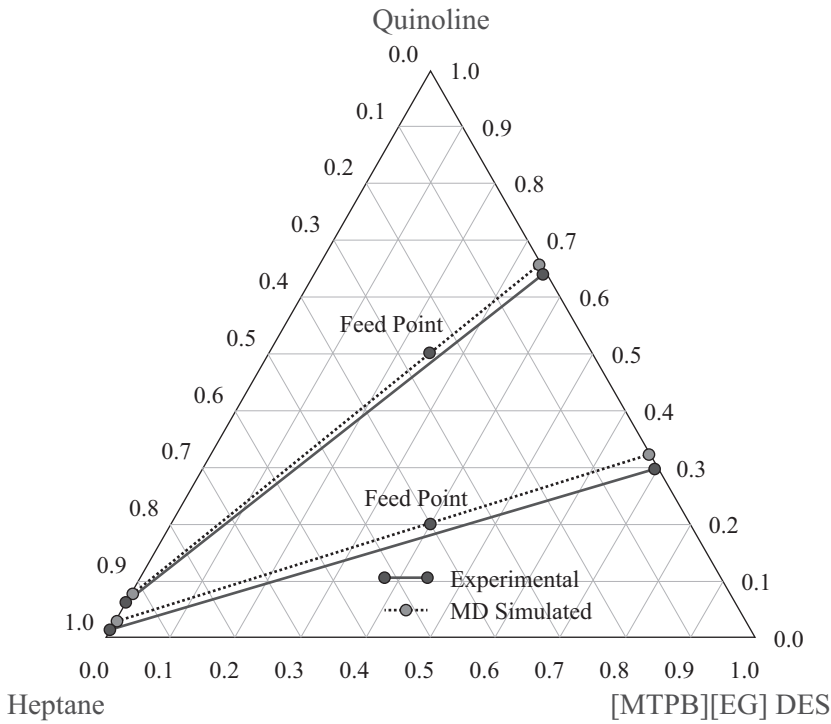

FIGURE 3.3 Experimental and MD simulation correlated tie-lines data points for the ternary system: DES (1) + quinoline (2)+ heptane (3) at T = 308.15 K and p = 1 atm.

and heptane–quinoline are completely immiscible. From Figure 3.3, it can be noticed that the raffinate-phase data occupy the extreme corner point of the ternary diagram. Thus, the quinoline molecules have actually transferred to the extract DES-rich phase. Moreover, in Figure 3.3 we have also compared the experimental ternary-phase diagram of the DES–quinoline–heptane system with that of the simulated one. It is clear that it gave good agreement between the experimental and simulated values. For the calculation of distribution coefficient (β) and selectivity (S), the following equations were used (Equations 3.1 and 3.2) [10].

$$\beta = \frac{x^{E}_{solute}}{x^{R}_{solute}} \tag{3.1}$$

$$S = \frac{\beta_{solute}}{\beta_{solvent}} = \frac{x^{E}_{solute} / x^{R}_{solute}}{x^{E}_{solvent} / x^{R}_{solvent}} \tag{3.2}$$

Here, x^{E}_{solute} and x^{R}_{solute} refer to the mole fractions of solute (quinoline/benzene) in extract and raffinate phases, respectively. $x^{E}_{solvent}$ and $x^{R}_{solvent}$ are the mole fractions of solvent (heptane/hexane) in extract and raffinate phases. As can be seen from Table 3.5, the values of β and S are greater than unity for both tie lines. The higher values of S indicate the better ability of DES for the extraction of quinoline

TABLE 3.5
Experimental and MD Simulated LLE Data for DES (x_1) + Quinoline (x_2) + Heptane (x_3) Ternary System at T= 308.15 K and 1 atm pressure[a]

System	Tie-line No	Type of data	DES-rich phase			Heptane-rich phase			Distribution coefficient (β)	Selectivity (S)
			x_1	x_2	x_3	x_1	x_2	x_3		
S1	2	Exp.	0.698	0.295	0.007	0.000	0.013	0.987	22.69	3204.70
		Comp.	0.676	0.321	0.003	0.005	0.027	0.968	11.88	3419.18
S2	5	Exp.	0.354	0.638	0.008	0.000	0.062	0.938	10.29	1298.20
		Comp.	0.340	0.655	0.005	0.004	0.075	0.921	8.73	1476.00

[a] Tie-line values are taken from Chapter 2 RMSD = 0.01%.

from heptane. The distribution coefficient indicates that the distribution of quinoline molecules from the heptane-rich phase to DES-rich phase. The higher the β value, the better the distribution of the quinoline from heptane- to DES-rich phase will be. This observation suggests a significant extraction of quinoline (from heptane solvent) by DES. From the observation of Table 5.3, the MD-predicted mole fraction of quinoline in both the raffinate and extract phases is quite higher than that of the experimental value. However, on the contrary, it gives a lower distribution coefficient for quinoline when compared to the experimental value.

A closer look into the β values for the first tie-line data reveals a reasonably lower value when compared to its experimental value. In specific for this tie-line, the experimental value of β is twice that of its simulated value. This difference in the β values may occur due to the failure in exactly locating the number of molecules at the predetermined interface because a small uncertainty can lead to a marked change in the distribution values. The reported mole fraction values are the average of three different random structural molecular simulation results. Similar deviations in the β values were also observed by Dehury et al. [12] during the extraction of butanol from water using IL as a solvent. The MD results show better selectivity values for both the tie-line data when compared to the experimental values (Table 3.5).

In Figure 3.4, we present the snapshots of system S1 at different simulation times, which reveal a gradual distribution of quinoline molecules from the heptane-rich phase to the DES-rich phase and hence supports the observations discussed earlier. The system with interfacial geometry, therefore, mimics the phase equilibria where the considered geometry was similar to the experimental procedure in a manner that quinoline molecules were randomly dispersed in the DES- and heptane-rich phases. The distribution of quinoline molecules from the heptane to DES phase starts from the beginning of the production run, and the maximum distribution is seen to complete at about 200 ns. At 200 ns, the system was observed to be DES in the middle and heptane on two sides (Figure 3.4(d)).

A similar slab geometry was also reported by Taha and Lee (2013) [21] in their study on the separation of water and organic solvents using the biological buffer as

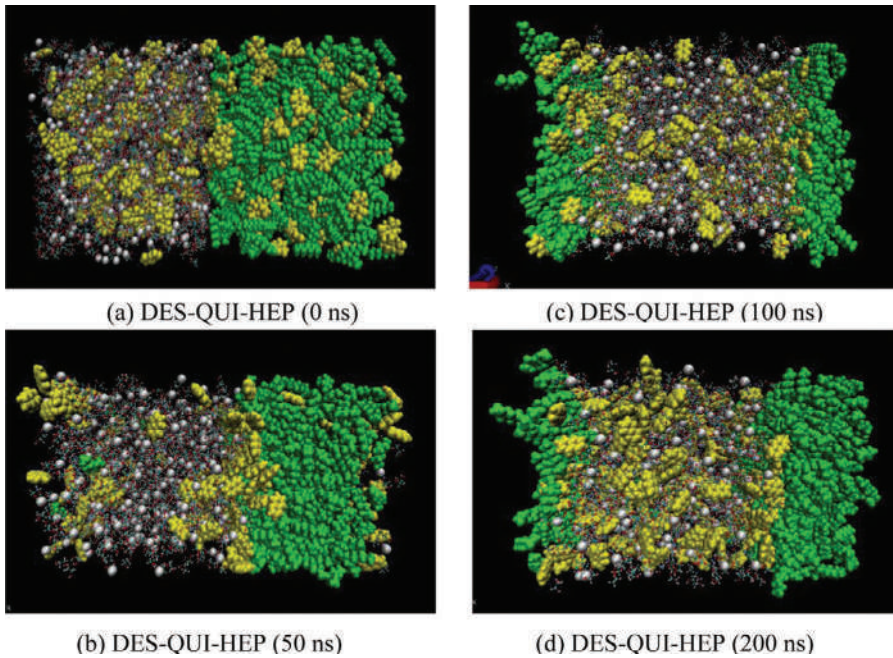

FIGURE 3.4 Distribution snapshots of quinoline in solvent throughout the system at different times (a) 0 ns, (b) 50 ns, (c) 100 ns, and (d) 200 ns, respectively (yellow: quinoline molecules; green: heptane molecules; gray: DES molecules) for system 1 (S1).

an external solvent. We also observed that an increase in the simulation runtime did not cause a significant change in the distribution of quinoline molecules. It should be noted that the selectivity of DES is much higher as compared to that of the ILs used in previous work [58–60]. Thus, the solvent DES is capable of extracting more of quinoline from the hydrocarbon solvent than that of ILs, which is an alternative green solvent.

In the case of DES + benzene + hexane system (S12), the concentrations in both the phases were compared with the existing experimental results by Kareem et al. [28] in order to validate the simulation. The investigated three LLE tie-lines data points are as per Table 3.2. The distribution coefficient and selectivity are seen to agree reasonably well with the experimental tie-line data (Table 3.6). The deviation in concentration is mainly observed in the hexane-rich phase owing to an absence of a sharp interface, which may not match with LLE experiments (Figure 3.5). Here, a detailed analysis was carried out for the second tie-line data (S12) as they all show similar trends. Initially the simulation was performed at 45°C because a maximum average selectivity was reported. Even though at 27°C, relatively good selectivity was achieved, distribution coefficients were small [6]. In order to see this effect of temperature, we have performed the same simulation with similar initial configurations and experimental conditions at 25°C. This will confirm us to recheck the reliability of the simulation process along with the effect of temperature on benzene

TABLE 3.6
Experimental and MD-Simulated LLE data for DES (x_1) + benzene (x_2) + hexane (x_3) ternary system at T= 318.15 K and 1 atm pressure[a]

System No.	Type of data	DES-rich phase			Hexane-rich phase			Distribution coefficient (β)	Selectivity (S)
		x_1	x_2	x_3	x_1	x_2	x_3		
S 11	Exp.	0.879	0.096	0.024	0.000	0.043	0.957	2.227	87.362
	Comp.	0.911	0.039	0.012	0.000	0.038	0.962	1.026	82.276
S 12	Exp.	0.599	0.378	0.022	0.000	0.236	0.764	1.604	61.292
	Comp.	0.650	0.325	0.025	0.000	0.195	0.805	1.505	57.500
S 13	Exp.	0.416	0.564	0.020	0.000	0.480	0.519	1.174	38.630
	Comp.	0.469	0.522	0.009	0.000	0.519	0.48	1.005	53.753

[a] Experimental value are taken from Kareem et al. [6], RMSD = 0.05%.

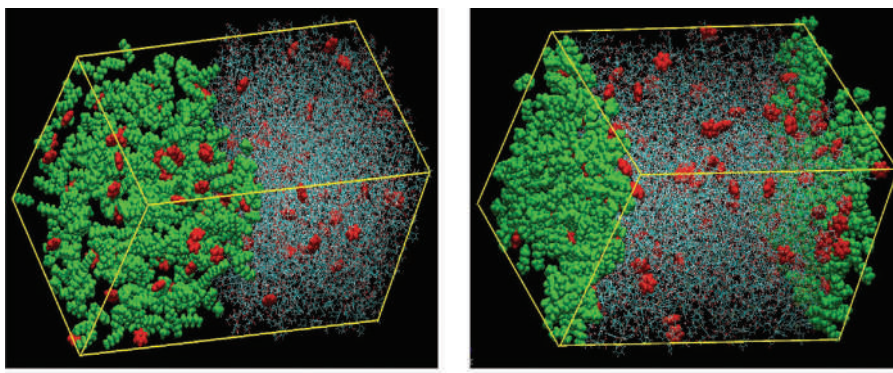

FIGURE 3.5 Distribution snapshots of benzene in the solvent throughout the system at different times: (a) 0 ns and (b) 100 ns, respectively (red: benzene, green: hexane, gray: DES [1:4] molecules).

extraction. The results below reconfirm the fact that the extraction efficiency at 45°C was higher as compared to lower temperatures. A comparison of the experimental (27°C) and the simulation result (25°C) is shown in Table 3.7.

Traditional organic solvents used for the extraction of benzene are sulfolane, furfuryl alcohol, EG, N-methyl pyrrolidone (NMP), and N-formylmorpholine (NFM). Industrially, the separation is carried out using sulfolane as solvent [61]. This process uses LLE with sulfolane as an extracting agent, followed by extractive distillation for solvent recovery. However, due to the high energy costs required for the sulfolane recovery, it becomes a noneconomical separation process especially for mixtures with aromatics content lower than 20 wt%. Consequently, if any DES shows distribution coefficient and selectivity values similar or higher to those of sulfolane, it would

TABLE 3.7
Experimental and MD-Simulated LLE Data for DES (x_1) + Benzene (x_2) + Hexane (x_3) Ternary System at Two Different Temperatures[a]

Temperature	Type of data	DES rich phase			Hexane rich phase			Distribution coefficient (β)	Selectivity (S)
		x_1	x_2	x_3	x_1	x_2	x_3		
27°C	Exp.	0.929	0.069	0.002	0.000	0.524	0.476	0.131	22.105
25°C	Comp.	0.947	0.051	0.002	0.000	0.544	.0456	0.094	21.375

[a] Experimental values are taken from Kareem et al. [6], RMSD = 0.05%.

TABLE 3.8
Comparison of Experimental and Simulated Data for Sulfolane (x_1) + Benzene (x_2) + Hexane (x_3) at T = 318.15 and 1 atm Pressure[a]

System No.	Type of data	Solvent-rich phase			Hexane-rich phase			Distribution coefficient (β)	Selectivity (S)
		x_1	x_2	x_3	x_1	x_2	x_3		
1	Exp.	0.833	0.146	0.021	0.048	0.300	0.651	0.485	15.120
	Comp.	0.858	0.124	0.018	0.052	0.235	0.713	0.527	20.901

[a] Experimental values are taken from Mahmoudi et al. [61] RMSD = 0.05%.

somewhat overcome both the solvent recovery issues of the conventional sulfolane process and the high synthesis price of the ILs. Mahmoudi et al. [61] have used sulfolane and NFM for the extraction of benzene from hexane at various temperatures. They found that sulfolane gives better performance of benzene extraction in terms of selectivity than NFM. A comparison of the experimental and predicted tie line is given in Table 3.8. The result clearly indicates that the MD simulation method for analyzing the extraction methodology is consistent with experiments.

3.3.1 Noncovalent Interaction Energy

In order to quantify the interactions between different system species, the total nonbonded interaction energies (IEs) were composed of electrostatic and van der Waals (vdW) components and computed by adopting different component pairs of moieties. First, considering the DES–quinoline–heptane system (S1), the nonbonded IEs were presented in Table 3.9. It can be noticed that the nonbonded interaction between DES–quinoline is more favorable than that for both DES–heptane and heptane–quinoline. A close inspection into the total interaction energies between these species suggests that the interaction between DES–heptane is the least favorable. This observation acts as corroborative evidence of what we discussed in our previous section.

A further investigation of the different components of total nonbonded IEs implies that it is the vdW that contributes significantly higher energy than does the

TABLE 3.9
MD-Simulated IEs (kJ/mole) between Different Ionic Pairs of DES–Quinoline–Heptane Ternary System Calculated at 308.15 K and 1 Atm. Pressure

Ionic pair	Electrostatic interactions (E_{elec})	van der Waals interactions (E_{vdW})	Total nonbonded interactions (E_{total}[a])
MTP–Quinoline	−7.02	−17.85	−24.87
MTP–Heptane	−0.12	−4.23	−4.35
Br–Quinoline	−2.04	−1.16	−3.21
Br–Heptane	0.08	−0.22	−0.14
EG–Quinoline	−4.25	−12.75	−17.01
EG–Heptane	−0.01	−4.32	−4.33
Quinoline–Heptane	−0.03	−7.73	−7.76
DES–Quinoline	−13.31	−31.76	−45.09
DES–Heptane	−0.05	−8.77	−8.82

[a] $E_{total} = E_{elec} + E_{vdW}$.

electrostatic energy component to total nonbonded IEs. For example, in the total nonbonded IE between DES and quinoline within the DES–heptane–quinoline ternary system, the electrostatic energy component contributes only −13.31 kJ/mol, whereas −31.76 kJ/mol energy comes from the vdW interactions. A further decomposition of total DES–quinoline interactions into MTP–quinoline, EG–quinoline and bromide ion–quinoline interaction indicates that it is the DES–quinoline interaction that is the most favorable, and this is then followed by the EG–quinoline interaction. The least favorable interaction among these three is the bromide ion–quinoline interaction. In a similar manner, the decomposition of DES–heptane total nonbonded interaction suggests that MTP–heptane and EG–heptane interactions contribute almost equally. Furthermore, it should be noted that the lower the interaction energy between the molecules, the lower the solubility and the higher the phase separations. The degree of interaction energy is found to be in the following order: DES–quinoline > DES–heptane > quinoline–heptane.

Similarly, for the DES–benzene–hexane system (S12), the nonbonded IEs were presented in Table 3.10. From the data, it can be concluded that the nonbonded interaction for DES–benzene is more than that of the DES–hexane and benzene–hexane pairs. A further close investigation reveals that the interaction energy of DES–benzene is four times (−41.970 kJ/mol) higher than the DES–hexane (−11.599 kJ/mol). It implies that the vdW energy is more prominent than the electrostatic energy within the total nonbonded IEs. It is also observed from the IE between DES and benzene (DES + hexane + benzene) that the electrostatic energy component contributes only −8.892 kJ/mol, whereas the values are about −33.079 kJ/mol for the vdW interactions. Total nonbonded interaction between DES-benzene can be decomposed into MTP−benzene, ETG−benzene, and bromide ion−benzene interaction (Table 3.10). It indicates that among all other interaction pairs, DES-benzene

TABLE 3.10
IEs (kJ/mol) between the Different Interacting Components of DES–Benzene–Hexane Calculated at 318.15 K and 1 atm Pressure

Interacting moiety	Electrostatic interactions (E_{elec})	vdW interactions (E_{vdW})	Total nonbonded interactions (E_{total} a)
MTP–BEN	1.328	−17.215	−15.887
MTP–HEX	0.222	−5.737	−5.515
Br–BEN	−8.080	−1.049	−9.129
Br–HEX	−0.254	−0.254	−0.508
ETG–BEN	−2.140	−14.815	−16.955
ETG–HEX	−0.023	−5.553	−5.576
BEN–HEX	−0.012	−3.940	−3.953
DES–BEN	−8.892	−33.079	−41.970
DES–HEX	−0.055	−11.544	−11.599

[a] $E_{total} = E_{elec} + E_{vdW}$.

interaction is most favorable and is followed by the ETG–benzene interaction. The least favorable interaction among these is bromide–hexane interaction. In a similar manner, the disintegration of DES–hexane total nonbonded interaction suggests that MTP–hexane and ETG–hexane interactions are similar. Furthermore, it could be noted that because of the lower IE between the molecules, the solubility is less, and this results in higher phase separations. The order of IE is found to be as follows: DES–benzene > DES–hexane > benzene–hexane. In order to further justify the extraction process, here we computed the hydrogen bonds within the systems.

3.3.2 Structural Information

The radial distribution functions (RDFs) give evidence about the entire assembly about the interactions between the different moieties of the system in forms of structural properties. The RDFs provide information about the overall structure and interactions between different species of the system considered, albeit qualitatively. For DES–quinoline–heptane ternary system (S1), we first concentrate on the selected site–site radial distribution functions. These RDFs are shown in Figure 3.6. The atomic sites that are considered for calculating these pair correlation functions are PC1 atom of MTP, bromide ion (i.e., Br1), OE1 and HEO atoms of EG, NQ1 atomic site of quinoline, and HH1 atom of heptane (Figure 3.1). Considering the distribution functions involving different atomic sites of solvent DES and quinoline (Figure 3.6a–c), we found a strong and well-defined first solvation peak for all of them. This suggests strong interactions between DES and quinoline.

From the observation of Figure 3.6a–c, the quinoline molecule reaches within bromide moiety at 3 Å, indicating the formation of a weak bond, whereas in the case of MTP and EG, quinoline reaches within 3 Å and 1.5 Å, respectively. In contrast,

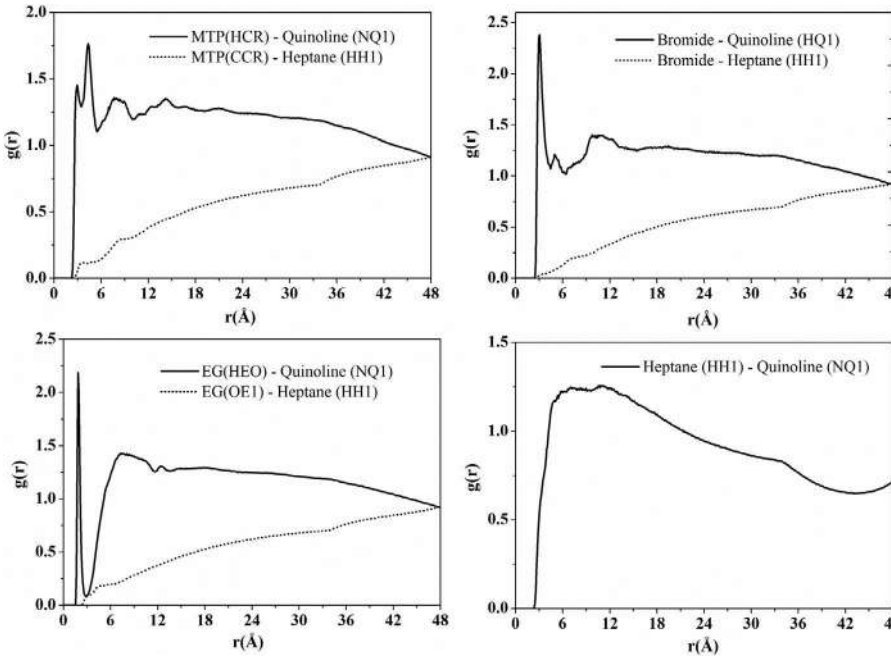

FIGURE 3.6 Atom–atom RDF plots between the different molecules present in the ternary system (a) MTP–quinoline and MTP–heptane, (b) bromide–quinoline and bromide–heptane; (c) EG–quinoline and EG–heptane, and (d) quinoline–heptane obtained at 200 ns.

the bromide ion exhibits a large g(r) peak when compared to other DES species. This signifies that the density distribution of quinoline molecule is higher for bromide ion. This phenomenon is further elucidated by the spatial distribution functions (discussed in Section 3.3.3). On the other hand, the intermolecular distances of DES species with quinoline and heptane is now calculated and reported in Table 3.11. As can be seen from Table 3.11, the intermolecular distances (which includes first and second solvation peaks) of bromide–quinoline is obtained at larger distances (7.64 Å) as compared to MTP–quinoline (4.97 Å) and EG–quinoline (7.03 Å).

In a similar manner, Figure 3.6 also presents the pair correlation functions involving different sites of DES and heptane. The unfavorable interactions between these molecules are quite apparent, as we do not find any sharp peak of these RDFs and the maximum peak heights are well below that of bulk density. The RDF involving the atomic sites of heptane and quinoline (Figure 3.6d) shows a broad peak with a maximum g(r) = 1.2, which is much lower than the maximum values of g(r) obtained for DES–quinoline RDFs. Furthermore, quinoline gave a larger g(r) peak with bromide compared to heptane, which reveals that the bromide ion also has a pronounced prominent role in the extraction process. On the other hand, the intermolecular distances between DES and heptane were obtained at 37–50 Å. Therefore, these findings suggest that the interactions between DES–quinoline are much more favorable than that of heptane and quinoline.

TABLE 3.11
Intermolecular Distances between the DES–Quinoline, DES–Heptane, and Quinoline–Heptane

Atom pairs	Distance (Å)
Br1–NQ1	7.64
HCR–NQ1	4.97
HEO–NQ1	7.03
OE1–HH1	45.84
CCR–HH1	49.86
OE1–HH1	37.01
NQ1–HH1	37.91

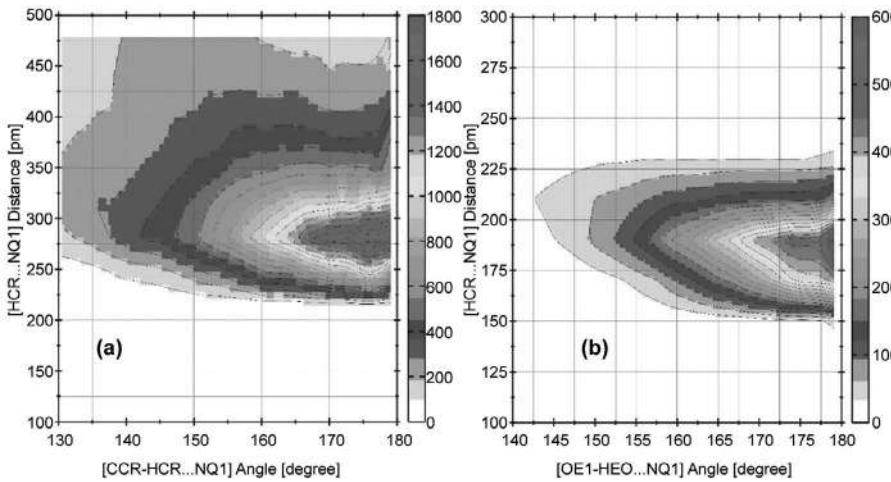

FIGURE 3.7 CDFs used to confirm the hydrogen bonds formed between the DES–quinoline by plotting the hydrogen bond distance (RDF) versus hydrogen bond angle (ADF) for the ternary system (a) CCR–HCR . . . NQ1 angle against corresponding HCR . . . NQ1 distance (MTP–quinoline) and (b) OE1–HEO . . . NQ1 angle against corresponding HEO . . . NQ1 distance (EG–quinoline).

Furthermore, CDFs (angular and radial) were also evaluated to confirm the presence of hydrogen bonding formation as a function of donor-acceptor distance and donor-hydrogen-acceptor angle, and the same is shown in Figure 3.7. For this, the CDF was plotted between the MTP (HCR)–quinoline (NQ1) and EG (HE1 and HEO)–quinoline (NQ1). The CDF was obtained by using the TRAVIS package, and the procedure for calculating this function were reported elsewhere [56]. From this analysis, we observed that the C–H . . . N bond was formed for both MTP–quinoline and EG–quinoline (Figures 3.7a and 3.8), while the O–H . . . N bond was formed for the EG–quinoline system (Figure 3.7b). These H-bonds were formed at approximately 3.0 Å and 1.95 Å for C–H . . . N and O–H . . . N with an angle of 140° to 180°,

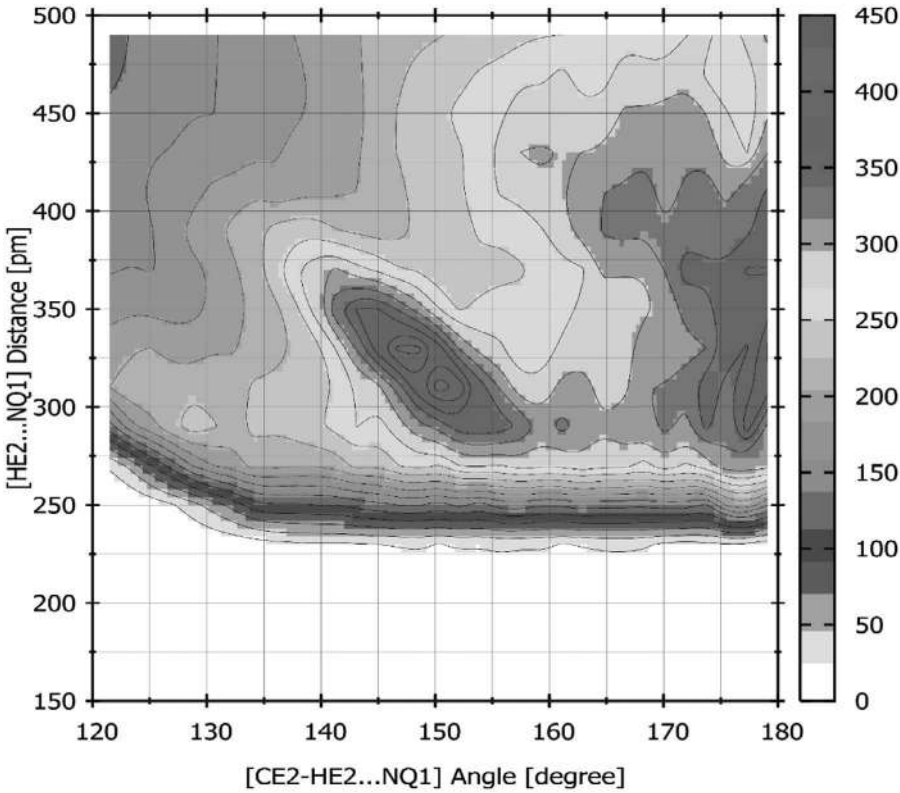

FIGURE 3.8 CDFs used to confirm the hydrogen bonds formed between the EG-quinoline by plotting the hydrogen bond distance (RDF) versus hydrogen bond angle (ADF) for the ternary system. CE1–HE1 . . . NQ1 angle against the corresponding HE1 . . . NQ1 distance.

respectively. Therefore, this confirms our observations with RDF peaks that were obtained at 3.0 Å and 1.95 Å for both molecular systems.

Similarly, for the DES–benzene–hexane system (S12), RDFs are shown in Figure 3.9. The atomic sites that are considered for calculating these pair correlation functions are C15 + P1 atom of MTP, bromide ion (Br1), O1 + C7 atoms of ETG, C1 atomic site of benzene, and C9 atom of hexane (Figure 3.1). From Figure 3.9a, a strong first solvation peak observed for MTP–benzene, which refers to interactions between DES and benzene. Figure 3.9b indicates the fact that the bromide ion are uniformly distributed around the benzene molecule as compared to hexane. This is due to the fact that benzene gave a larger g(r) peak with bromide as compared to hexane implying the fact that the bromide ion also helps in the extraction process along with the MTP cation. BEN–HEX also does not show a very sharp peak because of the higher selectivity of DES toward benzene as compared to hexane. It should be noted that the RDF of BEN–HEX would be different in the midst of the DES solvent molecule, which is the reason we do not observe a sharp peak for benzene-hexane

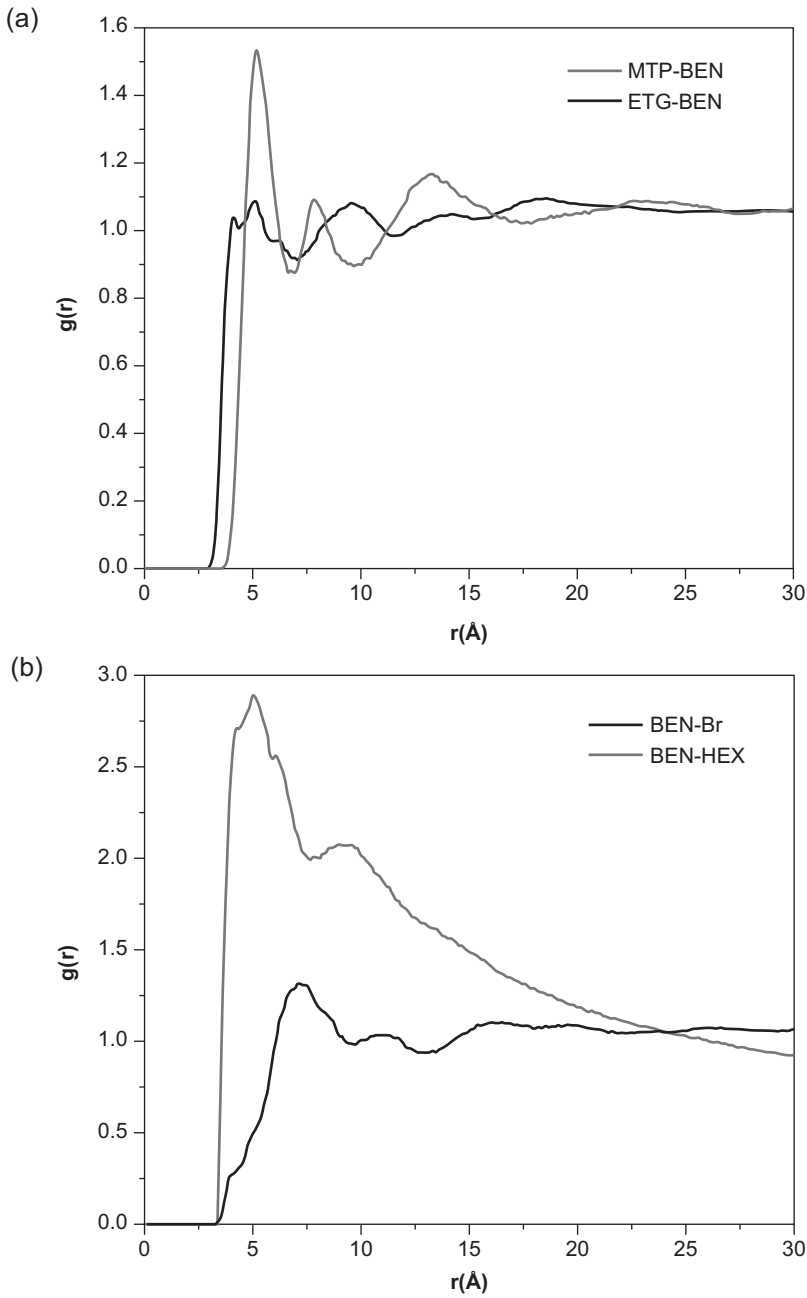

FIGURE 3.9 Atom–atom RDF plots between the different molecules present in the ternary system: (a) MTP–benzene and ETG–benzene and (b) benzene–bromide and benzene–hexane

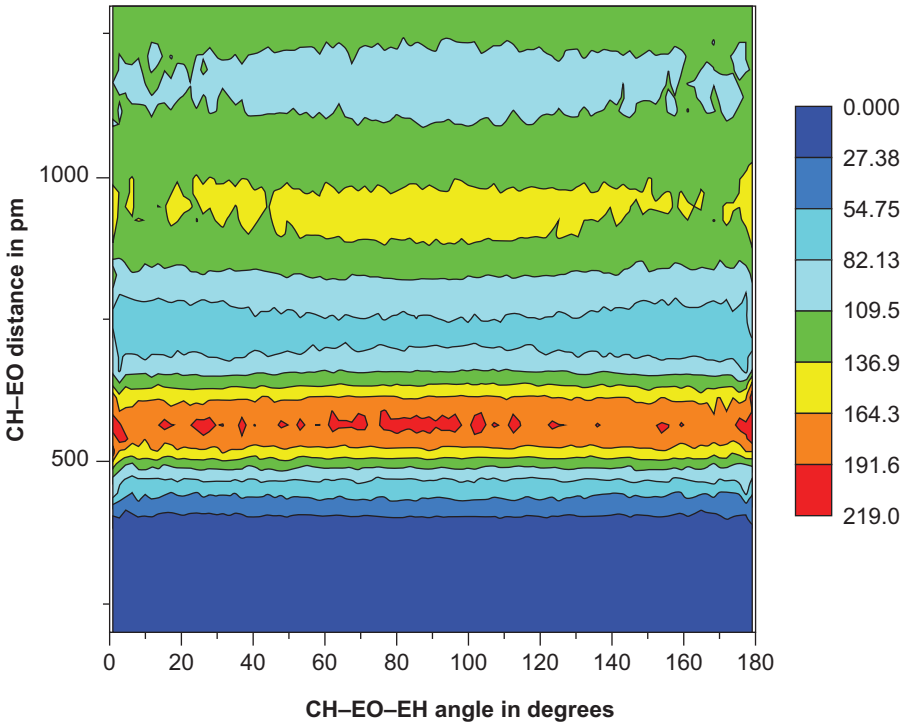

FIGURE 3.10 CDFs formed between the DES and benzene by plotting the hydrogen bond distance versus the hydrogen bond angle for C1–O1 . . . H7 angle against the corresponding C1 . . . O1 distance (BEN–ETG).

system. The first solvation shell coordination number for the DES components with benzene, such as MTP–BEN, ETG–BEN, and BEN–Br are 1.54, 1.04, and 2.9, respectively. The corresponding peaks are in a range of 4–5 Å. However, for the BEN–HEX, the coordination number is 1.3, with a prominent peak at 7 Å.

Furthermore, the CDFs were assessed to confirm the attraction of the DES–benzene pair. We have plotted the CDF in Figure 3.10, where the CDF was plotted between the angular and radial function of benzene–ETG. The TRAVIS package was used for calculating the CDF. A detailed procedure is reported elsewhere [56]. From Figure 3.10, we notice that the CH–EO . . . EH bond was formed for both benzene–ETG pairs. These H-bonds are formed in the range of approximately 3.0–5.0 Å (donor . . . acceptor) for the CH–OE . . . EH throughout the system. Thus, it agrees with previous RDF peaks (Figure 3.9), which are obtained at 4.15 Å for the ETG–benzene ionic pair of the systems.

3.3.3 SDFs

SDF give us details regarding the average density distribution of different type of species around a reference species. For DES–quinoline–heptane ternary system (S1),

SDFs of quinoline and heptane molecules in DES solution and are shown in Figure 3.11. The isovalues employed for the SDF corresponding to the DES–quinoline is 1.5 particle Å while the same for the DES–heptane is 0.05 particle Å. As can be seen that the more active ("N atom") sites of the quinoline molecule are surrounded by MTP molecule whereas the less active sites of quinoline surround the bromide ion and heptane. From the observation of Figure 3.11a–b, the bromide ion is highly distributed around the quinoline molecule as compared with other species. This fact is further confirmed by their RDF plots that the bromide ion exhibits a large g(r) peak with quinoline than with others. Therefore, the interaction energy between bromide and quinoline is lower than MTP–quinoline and EG–quinoline.

Moreover, the appearance of the distribution of EG molecule around the active side of quinoline is closer than that of MTP. In specific, the positions of the first peaks of these RDFs appeared at 1.95 Å and 2.85 Å, respectively. Furthermore, the densities of bromide ion and heptane molecules are distributed around the inactive side of quinoline (Figure 3.11a–c). It is also quite apparent that DES molecules are

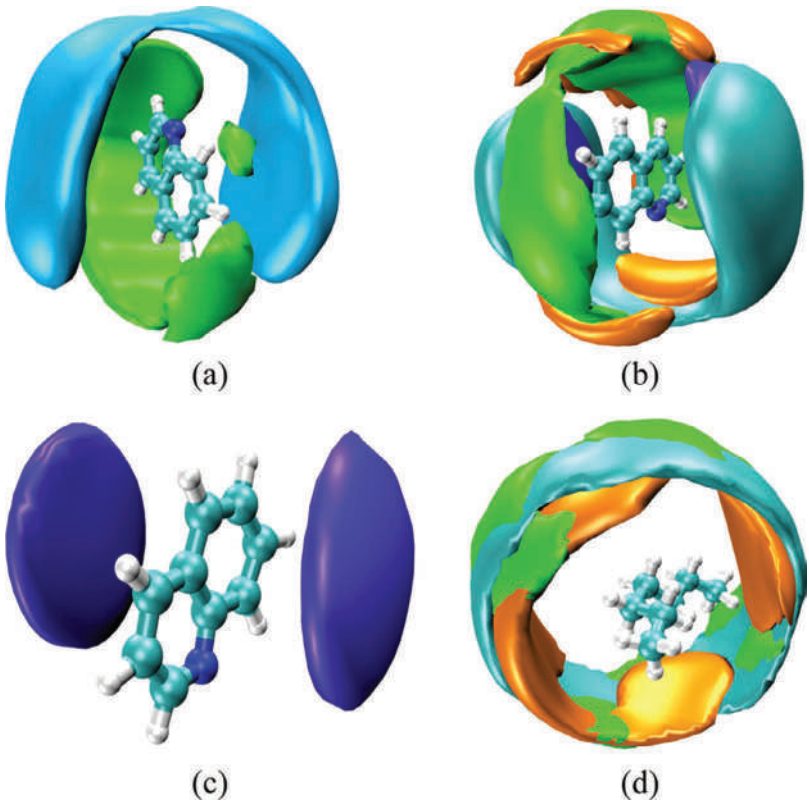

FIGURE 3.11 SDFs of the DES–quinoline–heptane system: (a) MTP and bromide around quinoline; (b) EG, bromide, MTP, and heptane around quinoline; (c) heptane around quinoline; and (d) DES around heptane molecule. Orange, green, cyan, and violet surfaces refer to EG, Br, MTP of DES, and heptane, respectively.

distributed at a distance that is very far from the heptane molecule (Figure 3.11d), which hinders the interactions between DES and heptane. Therefore, the surfaces of DES are very closely distributed around the active sides of quinoline. Thus, the quinoline molecules are susceptible in getting attracted to the DES molecule in the solution.

Similarly, for DES–benzene–hexane system (S12), Figure 3.12 shows the reference MTP and benzene molecules in the DES solution. Here, the active isovalues were used to plot the SDFs. The value of DES–benzene is 1.5 Å and that for MTP–hexane is 0.64 Å. The SDF plots suggest that the phenyl group of MTP acts as an electron-withdrawing group and attracts benzene electron cloud, enabling it to form CH–π type with MTP. Benzene is also set to form a CH–O-type hydrogen bond with ETG. This type of hydrogen bonding is also confirmed by two-dimensional (2D) nuclear magnetic resonance (NMR) by cross-peaks and active sites of benzene with DES components. Overall, from Figures 3.12a–b, it is clear that all the interactive moieties are highly distributed around the MTP molecule as compared with other species.

Therefore, the interaction energy between bromide and benzene is lower than that of MTP–benzene and ETG–benzene. Moreover, the appearance of the distribution of the ETG molecule around the benzene is closer than that of MTP. The positions of the first peaks of these RDFs appear for benzene–MTP and benzene–ETG at 4.95 and 5.15 Å, respectively. Furthermore, the densities of the bromide ion and hexane molecules are also distributed around the MTP (Figure 3.12a–e). The hexane molecules are distributed at a distance that is very far from the MTP molecule (Figure 3.12d),

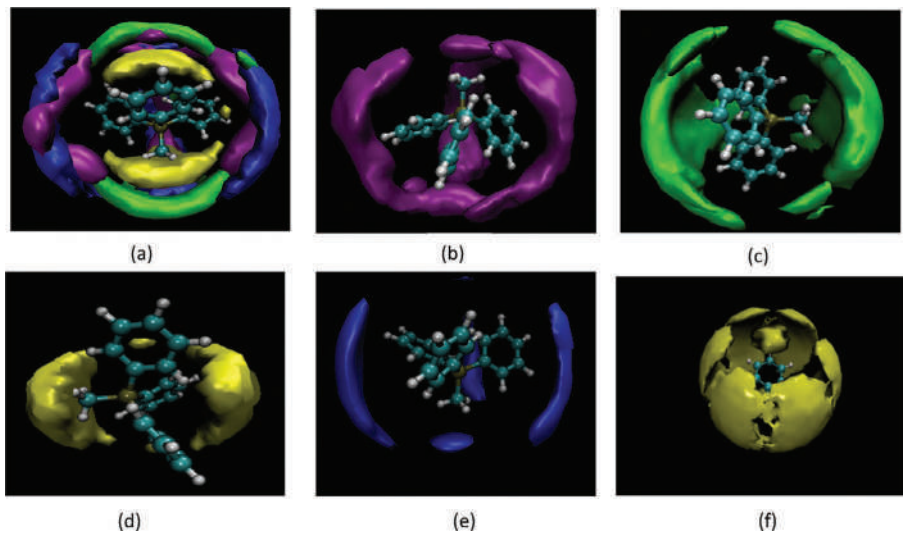

FIGURE 3.12 SDFs of the DES–benzene–hexane system: (a) benzene, hexane, Br, and ETG around MTP; (b) benzene around MTP; (c) Br around MTP; (d) ETG around the MTP molecule; (e) hexane around the MTP molecule; (f) ETG around the benzene molecule. Violet, green, blue, and yellow surfaces refer to benzene, Br, hexane, and ETG, respectively.

which can also be confirmed from the RDF plot. Figure 3.12f suggests that the ETG lies very close to the benzene moiety, initiating a high interaction compared to hexane. Hence, it is obvious that the isosurfaces of benzene are distributed around the active sites of DES, which implies that DES more effectively extracts the benzene molecules from the mixture. The interaction between the benzene and hexane needs to be overcome by the DES moiety so as to extract benzene from hexane. Both RDF and SDF indicate a strong H-bond as the interacting moieties of the DES get attracted to a larger extent toward benzene compared to hexane.

3.3.4 Hydrogen Bond Properties

For the formation of a hydrogen bond, a donor atom with a hydrogen atom bonded to it and an acceptor atom that is not bonded to donor atom are required. Furthermore, the absolute distance between donor and acceptor atoms should be less than or equal to the cutoff distance, and the angle between donor–hydrogen–acceptor pair or angle *D-H-A* should be greater or equal to the cutoff angle, where the angle and the distance are user-defined.

Figure 3.13 presents the average number of DES–quinoline hydrogen bonds per quinoline molecule as a function of simulation time. We have used geometric

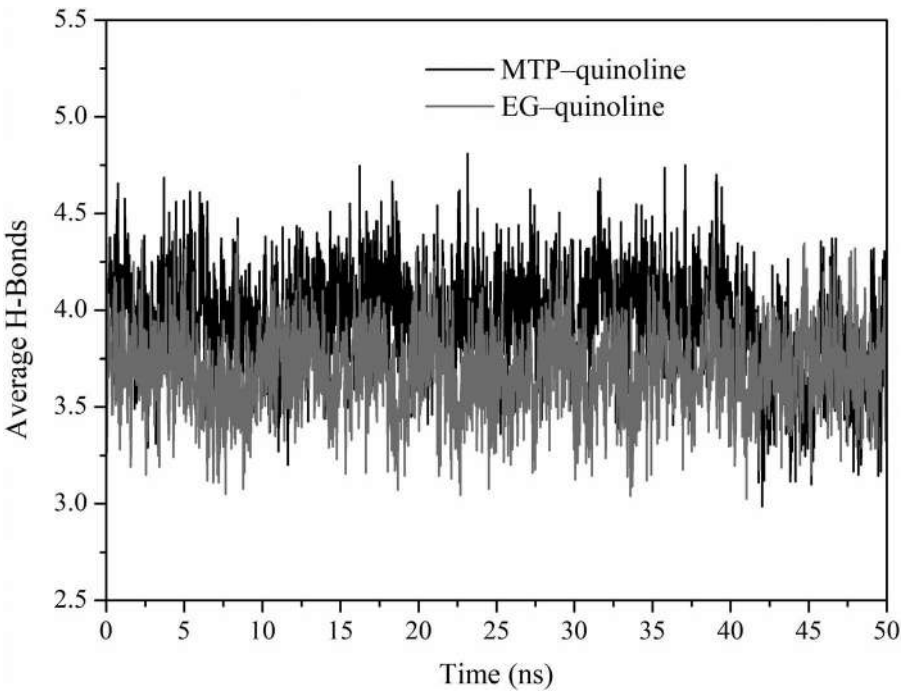

FIGURE 3.13 Average number of MTP–quinoline and EG–quinoline hydrogen bonds per quinoline molecule as a function of simulation time.

criteria of hydrogen bond calculation as used in some previous studies [62–64]. The last 50 ns of the production time was considered for criteria. It should be noted that MTP forms a C–H . . . N bond with quinoline at an average distance of approximately 3.0 Å (Figure 3.7a). In the case of EG, two different types of H-bonds are involved, namely, C–H . . . N (~3.0 Å; Figure 3.8) and O–H . . . N (1.95 Å; Figure 3.7b). Therefore, from the evidence of RDF (Figure 3.6) and CDF plots (Figure 3.7), the conditions for the acceptor–donor distance are fixed to 3.5 Å while the cutoff angle is taken from 140–180° for both the systems (MTP–quinoline and EG–quinoline). From Figure 3.13, it was observed that HBD of DES (i.e., EG) engages in forming a slightly lesser number of H-bonds with quinoline molecules than its salt partner (HBA, MTP). Again, between MTP–quinoline and bromide–quinoline molecules, MTP established a higher number of H-bonds with quinoline than with bromide. The average H-bond numbers of bromide–quinoline are not significant (not shown). Here, it is worth mentioning that, as expected, we do not notice any hydrogen bonding interactions between DES–heptane and quinoline–heptane molecules.

Figure 3.14 represents the average number of hydrogen bonds between the DES–benzene pair per benzene molecule as a function of simulation time. We have used

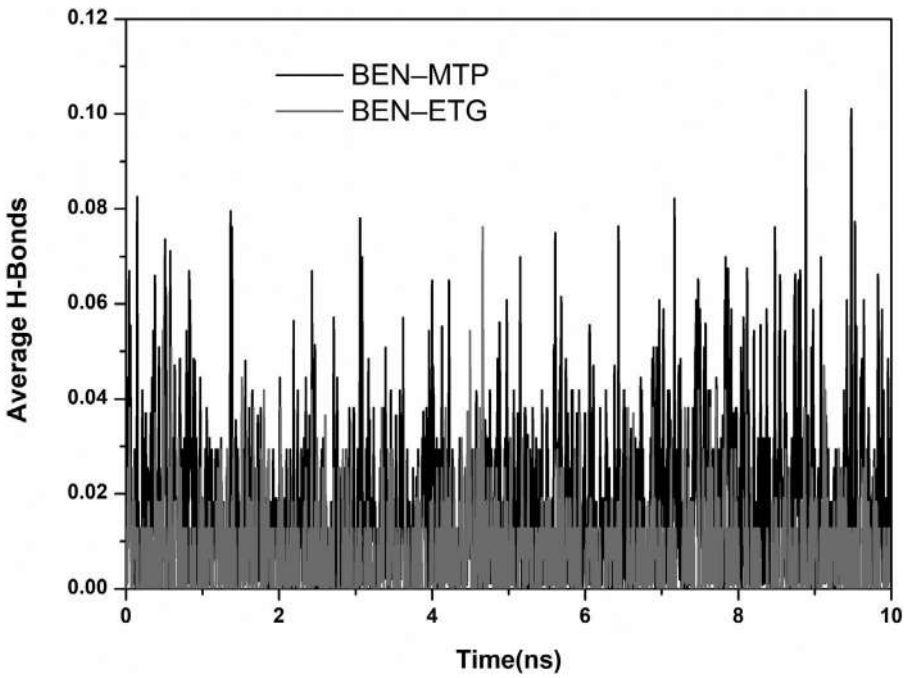

FIGURE 3.14 The average number of MTP–benzene and ETG–benzene hydrogen bonds per benzene molecule.

geometric criteria of hydrogen bond calculation as used in our previous studies [64], and the last 10 ns are considered for this computation. It should be noted that we have quantified the nonbonded interaction energies as in Table 3.10, while the hydrogen bonding interactions are discussed qualitatively. Overall, it can be said that the higher the number of average H-bonds, the stronger will be the interaction between the interacting pair. Furthermore, nonbonded interaction energies in Table 3.10 shows the energies between interacting pairs in kJ/mol. Therefore, here we cannot compare nonbonded energies directly with hydrogen bonding as it also indicates interactions due to induced dipoles, quadrupoles, and so on. However, the hydrogen bonding here is corroborated or related to a higher interaction due to the observed increase in the average number of hydrogen bonds [65, 66].

It should be noted that benzene forms C–H . . . P1 bond with MTP at an average distance of about 3.0 Å. The same can be revealed from the RDF (Figure 3.9), while the cutoff angle is taken from 10° to 180° for both the systems (MTP–benzene and ETG–benzene). From Figure 3.14, it is observed that the HBD of DES (i.e., ETG) has a slightly higher number of H-bonds with benzene molecules than its HBA part, namely, MTP. This is due to the fact that the oxygen atom in ETG acts as an active site for the formation of hydrogen bonds with benzene. Again, in between MTP–benzene and bromide–benzene molecules, MTP forms a higher number of H-bonds with benzene than bromide. The average number of H-bonds for bromide–benzene is much less in comparison to the benzene–MTP and benzene–ETG. There are no significant hydrogen bonding interactions found between DES–hexane and hexane–benzene pairs.

3.3.5 Transport and Diffusive Properties

The overall mobility of the different species in the phase equilibrium can be obtained by estimating the self-diffusion coefficient (D). The self-diffusion coefficients of different species were calculated by using Einstein's equation (Equation 3.3) [67–70].

$$D = \frac{1}{6}\lim_{t\to\infty}\frac{d}{dt}\left\langle \sum_{i=1}^{N}\left|r_i(t) - r_i(0)\right|^2 \right\rangle, \tag{3.3}$$

where $r_i(t)$ and $r_i(0)$ are the positions of the ith atom at time t and 0, respectively. Here, the expression in bracket indicates the MSD of the molecule. The presence of factor 1/6 is attributed to the three-dimensionality of the system. The self-diffusion coefficients of respective species are calculated from the long time slope of the MSD curve (Figure 3.15 and Figure 3.16). It shows that all the MSD plots have linearity. Here, it is worth mentioning that the diffusion coefficient values for different species were calculated by averaging over different time origins, which are listed against different time intervals with a time window of 10 ns.

For DES–quinoline–heptane ternary system (S1), Figure 3.15 shows the MSD curves of the different species of the system. This can shed some light on the overall transfer process of quinoline molecules from the heptane-rich phase to the DES

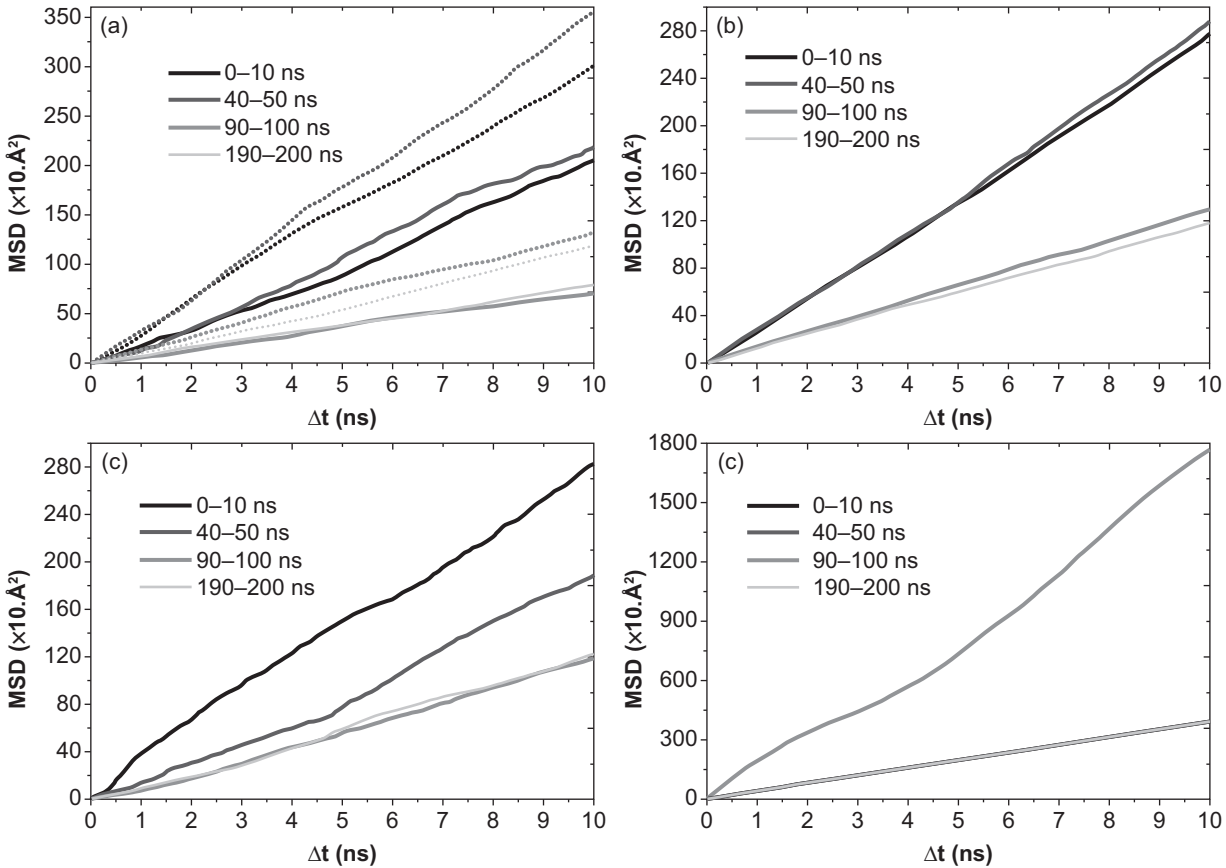

FIGURE 3.15 MSD plot of (a) MTPB (solid lines correspond to MTP and dashed lines correspond to Br), (b) EG, (c) quinoline, and (d) heptane.

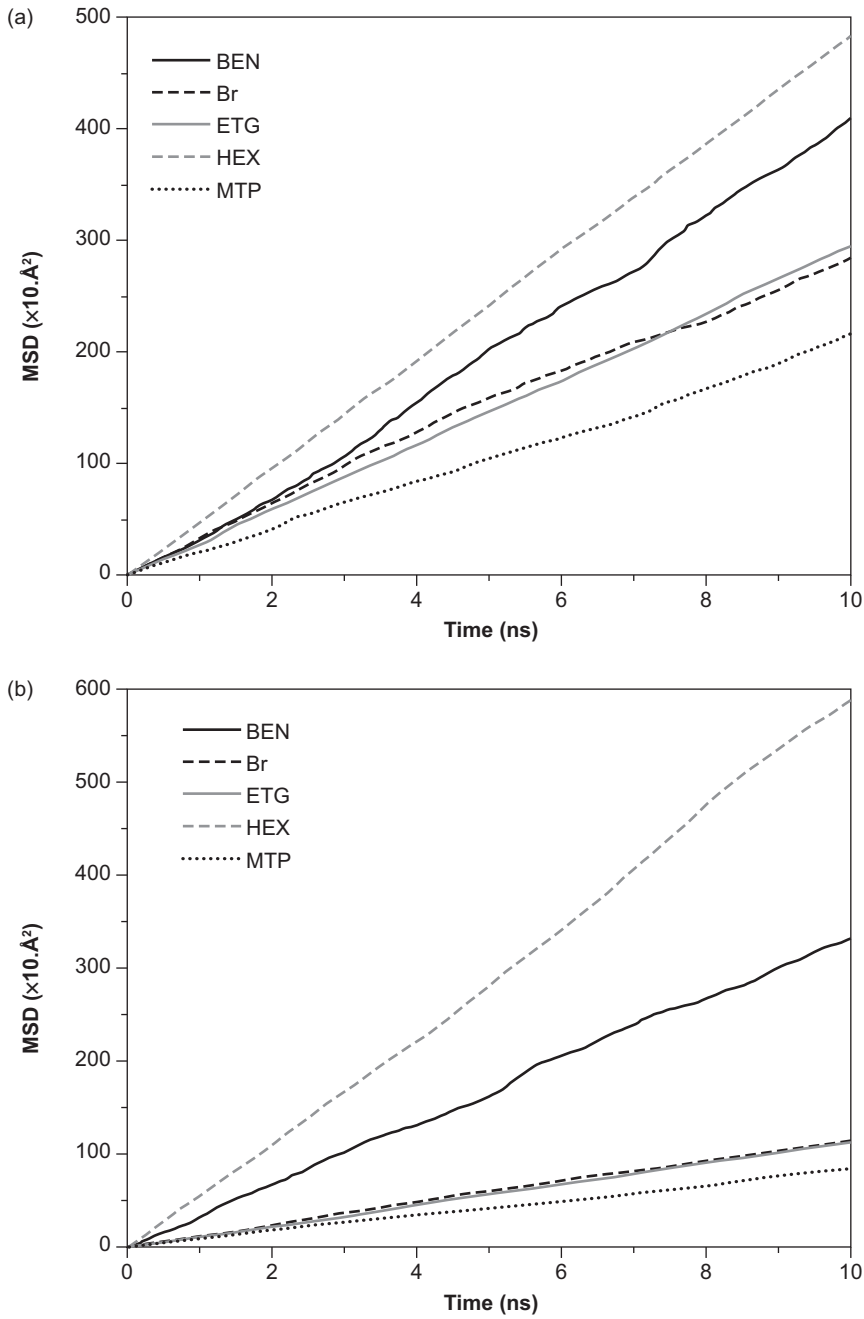

FIGURE 3.16 MSD curve of DES–benzene–hexane ternary system (a) 0–10 ns and (b) 90–100 ns.

phase. From Table 3.12, we make a few interesting observations: (1) at the beginning of the production run (0–10 ns), the self-diffusion coefficient values of all components were found to be relatively close, and (2) a further increase in simulation runtime tends to lower the diffusion coefficient of both quinoline and DES. These species possess similar self-diffusivities, which makes the transfer of quinoline molecules to the DES phase possible. On the other hand, it was observed that the closer the self-diffusion coefficient value of two components, the higher the interaction between the molecules and vice versa. The self-diffusion coefficient value of heptane remains practically unchanged throughout the simulation time.

From these observations, we propose the following: (1) The transfer of quinoline from the heptane phase to the DES phase takes place at about 50 ns. (2) The strong favorable electrostatic interactions between quinoline–MTP cation, quinoline–bromide ion, and quinoline–EG (Table 3.9) cause a sharp drop in the diffusion coefficient value of quinoline (i.e., quinoline moving along with the DES). This in turn, decreases the translational motion of MTP, bromide ions, and EG molecules, and (3) since the electrostatic interactions between quinoline–heptane are very weak, the removal of quinoline molecules from the heptane phase does not influence the self-diffusion coefficient of heptane.

For the DES–benzene–hexane ternary system (S12), Figure 3.16 shows the MSD curves of the different species of the system, and Table 3.13 summarizes about its diffusion coefficient values for different types of molecules over time bounds of 10 ns. This highlights the overall mass transfer process of benzene molecules from the hexane-rich phase to the DES phase. The self-diffusion coefficient (D) values of all species of the system were comparatively close in the initial stage of simulation at 0–10 ns. By the end of the simulation (90–100 ns), the values are lower for both benzene and DES components. The smaller diffusivity value of DES and benzene implies stability for extracted benzene within DES, indicating that they move together. The high diffusion coefficient value of hexane is nearly the same throughout the simulation. The strong interactions between benzene–MTP cation, benzene–bromide ion, and benzene–ETG (Table 3.10) cause

TABLE 3.12
Self-Diffusivity of Different Molecular Species for DES–Quinoline–Heptane Ternary System at 308.15 K[a]

Molecule species	Diffusion coefficient × 10^{-9} m^2 s^{-1}			
	0–10 ns	**40–50 ns**	**90–100 ns**	**190–200 ns**
Bromide ion	0.4921	0.5910	0.2196	0.2010
MTP cation	0.3503	0.3898	0.1231	0.1300
Ethylene glycol	0.4587	0.4776	0.2145	0.1940
Quinoline	0.4454	0.3264	0.2067	0.2110
Heptane	0.6466	0.6569	0.7006	0.6430

[a] Diffusion coefficient values are reported at a time window of 10 ns.

TABLE 3.13
Self-Diffusivity Value of Various Moiety of DES–Benzene–Hexane Ternary System at 318.15 K

Molecule species	Diffusion coefficient × 10^{-9} m^2 s^{-1}	
	0–10 ns	90–100 ns
Bromide ion	0.464	0.197
MTP cation	0.350	0.135
Ethylene glycol	0.491	0.190
Benzene	0.666	0.559
Hexane	0.809	1.000

a decrease in benzene diffusivity alone or, in other words, get attracted to DES. Due to weak interactions between benzene and hexane, the DES can extract benzene effectively.

3.3.6 2D NMR Analysis

The 2D ^{1}H–^{13}C heteronuclear multiple bond correlation (HMBC) NMR was performed in order to investigate the hydrogen bonding interactions among components of DES and benzene (Figure 3.17). In the DES–benzene system, there exists a hydrogen bond among benzene, MTP, and ETG, which is confirmed from our MD simulation. In particular, there exists a hydrogen bond of XH–π (X = C, O) type between benzene and DES. It should be noted that the XH–π (BEN) systems, such as benzene containing π-electrons, can also initiate the formation of XH–π bonds. The strength of such bonds depends on the nature of X attached to hydrogen. Figure 3.17 shows the ^{1}H–^{13}C HMBC spectrum of DES–benzene in DMSO-d_6 at 318.15 K. From the figure it is found that there exists a hydrogen-bond interaction between the ETG (CH)–π and MTP (CH)–π of benzene. The ^{1}H–^{13}C HMBC NMR provides information for protons and carbons that are connected via one and multiple (up to four) bonds, respectively. From Figure 3.17, the ETG (CH), which resonates at 3.20 ppm, shows cross-peaks with BEN(C) at 120.15 ppm, and MTP (CH) at 7.75 ppm shows cross-peaks with BEN(C) at 120.5 ppm. These cross-peaks indicate that a strong multiple bond correlation exists among the benzene and interactive moiety of DES. Furthermore, the cross-peaks of benzene with ETG and MTP in 2D ^{1}H–^{13}C HMBC is also confirmed from Figure 3.12 as it shows the presence of benzene in close vicinity of MTP, ETG, and bromine, which makes them capable of forming hydrogen bonding. This is in line with the findings for RDF and CDF as discussed in Section 3.3, giving evidence of close interaction between DES and benzene. The ^{1}H spectra of the DES are provided in the previous chapter (Figure 2.2) and the ^{13}C NMR spectra of the DES is reported in Figure 3.18.

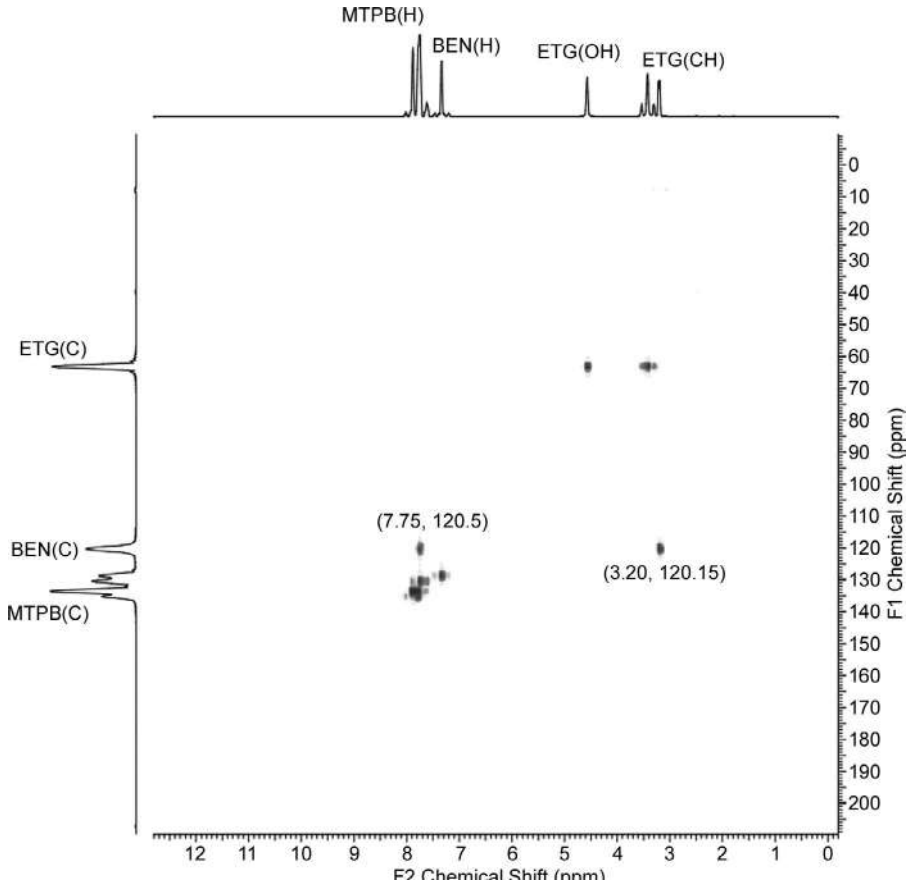

FIGURE 3.17 ^{1}H–^{13}C HMBC NMR spectra of DES–benzene.

3.4 EXTRACTION OF NITENPYRAM FROM AN AQUEOUS ENVIRONMENT

The extraction efficiency and selectivity of the pesticide nitenpyram were compared and validated against Florindo et al. [23] with DL-menthol–octanoic acid DES in a molar ratio 1:1. The simulation protocol was the same as mentioned earlier, albeit with a different simulation box configuration due to the addition of a new drug species (nitenpyram). Table 3.3 describes the number of molecules considered for the simulation. Figure 3.2 displays the structures with atomic notations of the molecules present in the system, and Figure 3.19 shows the snapshots of the system at two different time steps, 0 ns and 100 ns. After successful completion of the simulation, the nonbonded IE, RDF and CDF, SDF, hydrogen bonding properties, extraction efficiency, and selectivity of the pesticide were obtained and compared with the experimental results. All the simulations were carried out in triplicate for minimizing the error. For the calculation of distribution ratio (β) and selectivity (S), the following equations were used: [10]

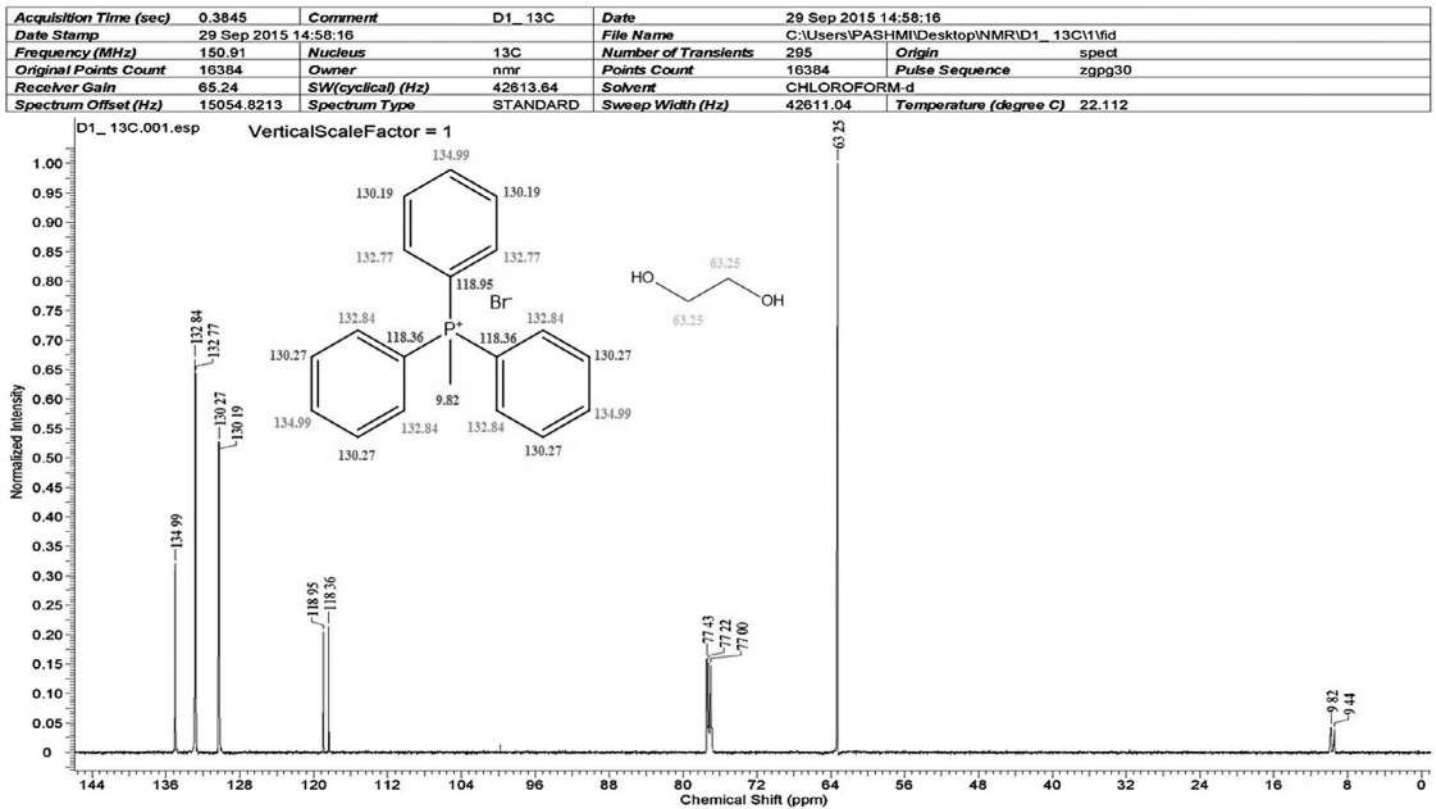

FIGURE 3.18 ^{13}C NMR spectra of DES.

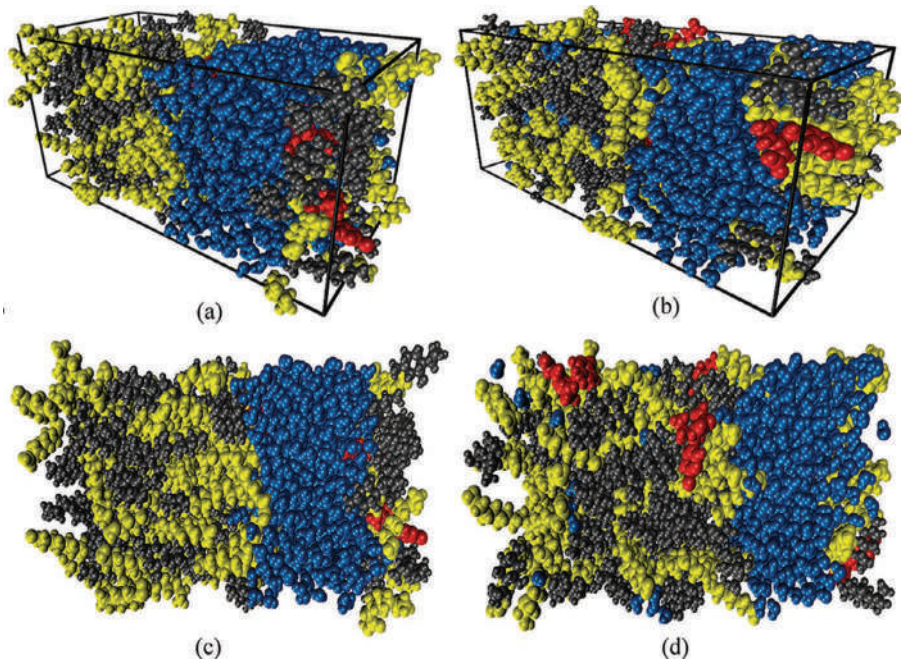

FIGURE 3.19 Distribution snapshots of nitenpyram in the solvent at different times: (a) and (b) 0 ns and (c) and (d) 100 ns, respectively (gray: menthol molecules; yellow: octanoic acid molecules; blue: water molecules; red: nitenpyram molecules).

$$\beta = \frac{x^E_{nitenpyram}}{x^R_{water}} \tag{3.4}$$

$$S = \frac{\beta_{nitenpyram}}{\beta_{water}} = \frac{x^E_{nitenpyram} / x^R_{nitenpyram}}{x^E_{water} / x^R_{water}} \tag{3.5}$$

Here, x^{E}nitenpyram and x^{R}nitenpyram denote the mole fractions of nitenpyram in DES-rich and water-rich phases, respectively. x^{E}water and x^{R}water denote the mole fractions of water in DES-rich and water-rich phases, respectively. Higher β values normally indicate a higher distribution of nitenpyram from the water phase to the DES phase. The higher the S, the greater the ability of DES in extracting nitenpyram from water. From Table 3.4, it can be concluded that the DES can be used for the extraction of nitenpyram from the water phase, and the MD simulation results confirmed the experimental nitenpyram extraction as shown in Table 3.14. To evaluate the extraction efficiency (%EE) of nitenpyram from water, the concentrations of nitenpyram in the aqueous phase before (C_o) and after extraction (C) can be used as follows:

$$\%E = [(C_0 - C) / C_0] \times 100 \tag{3.6}$$

TABLE 3.14
Comparison of Experimental and Simulated Result for DES (x_1) + Nitenpyram (x_2) + Water (x_3) at T = 298.15 K and 1 atm Pressure[a]

System No.	DES-rich phase			Water-rich phase			Distribution ratio (β)		Selectivity (S)	
1	x_1	x_2	x_3	x_1	x_2	x_3	Exp.	Comp.	Exp.	Comp.
	0.888	0.093	0.018	0.006	0.004	0.990	0.66	0.72	39.61	55.25

[a] The experimental value is taken from Florindo et al. [23].

TABLE 3.15
MD-Simulated Interaction Energies (kcal/mol) between the Different Component Pairs of Menthol–Octanoic Acid–Nitenpyram in 298.15 K and 1 Atm Pressure

Component pairs	Electrostatic interactions (*Eelec*)	Van der Waals interactions (*EvdW*)	Total nonbonded interactions (*Etotal a*)
Nitenpyram–water	–0.07	–0.03	–0.11
Nitenpyram–octanoic acid	–0.27	–0.54	–0.81
Nitenpyram–DL–menthol	–0.08	–0.60	–0.68
DL–menthol–octanoic acid	–4.35	–8.42	–12.77
DES–nitenpyram	–0.35	–1.13	–1.49

[a] $E_{total} = E_{elec} + E_{vdW}$.

The EE% calculated on the basis of simulated result ranged between 42–46.7%, whereas the experimental efficiency is 39.6% [24]. The slight variation in the simulated result occurred due to the presence of the molecules in the interfacial region leading to numerical inaccuracy in calculating the exact number of molecules present in that region. The simulated distribution ratio was also calculated, which is defined as the ratio of the concentration of the pesticide in the DES phase to the concentration in the water phase. The experimental distribution ratio [24] (0.67) was very close to the simulated distribution ratio (0.72) as shown in Table 3.14.

3.4.1 Nonbonded Energies

To study the interactions between the different molecules, we have quantified the total nonbonded interaction energies in terms of electrostatic and vdW interactions as shown in Table 3.15. It can be noticed that the nonbonded interactions between nitenpyram–menthol and nitenpyram–octanoic acid were more favorable than nitenpyram–water and menthol–water. A further investigation revealed that the vdW interactions were higher than electrostatic interactions between nitenpyram and DES

components (menthol and octanoic acid). However, in the case of nitenpyram–water and menthol–water, the electrostatic interactions were dominant compared to the vdW interactions. The total nonbonded interaction energy between DES and nitenpyram was −1.49 kcal/mol where the electrostatic contribution was an order of magnitude lower. This was contrary to that observed for nitenpyram and water.

The total nonbonded interaction energy (−12.78 kcal/mol) between the DES components was much higher than the other component pairs, which indicated a higher stability of the DES in the water system. Further evaluation of the interactions of DES, nitenpyram, and water suggested that the nitenpyram–octanoic acid interaction (−0.81 kcal/mol) was the most favorable, followed by nitenpyram–menthol (−0.68 kcal/mol). The interaction between nitenpyram and water was the least favorable (−0.11 kcal/mol).

3.4.2 Local Structural Ordering

RDFs are shown in Figure 3.20, where the selected atoms for different molecular species were O1 atom of nitenpyram, H51 and O5 atom of octanoic acid, H35 atom of DL-menthol, and H57 atom of the water molecule (notations as in Figure 3.2). It appeared that the well-defined first solvation shell for the DL-menthol and nitenpyram molecules was at 2 Å, suggesting a higher interaction between these two species (Figure 3.20a). The presence of water molecules at the first solvation shell (1.95 Å) was also observed, suggesting an interaction between nitenpyram and water. However, the coordination number of water molecules around nitenpyram moiety was 1.50, which was lower than DL-menthol around nitenpyram moiety (1.90), indicating a weaker interaction among them. For octanoic acid, it was at 3.35 Å (Figure 3.20a), justifying a relatively weaker interaction compared to nitenpyram–DL-menthol. A sharp peak was observed for DL-menthol and octanoic acid moiety at 2.05 Å (Figure 3.20b), reflecting a very strong HBA–HBD interaction and leading to the fact that the DES did not disintegrate in the presence of an aqueous environment. Moreover, a higher coordination number of HBA–HBD (5.50) compared to a very low value of HBD–water (0.75) strongly supports the higher stability of the DES in an aqueous medium.

In addition to the RDFs, CDFs are presented in Figure 3.21 to incorporate the angular structural analysis. The CDFs confirmed the formation of hydrogen bonding between donor and acceptor atoms. Figures 3.21a–b represent the CDF plots for nitenpyram–DL-menthol and nitenpyram–water, respectively, to identify possible hydrogen bonding between the species. The –NOO site of the nitenpyram molecule acquired a negative charge density due to the presence of a highly electronegative element and can be considered as an active site for other species containing a positive charge. Hence, we observed that of N–O . . . H bond was formed for both nitenpyram-DL-menthol and nitenpyram-water at a distance of approximately 2 Å (Figure 3.21). These bonds were formed with an angle ranging from 140–180°. Both interactions justify the criteria for the formation of hydrogen bonds. Comparing the color code values for both interactions, it can be observed that nitenpyram–menthol hydrogen bonding was higher than nitenpyram–water. Figure 3.21 confirmed the positions of the RDF peaks obtained in Figure 3.20. The presence of hydrogen bonding can further be analyzed by calculating the average hydrogen bond between the molecular species.

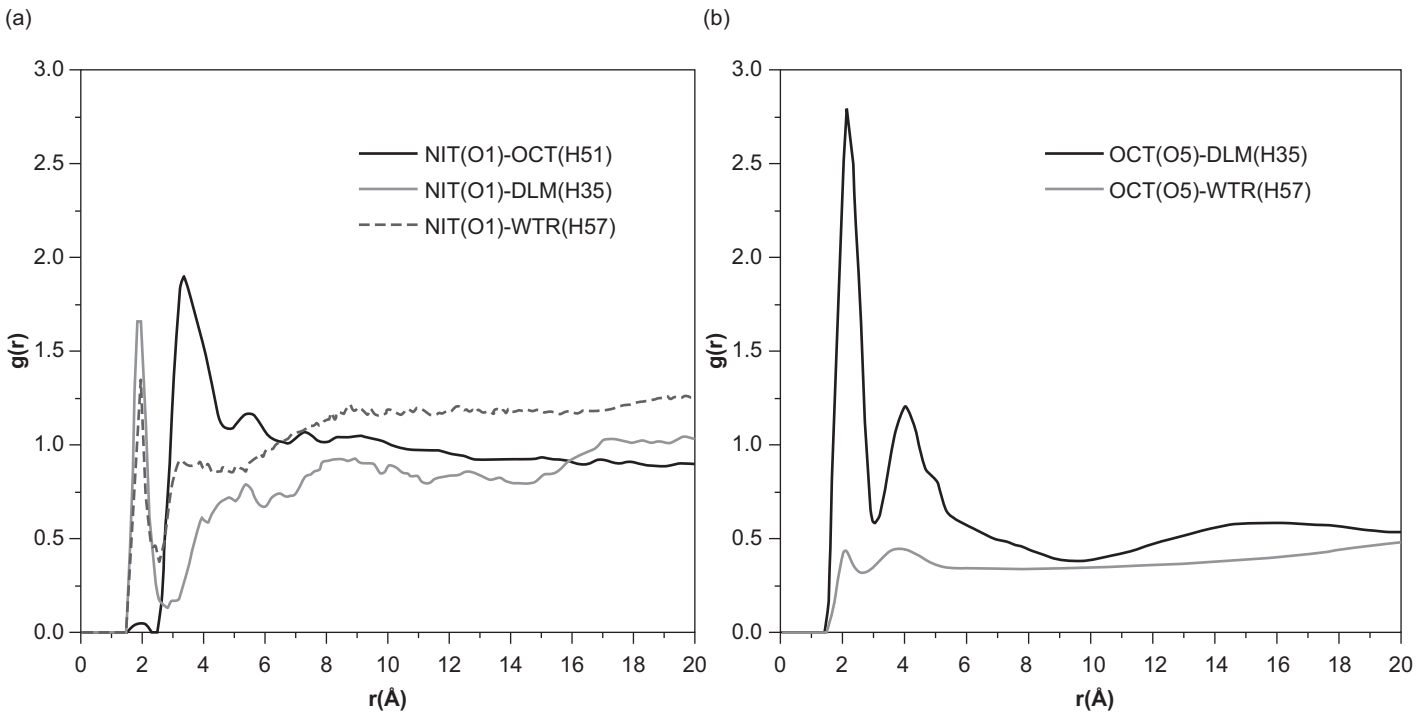

FIGURE 3.20 Comparison among atom-specific radial distribution function plots between the different molecular pairs present in the system: (a) nitenpyram–octanoic acid, nitenpyram–DL-menthol, and nitenpyram–water and (b) DL-menthol–octanoic acid and octanoic acid–water at 100 ns.

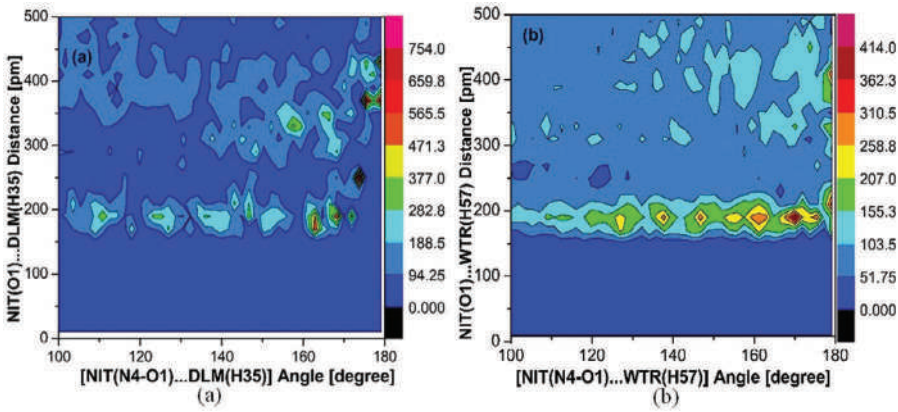

FIGURE 3.21 CDFs obtained by plotting the hydrogen bond distance versus the hydrogen bond angle for (a) N4-O1(nitenpyram) . . . H35 (DL-menthol) angle against O1 . . . H35 distance, (b) N4-O1(nitenpyram) . . . H57(water) angle against O1 . . . H57 distance

3.4.3 Density Distribution

SDFs are a convenient way to represent the three-dimensional density distribution. These are shown in Figure 3.22 obtained using the TRAVIS package [56]. These SDFs were generated to indicate the average density distribution of different molecules around a reference nitenpyram molecule. The isovalues employed for the SDFs corresponding to DES–nitenpyram were 1.5 Å, while that for nitenpyram–water was 0.05 Å. It can be observed that the nitenpyram molecule was closely surrounded by water (blue) and menthol molecules (green) at about 2 Å (Figure 3.22a). It justified the findings from the RDFs and CDFs as mentioned before (Figures 3.20 and 3.21). The smaller size of the water molecule and reasonably good interaction with nitenpyram made it feasible for higher distribution. The higher distribution of water was observed primarily around the N–O–O region of nitenpyram, which can be considered as probable active sites. Figure 3.22c certainly confirmed the higher density distribution of water molecules around nitenpyram. In fact, all the components displayed relatively comparable density distributions around nitenpyram. Octanoic acid molecules (yellow) were distributed around nitenpyram at a distance of approximately 3.3 Å. The appearance of the density distribution of menthol closer to the active site revealed its slightly higher interaction with nitenpyram when compared to the octanoic acid molecule (Figure 3.22b) in spite of the higher IE of the latter. One important aspect to be noticed here was the absence of water around the DES moieties, indicating the hydrophobic nature of the DES.

3.4.4 Hydrogen Bonding Associated with Nitenpyram

The average number of hydrogen bonds between nitenpyram and other molecular species present in the system as a function of simulation time is shown in Figure 3.23.

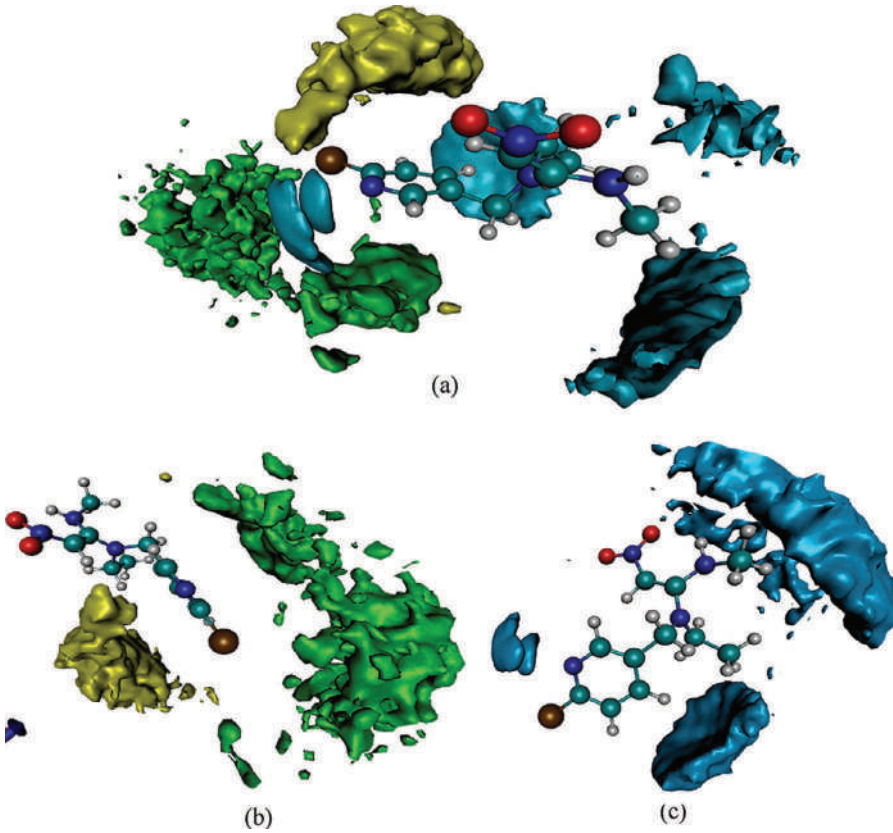

FIGURE 3.22 SDFs obtained for the system: (a) DLM, OCT, and water around NIT; (b) DES around NIT; (c) water around NIT molecule. Green, yellow and blue surfaces refer to DL-menthol, octanoic acid, and water, respectively

The geometric criteria of the hydrogen bond calculation were already mentioned [63]. The cutoff donor-acceptor distance was taken as 3.5 Å and the cutoff angle as 135–180° considering the results obtained in the RDF and the CDF as shown in Figures 3.20 and 3.21, respectively. As previously shown in the CDF calculation section, we performed a qualitative analysis in view of the probable formation of H-bonding between molecules. Thus, we obtained the quantitative analysis of hydrogen bonding of nitenpyram with DES molecules and water molecules. As revealed by Figure 3.23, the number of average hydrogen bonding between two species was found to be in the order of nitenpyram–octanoic acid (0.18) > nitenpyram–DL-menthol (0.14) > nitenpyram–water (0.12). The presence of carboxyl group (–COOH) in octanoic acid also aided in the formation of hydrogen bonds with the active site (–NOO) of nitenpyram. Meanwhile, it should be mentioned that, as expected, we do not observe any significant hydrogen bonding interaction between DES and water.

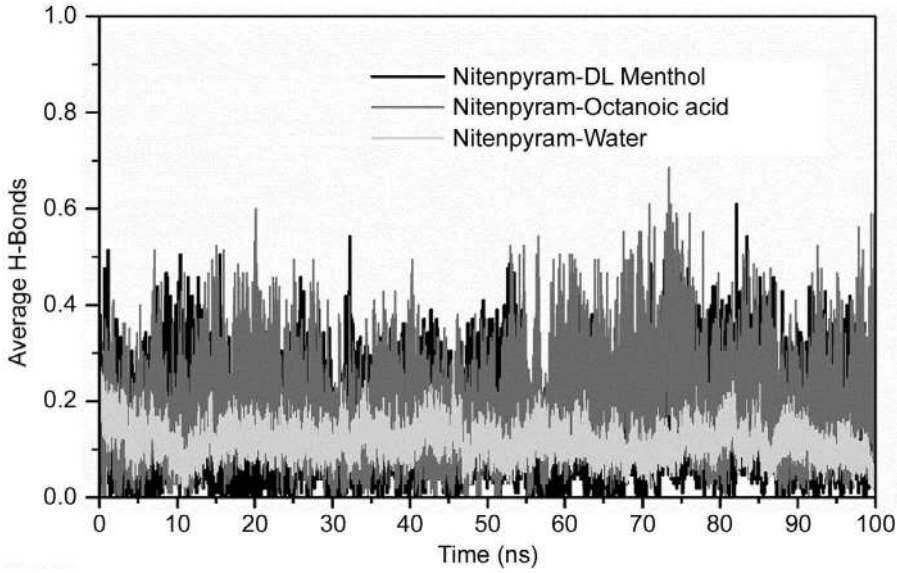

FIGURE 3.23 Average number of NIT–DLM, NIT–OCT, and NIT–water hydrogen bonds as a function of simulation time.

3.4.5 Diffusive Property Analysis of Nitenpyram

A detailed description of MSD and self-diffusivity coefficient was mentioned in the earlier section. Figure 3.24 represents the MSD plots for the DES–nitenpyram–water system at 0–10 ns and 90–100 ns, respectively. Linearity can be observed in all the plots. Initially, at the beginning of the simulation, the diffusivity of all the species is similar (Figure 3.24a), diverging only at the end, that is, 90–100 ns, where the water took a gradual shift (Figure 3.24b). The similar curves, other than water, indicate suitable transport properties among the molecules. From this, it can be assumed that the drug diffusivity is relatively higher in the DES. However, the water curve shown in both figures also suggests that water molecules maintained their mobility throughout the simulation implying a favorable transport property with nitenpyram. Table 3.16 presents the diffusion coefficient of each species in the system. It can be observed that the diffusion coefficients of DL-menthol and nitenpyram are close, and both indicate a similar trend. Overall, the following can be inferred: (1) the change in the diffusion coefficient of water is associated primarily with nitenpyram, and (2) from the diffusion coefficient data and the MSD plots, it can be confirmed that the nitenpyram molecules have sufficient mobility toward the DES phase. Both of these countereffective phenomena are responsible for the moderate extraction of nitenpyram from an aqueous environment.

3.5 SUMMARY

The classical MD simulation study was carried out to understand the experimental phase equilibria of a ternary system by means of their IE and structural properties.

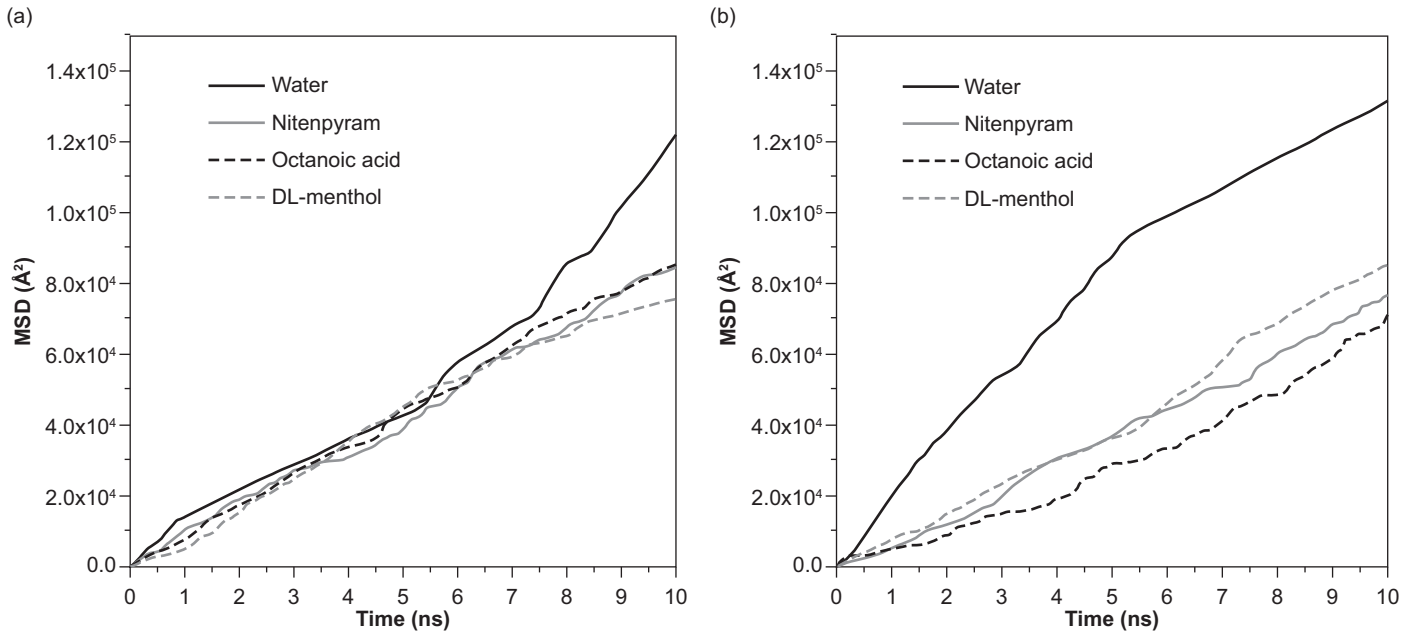

FIGURE 3.24 MSD plot at (a) 0–10 ns and (b) 90–100 ns, respectively, for DL-menthol–octanoic acid–nitenpyram–water system

TABLE 3.16
Self-Diffusivity of Different Molecular Species of DL-Menthol–Octanoic Acid–Nitenpyram–Water System at 298.15 K

		Diffusion coefficient (D) × 10^{-9} (m^2/s)		
System	**Molecule species**	**0–10 ns**	**40–50 ns**	**90–100 ns**
DES+ nitenpyram+ water	Water	0.914	1.001	1.088
	Octanoic acid	0.709	0.578	0.646
	Nitenpyram	0.732	0.776	0.568
	DL-menthol	0.684	0.672	0.729

The deviation between experimental and simulated data was found to give a fairly good agreement between them. Furthermore, the IEs between the investigated molecules were calculated for the ternary system using MD simulations. Overall, the vdW interactions were found to be higher than the electrostatic interactions, signifying that the vdW interactions are the controlling parameter for DES–quinoline/benzene–heptane/hexane interactions. In DES–quinoline system, MTP gave higher IE with quinoline, which is then followed by EG and bromide. This was further confirmed by their H-bonds and RDF plots. The SDF results suggest that the surfaces of DES were very closely distributed around the more active side of quinoline. From MSD, it is found that the closer the values of the self-diffusion coefficient within the species, the higher the miscibility and more interaction between the molecules. This makes quinoline to be more susceptible to the DES molecule. In the case of the DES–benzene pair, it possessed a higher IE compared to DES–hexane, which was also confirmed with the RDF plots. ETG–benzene gave a higher hydrogen bonding as compared to the MTP–benzene because of a higher fraction of active sites present in EG. The SDF results suggest that the surfaces of benzene are very closely distributed around the more active sites of DES. The self-diffusivity value also suggests higher miscibility with DES and benzene compared to hexane. The DES–benzene interaction was also confirmed from 2D NMR spectra. In summary, the cation MTPs of the HBA and the HBD both play a predominant role in the aromatic extraction process. Therefore, from the MD results, it was suggested that this study provides new insights for computational analysis of LLE equilibria in the absence of experimental data. Furthermore, the low-cost DES could be used as a potential solvent for the extraction of PAH compounds from fuel oil.

Furthermore, a pesticide drug (nitenpyram) extraction from an aqueous feed with DL-menthol:octanoic acid (1:1) DES was simulated, keeping similar experimental conditions to evaluate the MD simulation reliability. A simulated extraction efficiency of (42–46.7%) agreed with the 39% efficiency obtained in the experiments. Favorable interactions of nitenpyram were observed with both DES and water molecules. The average number of hydrogen bonds were obtained and follows nitenpyram–octanoic acid (0.18) > nitenpyram–DL-menthol (0.14) > nitenpyram–water (0.12). The presence of water molecules in the very close vicinity to the nitenpyram molecule was observed in the SDF plot, indicating a higher density distribution of water around

nitenpyram, whereas the RDF plot indicated a higher number of DES molecules, mainly HBA, within the solvation shell. A distribution coefficient (β) of 5.194 and selectivity (S) of 55.25 has been obtained in the simulation suggesting the suitability of the solvent in the extraction process. The simulated distribution ratio of 0.72 was in excellent agreement with the experimental distribution ratio of 0.67 for nitenpyram extraction.

Copyright Information (Entire Text, Figures and Tables)

1. Reprinted (adapted) with permission from Naik, P.K., et al., Molecular Dynamic Simulations for the Extraction of Quinoline from Heptane in the Presence of a Low-Cost Phosphonium-Based Deep Eutectic Solvent. *The Journal of Physical Chemistry B*, 2018. 122(14): p. 4006–4015. Copyright (2018) American Chemical Society [71].
2. Reprinted from *Journal of Molecular Liquids*, 317, N. Kumar, P. K. Naik, & T. Banerjee, Molecular modeling insights in the extraction of benzene from hydrocarbon stream using deep eutectic solvent. 113909, Copyright (2020), with permission from Elsevier [72].
3. Reprinted (adapted) with permission from Paul, N., et al., Molecular Dynamics Insights and Water Stability of Hydrophobic Deep Eutectic Solvents Aided Extraction of Nitenpyram from an Aqueous Environment. *The Journal of Physical Chemistry B*, 2020. 124(34): p. 7405–7420. Copyright (2020) American Chemical Society [73].

REFERENCES

1. Cassol, C.C., et al., *On the extraction of aromatic compounds from hydrocarbons by imidazolium ionic liquids*. International Journal of Molecular Sciences, 2007. **8**(7): p. 593–605.
2. Ravilla, U.K. and T. Banerjee, *Liquid liquid equilibria of imidazolium based ionic liquid+ pyridine+ hydrocarbon at 298.15 K: Experiments and correlations*. Fluid Phase Equilibria, 2012. **324**: p. 17–27.
3. Anantharaj, R. and T. Banerjee, *Liquid—liquid equilibria for quaternary systems of imidazolium based ionic liquid+ thiophene+ pyridine+ iso-octane at 298.15 K: Experiments and quantum chemical predictions*. Fluid Phase Equilibria, 2011. **312**: p. 20–30.
4. González, E.J., et al., *(Liquid+ liquid) equilibria for ternary mixtures of (alkane+ benzene+ [EMpy][ESO 4]) at several temperatures and atmospheric pressure*. The Journal of Chemical Thermodynamics, 2009. **41**(11): p. 1215–1221.
5. Hadj-Kali, M.K., et al., *Removal of thiophene from mixtures with n-heptane by selective extraction using deep eutectic solvents*. Industrial & Engineering Chemistry Research, 2016. **55**(30): p. 8415–8423.
6. Kareem, M.A., et al., *Liquid—liquid equilibria for the ternary system (phosphonium based deep eutectic solvent—benzene—hexane) at different temperatures: A new solvent introduced*. Fluid Phase Equilibria, 2012. **314**: p. 52–59.
7. Hou, Y., et al., *Separation of toluene from toluene/alkane mixtures with phosphonium salt based deep eutectic solvents*. Fuel Processing Technology, 2015. **135**: p. 99–104.
8. Ali, M.C., et al., *Efficient removal of both basic and non-basic nitrogen compounds from fuels by deep eutectic solvents*. Green Chemistry, 2016. **18**(1): p. 157–164.

9. Rodriguez, N.R., P.F. Requejo, and M.C. Kroon, *Aliphatic—aromatic separation using deep eutectic solvents as extracting agents*. Industrial & Engineering Chemistry Research, 2015. **54**(45): p. 11404–11412.
10. Oliveira, F.S., et al., *Deep eutectic solvents as extraction media for azeotropic mixtures*. Green Chemistry, 2013. **15**(5): p. 1326–1330.
11. Naik, P.K., S. Paul, and T. Banerjee, *Liquid Liquid Equilibria measurements for the extraction of poly aromatic nitrogen hydrocarbons with a low cost Deep Eutectic Solvent: Experimental and theoretical insights*. Journal of Molecular Liquids, 2017. **243**: p. 542–552.
12. Dehury, P., U. Mahanta, and T. Banerjee, *Partitioning of butanol between a hydrophobic ionic liquid and aqueous phase: Insights from Liquid Liquid Equilibria measurements and Molecular Dynamics simulations*. Fluid Phase Equilibria, 2016. **425**: p. 421–431.
13. Verma, R., et al., *Operational strategies and comprehensive evaluation of menthol based deep eutectic solvent for the extraction of lower alcohols from Aqueous media*. ACS Sustainable Chemistry & Engineering, 2018. **6**(12): p. 16920–16932.
14. Perkins, S.L., P. Painter, and C.M. Colina, *Experimental and computational studies of choline chloride-based deep eutectic solvents*. Journal of Chemical & Engineering Data, 2014. **59**(11): p. 3652–3662.
15. Naik, P.K., S. Paul, and T. Banerjee, *Physiochemical properties and molecular dynamics simulations of phosphonium and ammonium based deep eutectic solvents*. Journal of Solution Chemistry, 2019. **48**(7): p. 1046–1065.
16. Mohan, M., et al., *Solubility of glucose in tetrabutylammonium bromide based deep eutectic solvents: Experimental and molecular dynamic simulations*. Fluid Phase Equilibria, 2017. **448**: p. 168–177.
17. Jayaraman, S., *Computing thermodynamic and transport properties of room temperature ionic liquids and molten salts from atomistic simulations*. 2010: University of Notre Dame.
18. Naik, P.K., S. Paul, and T. Banerjee, *Thermal hydrogenation and degradation of quinoline from reactive force field simulations*. ChemistrySelect, 2019. **4**(44): p. 12996–13005.
19. Celebi, A.T., T.J. Vlugt, and O.A. Moultos, *Structural, thermodynamic and transport properties of aqueous reline and ethaline solutions from Molecular Dynamics Simulations*. The Journal of Physical Chemistry B, 2019.
20. Stephenson, S., et al., *Ethanol and water capacities of alcohols: A molecular dynamics study*. Chemical Engineering Science, 2006. **61**(17): p. 5834–5840.
21. Taha, M. and M.-J. Lee, *TES buffer-induced phase separation of aqueous solutions of several water-miscible organic solvents at 298.15 K: Phase diagrams and molecular dynamic simulations*. The Journal of Chemical Physics, 2013. **138**(24): p. 244501.
22. van Osch, D.J., et al., *Hydrophobic deep eutectic solvents as water-immiscible extractants*. Green Chemistry, 2015. **17**(9): p. 4518–4521.
23. Florindo, C., L. Branco, and I. Marrucho, *Development of hydrophobic deep eutectic solvents for extraction of pesticides from aqueous environments*. Fluid Phase Equilibria, 2017. **448**: p. 135–142.
24. Florindo, C., et al., *Hydrophobic deep eutectic solvents: A circular approach to purify water contaminated with Ciprofloxacin*. ACS Sustainable Chemistry & Engineering, 2019. **7**(17): p. 14739–14746.
25. Martins, M.n.A., et al., *Tunable hydrophobic eutectic solvents based on terpenes and monocarboxylic acids*. ACS Sustainable Chemistry & Engineering, 2018. **6**(7): p. 8836–8846.
26. Florindo, C., et al., *Hydrophobic deep eutectic solvents: A circular approach to purify water contaminated with ciprofloxacin*. ACS Sustainable Chemistry & Engineering, 2019. **7**(17): p. 14739–14746.

27. Morrison, H.G., C.C. Sun, and S. Neervannan, *Characterization of thermal behavior of deep eutectic solvents and their potential as drug solubilization vehicles*. International Journal of Pharmaceutics, 2009. **378**(1–2): p. 136–139.
28. Ge, D., et al., *A deep eutectic solvent as an extraction solvent to separate and preconcentrate parabens in water samples using in situ liquid-liquid microextraction*. Journal of the Brazilian Chemical Society, 2019. **30**(6): p. 1203–1210.
29. Zhu, S., et al., *Liquid—liquid microextraction of synthetic pigments in beverages using a hydrophobic deep eutectic solvent*. Food Chemistry, 2018. **243**: p. 351–356.
30. Ribeiro, B.D., et al., *Menthol-based eutectic mixtures: Hydrophobic low viscosity solvents*. ACS Sustainable Chemistry & Engineering, 2015. **3**(10): p. 2469–2477.
31. Pekel, A.G., et al., *Menthol-based deep eutectic solvent for the separation of carbamazepine: Reactive liquid-liquid extraction*. Biomass Conversion and Biorefinery, 2020: p. 1–8.
32. Dwamena, A.K., *Recent advances in hydrophobic deep eutectic solvents for extraction*. Separations, 2019. **6**(1): p. 9.
33. Sas, O.G., et al., *Removing phenolic pollutants using deep eutectic solvents*. Separation and Purification Technology, 2019. **227**: p. 115703.
34. Martins, M.A., S.P. Pinho, and J.A. Coutinho, *Insights into the nature of eutectic and deep eutectic mixtures*. Journal of Solution Chemistry, 2019. **48**(7): p. 962–982.
35. Verevkin, S.P., et al., *Separation performance of BioRenewable deep eutectic solvents*. Industrial & Engineering Chemistry Research, 2015. **54**(13): p. 3498–3504.
36. Pontes, P.V., et al., *Measurement and PC-SAFT modeling of solid-liquid equilibrium of deep eutectic solvents of quaternary ammonium chlorides and carboxylic acids*. Fluid Phase Equilibria, 2017. **448**: p. 69–80.
37. Dietz, C.H., et al., *Thermodynamic properties of hydrophobic deep eutectic solvents and solubility of water and HMF in them: Measurements and PC-SAFT modeling*. Fluid Phase Equilibria, 2019. **489**: p. 75–82.
38. Frisch, M., et al., *Gaussian 09 Revision B. 01*. 2010: Gaussian, Inc.
39. Kohn, W., A.D. Becke, and R.G. Parr, *Density functional theory of electronic structure*. The Journal of Physical Chemistry, 1996. **100**(31): p. 12974–12980.
40. Bayly, C.I., et al., *A well-behaved electrostatic potential based method using charge restraints for deriving atomic charges: the RESP model*. The Journal of Physical Chemistry, 1993. **97**(40): p. 10269–10280.
41. Case, D., et al., *Amber 12 reference manual*. 2012: University of California.
42. Wang, J., et al., *Development and testing of a general amber force field*. Journal of Computational Chemistry, 2004. **25**(9): p. 1157–1174.
43. Wang, J., et al., *Automatic atom type and bond type perception in molecular mechanical calculations*. Journal of Molecular Graphics and Modelling, 2006. **25**(2): p. 247–260.
44. Naik, P.K., et al., *Evaluation of deep eutectic solvent for the selective extraction of toluene and quinoline at T= 308.15 K and p= 1 bar*. Fluid Phase Equilibria, 2016. **423**: p. 146–155.
45. Martínez, L., et al., *PACKMOL: A package for building initial configurations for molecular dynamics simulations*. Journal of Computational Chemistry, 2009. **30**(13): p. 2157–2164.
46. Phillips, J.C., et al., *Scalable molecular dynamics with NAMD*. Journal of Computational Chemistry, 2005. **26**(16): p. 1781–1802.
47. Nosé, S., *A unified formulation of the constant temperature molecular dynamics methods*. The Journal of Chemical Physics, 1984. **81**(1): p. 511–519.
48. Hoover, W.G., *Canonical dynamics: Equilibrium phase-space distributions*. Physical Review A, 1985. **31**(3): p. 1695.
49. Hünenberger, P.H., *Thermostat algorithms for molecular dynamics simulations*. Advanced Computer Simulation, 2005: p. 130.

50. Feller, S.E., et al., *Constant pressure molecular dynamics simulation: The Langevin piston method*. The Journal of Chemical Physics, 1995. **103**(11): p. 4613–4621.
51. Andersen, H.C., *Rattle: A "velocity" version of the shake algorithm for molecular dynamics calculations*. Journal of Computational Physics, 1983. **52**(1): p. 24–34.
52. Essmann, U., et al., *A smooth particle mesh Ewald method*. The Journal of Chemical Physics, 1995. **103**(19): p. 8577–8593.
53. Zeron, I., J. Abascal, and C. Vega, *A force field of Li+, Na+, K+, Mg2+, Ca2+, Cl−, and SO 4 2− in aqueous solution based on the TIP4P/2005 water model and scaled charges for the ions*. The Journal of Chemical Physics, 2019. **151**(13): p. 134504.
54. Döpke, M.F., O.A. Moultos, and R. Hartkamp, *On the transferability of ion parameters to the TIP4P/2005 water model using molecular dynamics simulations*. The Journal of Chemical Physics, 2020. **152**(2): p. 024501.
55. Humphrey, W., A. Dalke, and K. Schulten, *VMD: Visual molecular dynamics*. Journal of Molecular Graphics, 1996. **14**(1): p. 33–38.
56. Brehm, M. and B. Kirchner, *TRAVIS-a free analyzer and visualizer for Monte Carlo and molecular dynamics trajectories*. Journal of Chemical Information and Modeling, 2011. **51**(8): p. 2007–2023.
57. Sørensen, J.M., et al., *Liquid-liquid equilibrium data: Their retrieval, correlation and prediction part I: Retrieval*. Fluid Phase Equilibria, 1979. **2**(4): p. 297–309.
58. Manohar, C., et al., *Liquid—liquid equilibria studies on ammonium and phosphonium based ionic liquid—aromatic—aliphatic component at T= 298.15 K and p= 1bar: correlations and a-priori predictions*. Fluid Phase Equilibria, 2013. **360**: p. 392–400.
59. Alonso, L., et al., *(Liquid+ liquid) equilibria of [C 8 mim][NTf 2] ionic liquid with a sulfur-component and hydrocarbons*. The Journal of Chemical Thermodynamics, 2008. **40**(2): p. 265–270.
60. Shah, M.R., et al., *Quaternary (liquid+ liquid) equilibria for systems of imidazolium based ionic liquid+ thiophene+ pyridine+ cyclohexane at 298.15 K: Experiments and quantum chemical predictions*. The Journal of Chemical Thermodynamics, 2013. **62**: p. 142–150.
61. Mahmoudi, J. and M.N. Lotfollahi, *(Liquid+ liquid) equilibria of (sulfolane+ benzene+ n-hexane), (N-formylmorpholine+ benzene+ n-hexane), and (sulfolane+ N-formylmorpholine+ benzene+ n-hexane) at temperatures ranging from (298.15 to 318.15) K: Experimental results and correlation*. The Journal of Chemical Thermodynamics, 2010. **42**(4): p. 466–471.
62. Sharma, B. and S. Paul, *Understanding the role of temperature change and the presence of NaCl salts on caffeine aggregation in aqueous solution: From structural and thermodynamics point of view*. The Journal of Physical Chemistry B, 2015. **119**(21): p. 6421–6432.
63. Paul, S. and S. Paul, *The influence of trehalose on hydrophobic interactions of small nonpolar solute: A molecular dynamics simulation study*. The Journal of Chemical Physics, 2013. **139**(4): p. 044508.
64. Borgohain, G. and S. Paul, *Temperature-mediated switching of protectant-denaturant behavior of trimethylamine-N-oxide and consequences on protein stability from a replica exchange molecular dynamics simulation study*. Molecular Simulation, 2017. **43**(1): p. 52–64.
65. Mata, I., et al., *Tuning the interaction energy of hydrogen bonds: The effect of the substituent*. The Journal of Physical Chemistry A, 2011. **115**(45): p. 12561–12571.
66. van der Lubbe, S.C. and C. Fonseca Guerra, *The nature of hydrogen bonds: A delineation of the role of different energy components on hydrogen bond strengths and lengths*. Chemistry—An Asian Journal, 2019. **14**(16): p. 2760–2769.
67. Allen, M.P. and D.J. Tildesley, *Computer simulation of liquids*. 1989: Oxford University Press.

68. Sarangi, S.S., et al., *Correlation between dynamic heterogeneity and local structure in a room-temperature ionic liquid: A molecular dynamics study of [bmim][PF6].* ChemPhysChem, 2010. **11**(9): p. 2001–2010.
69. Biswas, R., et al., *Interfacial insights on the dibenzo-based crown ether assisted cesium extraction in [BMIM][Tf2N]—water binary system.* Journal of Radioanalytical and Nuclear Chemistry, 2017. **311**(1): p. 427–438.
70. Sarkar, G., D. Kundu, and T. Banerjee, *Effects of functionality on the transport properties of thiol-ene/acrylate systems: A molecular dynamics study.* Journal of Molecular Liquids, 2016. **224**: p. 859–871.
71. Naik, P.K., et al., *Molecular dynamic simulations for the extraction of quinoline from heptane in the presence of a low-cost phosphonium-based deep eutectic solvent.* J. Phys. Chem. B, 2018. **122**(14): p. 4006.
72. Kumar, N., P.K. Naik, and T. Banerjee, *Molecular modeling insights in the extraction of benzene from hydrocarbon stream using deep eutectic solvent.* Journal of Molecular Liquids, 2020. **317**: p. 113909.
73. Paul, N., et al., *Molecular dynamics insights and water stability of hydrophobic deep eutectic solvents aided extraction of nitenpyram from an aqueous environment.* The Journal of Physical Chemistry B, 2020. **124**(34): p. 7405–7420.

4 Water Stability Studies on Hydrophobic Deep Eutectic Solvents and Extractive Desulfurization of Fuel

4.1 INTRODUCTION

In the previous chapters, different types of deep eutectic solvents (DESs) and their applications were discussed. One striking observation is that most of the DESs discovered till now are of the hydrophilic class, which can be efficiently applied in the fields such as metal processing, composite coatings, extraction of sugars and proteins, denitrification and desulfurization of fuel oil, synthesis of nanomaterials, and others in which water-based systems are not encountered [1]. However, for water purification by solvent extraction and separation of toxic, as well as valuable products from water, the solvents need to be hydrophobic in nature. In order to understand the applicability of the DESs in water-based extraction processes, one needs to study the different physicochemical properties of those solvent systems both experimentally and computationally. Researchers have come up to contribute to the synthesis of various hydrophobic DESs from natural substances. Six hydrophobic DESs were synthesized for the first time consisting of decanoic acid as a hydrogen bonding donor (HBD) and a range of quaternary ammonium salts as a hydrogen bonding agent (HBA) by the van Osch research group [2]. They studied the effect of the carbon chain length of the quaternary ammonium salts in the leaching of the HBA to the water phase and subsequently the overall hydrophobicity of the DESs. The study shows that all the DESs, which are initially believed to be hydrophobic, are not fully hydrophobic, but their overall behavior depends on the parent compound's affinity toward the aqueous phase. The ammonium salts consisting of higher carbon chain length have shown better hydrophobicity than the shorter ones.

Hydrophobic DESs based on menthol, ammonium salt, organic acids, and terpenes are synthesized and applied in the separation of pesticides and pharmaceuticals from aqueous environments [3–5]. Four different pesticides were extracted from aqueous environments successfully by DL-menthol and carboxylic acid-based DESs. Furthermore, their water stability was investigated experimentally by Marrucho's research group [3] for pesticides, such as neonicotinoids, imidacloprid, acetamiprid, nitenpyram, and thiamethoxam, from diluted aqueous solutions. Hydrophobic DESs

DOI: 10.1201/9781003231158-4

consisting of various combinations of DL-menthol, long-chain carboxylic acids (C_8–C_{12}), and quaternary ammonium salt have been applied to extract ciprofloxacin from an aqueous solution by Florindo et al. [4] They also studied the effect of various experimental conditions such as pH, stirring speed, contact time, and DES-to-water mass ratio. The extractability of the hydrophobic DESs hampered severely if the DES cannot stabilize in the presence of water. In other words, to maintain HBA–HBD integrity, the DES components need to be immiscible with water and should not leach out to the aqueous phase. Most of the DESs were liquid at room temperature, which allowed studying the DES–water solubility and drug extraction [6–8]. Recently, it was found that the menthol-based DESs were the most promising for these types of studies because of their hydrophobicity and physio-thermal properties [9–12].

A proper understanding of various solvent properties of DESs such as solubility and activity coefficient could help us in selecting suitable solvents for specific applications. Sufficient and authentic experimental data combined with efficient and robust mathematical models related to such solvent properties can be very much helpful in the effective selection of solvents. One such work is carried out by the research group of Verevkin et al. [13], where they have measured the activity coefficient at infinite dilution for 23 solutes in choline chloride: ethylene glycol (EG) DESs and validated the separation performances by PC-SAFT mathematical model for the first time for any DES system. Pontes et al. [14] studied the solid–liquid phase equilibrium of 15 DESs consisting of three quaternary ammonium salt and 5 carboxylic acids and then executed the PC-SAFT equation of state to measure possible hydrogen bonding among the species. Dietz et al. [15] have incorporated density and vapor pressure data in the PC-SAFT model to successfully measure various thermodynamic properties of eight hydrophobic DESs and further investigated the extraction of 5-hydroxymethylfurfural (HMF) from sugars in an aqueous environment. They also analyzed the solubility of water and HMF in the DES phase. One major advantage of these models is that they are useful in identifying the eutectic composition of the DES, that is, the composition at which the DES becomes liquid [15]. All these studies suggest that a proper combination of experimental study along with simulation strategies can certainly help us in the proper understanding of the DES systems and address the complexity of the DES systems. This combined strategy can be considered the way forward for predicting the phase equilibria and the selection of suitable solvents.

Classical molecular dynamics (MD) simulation can be advantageous to observe the process that cannot be carried out experimentally because of the extreme operating or hazardous conditions. It is also feasible in terms of time scale, experimental technique limitations, and from an economic point of view [16, 17]. Considering the complex nature of the eutectic systems and the price of various DES precursor materials, large-scale experimental studies cannot be maintained without a suitable screening technique. Furthermore, the experiments are in the order of hours/minutes or seconds, while the MD simulation analysis can be performed within the atomic scale and recorded at the nanosecond scale [18]. The chemical phenomena at the atomic level occur in a fraction of seconds. To analyze such an event, molecular dynamic simulations within a time scale in the order of nanoseconds are an effective

medium to understand such a phenomenon. It should be noted that such changes are usually not detected by digital instruments as in the experiment. Consequently, the goal of this simulation is to capture the phenomenon with the trajectory analysis. Overall, experiments and simulations can be carried out simultaneously to obtain a more efficient and precise pure component and phase equilibria data. Naik et al. carried out the experimental and MD simulation study for the extraction of quinoline from heptane with hydrophilic DES [19]. Furthermore, our group also studied the solubility of glucose in tetrabutylammonium bromide–based DESs [16].

Furthermore, the use of DESs as alternative solvents for the liquid–liquid extraction of organosulfur compounds from liquid fuels has also been investigated in the past several years [20]. DESs based on choline chloride [21, 22], as well as those produced from other quaternary ammonium halide salts, amino acids, and metal halides, are examples of this kind of compound (e.g., $ZnCl_2$, $FeCl_3$) [23, 24]. There has been a big rise in the use of computational tools to better understand the structure, dynamics, and interactions of DES systems [25–28], but little is known about how DES molecular structure and composition affect interactions with aromatic sulfur compounds, which are very important in the desulfurization of fuels.

The present chapter exemplifies the molecular-level understanding of the stability of hydrophobic DESs in water at a temperature of 298.15 K and 1 atm atmospheric pressure. Here, the MD simulation study is carried out for the stability of (a) DL-menthol–organic acid-based DESs and (b) tetrabutylammonium chloride-organic acid-based DESs in aqueous solutions. The composition of each system considered in the simulation work is kept identical to that of the experimental work of Florindo et al. [3] The ensuing section starts with the computational details and thereafter discusses the evaluation of nonbonded interaction. Furthermore, the radial and combined distribution functions (RDFs and CDFs, respectively) between the different components of the DES and water, spatial distribution function (SDF), mean square displacement (MSD), and self-diffusivity analysis, among others, are evaluated. The ‘relative stability factor’ is introduced as a new means for measuring the stability of a DES in contact with water. Hydrogen bonding analysis of the DES systems has been carried out to get valuable insights into the DES interactions. To manage the extraction of the target molecules from sulfur-contaminated liquid fuels, quantum mechanical (QM) simulations are used to get a molecular-level knowledge of how certain components inside traditional DESs interact with model aromatic sulfur compounds (ASCs). DESs containing 1:2 molar ratios of choline chloride:urea (reline) and choline chloride:EG (ethaline) were studied in detail, as were the model ASCs benzothiophene (BT) and dibenzothiophene (DBT), and the sulfoxide/sulfone oxidation products oxides and dioxides of BT and DBT.

4.2 SIMULATION METHODOLOGIES

Initially, the structures of individual molecules of HBA, HBD, and water were drawn in GaussView 05 with geometry optimization using Gaussian 09 [29] at the B3LYP/6–31G* theory [30]. Figures 4.1 and 4.2 present the chemical structures of all the molecules along with atomic notations. The partial atomic charges of the molecules were obtained by the restricted electrostatic potential (RESP) [31] module

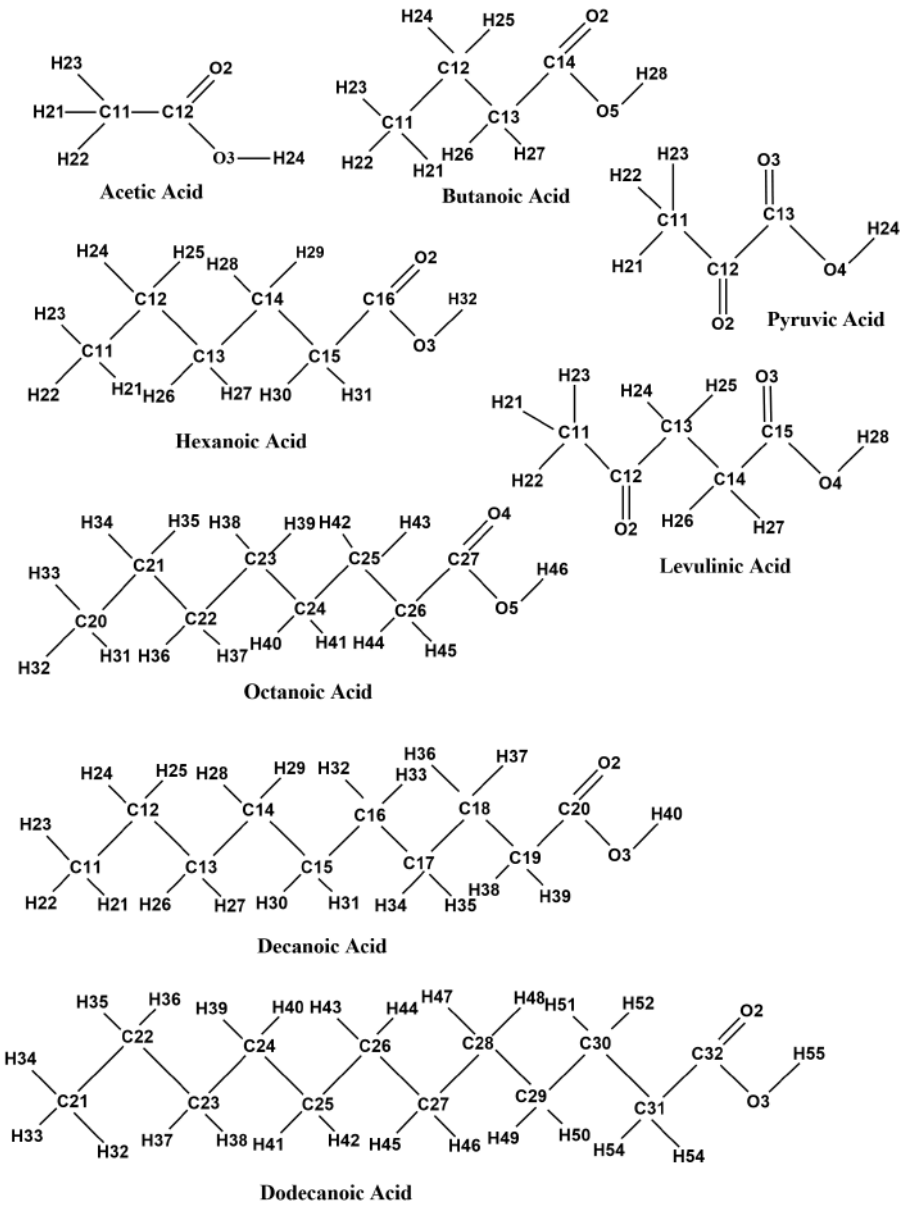

FIGURE 4.1 Structures of all the HBD molecules with atom notations.

of AMBER 14 [32]. They were used to fit the partial charges for different species that were obtained from the optimized geometry as before. Table 4.1 represents the compound name and composition of various hydrophobic DES studied. The generalized amber force field [33] functional of the ANTECHAMBER [34, 35], a module of AMBER 14 [32] was used to generate all force field parameters. The validation of

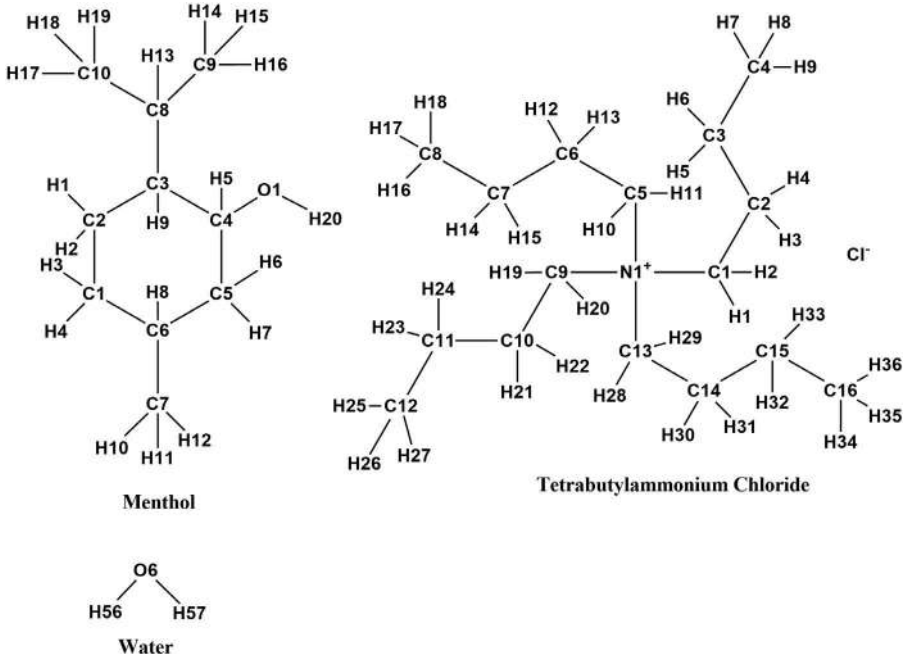

FIGURE 4.2 Structures of HBA molecules and water with atom notations.

TABLE 4.1
Composition of Various Hydrophobic DESs

Sl. No.	Name of DES	DES		Molar ratio
		HBA	HBD	
1	DES1	DL-menthol	Acetic acid	1:1
2	DES2	DL-menthol	Butanoic acid	1:1
3	DES3	DL-menthol	Hexanoic acid	1:1
4	DES4	DL-menthol	Octanoic acid	1:1
5	DES5	DL-menthol	Decanoic acid	1:1
6	DES6	DL-menthol	Dodecanoic acid	2:1
7	DES7	DL-menthol	Pyruvic acid	1:2
8	DES8	DL-menthol	Levulinic acid	1:1
9	DES9	$N_{4444}Cl$	Acetic acid	1:1
10	DES10	$N_{4444}Cl$	Octanoic acid	1:2

the generated force-field parameters was done by comparing the simulated density of DES1 (0.929 gm/cm^3) at 298.15 K temperature and 1 atm pressure condition with that of the experimental density (0.931 gm/cm^3) at the same temperature–pressure condition. The composition of the different systems has been presented in Table 4.2.

TABLE 4.2
Composition of Different Systems Considering 1:1 Mass Ratio of DES and Water and the Number of Molecules Considered for MD Simulation

System No.	DES		Number of molecules				Periodic box size
	HBA	HBD	HBA	HBD	Water	Total	(Å × Å × Å)
S1	DL-menthol	Acetic acid	30	30	181	241	35.38 × 21.23 × 21.23
S2	DL-menthol	Butanoic acid	30	30	204	264	36.89 × 22.13 × 22.13
S3	DL-menthol	Hexanoic acid	30	30	227	287	38.61 × 23.17 × 23.17
S4	DL-menthol	Octanoic acid	25	25	209	259	37.62 × 22.57 × 22.57
S5	DL-menthol	Decanoic acid	30	30	274	334	41.67 × 25.00 × 25.00
S6	DL-menthol	Dodecanoic acid	50	25	238	313	43.71 × 26.22 × 26.22
S7	DL-menthol	Pyruvic acid	30	60	185	275	38.49 × 23.09 × 23.09
S8	DL-menthol	Levulinic acid	30	30	227	287	38.10 × 22.86 × 22.86
S9	$N_{4444}Cl$	Acetic acid	30	30	282	342	40.49 × 24.29 × 24.29
S10	$N_{4444}Cl$	Octanoic acid	30	60	315	405	45.35 × 28.86 × 28.86

PACKMOL was used to generate the initial configuration of different systems consisting of DES and water molecules [36].

The binary systems were considered for studying the stability of the DESs in water. Those systems consisted of two components, that is, DES and water. Initially, the HBA and HBD molecules were inserted in a cubic box, while water molecules were packed in a separate cubic box. Thereafter, the two boxes were placed close to each other to mimic a two-phase system having a DES-rich phase and a water-rich phase, respectively. All the MD simulations were carried out in NAMD 2.10 package [37]. The systems were initially minimized for 6 ns in an NVE ensemble, thereafter all the systems were gradually heated from 0 K to 298.15 K within 0.5 ns. The systems were then subjected to an equilibration step for 10 ns in an NPT ensemble at 298.15 K and atmospheric pressure.

The Langevin dynamics method [38] with a collision frequency of 1 ps^{-1} was used for maintaining the desired temperature. The Nosé–Hoover Langevin piston was used for pressure control with an oscillation period of 100 fs and a damping factor of 50 fs [39]. Subsequently, the production runs were carried out for 100 ns for each of the systems with the NVT ensemble. The trajectory data were saved at every 5 ps. The SHAKE algorithm was considered to restrain the bonds involving hydrogen atoms [40]. VMD 1.9.3 package was used for visualizing the trajectory of the molecules within the systems [41]. The particle mesh Ewald method was used for the calculation of the long-range intermolecular electrostatic interactions [42]. A cutoff distance of 12 Å was considered for short-range interactions. Periodic boundary condition (PBC) was applied in each system [43]. The box size of the individual systems is provided in Table 4.2. Each system was initiated with three different starting configurations so to ensure successful completion and reproducibility of the simulation that can provide a realistic estimate of the trajectory and the thermodynamic properties.

This was performed to remove any numerical or modeling bias in the simulation procedure.

After successful completion of the production run, a trajectory file was obtained that contains the trajectory of the molecules of the system. The parameter file and the trajectory files were then inserted into the VMD software package [41]. The nonbonded interaction energy, average hydrogen bonding, and radial distribution function on the specification of the requisite criteria were obtained directly using the tools provided in VMD. TRAVIS package [44] was used to obtain the CDF and the SDF, where the final coordinate file was used as the input. Specific molecules and atoms along with required criteria such as reference molecule and observed molecule were selected to get the CDF datasheet SDF coordinate file. The data ware then plotted in a graph sheet. Proper isovalues were set to view the three-dimensional SDF. The MSD curves were obtained by solving the Einstein equation of self-diffusivity through VMD. The diffusion coefficient was obtained from the linear slope of the MSD curve.

The percentage loss of the DES components (HBA, HBD) to the aqueous phase was obtained by calculating the number of the molecules present in the water-rich phase after 100 ns that initially were present in the DES phase. Later, the number was averaged out from all the three simulation runs carried out for each system and then subsequently divided by the total number of molecules of that species. It was then converted to a percentage to obtain the percentage loss.

4.3 INSIGHTS INTO WATER STABILITY OF DES FROM MD SIMULATIONS

In our MD simulations, DL-menthol and tetrabutylammonium chloride were taken as HBAs and organic acids, such as acetic acid, pyruvic acid, butanoic acid, hexanoic acid, levulinic acid, octanoic acid, decanoic acid, and dodecanoic acid, were taken as HBDs, respectively, with appropriate compositions. Each system consisted of a 1:1 mass ratio of DES and water, which was the same as the experiments [3]. The snapshots were captured at 0 ns and 100 ns of production run respectively for each system to compare the initial and the final molecular arrangements. The snapshots of the systems S1 to S10 at 0 ns and 100 ns were provided in Figures 4.3a–t.

The water-stability of DES or DES stability in water can be explained as to whether one DES could maintain its chemical and physical integrity when placed in an aqueous or other environment while retaining its identity or structure. A DES can be termed “water-stable” if it can sustain itself in the presence of an aqueous environment and significantly not leach to the aqueous phase or allow water molecules to disrupt its structure.

From Figure 4.3, it can be observed that the menthol-based DESs consisting of acetic acid, butanoic acid, and hexanoic acid are much less water-stable. The order of stability of the DESs based on the distribution of HBD molecules in the water phase can be witnessed as DES1 < DES8 < DES2 < DES7 < DES3 < DES4 < DES5 < DES6. In system S1, the disruption of the DES integrity was witnessed in contact with water, where a loss of acid about 95% takes place toward the water-rich phase. On a similar note, the loss of acid decreases to about 35% and 15% for systems S2 and

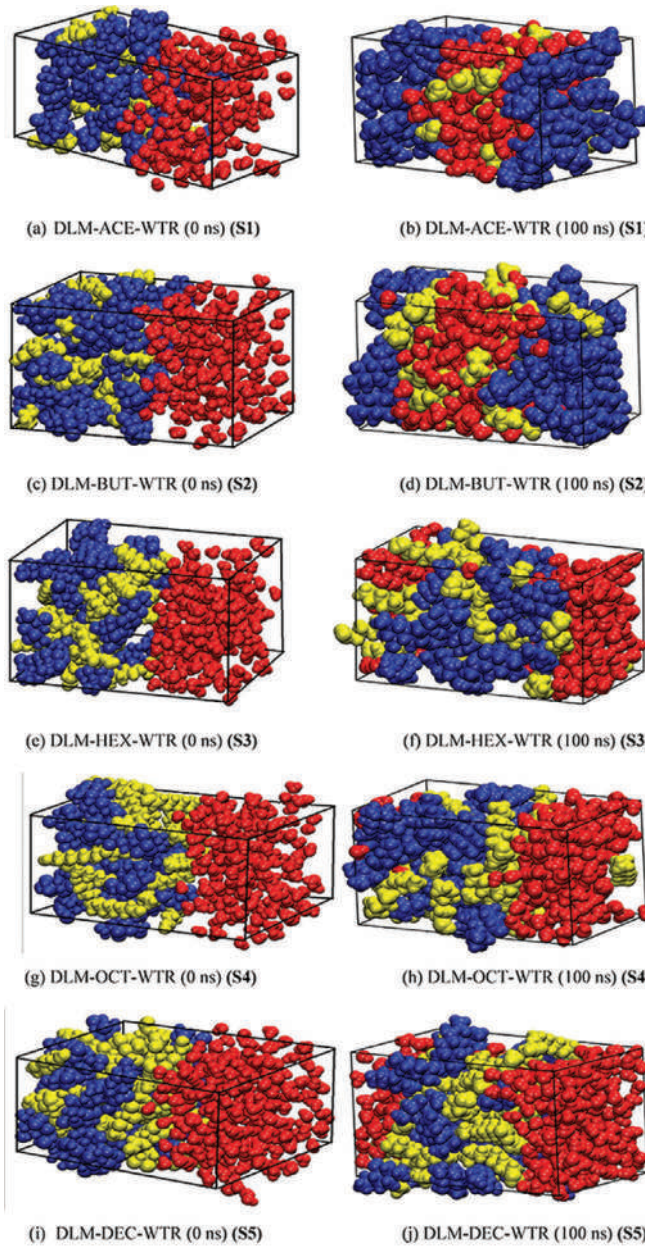

FIGURE 4.3 Distribution snapshots of different DES–water systems at 0 ns and 100 ns for (a), (b) system S1; (c), (d) system S2; (e) (f) system S3; (g), (h) system S4; (i), (j) system S5; (k), (l) system S6; (m), (n) system S7; (o), (p) system S8; (q), (r) system S9 and (s), (t) system S10; (DLM and TBACl denote DL-menthol and tetrabutylammonium molecules, respectively, both in blue, chloride ions in green; WTR denotes water molecules in red; ACE, BUT, HEX, OCT, DEC, DODEC, PYR, and LEV denote acetic acid, butanoic acid, hexanoic acid, octanoic acid, decanoic acid, dodecanoic acid, pyruvic acid, and levulinic acid molecules, respectively, in yellow).

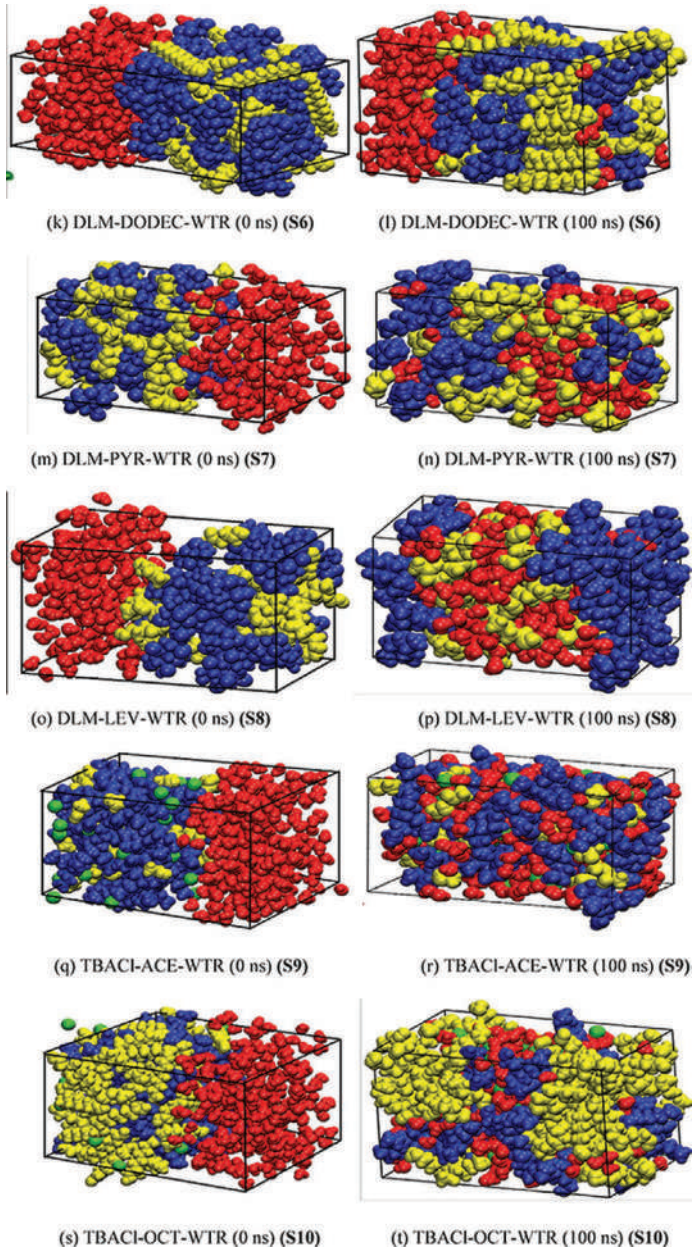

FIGURE 4.3 (Continued)

S3, respectively. These can be visualized from the molecular arrangements captured at 0 ns and 100 ns of the simulation run in Figure 4.3a–f.

Among all the systems containing DL-menthol as HBA, DES4, DES5, and DES6 have shown hydrophobic nature (Figure 4.3g–l) with low contamination

of the hydrophobic long-chain organic acids (HBDs) in the water-rich phase. On the contrary, the systems containing DES1, DES2, DES3, DES7, and DES8 were unstable in contact with water because of the presence of hydrophilic organic groups as HBDs. In the case of $N_{4444}Cl$-based DESs, all the DESs, such as DES9 and DES10, were found to be water-miscible because of the hydrophilic nature of $N_{4444}Cl$ (Figure 4.3q–t). In contrast to the menthol-based DESs, where hydrophilic HBDs played a major role in its leaching toward the water-rich phase, the hydrophilic $N_{4444}Cl$ got transported primarily to the water-rich phase in the case of $N_{4444}Cl$-based DESs. This is, in fact, the main reason behind the instability of ammonium-based DESs in contact with water. From the snapshots of the systems S9 (Figures 4.3q and 4.3r), it can be visualized that both HBA (tetrabutylammonium chloride) and HBD (acetic acid) were miscible with the water molecules, turning the whole system unstable with water. System S10 confirmed the transport of only hydrophilic ammonium salt to the water-rich phase, whereas the contamination of the HBDs such as octanoic acid to the water-rich phase was very negligible (Figure 4.3s and 4.3t).

When compared to experiments, Florindo et al. [3] studied the water stability of different DESs by comparing the ^1H nuclear magnetic resonance (NMR) spectra for the DES-rich phase and water-rich phase as presented in Figure 4.4. They confirmed the presence of the hydrophilic HBDs (such as acetic acid, butanoic acid, and hexanoic acid) in the water-rich phase for the systems S1, S2, and S3. With detailed scrutiny of the ^1H NMR data for acetic acid–, butanoic acid–, and levulinic acid–based DESs, it was observed that the acid molecules (HBD) leached out to the water phase while the menthol molecules kept themselves isolated from the water phase. Similar results can be viewed in Figures 4.3a–b, 4.3c–d and 4.3o–p, respectively. However, in the case of octanoic acid– and dodecanoic acid–based systems, no transport of menthol, as well as acid molecules (HBA and HBD), were observed. This has been confirmed and depicted in Figures 4.3g–h and 4.3k–l. From the analysis of the tetrabutylammonium chloride–octanoic acid-based system, it was observed that the ammonium salt molecules have a strong affinity to the water phase, whereas the octanoic acid molecules maintained their hydrophobic characteristic (Figures 4.3s and 4.3t). The experimental results hence can be seen in excellent agreement with the simulation results that were obtained in the present work. We further analyzed the nonbonded interaction energy, average hydrogen bonding, RDF, CDF, and the MSD self-diffusion coefficient to have an insight into the molecular-level understanding within the different systems.

4.3.1 Nonbonded Interaction Energy

Table 4.3 represents the non-bonded interaction energies, subdivided further into electrostatic and van der Waals (vdW) interactions, among the different components in each system. To study the interaction energies, a comparison analysis is carried out for short-chain organic acid, such as acetic acid, with long-chain organic acids, such as octanoic acid, decanoic acid, and dodecanoic acid, as HBD. Interaction between acetic acid and water was much more favorable (–3.17 kcal/mol; system S1) than that of octanoic acid–water (–2.40 kcal/mol), decanoic acid–water (–1.94 kcal/mol),

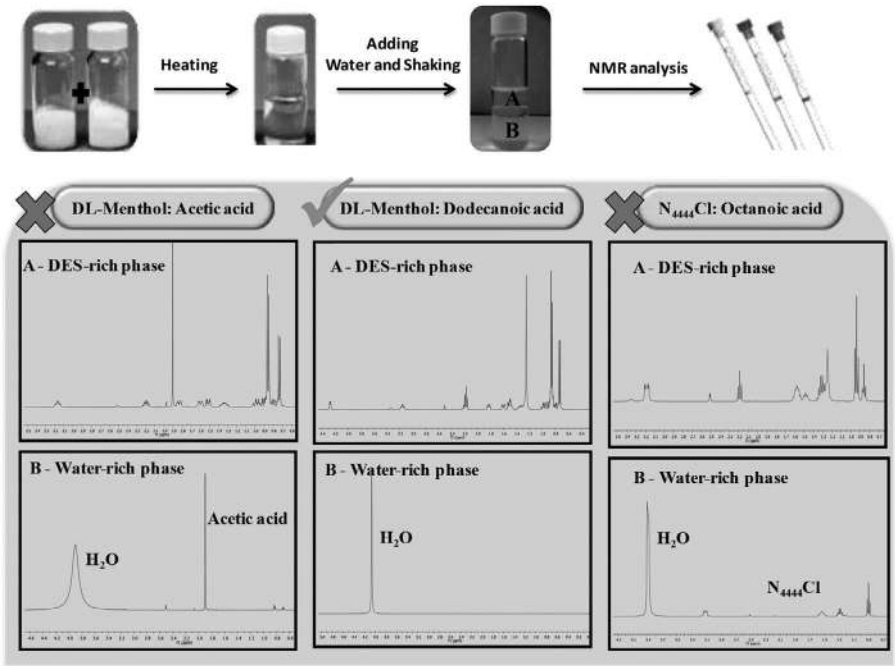

FIGURE 4.4 NMR analysis of DES- and water-rich phases after liquid–liquid extraction technique.

Source: Reprinted from *Fluid Phase Equilibria*, 448, C, Florindo, L.C. Branco and I.M. Marrucho, Development of hydrophobic deep eutectic solvents for extraction of pesticides from aqueous environments, pp. 135–142, Copyright (2017), with permission from Elsevier [3].

and dodecanoic acid–water (−1.83 kcal/mol; systems S4, S5, and S6, respectively). It implied that when in contact with water, acetic acid would have a higher affinity toward the water-rich phase than the longer carboxylic acids such as C_8 to C_{12}. A further breakup of the interaction energy into electrostatic and vdW components of system S1 revealed that the electrostatic interaction between acetic acid and water (−2.75 kcal/mol) was more dominant than the vdW interaction (−0.42 kcal/mol). However, an opposite trend was seen between menthol and acetic acid as the vdW component (−2.48 kcal/mol) between the HBA and the HBD molecule was higher than the electrostatic part (−1.72 kcal/mol). A probable explanation for this could be the large size of the menthol molecule as compared to that of acetic acid, which leads to steric hindrance between the molecules, thus reducing the electrostatic effect. It should be noted that the HBA and the HBD were nonionic compounds, for which electrostatic interactions were less likely to dominate and entropic effects predominate. The hydroxyl (–OH) group present in the menthol structure was more likely to participate in H-bonding with the polar carboxyl (–COOH) group present in the acetic acid.

DES2, DES3, DES7, and DES8 have also appeared to be hydrophilic. For systems S2 and S3, we observed the distribution of the HBD molecules, that is, butanoic acid and hexanoic acid, toward the water-rich phase was observed, although the numbers drastically reduced in the case of hexanoic acid. Whereas, both the HBA and the HBD molecules showed affinity toward the aqueous phase for systems S7 and S8. Interestingly, the stability of DES2 and DES3 in water was higher as compared to DES1 even though all possessed hydrophilic nature as the total HBA–HBD interaction was higher than the HBD–water interaction, which thereby improved the overall hydrophobicity.

This can be explained based on total nonbonded energies as presented in Table 4.3. Here, the menthol-organic acid energies are always greater than the water-organic acid systems. However, the difference is the lowest in acetic acid while the highest in dodecanoic acid. This implies that the higher the difference, the more strongly it is attached to the HBA (menthol). So with acetic acid, it has almost equal magnitude indicating its higher preference in leaching out to the water phase. Among all the menthol-based DESs studied in this work, DESs based on octanoic acid, decanoic acid, and dodecanoic acid depicted very low HBD–water interaction. This explains why DES4, DES5, and DES6 are stable in water. The hydrophobic tail of the HBD molecules (higher carboxylic acids with C_8–C_{12}) pushes the water molecules, owing to steric hindrance, and hence contributes to a strong interaction between the HBA and HBD.

It can be observed from Table 4.3 for systems S1 to S6, that the total nonbonded interaction energy (E_{total}) between the HBD (carboxylic acids) and water gradually decreased (system S1 to S6), with an increase in the chain length of the organic acids (from C_1–C_{12}). This happens because, with the increase in chain length, the HBA–HBD interaction also increased continuously. The total nonbonded HBA–HBD interaction (−4.20 kcal/mol) for system S1 increased to (−22.87 kcal/mol) for system S6, whereas the HBD–water interaction for system S1 (−3.17 kcal/mol) reduced to (−1.83 kcal/mol) for system S6 (Table 4.3). For systems S9 and S10, it can be noticed that the N_{4444}Cl–octanoic acid interaction (−31.36 kcal/mol) is much greater than that of N_{4444}Cl–acetic acid (−22.84 kcal/mol). The effect of individual properties of HBA and HBD for the stability of DES in a specific medium can be explained in terms of their interactions with the molecules of that medium. Systems S4 and S10 do follow this behavior (Table 4.3). In both the systems, octanoic acid was present as the HBD, whereas DL-menthol and N_{4444}Cl were present as HBA for S4 and S10, respectively. Octanoic acid showed higher interaction with N_{4444}Cl (−31.36 kcal/mol) than DL-menthol (−12.52 kcal/mol), which could imply greater stability of DES10 than that of DES4. However, when HBA–water interaction of both the systems was compared, it was observed that N_{4444}Cl had greater interaction energy (−13.99 kcal/mol) with water than did DL-menthol (−0.99 kcal/mol). For both systems, octanoic acid exhibited very low interactions with water. From the preceding observations, it can be concluded that N_{4444}Cl–octanoic acid DES did not maintain its chemical and physical integrity in an aqueous environment largely due to the hydrophilic character of the HBA molecules, suggesting a possible disruption of DES structure. Figures 4.3s and 4.3t visually suggest the same for DES10. The difference in the relative stability factor of DES4 (3.70) and DES10 (2.0) can be justified by the preceding explanation.

TABLE 4.3
MD-Simulated Nonbonded Interaction Energies (kcal/mol) between the Different Pairs of HBA–HBD–Water for the Different Systems Calculated at 298.15 K and 1 atm Pressure

System No	Component pairs	Electrostatic interactions (E_{elec})	van der Waals interactions (E_{vdW})	Total nonbonded interactions (E_{total})	Relative Stability Factor (S)
S1	Menthol–water	−1.18	−0.21	−1.39	
	Menthol–acetic acid	−1.72	−2.48	−4.20	0.92
	Acetic acid–water	−2.75	−0.42	−3.17	
S2	Menthol–water	−1.08	−0.15	−1.23	
	Menthol–butanoic acid	−2.65	−5.44	−8.09	1.94
	Butanoic acid–water	−2.44	−0.50	−2.94	
S3	Menthol–water	−0.87	−0.15	−1.02	
	Menthol–hexanoic acid	−3.32	−8.15	−11.47	3.21
	Hexanoic acid–water	−2.14	−0.41	−2.55	
S4	Menthol–water	−0.84	−0.15	−0.99	
	Menthol–octanoic acid	−3.01	−9.51	−12.52	3.70
	Octanoic acid–water	−2.04	−0.36	−2.40	
S5	Menthol–water	−0.90	−0.19	−1.09	
	Menthol–decanoic acid	−2.56	−11.40	−13.96	4.61
	Decanoic acid–water	−1.69	−0.25	−1.94	
S6	Menthol–water	−1.68	−0.24	−1.92	
	Menthol–dodecanoic acid	−4.10	−18.77	−22.87	6.10
	Dodecanoic acid–water	−1.57	−0.26	−1.83	
S7	Menthol–water	−0.99	−0.14	−1.13	
	Menthol–pyruvic acid	−4.97	−7.35	−12.32	2.48
	Pyruvic acid–water	−3.43	−0.40	−3.83	
S8	Menthol–water	−1.16	−0.17	−1.33	
	Menthol–levulinic acid	−2.11	−4.07	−6.18	1.22
	Levulinic acid–water	−3.14	−0.61	−3.74	
S9	$N_{4444}Cl$–water	−13.42	−0.28	−13.70	
	$N_{4444}Cl$–acetic acid	−16.76	−6.08	−22.84	1.57
	Acetic acid–water	−0.72	−0.12	−0.84	
S10	$N_{4444}Cl$–water	−13.81	−0.18	−13.99	
	$N_{4444}Cl$–octanoic acid	−15.25	−16.11	−31.36	2.00
	Octanoic acid–water	−1.46	−0.24	−1.70	

Here, the HBA characteristic determined the overall stability of the DES in an aqueous medium.

4.3.2 RDF AND CDF

RDFs provide an insight into the structural properties of the different eutectic systems and their interactions in the presence of water. The RDFs presented the overall

structural properties of a molecule with different species in the system as shown in Figures 4.5, 4.6, and 4.7. Figure 4.5 presented the comparative analysis of the RDFs between HBD–water (Figure 4.5a) and HBA–HBD (Figure 4.5b). Figures 4.6 and 4.7 depicted the individual RDFs of HBA–HBD and HBD–water, respectively, for the menthol-based systems. The respective atomic sites that were selected for the RDFs are H24 and O2 for acetic acid, O2 for butanoic acid, H46 and O4 for octanoic acid, H40 and O2 for decanoic acid, O6 for water, and H20 for DL-menthol (refer to Figures 4.1 and 4.2 for detailed notations of all the molecules, and Figures 4.6 and 4.7 for the rest of the DESs). From Figure 4.5a, it can be observed that acetic acid had the most favorable interaction with water among all the HBD molecules. It gave a significantly sharp peak indicating the first solvation shell at around 3.15 Å. With an increase in the alkyl chain length of the HBD molecules, the subsequent reduction in the g(r) values of the RDFs was observed. This comparative plot suggested that acetic acid had significant interaction with the water molecules and lower organic acid-based DESs were not stable with water as they tend to interact favorably with water. Conversely, higher organic acids have shown reduced interaction with water molecules as shown in Figure 4.5a.

Furthermore, from Figure 4.5b, we observed a sharp first solvation shell between DL-menthol and organic acids within 3Å. Interestingly, the maximum g(r) value sharply increased with an increase in the chain length of the organic acids. The maximum g(r) for decanoic acid, octanoic acid, and acetic acid were 3.5, 2.9, and 1.4, respectively (Figure 4.5b). It signified that the interaction of acetic acid and DL-menthol was less as compared to acetic acid–water; thus, DES1 became unstable in water. On the other hand, octanoic acid and decanoic acid showed increased interaction with DL-menthol and less with water. This initiated higher stability to both the DESs toward an aqueous environment. The respective coordination numbers were shown in Table 4.4, which also validated the analysis of the RDFs.

For tetrabutylammonium chloride–based DESs, we obtained the atom–atom RDF plots and tried to formulate a comparison among the species present, as shown in Figure 4.8. The ammonium cation exhibited higher interaction with water for system S10 as compared to system S9. For both cases, the maximum intensity g(r) peak appeared at about 4.15 Å, but the peak intensity differed (Figure 4.8a). We observed increased interaction of acetic acid–water as compared to octanoic acid–water as shown in Figure 4.8d. As water displayed less favorable interaction with octanoic acid (system S10), the ammonium cation present in the system exhibited higher interaction with water. It was also observed that ammonium cation displayed similar interaction with acetic acid and octanoic acid as well (Figure 4.8b). A very sharp g(r) peak of 14 and 17.8 was obtained between chloride ion and water for S9 and S10, respectively (Figure 4.8c), at about 2.0 Å. Overall, the RDFs in Figure 4.8 suggested that both DES9 and DES10 had favorable interaction with water mainly because of the presence of hydrophilic moieties, such as ammonium cation, chloride ion, and acetic acid. This revealed the fact that DES components got disrupted in the presence of water disturbed the DES integrity and exposed the instability of ammonium-based DESs in the aqueous environment.

Furthermore, for the confirmation of the hydrogen bonding, we have obtained the CDF (angular and radial). The CDF was evaluated as a function of HBD–HBA distance and donor–acceptor angle as shown in Figure 4.9. The TRAVIS package

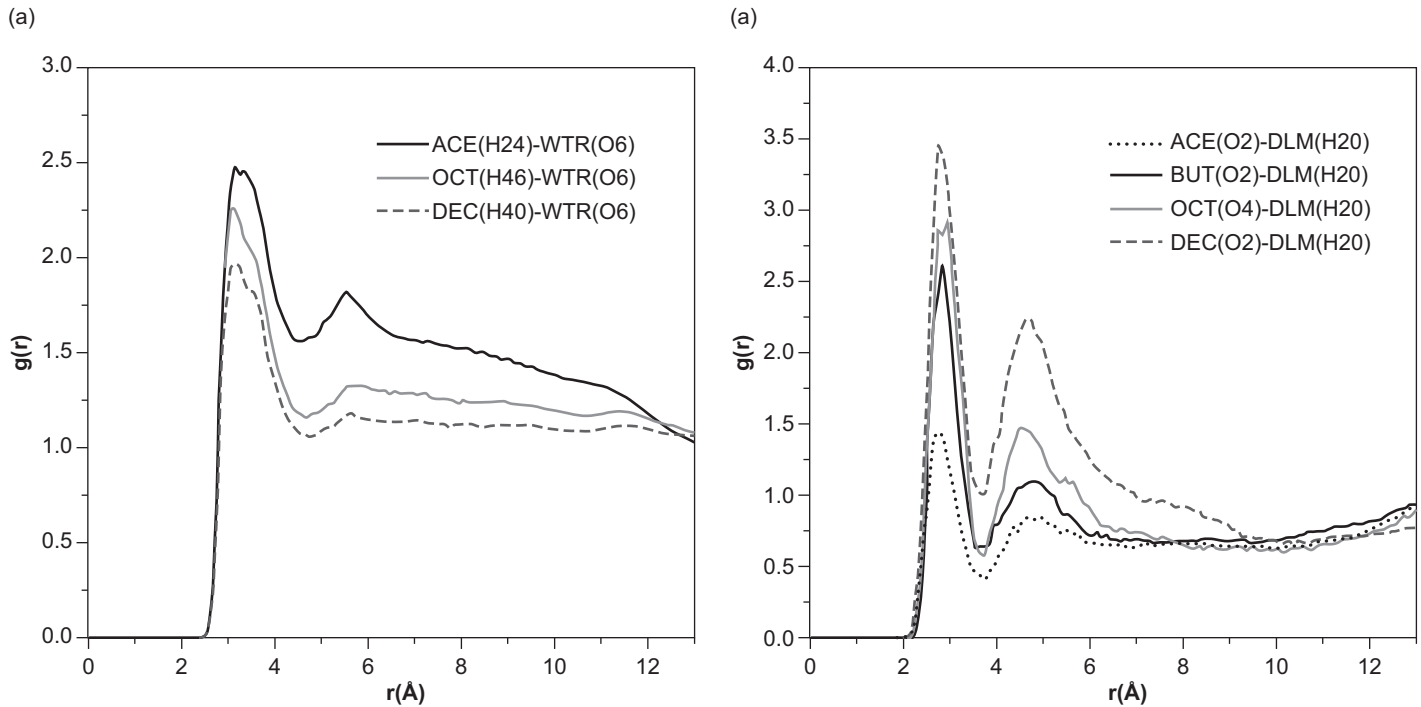

FIGURE 4.5 Comparison among atom-specific RDF plots between the different molecular pairs present in the different DES–water systems: (a) acetic acid–water, octanoic acid–water, and decanoic acid–water, for systems S1, S4, and S5, respectively; (b) DL-menthol–acetic acid, DL-menthol–butanoic acid, DL-menthol–octanoic acid, and DL-menthol–decanoic acid, for systems S1, S2, S4, and S5, respectively, at 100 ns.

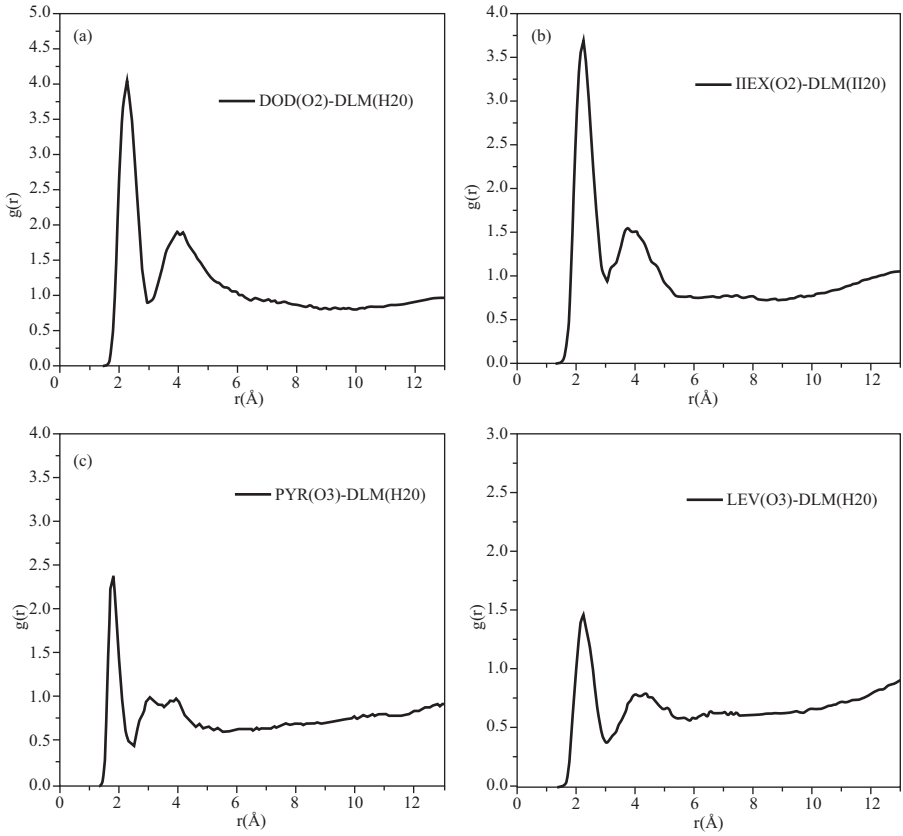

FIGURE 4.6 Atom–atom RDF plots between DL-menthol and (a) dodecanoic acid (S6), (b) hexanoic acid (S3), (c) pyruvic acid (S7), and (d) levulinic acid (S8), at 100 ns.

[44] was used to obtain the CDF, and the calculation procedure to evaluate CDF was followed as mentioned in the literature [44]. The CDF confirmed the presence of hydrogen bonding among molecules and helps us in verifying the observations of RDFs. From Figure 4.9a, it was observed that acetic acid formed an O-H . . . O bond with water at a distance about 3.15 Å. It also had an angle between 160–180°, which followed the criteria of hydrogen bonding. Thus, the –OH group of acetic acid formed a hydrogen bond with the O atom of the water molecule with a distance of 3.15 Å and the bond was formed at an angle of 160–180° (for system S1). Similarly, Figure 4.9b pointed out the fact that DL-menthol formed O-H . . . O bond with decanoic acid at 3 Å keeping the angle between the bonds ranging from 120–160°. This confirms the results obtained by the RDFs and also possible hydrogen bonding between DL-menthol and decanoic acid (for system S5). Similar to menthol–decanoic acid, DL-menthol displayed a possible O-H . . . O hydrogen bond with octanoic acid (for system S4; Figure 4.9d). No significant interaction, such as hydrogen bonding and molecular distribution, was observed between octanoic

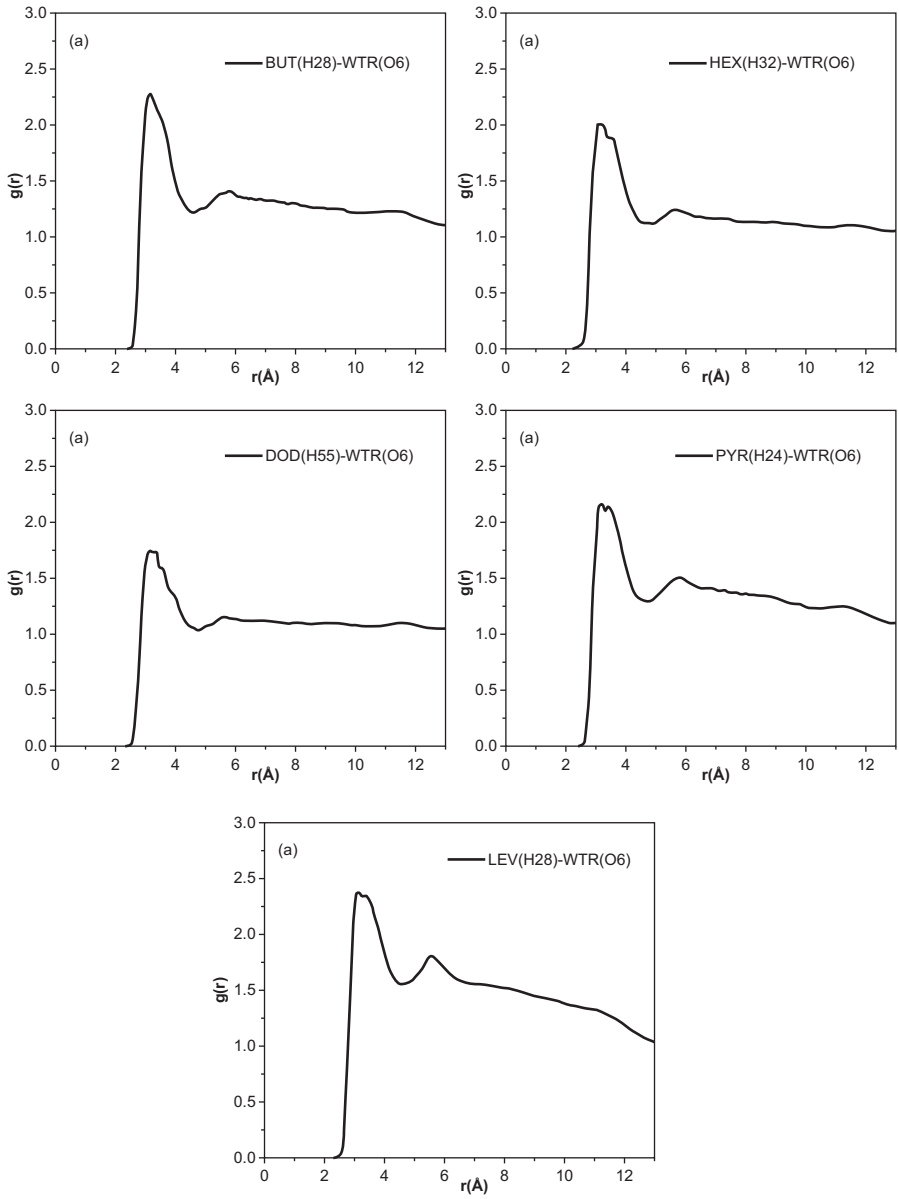

FIGURE 4.7 Atom–atom RDF plots for individual systems of DL-menthol–based DESs between (a) butanoic acid–water (S2), (b) hexanoic acid–water (S3), (c) dodecanoic acid–water (S6), (d) pyruvic acid–water (S7), and (e) levulinic acid–water (S8) at 100 ns.

acid and water (for system S4) as per Figure 4.9c. A significantly higher degree of hydrogen bonding was observed for decanoic acid and octanoic acid than for acetic acid, which is shown in Figures 4.9a, 4.9b, and 4.9c. A higher value of the color code suggests a higher degree of hydrogen bonding. We did not observe hydrogen

TABLE 4.4
Coordination Number Obtained from the RDF for Different DES Systems

System	Component pairs	Coordination number (Z)
S1	Menthol–water	0.70
	Menthol–acetic acid	1.50
	Acetic acid–water	2.60
S2	Menthol–water	0.55
	Menthol–butanoic acid	2.60
	Butanoic acid–water	2.30
S3	Menthol–water	0.60
	Menthol–hexanoic acid	3.40
	Hexanoic acid–water	2.15
S4	Menthol–water	0.45
	Menthol–octanoic acid	3.60
	Octanoic acid–water	2.05
S5	Menthol–water	0.40
	Menthol–decanoic acid	3.8
	Decanoic acid–water	1.97
S6	Menthol–water	0.50
	Menthol–dodecanoic acid	4.0
	Dodecanoic acid–water	1.77
S7	Menthol–water	0.85
	Menthol–pyruvic acid	2.4
	Pyruvic acid–water	2.2
S8	Menthol–water	0.75
	Menthol–levulinic acid	1.3
	Levulinic acid–water	2.37
S9	$N_{4444}Cl$–water	1.65
	$N_{4444}Cl$–acetic acid	1.70
	Acetic acid–water	1.45
S10	$N_{4444}Cl$–water	2.40
	$N_{4444}Cl$–octanoic acid	1.75
	Octanoic acid–water	1.25

bonding between decanoic acid and water. It signified that there was very little interaction between decanoic acid and water. Similar results were also obtained for octanoic acid and water.

4.3.3 Hydrogen Bond Properties

Figure 4.10a represents the average number of HBD–water hydrogen bonds per HBD molecule, and Figure 4.10b represents the average number of HBA–HBD hydrogen bonds per DES molecule, both as a function of simulation time. The geometric criteria for hydrogen bonding were considered based on the literature [17]. The criteria were defined by a cutoff value for distance and angles between the atoms that were

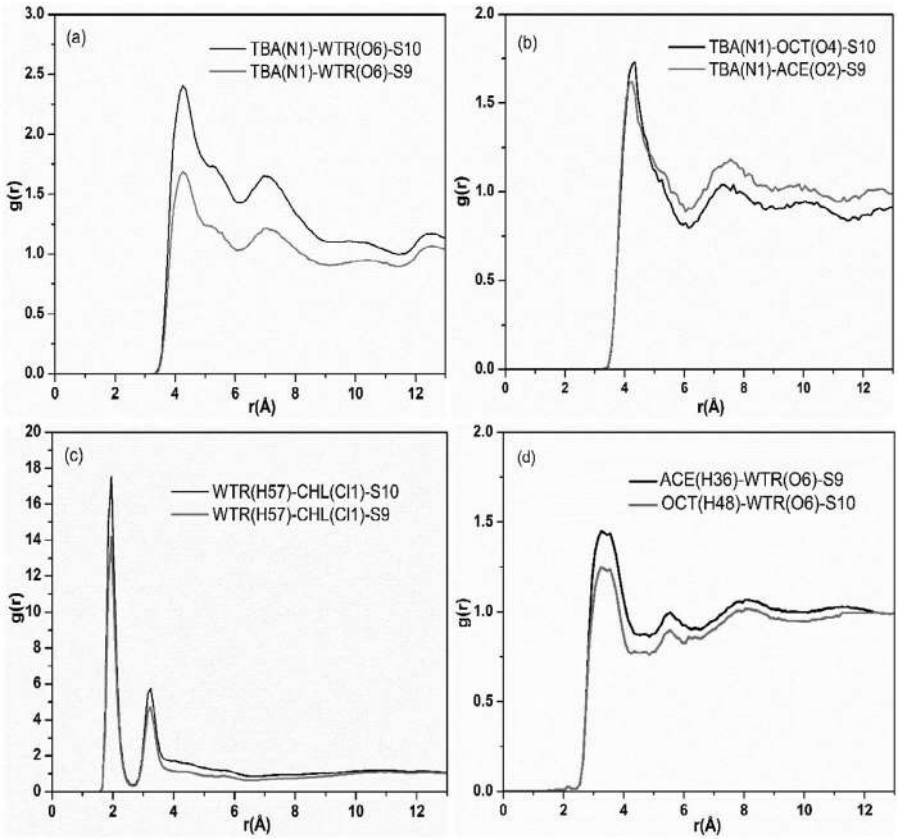

FIGURE 4.8 Comparison among atom-specific RDF plots for different DES–water systems for the different molecular pairs between (a) tetrabutylammonium cation–water, for system S9 and S10; (b) tetrabutylammonium cation–acetic acid, for system S9 and tetrabutylammonium cation–octanoic acid, for system S10; (c) water–chloride ion for system S9 and S10, at 100 ns; (d) acetic acid–water, for system S9 and octanoic acid-water, for system S10.

involved in hydrogen bonding. It can be observed that the hydrogen bond donors (carboxylic acids) form O-H–O hydrogen bonds with water at an average distance of approximately 3.1 Å (Figure 4.9a). Additionally, the HBD molecules formed O . . . H-O bonds with DL-menthol at an average distance of about 3 Å (Figure 4.9b). Because of this, 3.5 Å was considered as the cutoff distance, while the cutoff angle was considered from 120–180° for all the systems. The menthol–water hydrogen bonding for the systems S1, S2, S4, and S5 were shown in Figure 4.10c. The degree of hydrogen bonding between menthol and water was almost the same for all the systems, and the value was quite less, indicating a minimum interaction between them. In Figure S5, the average value of the average number of hydrogen bonds was obtained between HBD–water, HBA–HBD, and HBA–water, for the DL-menthol–based systems (S1–S8), as a function of simulation time.

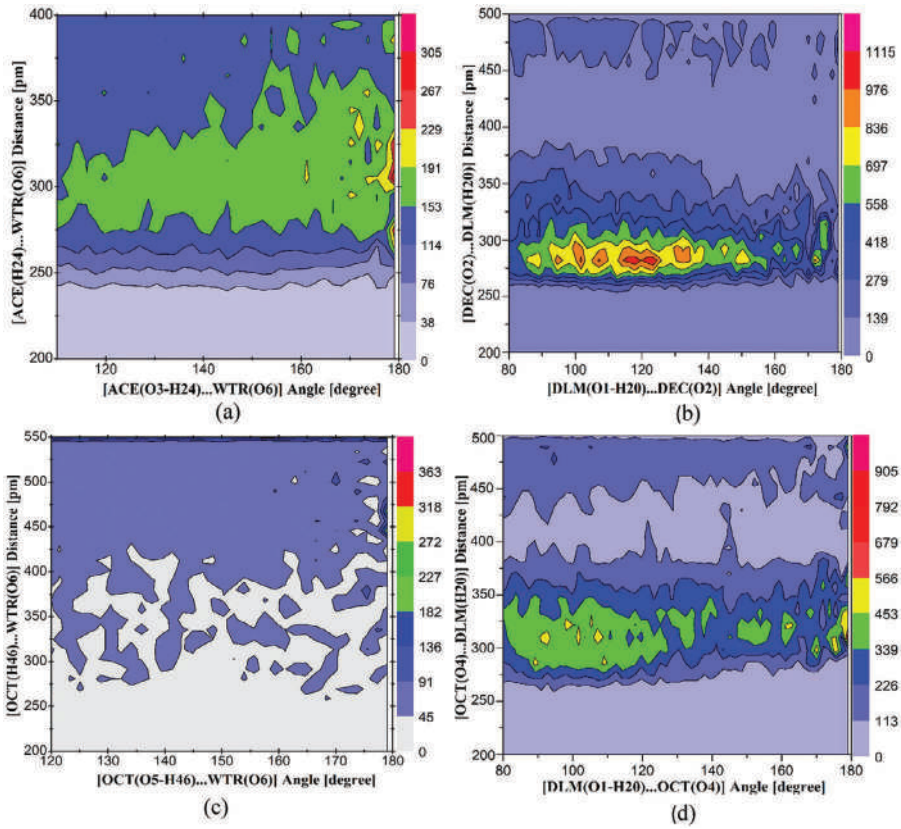

FIGURE 4.9 CDFs obtained by plotting the hydrogen bond distance (RDF) versus the hydrogen bond angle (ADF) for (a) O3-H24 . . . O6 angle against H24 . . . O6 distance (acetic acid–water); (b) O1-H20 . . . O2 angle against H20 . . . O2 distance (DL-menthol–decanoic acid); (c) O5-H46 . . . O6 angle against H46 . . . O6 distance (octanoic acid–water); and (d) O1-H20 . . . O4 angle against H20 . . . O4 distance (DL-menthol–octanoic acid).

In Figure 4.10a, it can be observed that the average number of hydrogen bonds between HBD and water decreased from the acetic acid system to the dodecanoic acid system in the case of DL-menthol–based DESs. It can be deduced that dodecanoic acid–based DES is more stable than acetic acid–based DES in an aqueous medium. The degree of hydrogen bonding between HBD–water can be presented as acetic acid > levulinic acid > butanoic acid > pyruvic acid > hexanoic acid > octanoic acid > decanoic acid > dodecanoic acid. The exact opposite order of the hydrogen bonding can be witnessed between HBA–HBD in Figure 4.10b. Fewer hydrogen bondings were witnessed between menthol and water for all the systems (Figure 4.10c).

The hydrogen bonding between the different species for the $N_{4444}Cl$-based systems was obtained as shown in Figure 4.11. It can be noticed that acetic acid formed a higher number of hydrogen bonds with water as compared to octanoic acid (Figure

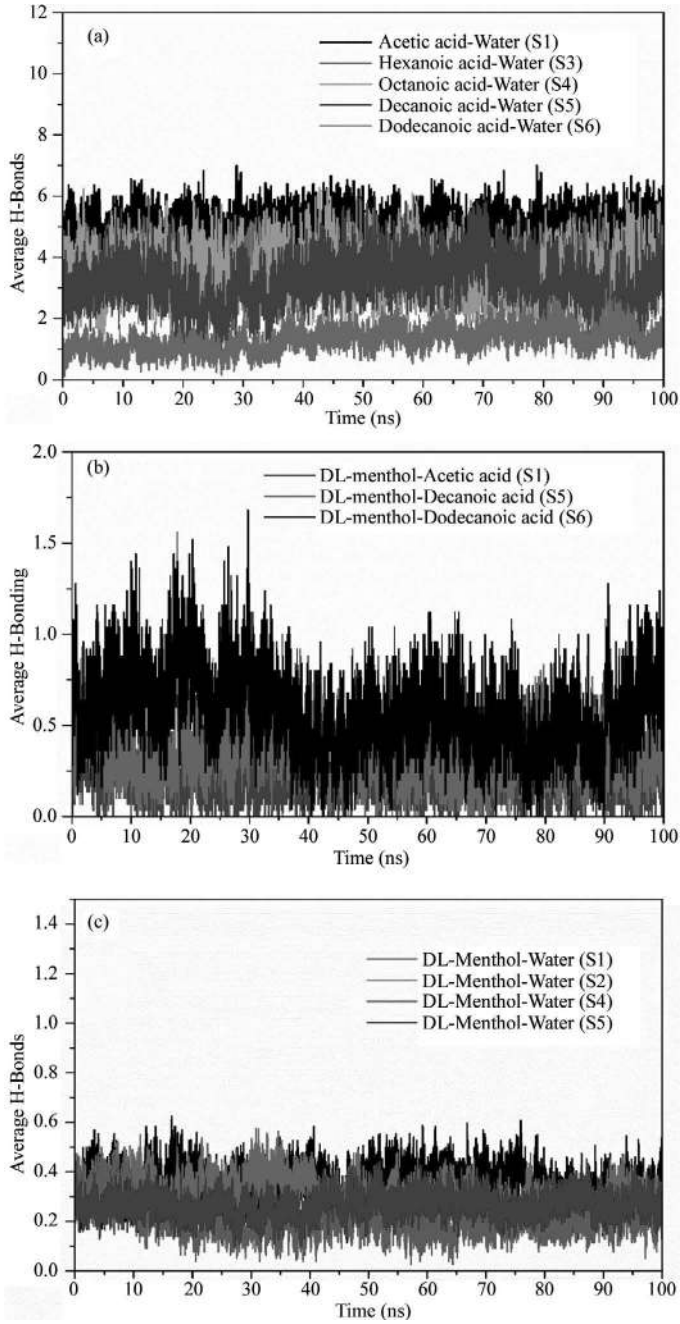

FIGURE 4.10 The average number of hydrogen bonds between (a) HBD–water per HBD molecule, for systems S1, S3, S4, S5, and S6; (b) HBA–HBD per DES molecule, for systems S1, S5, and S6; and (c) HBA–water per HBA molecule, for systems S1, S2, S4, and S5 as a function of simulation time.

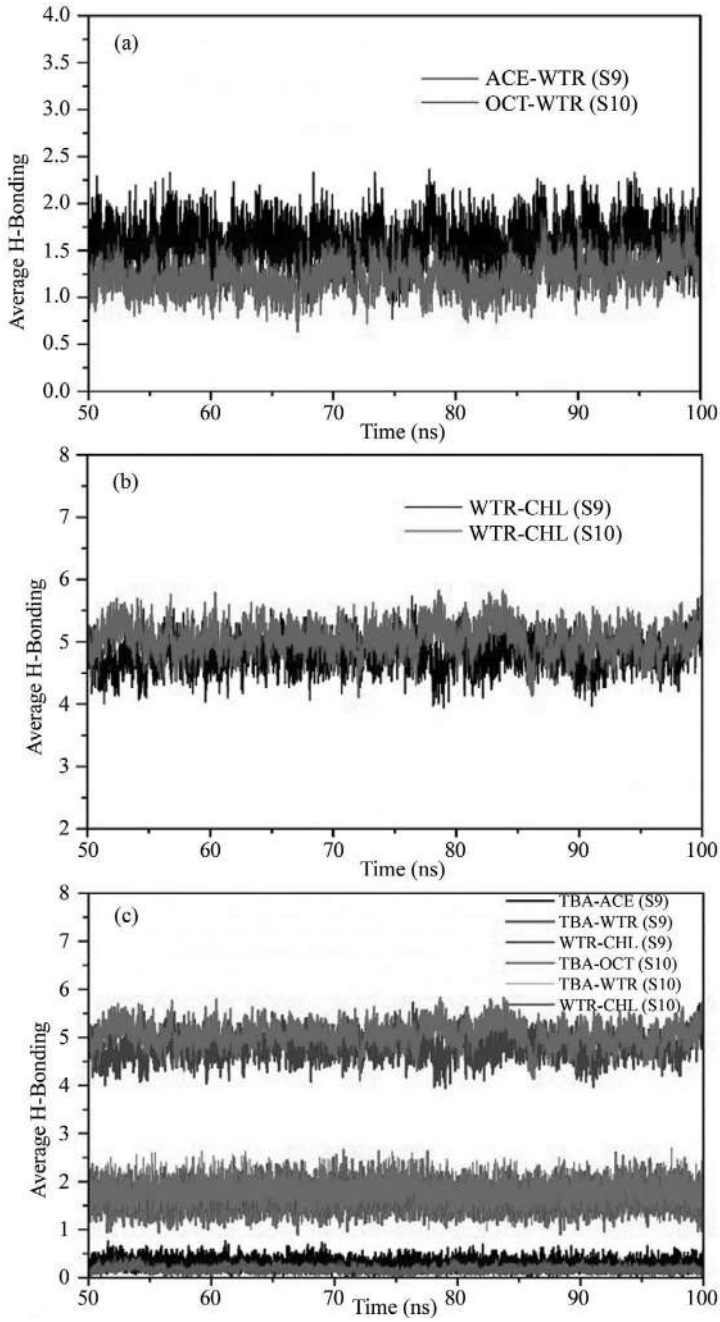

FIGURE 4.11 The average number of hydrogen bonds between (a) HBD–water per HBD molecule, for systems S9 and S10; (b) chloride anion–water per chloride ion, for systems S9 and S10; (c) various combinations among tetrabutylammonium cation, water, acetic acid, octanoic acid, and chloride ion for systems S9 and S10 as a function of simulation time

4.11a). Also, a very high degree of hydrogen bonding was observed between water molecules and chloride ions (Figure 4.11b), leading to the fact that DES integrity was compromised as breakage of hydrogen bonding was witnessed between the ammonium cation and chloride anion. Here, hydration by chlorine atoms through water molecules was automatically addressed in the calculation of the average H-bonding ion. The overall nature of hydrogen bonding between the various components in the systems S9 and S10 are plotted in Figure 4.11c. From this plot, one can observe the following order of hydrogen bonding in both the systems S9 and S10, such as chloride ion–water molecule > tetrabutylammonium cation–water molecule > tetrabutylammonium cation–HBD molecule. The change in integral values of the ^{1}H-NMR spectra obtained by Florindo et al. [3] suggested that a large quantity of tetra butyl ammonium (TBA) cation was lost to the water phase as shown in Figure 4.4. In contrast, octanoic acid remained intact even after mixing with water. Overall, the simulation results were found to be in excellent support with that of the experiment [3].

4.3.4 Relative Stability Factor

Based on the nonbonded interaction energy among different species in a system, the stability of the eutectic systems in an aqueous environment can be predicted. For that, a new term, 'Relative Stability Factor,' is introduced to evaluate the relative stability of a eutectic system. It is a relative measure to analyze the stability of the hydrophobic DESs in an aqueous environment. The relative stability of hydrophobic DESs in water can be obtained from the ratio of the interaction energies between HBA–HBD and the sum of interaction energies between HBA–water and between HBD–water. Here, electrostatic interactions and vdW interactions were considered the two components of nonbonded interaction. This factor revealed the order of stability of different DES systems in contact with an aqueous environment. It does not exactly quantify the stability of a system. Since the interaction between HBA–water is almost constant in the case of menthol-based DESs, the stability factor primarily is a function of the HBD–water interaction. Hence, we defined the same as follows:

$$\text{Relative stability factor of hydrophobic DES } (\text{S}) = \frac{\text{IE}(\text{HBA} - \text{HBD})}{\text{IE}(\text{HBA} - \text{WATER}) + \text{IE}(\text{HBD} - \text{WATER})} \tag{4.1}$$

The factor was presented in Table 4.3. The higher the stability factor (S), the higher the stability of DES in water. From the experimental work of Florindo et al. [3], long-chain organic acid–based DESs were found to be more stable than the short-chain ones (menthol-based), whereas all the ammonium-based DESs were found to be hydrophilic. This can be verified by examining the relative stability factor (*S*) obtained with the help of MD simulation (Table 4.3). Initially, we compared the stability factor values obtained in this work (Table 4.3) to the experimental findings of the stability of DESs in water by Florindo et al. [3]. It was discovered

that a stability factor ranging from 0–3.30 can be labeled as "miscible in water" or "unstable in water". According to this assessment of the water stability of menthol-based DESs, acetic acid (S = 0.92) was found to be the "most unstable". Butanoic acid (S = 1.94), hexanoic acid (S = 3.21), pyruvic acid (S = 2.48), and levulinic acid (S = 1.22) is also termed as "unstable in water". However, octanoic acid (S = 3.70), decanoic acid (S = 4.60), and dodecanoic acid (S = 6.10) emerged to be "stable in water" (for menthol-based DESs). For $N_{4444}Cl$-based DESs, both acetic acid (S = 1.57) and octanoic acid (S = 2.00) were 'unstable in water. Overall, from the observation of the relative stability factor data (Table 4.3), the order of stability of menthol-based DESs in an aqueous medium in terms of HBD was found to be in the order: dodecanoic acid > decanoic acid > octanoic acid > hexanoic acid > pyruvic acid > butanoic acid > levulinic acid > acetic acid. The ammonium-based DESs it was found to be in the order of octanoic acid > acetic acid.

4.3.5 MSD

Estimation of the self-diffusion coefficient (D) is carried out by using Einstein's equation (Equation 3.3, Chapter 3), which involves the MSD of the molecule. It is a useful parameter to measure the overall mobility of various species in the system. From the slope of the MSD curve obtained by the simulation, we can calculate the self-diffusion coefficient for each species. From Figure 4.12, the linear trend of the MSD plots can be observed. In Figures 4.12a and 4.12b, one can note that the acetic acid and water curves have come close to each other, indicating higher mobility within the system. The menthol curve is also shifted at 90–100 ns (Figure 4.12b) as compared to 0–10 ns (Figure 4.12a). One possible explanation for this can be a disruption of DES structure as acetic acid might leach through the DES phase. Thereby, we have observed the movement of the menthol molecule along with it. Figures 4.12c and 4.12d depict less movement for both menthol and octanoic acid molecule. Since both components are hydrophobic in nature, accordingly less mobility was observed. This certainly leads to the fact that both DES components were quite stable within the system. The self-diffusivity coefficient data for different systems are provided in Table 4.5. From the self-diffusivity values of the species the following conclusions can be drawn:

1. With an increase in simulation time, the diffusion coefficient values of both acetic acid and water are decreased. The increased movement and transport tendency of acetic acid and water molecules are suggested as both molecules followed a similar trend in diffusivity (system S1). Similar trends were observed between butanoic acid–water and pyruvic acid–water for the systems S2 and S7, respectively (Table 4.5). The similar diffusivity values trigger the higher movement of molecules with a possibility to move through the phases.
2. Octanoic acid and DL-menthol have a significant difference in their self-diffusion coefficient with water both at the beginning as well as at the end of the production run. Furthermore, the diffusivity values of both molecules did not change much throughout the simulation (system S4). Similar results

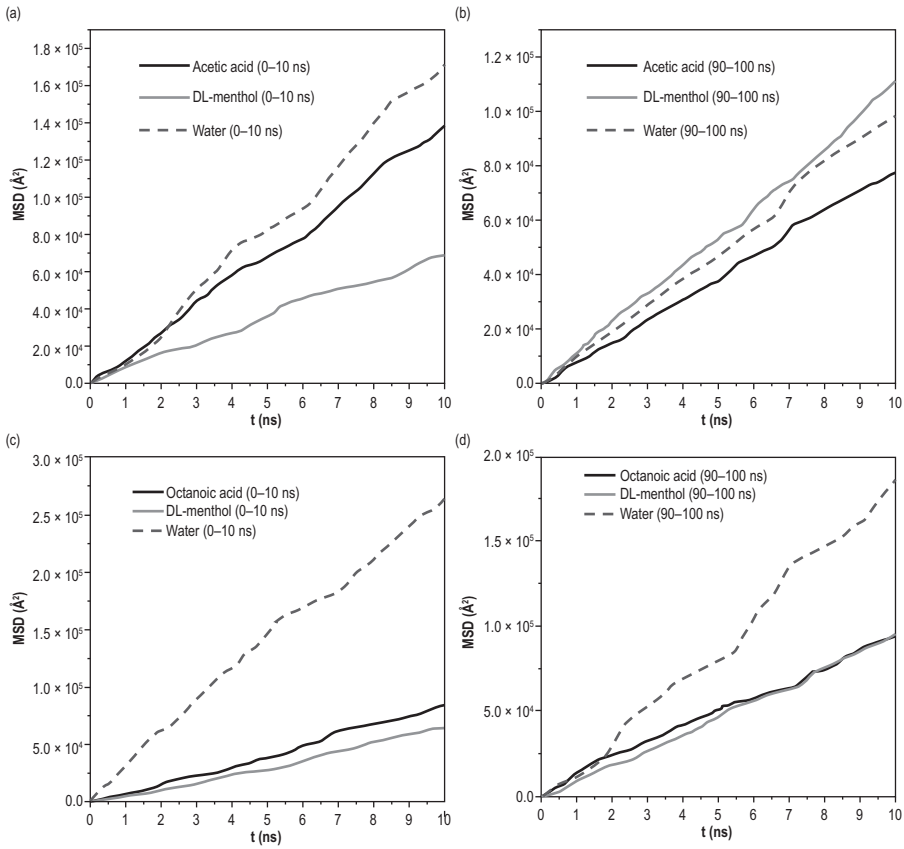

FIGURE 4.12 MSD plot at (a) 0–10 ns and (b) 90–100 ns, respectively, for system S1 and at (c) 0–10 ns and (d) 90–100 ns, respectively, for system S4.

were observed for DL-menthol–dodecanoic acid system (system S6) with similar self-diffusion coefficient values between these two species. Overall, it suggests that these DESs are quite stable in the DES phase and do not tend to move freely through the phases.

3. The diffusion coefficient values of acetic acid, chloride ion, and water were very close to each other, and in addition, the diffusivity value of TBA cation (system S9) decreased in the last 90–100 ns run (Table 4.5). This suggests a high diffusive property of all the molecular species. In the case of system S10, though octanoic acid is present in the system, similar results were observed as compared to system S9. Additionally, the diffusion coefficients of octanoic acid and DL-menthol were very close to the unity implying a very stable assembly of the species.

From all the preceding findings, the following outcomes can be suggested: (1) DL-menthol–based DESs with acetic acid, butanoic acid, hexanoic acid, and pyruvic

TABLE 4.5
Self-Diffusivity for Different Molecular Species of DL-Menthol–Based and Tetrabutylammonium-Based DES Systems with Water at 298.15 K at Different Time Intervals

System number	Molecule species	Diffusion coefficient (D) × 10^{-9} (m^2/s)		
		0–10 ns	40–50 ns	90–100 ns
S1	Acetic acid	1.150	0.884	0.665
	DL-menthol	0.564	0.705	0.905
	Water	1.484	1.162	0.844
S2	Butanoic acid	1.003	0.918	0.601
	DL-menthol	0.656	0.495	0.960
	Water	1.239	1.765	0.828
S3	Hexanoic acid	0.834	0.818	0.728
	DL-menthol	0.775	0.975	0.450
	Water	1.506	0.841	2.438
S4	Octanoic acid	0.722	0.840	0.734
	DL-menthol	0.560	0.793	0.793
	Water	2.145	1.463	1.557
S5	Decanoic acid	0.944	0.632	0.916
	DL-menthol	1.002	0.627	0.592
	Water	1.078	2.633	2.385
S6	Dodecanoic acid	0.908	0.980	0.774
	DL-menthol	0.808	0.806	0.852
	Water	1.091	1.182	1.365
S7	Pyruvic acid	0.804	0.944	0.608
	DL-menthol	0.613	0.433	0.912
	Water	1.301	1.848	0.846
S8	Levulinic acid	0.904	0.566	0.887
	DL-menthol	0.729	1.042	0.700
	Water	1.291	0.950	1.309
S9	Acetic acid	0.745	0.658	0.890
	TBA cation	0.633	0.661	0.597
	Chloride ion	0.740	0.822	0.835
	Water	0.912	0.964	0.963
S10	Octanoic acid	0.813	1.068	0.994
	TBA cation	0.657	0.546	0.551
	Chloride ion	0.851	0.702	0.908
	Water	0.925	0.803	0.941

acid are not stable in an aqueous environment as they possess similar diffusivity to water and high mobility within the system. Also, the transfer of acetic acid and butanoic acid to the water phase starts at the beginning of the simulation and happens at a similar rate throughout the simulation. (2) DL-menthol–based DESs with octanoic

acid and higher organic acids have shown higher stability in water and can be utilized as hydrophobic solvents. (3) Tetrabutylammonium chloride–based DESs are very hydrophilic in nature as observed from the self-diffusivity values, and the transport of the ions to the water phase was observed from 0–40 ns of the simulation run. The next section discusses the extractive desulfurization (ED) of fuel in the context of DESs.

4.4 DENSITY FUNCTIONAL THEORY AND NATURAL BONDING ORBITAL ANALYSIS ON ED OF FUEL

Density functional theory (DFT) can be very much helpful in the atomistic level understanding of DES formation and nonbonded interaction mechanism. MD simulation gives a bulk system property analysis whereas the DFT-based QC calculations highlight the atom- and molecular-level insights, which, in turn, gives valuable information regarding hydrogen bonding interactions and thermochemical analysis with thermodynamic and chemical property evaluations. Natural bonding orbital (NBO) analysis shows light in calculating the charge transfer (CT) process in a given system. Overall, these studies are useful in better understanding of the DES systems.

4.4.1 Optimized Geometries of DESs and Their Complexes with ASCs

In this study, the structures of the DES and the ASCs were optimized using the M06–2X/6–31++G(d,p) level of calculation [45]. The DESs selected for this study were reline and ethaline whereas the ASCs were BT, DBT, and their oxides. The optimized structures of the DESs are presented in Figure 4.13. Similarly, the optimized structures of the DES–ASC clusters are displayed in Figures 4.14 and 4.15 for reline and ethaline, respectively. The M06–2X functional has been selected due to its

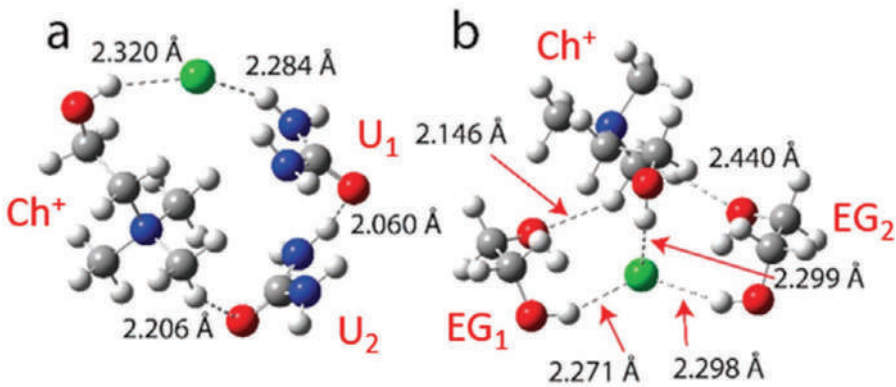

FIGURE 4.13 M06–2X/6–31++G(d,p) optimized geometries of (a) reline and (b) ethaline DES clusters. Dark gray: carbon, light gray: hydrogen, red: oxygen, green: chlorine, and blue: nitrogen. Ch+ denotes choline; U1 and U2 denote urea, and EG1 and EG2 represent ethylene glycol. Reprinted (adapted) with permission from Wagle, Durgesh V., et al. "Quantum chemical evaluation of deep eutectic solvents for the extractive desulfurization of fuel." ACS Sustainable Chemistry & Engineering, 2018, 6(6) p. 7525–75313. Copyright (2018) American Chemical Society [47].

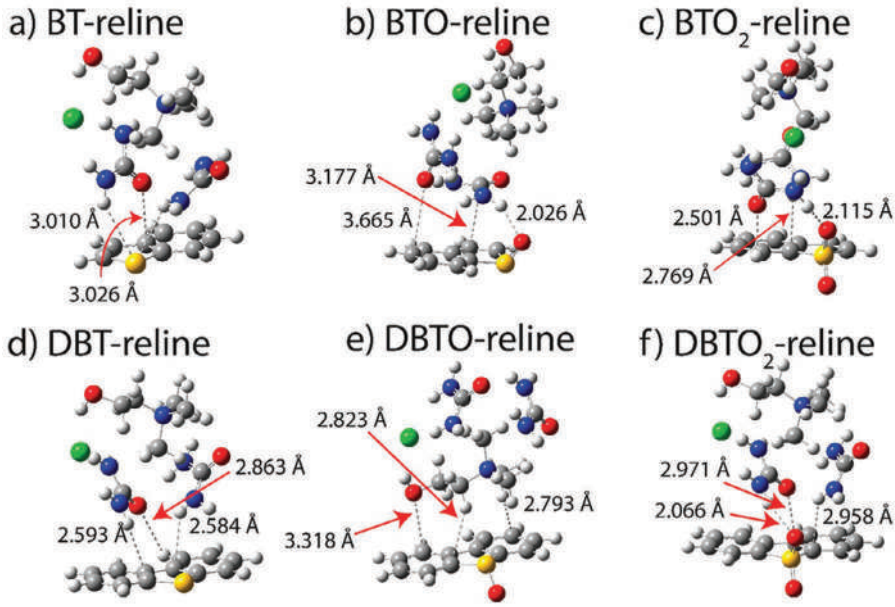

FIGURE 4.14 M06–2X/6–31++G(d,p) optimized geometries of reline and aromatic sulfur compound complexes. Dark gray is used to color carbon, light gray for hydrogen, red for oxygen, yellow for sulfur, green for chlorine, and blue for nitrogen. Reprinted (adapted) with permission from Wagle, Durgesh V., et al. "Quantum chemical evaluation of deep eutectic solvents for the extractive desulfurization of fuel." *ACS Sustainable Chemistry & Engineering*, 2018, 6(6) p. 7525–7531. Copyright (2018) American Chemical Society [47].

accurate insights into dipole interactions, hydrogen-bonding interactions, noncovalent interactions, and charge transfer processes [45–47]. The desulfurization process and the selective performance of DESs were evaluated in the study.

The optimized reline and ethaline structures consist of choline chloride:urea and choline chloride:EG, respectively, at a molar ratio of 1:2. A complex but favorable combination of nonbonded interactions was observed among the components of the DES. The negative chloride atom present in choline chloride as seen in Figure 4.13a for reline, there is a significant hydrogen bonding contact between urea and Cl through N-H . . . Cl^- hydrogen bonds, with the shortest H . . . Cl interaction lengths of 2.284 Å. DES structure involved two weaker cis-N-H . . . O=C hydrogen bonds with the shortest H . . . O distance being 2.060 Å. Finally, the C=O on urea and the C-H on the choline cation's methyl groups are seen to have a significant interaction, with 2.206 Å as the shortest C=O . . . H-C distance, indicating C interactions between lone pairs (Figure 4.13a). Similarly, oxygen atoms of EG interact with the choline cation's methyl protons through C-H . . . O hydrogen connections that are not normal, having the shortest distance of 2.440 Å (Figure 4.13b), with ethaline having numerous hydrogen bonds between EG and Cl^-.

Figures 4.14 and 4.15 demonstrated the optimized interactions of ASCs with reline and ethaline, respectively. In particular, the optimized geometries demonstrate

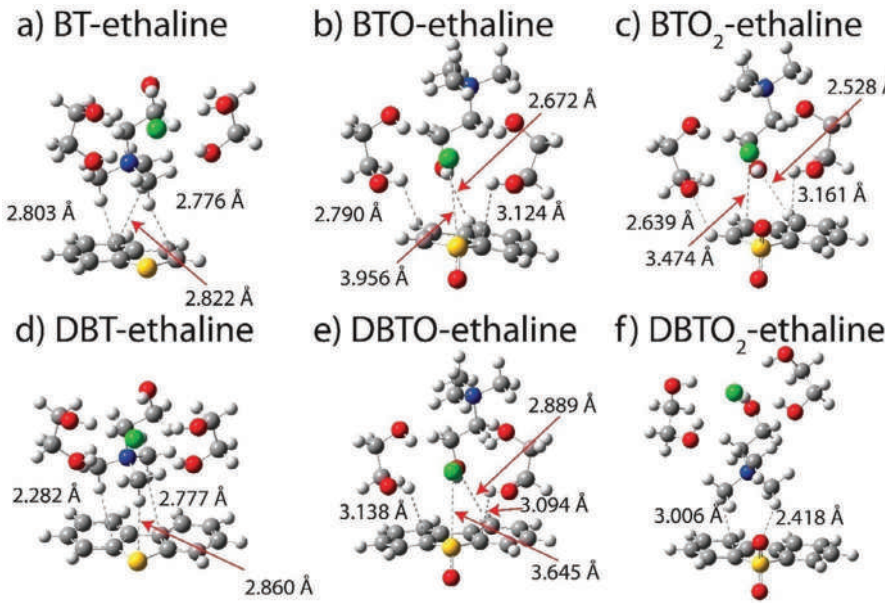

FIGURE 4.15 M06–2X/6–31++G(d,p) optimized geometries of ethaline and ASC complexes. Dark gray is used to color carbon, light gray for hydrogen, red for oxygen, yellow for sulfur, green for chlorine, and blue for nitrogen. Reprinted (adapted) with permission from Wagle, Durgesh V., et al. "Quantum chemical evaluation of deep eutectic solvents for the extractive desulfurization of fuel." *ACS Sustainable Chemistry & Engineering*, 2018, 6(6) p. 7525–7531. Copyright (2018) American Chemical Society [47].

that there is no interaction between chloride ion (Cl) and BT or DBT, but choline ion (Cho) interacts with both BT and DBT as well as the HBD species (urea and EG in reline and ethaline, respectively) by which they interact with the aromatic rings of BT or DBT, respectively. However, the bonding is weak when it comes to noncovalent (C–H . . . π, C–O . . . π, O–H . . . π, and N–H . . . π) interactions. The DES clusters maintain the majority of their original characteristics of the hydrogen-bonding network formed between the HBA and HBD molecules upon the injection of an ASC that has not been oxidized, showing a preference for retaining the connection between hydrogen-bonding contacts inside the DES cluster. The development of new contacts with the nonpolar, unoxidized aromatic substance (BT or DBT) could not hamper the inherent DES forming ability of the DES components. Specifically, the presence of an oxygen atom on the sulfur atom of the aromatic rings (designated Os) in the monoxide (BTO and DBTO) and dioxide (BTO2 and DBTO2) forms of ASCs enables for the establishment of typical hydrogen bonds between the ASCs and the choline or HDB components of the DES. Although the presence of Os facilitates additional interactions (such as C–H . . . Os, N–H . . . Os, and O–H . . . Os), it also significantly weakens the choline and HBD interactions with the aromatic ring, as evidenced by the increased interaction distances between the DES components and the aromatic rings (see panels b, e, and f in Figure 4.14 and panels b, c, and e in

Figure 4.15). It should be noted that the sole exception to this pattern is the reline–BTO2 system, in which one of the urea molecules is close to the BTO2 as a result of the absence of interaction between that urea and Os.

4.4.2 Gas Phase Thermodynamics

When an ASC and DES complex is formed, there are changes in enthalpy and free energy associated with the formation of the complex. This information can be used to determine whether the interaction between a given DES and ASC is thermodynamically favorable, which is an important factor influencing the ED of fuels. The thermochemical parameters in this table were calculated using Equation 4.2:

$$\Delta X_{ASC-DES} = X_{ASC-DES} - X_{ASC} - X_{DES} \tag{4.2}$$

All ASC–DES complexes except BTO have ΔG values that are positive, but all the complexes have negative ΔH values (Table 4.6). The BTO–DES complexes only display advantageous thermodynamic behavior in a gas phase environment because of their strong intermolecular interactions. BTO's smaller size and greater polarity than the other ASCs result in this beneficial interaction between BTO and DESs.

4.4.3 Continuum Solvation Study

As it turns out, continuum solvation models offer the best conceptual framework for describing solvent effects in the context of the QM method. Because the polarization of the dielectric due to the presence of a solute (or, in Onsager's terminology, its reaction field) is induced by the solute, and the solute itself is polarised back by the solvent, an iterative self-consistent field approach is used to calculate the polarization of the dielectric [47, 48]. To determine the change in solvation free energy (G°_{solv}) when an ASC molecule is transported from one phase (octane) to another (DES), a liquid–phase investigation was performed (Figure 4.16). The SMD solvation model developed by Truhlar and coworkers [49] was used to calculate the free solvation energies at the M06–2X/6–31++G(d,p) level of theory. It was found that the efficiency of ASC transfer from the liquid fuel phase to the DES may be better understood by measuring the standard free energy of solvation. Liquid fuel was mimicked by using an octane solvent.

TABLE 4.6
Free Energy Changes (ΔG/kcal mol^{-1}) and Enthalpy Changes (ΔH/kcal mol^{-1}) Associated with the Formation of the Various DES–ASC Complexes

	DES	BT	DBT	BTO	DBTO	BTO_2	$DBTO_2$
Free Energy Changes	Reline	8.58	5.44	−20.68	5.85	4.12	2.92
	Ethaline	5.28	3.15	−19.53	3.89	5.80	3.24
Enthalpy Changes	Reline	−3.48	−6.87	−32.13	−6.64	−8.39	−10.03
	Ethaline	−6.85	−6.46	−30.82	−7.57	−6.26	−7.73

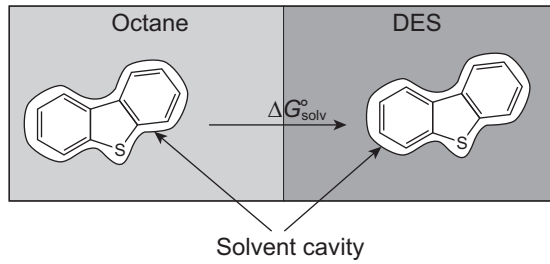

FIGURE 4.16 Schematic representation of the determination of the free energy of solvation for aromatic sulfur compounds for transfer from an octane phase to a DES phase. Reprinted (adapted) with permission from Wagle, Durgesh V., et al. "Quantum chemical evaluation of deep eutectic solvents for the extractive desulfurization of fuel." *ACS Sustainable Chemistry & Engineering*, 2018, 6(6) p. 7525–7531. Copyright (2018) American Chemical Society [47].

TABLE 4.7
Free Energy of Solvation Changes (ΔG°_{solv}) of an ASC for Transfer from the Octane Phase to DES Phase

DES	BT	DBT	BTO	DBTO	BTO_2	$DBTO_2$
Reline	0.62	0.59	−3.12	−2.12	−3.50	−2.03
Ethaline	0.60	0.91	−4.42	−3.76	−4.74	−3.74

$$\Delta G^{\circ}_{solv} = G_{DES} - G_{octane} \tag{4.3}$$

The ΔG°_{solv} was calculated as the difference in free energy in the DES phase and octane phase for the ASCs as expressed by Equation 4.3 and presented in Table 4.7. The Truhlar group's SMD solvation model [49] was utilized to calculate ΔG°_{solv}. BT and DBT (Table 4.7) have positive ΔG°_{solv} values, but the mono- and dioxides have negative ones. This shows an increase in the likelihood of an ASC moving from the octane to the DES phase following oxidation of the aromatic sulfur. As the sulfur atom is oxidized, the ASC's capacity to form hydrogen bonds with the DES through Os increases, leading to a preference for the DES phase (Figures 4.14 and 4.15). Although the ΔG°_{solv} of the ASCs improved slightly when the sulphur atom was oxidized from monoxide to dioxide, the overall improvement was negligible. This finding indicates that sulfur mono-oxidation is adequate to remove ASCs from octane and transfer it to DES. Furthermore, BT compounds have better ΔG°_{solv} values than dibenzothiophene derivatives. BT derivatives have a lower hydrophobicity than DBT derivatives, making them more compatible with hydrophilic DESs. This tendency is a result of this fact.

4.5 SUMMARY

A MD simulation study was performed to understand the relative partitioning and distribution of the components of the organic acid–based DESs in the presence of

an aqueous environment utilizing thermodynamic properties, such as interaction energy and structural, as well as diffusive, properties. Their molecular-level activities were studied when exposed to an aqueous environment. The interaction energy study revealed that menthol and higher fatty acid (C_8–C_{12})–based DESs have maintained their chemical and physical integrity in contact with water. The term 'Relative Stability Factor' was introduced to successfully measure the relative stability of a DES in an aqueous medium based on the nonbonded interaction energies among the components of the DESs. The sequence of stability of the menthol-based DESs in terms of HBD was found as dodecanoic acid > decanoic acid > octanoic acid > hexanoic acid > pyruvic acid > butanoic acid > levulinic acid > acetic acid. For ammonium-based DESs the order was found to be octanoic acid > acetic acid. The interaction mechanism between components of DES and water further revealed that vdW interactions were dominant between HBA-HBD while O–H–O hydrogen bond played a crucial role when interacting with water. The average hydrogen bond measured between HBA and HBD followed the same order as given earlier in terms of stability. The structural properties such as RDF and the CDF analysis provided significant evidence of strong HBA–HBD interactions in higher organic acid–based DESs and how short-chain fatty acid HBDs interact with water. The MSD plots and diffusion coefficient analysis regarding the transport properties revealed that HBDs and HBAs distributed themselves between the aqueous and DES phase in terms of their relative affinity toward that phase and stability of the DES was dependent on those interactions. The subsequent leaching of hydrophilic groups to the water phase was observed that was validated with the ^{1}H NMR data as obtained from the experimental literature.

To examine the usefulness of standard solvents for ED of fossil fuels, quantum chemical research of the ASC–DES interaction was done. The choline cation and the HBD components of the DES interact with the ASCs through several weak noncovalent interactions but do not directly interact with the chloride ion. When the ASC–DES complexes are formed, many strong hydrogen bonds between the Cl^- and the choline and HBD species are retained, and as a consequence, there are no ASC–Cl^- interactions. Remarkably, the DES cluster's intermolecular connections are entirely preserved during complex formation. Even more encouraging is the fact that after oxidation, the ASCs show a considerable increase in the free energy of solvation change. This indicates an improved ability to extract ASCs from a liquid fuel phase to the DES phase that may be used in desulfurization operations.

REFERENCES

1. Smith, E.L., A.P. Abbott, and K.S. Ryder, *Deep Eutectic Solvents (DESs) and their applications*. Chem. Rev., 2014. **114**: p. 11060–11082.

2. Van Osch, D.J.G.P., L.F. Zubeir, A. Van Den Bruinhorst, M.A.A. Rocha, and M.C. Kroon, *Hydrophobic deep eutectic solvents as water-immiscible extractants*. Green Chem., 2015. **17**: p. 4518–4521.
3. Florindo, C., L.C. Branco, and I.M. Marrucho, *Development of hydrophobic deep eutectic solvents for extraction of pesticides from aqueous environments*. Fluid Phase Equilib., 2017. **448**: p. 135–142.
4. Florindo, C., F. Lima, L.C. Branco, and I.M. Marrucho, *Hydrophobic deep eutectic solvents: A circular approach to purify water contaminated with Ciprofloxacin*. ACS Sustain. Chem. Eng., 2019. **7**: p. 14739–14746.
5. Martins, M.A.R., E.A. Crespo, P.V.A. Pontes, L.P. Silva, M. Bülow, G.J. Maximo et al., *Tunable hydrophobic eutectic solvents based on terpenes and monocarboxylic acids*. ACS Sustain. Chem. Eng., 2018. **6**: p. 8836–8846.
6. Morrison, H.G., C.C. Sun, and S. Neervannan, *Characterization of thermal behavior of deep eutectic solvents and their potential as drug solubilization vehicles*. Int. J. Pharm., 2009. **378**: p. 136–139.
7. Ge, D., Y. Wang, Q. Jiang, and E. Dai, *A deep eutectic solvent as an extraction solvent to separate and preconcentrate parabens in water samples using in situ liquid-liquid microextraction*. J. Braz. Chem. Soc., 2019. **30**: p. 1203–1210.
8. Zhu, S., J. Zhou, H. Jia, and H. Zhang, *Liquid—liquid microextraction of synthetic pigments in beverages using a hydrophobic deep eutectic solvent*. Food Chem., 2018. **243**: p. 351–356.
9. Ribeiro, B.D., C. Florindo, L.C. Iff, M.A.Z. Coelho, and I.M. Marrucho, *Menthol-based eutectic mixtures: Hydrophobic low viscosity solvents*. ACS Sustain. Chem. Eng., 2015. **3**: p. 2469–2477.
10. Dwamena, A.K., *Recent advances in hydrophobic deep eutectic solvents for extraction*. Separations, 2019. **6**.
11. Sas, O.G., M. Castro, Á. Domínguez, and B. González, *Removing phenolic pollutants using deep eutectic solvents*. Sep. Purif. Technol., 2019. **227**: p. 115703.
12. Martins, M.A.R., S.P. Pinho, and J.A.P. Coutinho, *Insights into the nature of eutectic and deep eutectic mixtures*. J. Solution Chem., 2019. **48**: p. 962–982.
13. Verevkin, S.P., A.Y. Sazonova, A.K. Frolkova, D.H. Zaitsau, I. V. Prikhodko, and C. Held, *Separation performance of BioRenewable deep eutectic solvents*. Ind. Eng. Chem. Res., 2015. **54**: p. 3498–3504.
14. Pontes, P.V.A., E.A. Crespo, M.A.R. Martins, L.P. Silva, C.M.S.S. Neves, G.J. Maximo et al., *Measurement and PC-SAFT modeling of solid-liquid equilibrium of deep eutectic solvents of quaternary ammonium chlorides and carboxylic acids*. Fluid Phase Equilib., 2017. **448**: p. 69–80.
15. Dietz, C.H.J.T., A. Erve, M.C. Kroon, M. van Sint Annaland, F. Gallucci, and C. Held, *Thermodynamic properties of hydrophobic deep eutectic solvents and solubility of water and HMF in them: Measurements and PC-SAFT modeling*. Fluid Phase Equilib., 2019. **489**: p. 75–82.
16. Mohan, M., P.K. Naik, T. Banerjee, V.V. Goud, and S. Paul, *Solubility of glucose in tetrabutylammonium bromide based deep eutectic solvents: Experimental and molecular dynamic simulations*. Fluid Phase Equilib., 2017. **448**: p. 168–177.
17. Paul, S. and S. Paul, *The influence of trehalose on hydrophobic interactions of small nonpolar solute: A molecular dynamics simulation study*. J. Chem. Phys., 2013. **139**.
18. Naik, P.K., S. Paul, and T. Banerjee, *Physiochemical properties and molecular dynamics simulations of phosphonium and ammonium based deep eutectic solvents*. J. Solution Chem., 2019. **48**: p. 1046–1065.
19. Naik, P.K., M. Mohan, T. Banerjee, S. Paul, and V.V. Goud, *Molecular dynamic simulations for the extraction of quinoline from heptane in the presence of a low-cost phosphonium-based deep eutectic solvent*. J. Phys. Chem. B, 2018. **122**: p. 4006–4015.

20. Warrag, S.E.E., C.J. Peters, and M.C. Kroon, *Deep eutectic solvents for highly efficient separations in oil and gas industries*. Curr. Opin. Green Sustain. Chem., 2017. **5**: p. 55–60.
21. Gutiérrez, M.C., D. Carriazo, C.O. Ania, J.B. Parra, M.L. Ferrer, and F. Del Monte, *Deep eutectic solvents as both precursors and structure directing agents in the synthesis of nitrogen doped hierarchical carbons highly suitable for CO 2 capture*. Energy Environ. Sci., 2011. **4**: p. 3535–3544.
22. Liu, W., W. Jiang, W. Zhu, W. Zhu, H. Li, T. Guo, et al., *Oxidative desulfurization of fuels promoted by choline chloride-based deep eutectic solvents*. J. Mol. Catal. A Chem., 2016. **424**: p. 261–268.
23. Jiang, W., L. Dong, W. Liu, T. Guo, H. Li, S. Yin, et al., *Biodegradable choline-like deep eutectic solvents for extractive desulfurization of fuel*. Chem. Eng. Process. Process Intensif., 2017. **115**: p. 34–38.
24. Warrag, S.E.E., N.R. Rodriguez, I.M. Nashef, M. Van Sint Annaland, J.I. Siepmann, M.C. Kroon, et al., *Separation of thiophene from aliphatic hydrocarbons using tetrahexylammonium-based deep eutectic solvents as extracting agents*. J. Chem. Eng. Data, 2017. **62**: p. 2911–2919.
25. Das, S., R. Biswas, and B. Mukherjee, *Collective dynamic dipole moment and orientation fluctuations, cooperative hydrogen bond relaxations, and their connections to dielectric relaxation in ionic acetamide deep eutectics: Microscopic insight from simulations*. J. Chem. Phys., 2016. **145**.
26. Kaur, S., A. Gupta, and H.K. Kashyap, *Nanoscale spatial heterogeneity in deep eutectic solvents*. J. Phys. Chem. B, 2016. **120**: p. 6712–6720.
27. Wagle, D.V., G.A. Baker, and E. Mamontov, *Differential microscopic mobility of components within a deep eutectic solvent*. J. Phys. Chem. Lett., 2015. **6**: p. 2924–2928.
28. Zahn, S., B. Kirchner, and D. Mollenhauer, *Charge spreading in deep eutectic solvents*. ChemPhysChem, 2016. **17**: p. 3354–3358.
29. *Gaussian 16*. Gaussian, Inc., Wallingford, CT, 2016.
30. Kohn, W., A.D. Becke, and R.G. Parr, *Density functional theory of electronic structure*. J. Phys. Chem., 1996. **100**: p. 12974–12980.
31. Bayly, C.I., P. Cieplak, W.D. Cornell, and P.A. Kollman, *A well-behaved electrostatic potential based method using charge restraints for deriving atomic charges: The RESP model*. J. Phys. Chem., 1993. **97**: p. 10269–10280.
32. *AMBER 14*. University of California, San Francisco, 2014.
33. Wang, J., R.M. Wolf, J.W. Caldwell, P.A. Kollman, and D.A. Case, *Development and testing of a general Amber force field*. J. Comput. Chem., 2004. **25**: p. 1157–1174.
34. Wang, J., W. Wang, P.A. Kollman, and D.A. Case, *Antechamber, an accessory software package for molecular mechanical calculations*. J. Am. Chem. Soc., 2001. **222**: p. U403.
35. Wang, J., W. Wang, P.A. Kollman, and D.A. Case, *Automatic atom type and bond type perception in molecular mechanical calculations*. J. Mol. Graph. Model., 2006. **25**: p. 247–260.
36. Martinez, L., R. Andrade, E.G. Birgin, and J.M. Martínez, *PACKMOL: A package for building initial configurations for molecular dynamics simulations*. J. Comput. Chem., 2009. **30**: p. 2157–2164.
37. Phillips, J.C., R. Braun, W. Wang, J. Gumbart, E. Tajkhorshid, E. Villa, et al., *Scalable molecular dynamics with NAMD*. J. Comput. Chem., 2005. **26**: p. 1781–1802.
38. Hünenberger, P.H., *Thermostat algorithms for molecular dynamics simulations*. Adv. Polym. Sci., 2005. **173**: p. 105–147.
39. Feller, S.E., Y. Zhang, R.W. Pastor, and B.R. Brooks, *Constant pressure molecular dynamics simulation: The Langevin piston method*. J. Chem. Phys., 1995. **103**: p. 4613–4621.

40. Andersen, H.C., *Rattle: A "velocity" version of the shake algorithm for molecular dynamics calculations*. J. Comput. Phys., 1983. **52**: p. 24–34.
41. Humphrey, W., A. Dalke, and K. Schulten, *Sartorius products*. J. Mol. Graph. 1996. **14**: p. 33–38.
42. Essmann, U., L. Perera, M.L. Berkowitz, T. Darden, H. Lee, and L.G. Pedersen, *A smooth particle mesh Ewald method*. J. Chem. Phys., 1995. **103**: p. 8577–8593.
43. Brooks, C.L., *Computer simulation of liquids*. J. Solution Chem., 1989, **18**, p. 99.
44. Brehm, M., and B. Kirchner, *TRAVIS—A free analyzer and visualizer for monte carlo and molecular dynamics trajectories*. J. Chem. Inf. Model., 2011. **51**: p. 2007–2023.
45. Zhao, Y., and D.G. Truhlar, *The M06 suite of density functionals for main group thermochemistry, thermochemical kinetics, noncovalent interactions, excited states, and transition elements: Two new functionals and systematic testing of four M06-class functionals and 12 other function*. Theor. Chem. Acc., 2008. **120**: p. 215–241.
46. Zhao, Y., and D.G. Truhlar, *Density functionals with broad applicability in chemistry*. Acc. Chem. Res., 2008. **41**: p. 157–167.
47. Wagle, D.V., H. Zhao, C.A. Deakyne, and G.A. Baker, *Quantum chemical evaluation of deep eutectic solvents for the extractive desulfurization of fuel*. ACS Sustain. Chem. Eng., 2018. **6**: p. 7525–7531.
48. Mennucci, B., *Continuum solvation models: What else can we learn from them?* J. Phys. Chem. Lett., 2010. **1**: p. 1666–1674.
49. Bernales, V.S., A.V. Marenich, R. Contreras, C.J. Cramer, and D.G. Truhlar, *Quantum mechanical continuum solvation models for ionic liquids*. J. Phys. Chem. B, 2012. **116**: p. 9122–9129.
50. Paul, N., P.K. Naik, B.D. Ribeiro, P.S. Gooh Pattader, I.M. Marrucho, &, T. Banerjee, *Molecular dynamics insights and water stability of hydrophobic deep eutectic solvents aided extraction of nitenpyram from an aqueous environment*. J. Phys. Chem. B, 2020. **124**(34): p. 7405–7420.

5 Industrial and Environmental Applications with Limitations of Deep Eutectic Solvents

5.1 INTRODUCTION

Because of the detrimental effects of existing chemicals on humankind and the environment, new alternative solvents are gaining more attention in research. As a result, they are used as environmentally responsive extracting agents and sorbents as a replacement for the conventional substances. Ionic liquids (ILs) and deep eutectic solvents (DESs) make significant contributions in the field of separation because, in addition to serving as an extraction medium, they can help adsorbents to increase separation performance by disaggregating various nanomaterials into it. The use of nontoxic precursor materials for solvent formulation is causing a progressive shift in modern scientific study around the world. Most of today's scientific study is based on 21st-century conceptions of "green chemistry". The chief source of understanding of this perception is to give alternate routes for reducing the manufacture and use of toxic products that affects both humans and the environment by utilizing renewable, inexpensive, and ecologically friendly precursor materials.

Since the green idea was presented in chemistry, there have been significant efforts to identify new and benign solvents that are safe for both man and the environment to replace the usage of harmful solvents in chemical productions and processes. The use of volatile organic solvents is currently a popular method for extracting phytochemical and bioactive elements from plant materials [1]. However, the majority of conventional solvents used in the extraction of plant extracts are associated with high solvent utilization and long extraction times [2], producing unacceptable residues in the extract, which are highly volatile and thus end up in the atmosphere or groundwater, causing pollution [3, 4]. Furthermore, most typical organic solvents have a threshold temperature (>200°C) that makes them unsuitable for isolating bioactive compounds, as this could result in the loss of the majority of the volatile components in the plants [5]. Since green solvents are safe and produce high-quality extracts, they are becoming increasingly popular as an alternative to environmentally hazardous solvents in current extraction techniques [6, 7].

DOI: 10.1201/9781003231158-5

In recent years, Abbott and coworkers explored a whole new class of multicomponent mixture solvents known as DESs [8, 9]. DESs have been shown to be environmentally friendly by various study teams, and this has been validated by multiple other groups [10, 11]. Organic chemicals, which are typically synthesized by biotechnological processes, are the most common constituents of DESs [12]. In addition to their engagement in chemical processes, the use of DESs in biochemical and biotechnological processes has been convincingly established in various articles, and growth in this employment can be reasonably anticipated in the future [13, 14]. The majority of DESs are nontoxic and biodegradable. The importance of DESs in the previously mentioned elements is specifically discussed and appraised in this chapter.

5.2 INDUSTRIAL USES OF DESs

DESs have developed a great deal of interest in the past five years of scientific investigation. Up until 2013, very little had been done to investigate these systems [15, 16], both in terms of their basics and their applications. It is still debatable what constitutes a deep eutectic system; therefore, in this chapter, we highlight the various applications that have been proposed or studied in the literature and discuss what should be pursued in order to achieve consensus among the researchers studying this field. From the basic fundamentals to its applications, there have also been some intriguing shifts in the themes of DES that have been covered in the literature [17]. The field progresses as fresh aftermaths on DES characteristics are discovered, ranging from electrochemistry to emerging applications, such as cryopreservation, and the domain is expected to continue to evolve [18]. New research trends in decentralized energy systems of DES are presented and discussed in this chapter, as are some insights into the most potential DES applications at the industrial scale.

It is advantageous to use DESs over other green solvents, such as ILs, since DESs are less expensive and simpler to create in large-scale quantities, making them ideal for industrial use. Scaling up alternative greener techniques, however, might take several years to persuade industry that they are worthwhile, needing similar stages between the original idea and completed production arrangement as any other emerging technology. Scaling up from a bench to a pilot plant, then from that to a full-scale process, and then optimizing that process are the primary operational processes. Pilot plants are often essential, even if the ultimate aim is to go straight from process improvement to full-scale production. An improved understanding of the whole process may be gained by pilot plant studies, which aids in the scaling up of the technology. DES, in particular, is a relatively new technology. The application of novel methods into industry has yet to be established, despite tremendous success at the lab scale, and only a few pilot-size studies have been done or have previously been published.

5.3 SCALING UP STUDIES

There are several important benefits of DES over other unconventional green solvents, such as ILs, including the fact that DESs are less expensive and much easier to manufacture in large batches, allowing for the scaling up of DES-based operations in an industrial environment [19, 20]. However, scaling up alternative greener technologies

is a challenging task that takes several years to persuade industries that they are worthwhile. As with any new advancing technology, there are a lot of steps linking the preliminary model and the construction of the finished manufacturing plant. The primary functioning steps are the scaling up from (1) the bench to a pilot plant, (2) the pilot plant to a full-scale progression, and (3) the full-scale process to optimization of the process. The decisive purpose is to proceed directly from optimized process to full-scale industry, but in most cases, a pilot plant is an essential stage in the process. The knowledge gained from the pilot or prototype plant investigation provides for a more comprehensive understanding of the whole process, and this stage aids in the efficient and safe scaling up of the technology at a larger scale [20].

In particular, the deployment of DES is a relatively new technological development. Although great developments have been made at the lab scale, the application of new processes in the industry has not been established so far, and only a few pilot size studies have been done or have previously been published, despite significant progress at the lab scale. Numerous European Union (EU)–funded research initiatives have focused on DES-linked metal processing units recently, having focused on the scale-up of metal surface finishing and extraction industries, concentrating on commercialization. For example, one of the most common uses for DESs is as an alternate media for metals that are generally difficult to process, or that require the use of ecologically harmful processing methods. When compared to water-based electrolytes, DES exhibits better solubility of metal salts in the lack of presence of water, as well as high conductivity when compared to non-water-based solvents, among other characteristics. DESs have been shown to serve as effective metal-plating solvents in a wide variety of applications, including copper, zinc, nickel, tin, gold, and silver, and several collaborations combining academia and large corporations, such as Rolls-Royce, are still in progress, with the focus on scaling up and process optimization being the primary objectives. Nonetheless, the deposition of aluminum is still at a laboratory size, and further research into the issue of increasing the deposition rate is required [21].

Sulfuric compound removal from fuel oil is another interesting area of research that has piqued the interest of many researchers and is being pursued in conjunction with DES. Additionally, the process of separating hydrocarbons with the same number of carbon atoms into aromatic and aliphatic types can prove to be a difficult procedure, particularly at very low aromatic concentrations. It has only been a few years since lab-scale investigations into the liquid–liquid extraction (LLE) techniques used to separate aromatic compounds have been conducted, and the selectivity and distribution ratio data have proved the advantages of utilizing DESs in this separation task. Because of the encouraging results, Ali and his colleagues have already conducted investigations at the pilot stage in order to validate the results obtained at the laboratory scale. Despite the positive results, more pilot plant–scale prospective studies are needed for LLE methods using DES to be implemented in the industrial sector. For the partition of aromatics from fuel, the optimization of the working parameters necessarily needs to be accomplished using gasoline itself as a fuel, rather than a simulated mixture, in order to commercialize the technology [22]. A significant step forward in the deployment of this technology on an industrial scale may have been taken with this development.

DES is being used in a variety of other fields, with the possibility of scaling up several years down the road, on an industrial level [23]. DESs can be used as solvents, co-solvents, or extracting solvents in a variety of biocatalytic reactions, depending on the reaction [24]. Surprisingly, when used as solvents, DESs may both activate and stabilize enzymes, resulting in the best possible efficiency. As of today, various enzymes including lipases, proteases, and epoxide hydrolases exhibit outstanding catalytic activity when used in DES, indicating that they have the potential to replace ILs and/or organic solvents in biocatalytic processes. In spite of this, there are still some questions that need to be answered. For example, a better understanding of how DESs can activate and stabilize enzymes, as well as how the biocatalysis products can be separated from their DES sources, will help to advance the application of these compounds in biocatalysis at a laboratory or industrial scale [25]. We discuss some case studies concerning electroplating and the desulfurization process involving DES.

5.3.1 Electroplating Studies

Many EU research initiatives have focused on scaling up and commercializing DES-based metal processing for the metal polishing and extraction sectors in the last few years, making it an attractive study topic. DESs may be used as an alternative medium for metals that have historically been difficult to plate or treat or that require ecologically harmful methods. When compared to aqueous electrolytes, DES exhibits greater metal salt solubility and conductivity in the absence of water. It has been shown that DESs are acceptable as solvents for the deposition of many metals, such as copper, nickel, zinc, tin, and silver. Numerous cooperative studies between academics and big enterprises are currently underway, focused on process optimization and scaling up. Further research is needed to determine how aluminum deposition might be increased in the lab. When compared to aqueous electrolytes, DES exhibits greater metal-salt solubility and conductivity in the absence of water.

Comparisons have been made between the electrochemical deposition of copper from a solution of $CuCl_2$ in choline chloride (ChCl) using hydrogen bond donors (HBDs), such as oxalic acid or urea as the electrolyte [26]. ChCl:oxalic acid and ChCl:ethylene glycol were found to produce finer, more homogeneous, and more adhesive deposits. ChCl:ethylene glycol is claimed to include $[CuCl_3]_2$ and $[CuCl_4]_2$ metal species, which were identified by ultraviolet-visible spectroscopy. During the deposition of Cu in ChCl:glycerol, ultrasound was shown to enhance the current by a factor of five compared to undisturbed circumstances. When nickel chloride dihydrate is dissolved in ChCl:urea or ChCl:ethylene glycol, the kinetics and thermodynamics of nickel chloride dihydrate deposition vary from those of the aqueous process, leading to distinct deposit morphologies [26].

5.3.2 Desulphurization of Fuel Oil

Cleaning up gasoline by removing sulfuric components is another interesting area of study employing DES that is attracting a lot of attention. At low aromatic concentrations, the process of separating hydrocarbons with the same number of carbon

atoms into aromatic and aliphatic types is a difficult task. Lab-scale studies have revealed the advantages of DESs for aromatic separation utilizing LLE techniques in recent years. Both distribution ratio and selectivity data have shown this. Ali and coworkers have previously completed tests at pilot size to validate the outcomes of prior laboratory-scale investigations due to the positive results [22]. The effectiveness of extraction can reach up to 82.83% in one cycle and 99.8% after five cycles under ideal circumstances. The past study on LLE has all been done in the laboratory environment, regardless of the solvent employed. Using extractive desulfurization on a pilot plant size has not been attempted to our knowledge, at least for the DES. In reality, pilot plant tests and optimization of operating parameters are required before DES for LLE processes and in particular deep desulfurization can be industrially implemented.

5.3.3 Pilot Plant Studies

A three-stage LLE machine (BP 17–3) conceived and manufactured in partnership with SOLTEQ® is under consideration for the investigation of LLE. This becomes a research-grade container of intermediate size that can hold up to 10 liters of liquid, heavy or light. Centrifugal separators, tanks for storing heavy and light liquid phases, and a pumping and heating circuit are the primary components of the unit (Figure 5.1). The component nomenclature is provided in Table 5.1. This has been used in experiments involving the optimization of various operational process parameters, such as flow rates, temperatures, and the number of stages. Experiments on LLE, especially with DESs, have been operational with thiophene–aliphatic separation. Figure 5.1 shows a schematic diagram of this pilot plant which is a typical LLE equipment, detailed in Table 5.1. It is still necessary to carry out optimization of operating parameters using gasoline fuel rather than a model mixture in pilot plant–scale studies to adopt DES industrially, in LLE processes and in particular in the process of separating aromatic compounds from gasoline. If successful, this might be a huge step toward the industrialization of this technology.

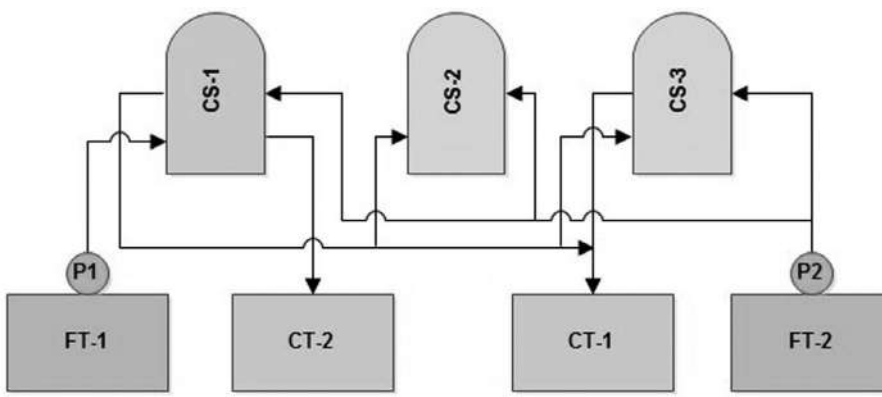

FIGURE 5.1 Schematic concept of a typical pilot plant.

TABLE 5.1
Nomenclature of Pilot Plant

Unit	Description
CS-1	Steel motorized centrifugal extractors
CS-2	(Max flow rate 1.9 Lpm; Max volume 2L; Motor 1/8 HP and
CS-3	max 3450 rpm)
FT-1	Light phase feed tank
	Steel container, Max volume 10 L
FT-2	Heavy phase feed tank:
	Steel container, Max volume 10 L
CT-1	Light phase collection tank:
	Steel container, Max volume 10 L
CT-2	Heavy phase collection tank:
	Steel container, Max volume 10 L
P-1	Light phase pump: motor 0.05 kW, Max flow rate 2.5 Lpm, 3bar
P-2	Heavy phase pump: motor 0.15 kW, Max flow rate 2.5 Lpm, 8bar

5.3.4 DESs and Biocatalysis

Biocatalysis is another area in which DES is being explored and might be scaled up to industrial levels in the next few years. In certain biocatalytic processes, DESs may serve as solvents, co-solvents, or extraction solvents. Astonishingly, DESs are solvents that can activate and stabilize enzymes, resulting in the greatest levels of efficiency in the process. Today, a number of proteins and epoxide hydrolases have shown excellent catalytic activity in DES, suggesting their potential to take the role of ILs and organic solvents in biocatalytic processes. A deeper knowledge of how DESs activate and stabilize enzymes, as well as how the biocatalysis products can really be isolated from DES, will lead to the widespread use of DESs in biocatalysis in the laboratory and the industrial sector.

Among the base-catalyzed reactions in DES, DES-catalyzed Perkin- and Knoevenagel-type condensations employing a 1:2 ChCl/urea (molar ratio) DES were reported. Both techniques resulted in moderate to excellent isolated yields (typically >90%) with response times ranging from minutes (Knoevenagel-based reactions) to a few hours (Perkin-based reactions). In the majority of these situations, the results were considerably superior to those obtained under traditional reaction circumstances in terms of reaction time, recyclability, and work-up ease. Additionally, as predicted by the DES characteristics, substrate loadings might be greatly increased allowing for the possibility of industrially viable substrate loadings and productivities under very mild reaction conditions and competitive durations. Additionally, water is added to break down the DES and initiate product precipitation. The DES was reused numerous times (up to five times) after water evaporation without substantial loss of activity. Paal–Knorr reactions in 1:2 ChCl/urea (molar ratio) have been achieved effectively in the identical base-catalyzed procedures employing DES as solvents and catalysts. Additionally, high isolated yields (about 95%) were

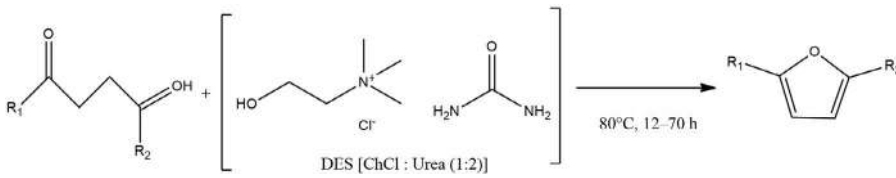

FIGURE 5.2 Paal–Knorr reaction in DES using ChCl/urea (1:2) and 2,5-diones

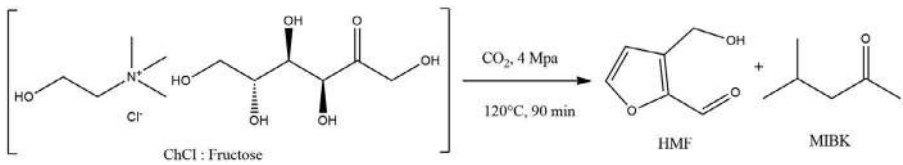

FIGURE 5.3 Use of DES and CO_2 to form HMF and MIBK.

achieved in all instances but with very lengthy reaction durations (12–70 h) that were substantially dependent on the substrate used (Figure 5.2).

An innovative and intriguing idea in case of acid-catalyzed reactions utilizes chloroform and fructose as DES (melting values of 60–80 °C) and CO_2 as the acidic source. The generated DES is acidic as a consequence of the creation of carbonic acid, and carbonic acid is quite dominant in dehydration of fructose to 5-hydroxymethylfurfural (HMF). Following that extraction (biphasic) with methyl isobutyl ketone (MIBK) effectively yields HMF. The disclosed system is capable of successfully converting very large fructose loadings (up to 250 wt%; Figure 5.3).

DESs have been employed as a solvent/separator in (bio)catalytic processes. Here it is capable of dissolving HBD molecules (e.g., alcohols) and forming a second phase with compounds lacking HBD groups (esters). Thus, using DES (Figure 5.4), it is feasible to separate esters and alcohols. When DES is added to the alcohol/ester combination, the alcohol dissolves in the DES phase, while the ester forms a second phase. After separating the phases, the DES-dissolved alcohol may be recovered using a solvent such as ethyl acetate and the phases can be recycled (Figure 5.4). This concept has been applied to the lipase-catalyzed kinetic resolution of alcohols in order to separate the formed R-esters from remnant S-alcohols by selectively dissolving the alcohols in DES, as well as to the separation of HMF esters and HMF51 with high purity (>99%) and yields (>90%).

5.3.5 Recovery of Drugs and Recycle of DESs

Another promising area can be the isolation of products in the pharmceutical industry. LLE can be carried out for extraction of drugs from an aqueous phase. Here, the DES is a part of the component in (water + drugs + DES) or aqueous biphasic systems (ABSs) [27]. When it comes to the extraction and purification of biomolecules, bioactives, medicines, and dyes, DES-ABS has proved tremendous potential (Figures 5.5 and 5.6). Undoubtedly, DES (choline-based) was initially investigated

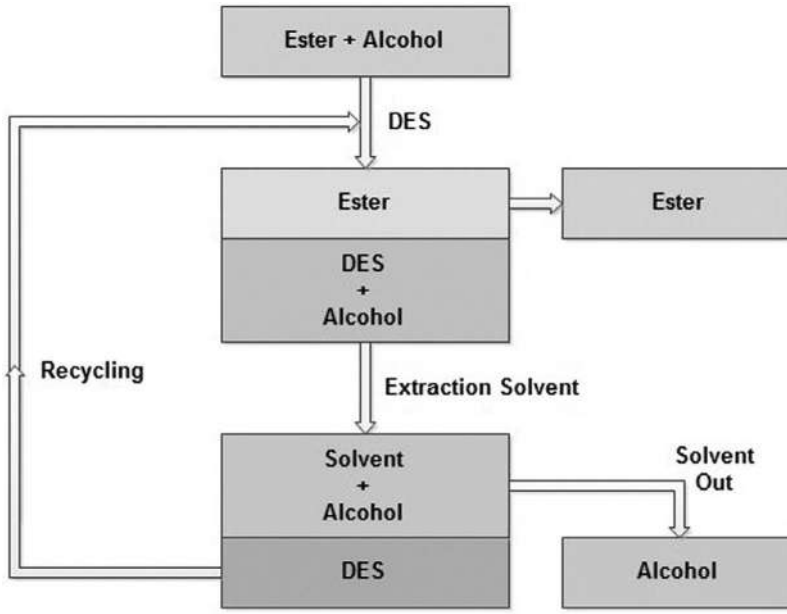

FIGURE 5.4 Concept to use DES as separation agents for alcohols and esters.

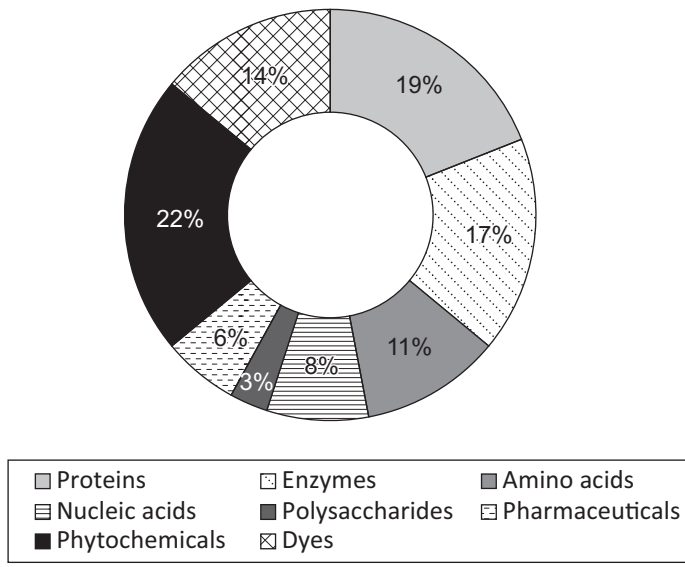

FIGURE 5.5 Applications of DES-ABS in separation and purification of compounds. Reprinted from *Biochemical Engineering Journal*, 176, E. A. Oke, & S. P. Ijardar, Advances in the application of deep eutectic solvents based aqueous biphasic systems: An up-to-date review, 108211, Copyright (2021), with permission from Elsevier [27].

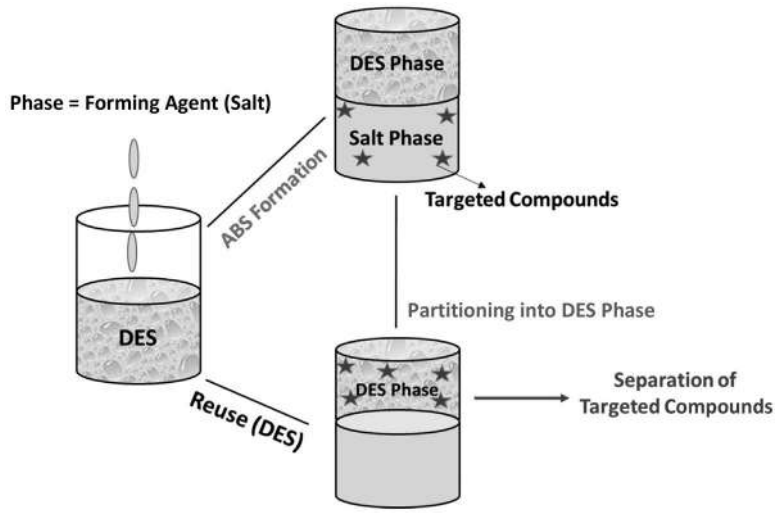

FIGURE 5.6 Schematic diagram on separation of targeted compounds in DES-ABS. Reprinted from *Biochemical Engineering Journal*, 176, E. A. Oke, & S. P. Ijardar, Advances in the application of deep eutectic solvents based aqueous biphasic systems: An up-to-date review, 108211, Copyright (2021), with permission from Elsevier [27].

for the separation and purification of biomolecules such as proteins, enzymes, amino acids and nucleic acids, phytochemicals polysaccharides, and medicines, as well as for the production of colors. The biodegradable nature of choline-based DES and citrate/buffer, Good's polymer, and an increased amount of water in the ABS system creates an environment that is suitable for the partitioning of biomolecules to occur [28, 29].

In usual processes within the extraction step and drug partitioning into the DES-rich phase, two strategies for DES cleaning and drug recovery can be attempted: (a) addition of water for the most insoluble drugs and (b) pH change to a neutral form. Both strategies aim at precipitating the drug. Since drugs have low water-solubility, the precipitation of drugs occurs, and they can be recovered by centrifugation, followed by filtration. The obtained precipitate may be further washed in DI water and then dried at 60–70°C and weighted until constant weight is obtained, which means all the moisture has been removed from the recovered drug.

The percentage recovery drug can be calculated using the following expression:

$$\left(\%\ \text{Recovery}\right) = \frac{\left(W_{Drug}\right)_{recovered}}{\left(W_{Drug}\right)_{DES-richphase}} \times 100 \tag{5.1}$$

$\left(W_{Drug}\right)_{recovered}$ = Total weight of each drug after filtration and drying step.

$\left(W_{Drug}\right)_{DES-richphase}$ = Total weight of each drug present in the DES-rich phase.

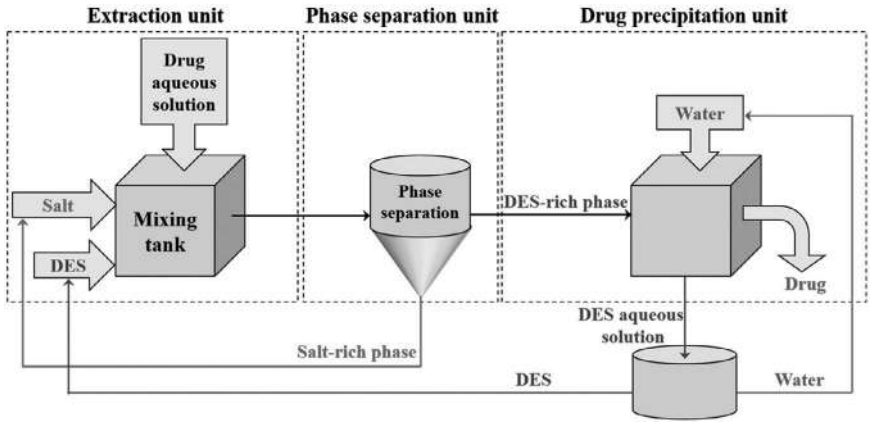

FIGURE 5.7 Conceptual process flow diagram for the recycling of the DES phase and recovery of the drugs.

After the recovery of drugs, the DES can be cleaned and reused in the preparation of ABS and LLE (Figure 5.7). In particular, it will be more difficult to achieve a full circular process for ABS systems due to the complexity of these systems but comparatively easier for hydrophobic DES.

5.4 RECENT ADVANCEMENTS IN THE APPLICATION OF DESS

In most industries and all fields of science, solvents are vital fundamentals. They are used in synthesis, testing, pharmaceutical, nutrition, and flavor science, as well as the materials and painting industries [19, 30]. Because of its environmentally friendly characteristics, DES is increasingly being used to replace these conventional solvents. Natural DESs are used to describe DESs that are made from neutral, acidic, or basic chemicals that are produced through natural means (NADES) [31]. NADESs have been utilized to substitute organic solvents in a variety of fields. The development of NADES, which contain naturally occurring components such as organic acids, amino acids, and sugars, for potential use in the natural product area has recently been completed [32]. The hydrogen bond acceptor (HBA; usually ChCl, betaine hydrochloride, lactic acid, tetrabutylammonium chloride, or trioctyl ammonium chloride) and HBD (generally natural plant-based organic species, such as carboxylic acids, sugars, and sugar alcohols, amino acids, etc.) are mixed in a definite molar ratio [33, 34] to prepare NADES.

A therapeutic deep eutectic system (THEDES) is one in which an active pharmaceutical ingredient (API) is among the eutectic system's components. In the pharmaceutical area, the solvent has been used in a variety of applications, including medication solubility enhancement, permeation enhancement, and absorption enhancement, as well as serving as the oil phase in an emulsion system [35–37]. Furthermore, any polymer that is dissolved into the formulated eutectic mixture is referred to as a polymeric DES (PODES). To prepare the polymeric eutectic system, a

variety of polymers can be dissolved in the solvent and mixed together. Artificial and natural polymers can be used to formulate the same. This includes urea- and sugar-based polymers (citric acid–glucose), organic acid– and amino acid–based polymers (malic acid, glutamic acid, lactic acid, etc.), and ChCl-based polymers[38, 39]. The type of the polymer determines whether the medicine is released immediately or over a longer period from formulations including polymeric liquid PODES [35, 39]. The advantage of this type of DES is that it is less toxic and often biodegradable, and it is less expensive to manufacture because of the lower cost of the raw components. The downside of DES is their high viscosity, and the fact that most DES are solid at ambient temperature prevents them from being used as extraction solvents [40].

Again, DESs also can be categorized into two types based on their solubility in water: hydrophilic DESs and hydrophobic DESs, which are related to the solubility in water [41]. Because of their propensity to form hydrogen bonds, DESs are largely water-loving and dissolve promptly in aqueous solutions [42]. In a variety of domains, hydrophilic DESs are used as catalysts for chemical reactions or as solvents for chemical reactions. Other applications include electrochemistry, medicines, and separation processes. The hydrophilic DESs were the majority of the DESs proposed in the published articles, and they were found to be miscible with water. The most significant disadvantage of hydrophilic DES is that it can only separate polar molecules [43]. Hydrophobic DESs have recently been developed as substitute extractive agents for the extraction of nonpolar organic and inorganic compounds from aqueous solutions [44]. Water-insoluble volatile organic molecules were extracted using a water-impermeable solvent, and the results showed that the extraction yield and efficiency were both very high [45–47].

Florindo et al. studied the development of hydrophobic DESs as low-cost extractants for the removal of four neonicotinoids from dilute wastewater using the LLE method, namely, imidacloprid, acetamiprid, nitenpyram, and thiamethoxam [48]. DESs were used in their studies, with one based on natural neutral ingredients (DL-menthol and natural organic acids) and the other either on quaternary ammonium salts ($N_{4444}Cl$) or organic acids (acetic acid, levulinic acid, pyruvic acid, butyric acid, octanoic acid, decanoic acid, and dodecanoic acid). DL-menthol:octanoic acid was found to be the most appropriate DES for removing pesticides from wastewater. Yousefi et al. and his team [49] investigated the use of carboxylic acid and tetrabutylammonium bromide (TBAB) as hydrophobic DESs in microextraction procedures based on the solidification of floating droplet (SFD) suspensions. According to this study, the hydrogen bond acceptor TBAB and the hydrogen bond donors, oleic acid, decanoic acid, octanoic acid, propionic acid, acrylic acid, acetic acid, and butyric acid, in a 1:2 mol ratio, serve as hydrogen bond acceptors. The TBAB/2-decanoic acid DES was found to have the most favorable qualities as an extraction solvent in SFD when compared to others. Osch et al. [42] discovered and described a terpenes-based DES for extracting riboflavin from water, which they used in their research. They discovered 17 novel hydrophobic DESs by experimenting with 507 different solid component combinations. The combination of Decanoic acid and Lidocaine was shown to be the most effective for extracting riboflavin from water (81%; 2:1). There are so many research studies already published regarding THEDES; some more discussion on these DESs continues in the following sections.

Eutectic liquids prepared from eutectic-forming active ingredients in the oil phase are an appealing but less costly substitute for oil-in-water emulsion preparations with the removal from emulsions containing oils and antioxidant molecules, and as an added bonus, it's a more affordable choice or substitution. Tamilvanan et al. [50] developed an oil-free emulsion, having powder from coriander seed in a eutectic solvent produced with camphor and menthol, as well as tween 80 as a surfactant, to be used in a variety of applications. After much deliberation, they came to the conclusion that the potential for topical therapeutic application of coriander-based oil-less emulsion is very high. Microemulsion-based external hydrogels encapsulating lornoxicam were developed and tested by Biswal et al. [51] The oily phase (with a maximum concentration of 10%), which serves as a solvent for lornoxicam and also acts as a potent penetration enhancer, was composed of a eutectic blend of camphor and menthol. Shen et al. [52] found that putting daidzein in a microemulsion formulation with the use of a borneol/menthol eutectic mixture increased intestinal absorption of the compound (1:4). In their pharmacokinetic analysis, they discovered that the relative bioavailability of borneol:menthol eutectic solvents and microemulsions increased the absorption of daidzein by roughly 1.5-fold and 3.65-fold, respectively, when compared to the absorption of a daidzein solution. Similar to this, a number of recent studies on the application of DES have been described.

5.5 DESs FOR IONOTHERMAL SYNTHESIS

It is possible to use DESs for applications that are of industrial relevance, for instance, porous materials synthesis, because they allow for the customization of the DES structure by modifying the characteristics of the HBA and HBD, as well as the modulation of the preparation process. For the fabrication of new zeotypes frameworks, Cooper and colleagues published an alternate convention to the well-known hydrothermal synthesis method in 2004 [53]. This methodology was based on unique features of the deuterated choline chloride and urea (DES) generated by these two chemicals. According to the authors, an inventive procedure for the generation of novel porous materials was developed by combining amplified solvent proficiency of an organic DES in conjunction with its recognized molecular arrangement, which resulted in an improved capability of tailoring the synthesis to exclusive spatial parameters. For the first time, it became possible to use the DES as a solvent and a structure-directing agent (SDA) that unwrapped a number of new research directions in applied chemistry. By utilizing certain combinations of HBA and HBD, several porous constituents have been produced in the laboratory scale to date [54]. The technique, known as ionothermal synthesis, can be carried out using ILs or dielectric solvents (DESs) and can be expanded to the manufacture of a variety of porous materials [55, 56]. Gao et al. synthesized an ultra-thin-layered double hydroxides (LDHs) with small particle sizes by using ChCl–urea-based DES and applied to boron removal [56] (Figure 5.8).

5.6 DESs FOR GAS SOLUBILIZATION

Experimentation with DESs has revealed that their unique structure, with multiple functional groups by selecting convenient sequences of HBAs and HBDs, can be

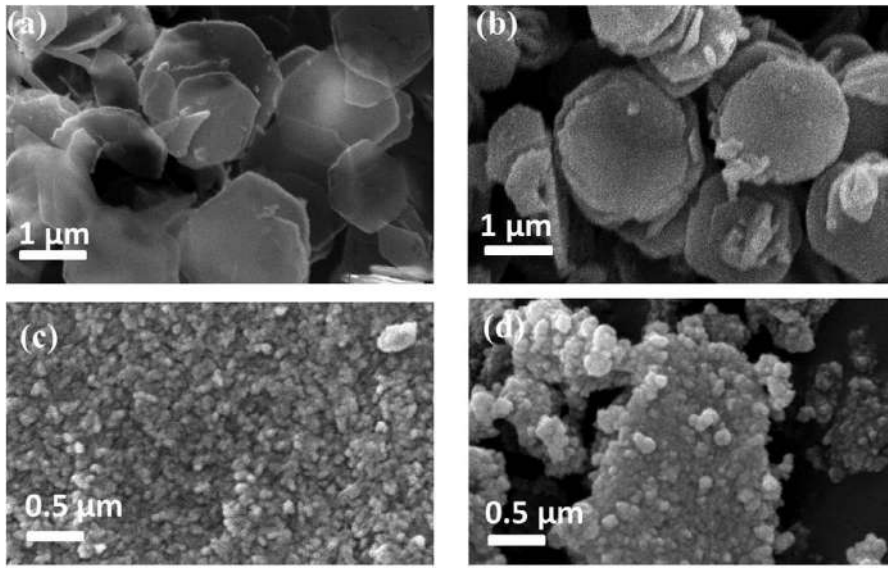

FIGURE 5.8 Scanning electron microscopy images of (a) U-LDH, (b) U-CLDH, (c) I-LDH and (d) I-CLDH.

Source: Reprinted from *Chemical Engineering Journal*, 319, Z. Gao, S. Xie, B. Zhang, X. Qiu, & F. Chen, Ultrathin Mg-Al layered double hydroxide prepared by ionothermal synthesis in a deep eutectic solvent for highly effective boron removal, 108–118, Copyright (2017), with permission from Elsevier [56].

used to improve their gas sorption capacity. A special interest in this area is volatile organic compounds (VOCs), which are typical derivatives of numerous industrial activities [57], and they are believed to be hazardous substances that are frequently related with a variety of ailments [80][58]. Volatile organic compounds (VOCs) are created in huge quantities in the transportation division, and they are frequent constituents in several cleaning commodities, making them one of the most significant bases of air impurities [59, 60]. The reduction of VOC emissions is a top precedence, and as declared obligatory by a number of national and international regulatory bodies [61]. Technologically saying, capturing VOCs from gas flows with liquid sorbents is a highly effective method of slashing them from the environment. The usefulness of this strategy is dependent on two key factors: (1) the accessibility of high-performance sorbents and (2) the long-term viability of the sorbents that have been produced. Since a few years ago, it has been demonstrated that the methodologies used to handle the difficulties listed above are inefficient. Because of the deadliness and contamination allied with sorbent devices, the use of organic solvents for VOC elimination cannot be practiced [62, 63].

The research on and advancement of the manufacture of water-based absorbent materials, on the other hand, would be the most environmentally friendly option. Unfortunately, due to the limited solubility of the hydrophobic constituents included in VOCs in water-existing conditions, this option is ruled out. More recently, the prospect

of using ionic liquids to capture VOCs has been investigated, with promising findings [64]. In spite of this, the cost-ineffectiveness and the difficult synthesis specifications of ILs have a significant negative impact on the overall sustainability of the process [65]. With the use of DESs, it is feasible to indicate a step forward in the current available technology for VOCs treatment by demonstrating a potential advancement. Aside from being inexpensive and environmentally friendly, DESs are also liquid at ambient temperature and exhibit significant interactions with organic molecules, as previously described. The development of extremely efficient DES-based VOC sorbents, according to theory, represents the most promising technical elucidation in air pollution. The use of ammonium-based eutectics as a CO_2 solvent has been described since 2015 [66–69], and the technology has been expanded to include other VOCs later by Moura and colleagues [70]. For toluene, acetaldehyde, and dichloromethane, Moura described the possibility of using hydrophilic ChCl-based DESs in combination with tetrabutylphosphonium bromide–based DESs as hydrophobic adsorbents. Excellent results were recorded, particularly in the instance of acetaldehyde, which was adsorbed nearly 99% when compared to the starting level. Since these groundbreaking studies, only a few further developments on the subject have been recorded, particularly in terms of the amount of VOCs adsorbed. DESs based on quaternary ammonium salts (HBD = glycerol [71], levulinic acid [72], guaiacol or cardanol [73]), certain thiocyanate-based DESs [74], and eutectics produced by betaine or L-carnitine and ethylene glycol [75] have all been found to be effective in SO_2 adsorption applications.

In recent years, a family of DESs has been created for use in the sorption of ammonia, and this family has been used for a variety of applications. According to Akhmetshina et al., gas sorbent characteristics of 1-butyl-3-methyl imidazolium methanesulfonate/urea toward ammonia, hydrogen sulfide, and carbon anhydride was carried out, and the results were favorable in comparison to the competence of ammonia in sorption [76] and carbon anhydride. The detailed description of the apparatus used was represented in Figure 5.9. This study builds on the findings of Zhong [77, 78] regarding phenol-based ternary DESs, Yang [79] with respect to hybrid DES ChCl/resorcinol/glycerol (1:3:5), and Deng [80] through protic NH_4SCN-based DESs are some of the pioneering work. Di Pietro and colleagues describe a novel method to the creation of acceptable DESs-based devices for trapping VOCs that differs from the conventional technique [81]. In DES (choline chloride/urea 1:2), the authors proved that it is possible execute the procedure in DES in order to change the ability of cyclodextrins encapsulation of toluene and aniline. The discovery of this DES-cyclodextrin hybrid system unwraps the door to firsthand engineering options, such as the development of opportune eutectics and the combination of these with certain macromolecules.

5.7 DESs IN MEDICINE

One of the most significant challenges facing the pharmaceutical industry is the enhancement of existing APIs in terms of efficacy and pharmacological action, which are highly correlated with a variety of physico-chemical parameters such as solubility, permeation, and bioavailability [82, 83]. This strategy is critical in the development of new therapeutic medicines since it reduces the expenses associated with clinical trials, which are otherwise incurred during the drug development

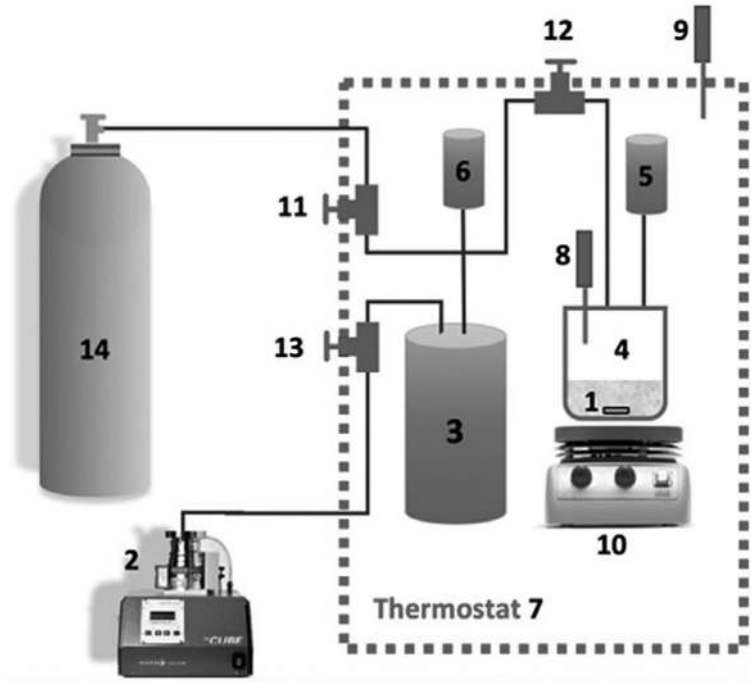

FIGURE 5.9 Experimental apparatus for the measurement of gas solubility. Sample of DES (1), vacuum post (2), a container with gas (3), a high-pressure equilibrium cell (4), pressure transducers (5, 6), a thermostatic bath (7), temperature sensors (8, 9), magnetic stirring system (10), valves (11, 12, 13), and cylinder with testing gas (14).

Source: Reprinted (adapted) with permission from Akhmetshina, A.I., et al., Evaluation of methanesulfonate-based deep eutectic solvent for ammonia sorption. *Journal of Chemical and Engineering Data*, 2018. 63(6): p. 1896–1904. Copyright (2018) American Chemical Society [76].

process. Accordingly, eutectic compositions have been used in the pharmaceutical discipline for a long time and have been successful in numerous uses, including drug administration, where eutecticity increases drug solubility and penetrability in biocatalyzed reactions [84, 85]. Following recent research [86, 87], it has been discovered that DESs and their products offer a great deal of intriguing prospects as systems for drug delivery due to quite remarkable physico-chemical features in terms of tunability, stability, and minimal toxicity reports. Besides, particular grades of DESs are explored as possible intrinsic therapeutic moieties, with preluded bioactivity in vitro alongside specified bacteria and cancer cell lines, indicating that this is a promising avenue for future research. The use of DESs as medicinal instruments has been the subject of a significant amount of study over the last five years, and their enhancement is currently being worked on in a continuous cycle.

For the solubilization of APIs that are insoluble in water, DESs are a better option than organic solvents since they are less toxic and more biocompatible, which is

particularly important for topical applications. A number of encouraging outcomes on the solubilization of various medication classes (including nonsteroidal anti-inflammatory medicines, antifungals, anesthetics, and analgesics) have been demonstrated utilizing eutectic mixtures that are predominantly based on chloride. These DESs have a safe and inexpensive HBA part (ChCl) that complies with the majority of sustainability standards; however, great consideration must be given to the selection of the HBDs because many HBD components have the potential to be harmful in high quantities.

Quite a lot of drugs have demonstrated a dramatic escalation in being solubilized in DESs when competed to water, with ibuprofen solubility increasing by up to 5400-fold [88], posaconazole solubility increasing by up to 6400-fold in binary eutectic systems [89], and the antifungal drug itraconazole increasing by up to 53,600-fold in a ternary deep eutectic mixture of glycolic acid, oxalic acid, and water [90]. Furthermore, it has been found effective for aspirin [87] and -lactam antibiotics [91], DESs have the potential to increase the chemical stability of APIs. Multiple factors influence the solution properties of APIs in DESs, including the HBD proportions, that can either increase or reduce the solubility, which depends on the class of the medication and eutectic as a result of the various substrate-environment interactions [88]. Even when DESs or NADESs are given a suitable amount of water, it can have a meaningful impression on their physicochemical properties and the solubility of APIs [92]. In illustration, benzylisoquinoline alkaloid berberine's solubility can be increased up to 12-fold in a succession of NADESs when transitioning from binary eutectics, as reduced solubility can be observed in comparison to water, to quaternary NADESs comprising having water to be a constituent [93].

The integration of the active pharmacological species as a member of the deep eutectic mixture itself (API–DES or THEDES) [93] has been shown to be a strong strategy for increasing API solubility and has been extensively researched [94]. For specific therapeutic goals, these eutectic substances can be developed employing a collection of APIs (functioning as HBAs or HBDs) and equivalents (e.g., metabolites) to achieve the desired results [94]. When it comes to improving the penetration of transdermal drug delivery systems, API–DES formulations have demonstrated outstanding outcomes. The incorporation of many permeation enrichers (terpenes or such medicines) into API–DES mixes, such as ibuprofen [95], lidocaine [96], and itraconazole [97], has demonstrated both a substantial increase in solubility and an increase in transdermal delivery in an isotonic solution. Some medications' oral bioavailability (e.g., CoQ10) [98], absorption of daidzein in the intestine [52] and the capacity to dissolve and permeate numerous pharmaceuticals (e.g., paeonol [99], ibuprofen, and aspirin [100]) have all been improved by the use of API–DESs. Furthermore, the occurrence of eutectic systems, including two drugs that combine two different APIs in a single eutectic formulation, has paved the way for the development of novel and intriguing strategies for synergic multimodal therapies that make use of drugs with improved solubility and permeation properties [101–103].

It has also been discovered that API–DES can be used to manage drug distribution when used as monomers in polymer synthesis. They epitomize a substantial advancement in the expansion of controlled drug delivery approaches because they are capable of (a) providing the API and (b) acting as both a monomer and a reaction medium for the polymerization process in a single formulation [104]. A controlled release of the anesthetic medication lidocaine has been achieved by incorporating it into acrylic

or methacrylic acid–containing DESs following polymerization, which was activated by a variety of factors such as pH and ionic strength [105]. Furthermore, polymeric eutectic systems offer a more straightforward and environmentally friendly technique of incorporating medicines and polymers into pharmaceutical formulations. (Bio)polymer-based API–DES combinations have been tested for a variety of drug delivery methods, including anticancer (doxorubicin [106], Paclitaxel [107], anti-inflammatory (ibuprofen [108], dexamethasone [36]), anesthetic (prilocaine [109], lidocaine [110]) drugs, with poly(vinyl alcohol) (PV) and poly(acrylic acid) (PA) polymers, ammonium salts, SPCL (starch and poly-ε-caprolactone polymeric blend), cellulose [111], poly(octanediol-co-citrate) elastomers and gelatine [112] in modifying the APIs release profiles (Figures 5.10 and 5.11).

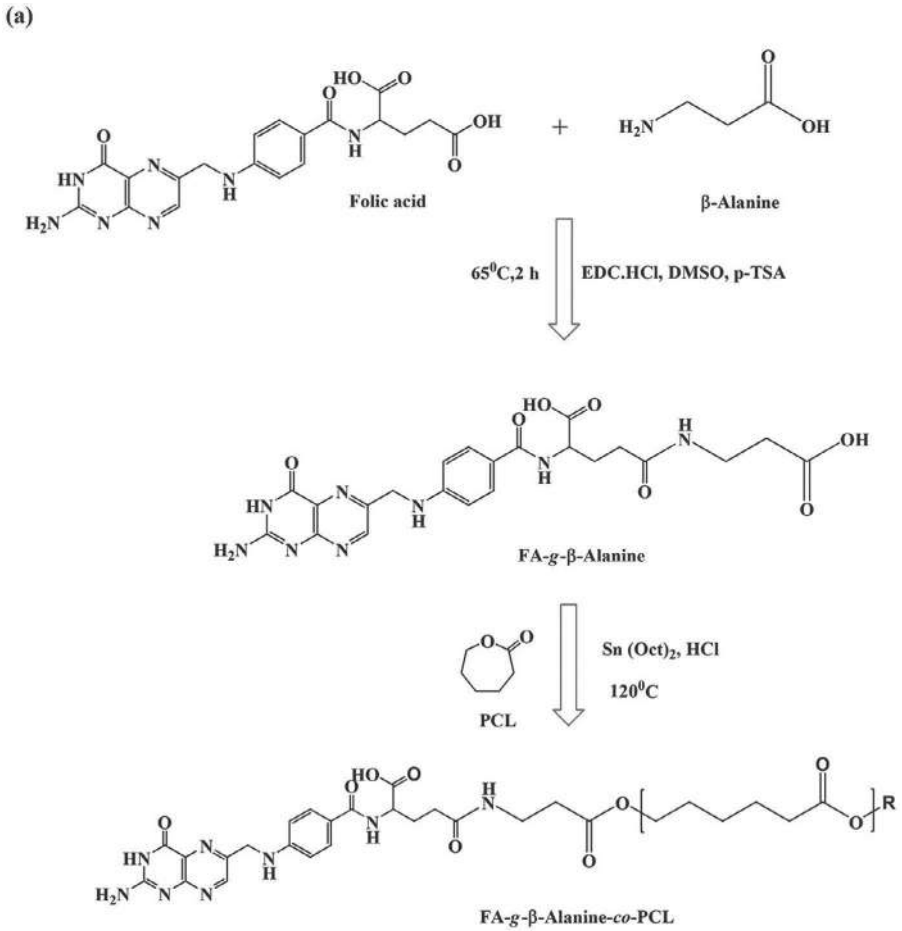

FIGURE 5.10 Schematic representation of the (a) synthetic route of the FA-g-β-alanine-co-PCL, (b) synthesis of the DES@FA-g-β-alanine-co-PCL.

Source: Reprinted (adapted) with permission from Pradeepkumar, P., et al., Deep eutectic solvent-mediated FA-g-β-alanine-co-PCL drug carrier for sustainable and site-specific drug delivery. *ACS Applied Bio Materials*, 2018. 1(6): p. 2094–2109. Copyright (2018) American Chemical Society [106].

(b)

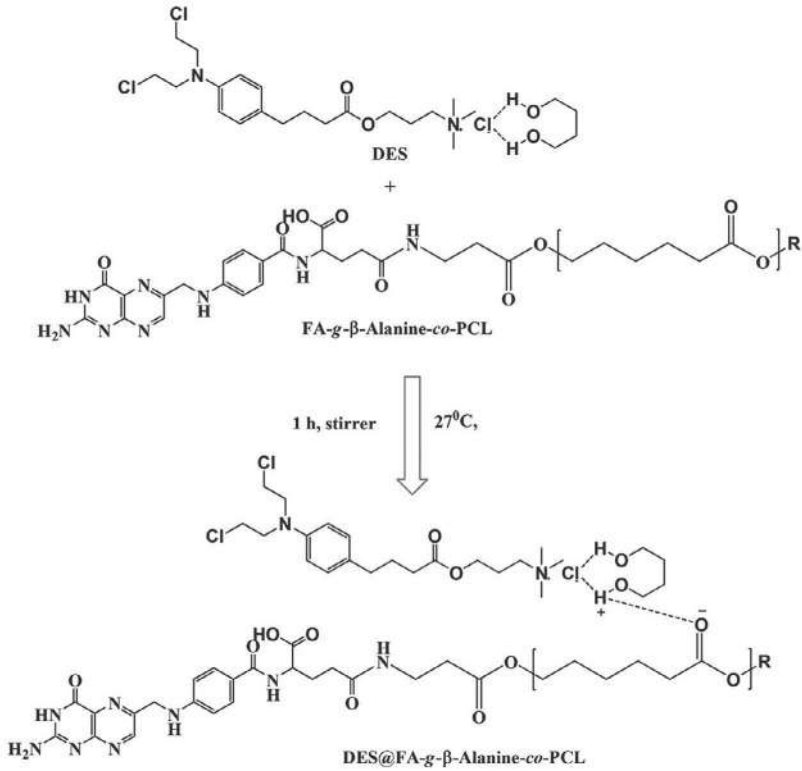

FIGURE 5.10 (Continued)

Raja Sekharan et al. [37] and their colleagues developed an emulsion containing ibuprofen that was derived from a hydrophobic eutectic solvent derived from camphor and menthol. After doing their research, they discovered that an ibuprofen emulsion could be successfully made using Eudragit RL 100 in a eutectic combination. In a study conducted by Stott and colleagues [95], using a terpene eutectic system, they were able to increase the permeation of an ibuprofen drug through the skin. They came to the conclusion that ibuprofen creates eutectic systems with certain terpene penetration enhancers when combined with other terpenes. A considerable increase in transdermal flux was seen following the interaction of the terpene with ibuprofen and the disruption of hydrogen-bonded dimers. The consequent melting point depression of the formulation coincided with a significant increase in transdermal flux. With the use of salicylic acid—menthol and benzocaine—menthol as eutectic mixtures, Zu et al. [113] were able to manufacture fluconazole cream that was assessed for its physical qualities. When comparing the physical qualities of fluconazole creams with eutectic mixtures to those of fluconazole creams without eutectic mixtures, the eutectic mixtures had improved

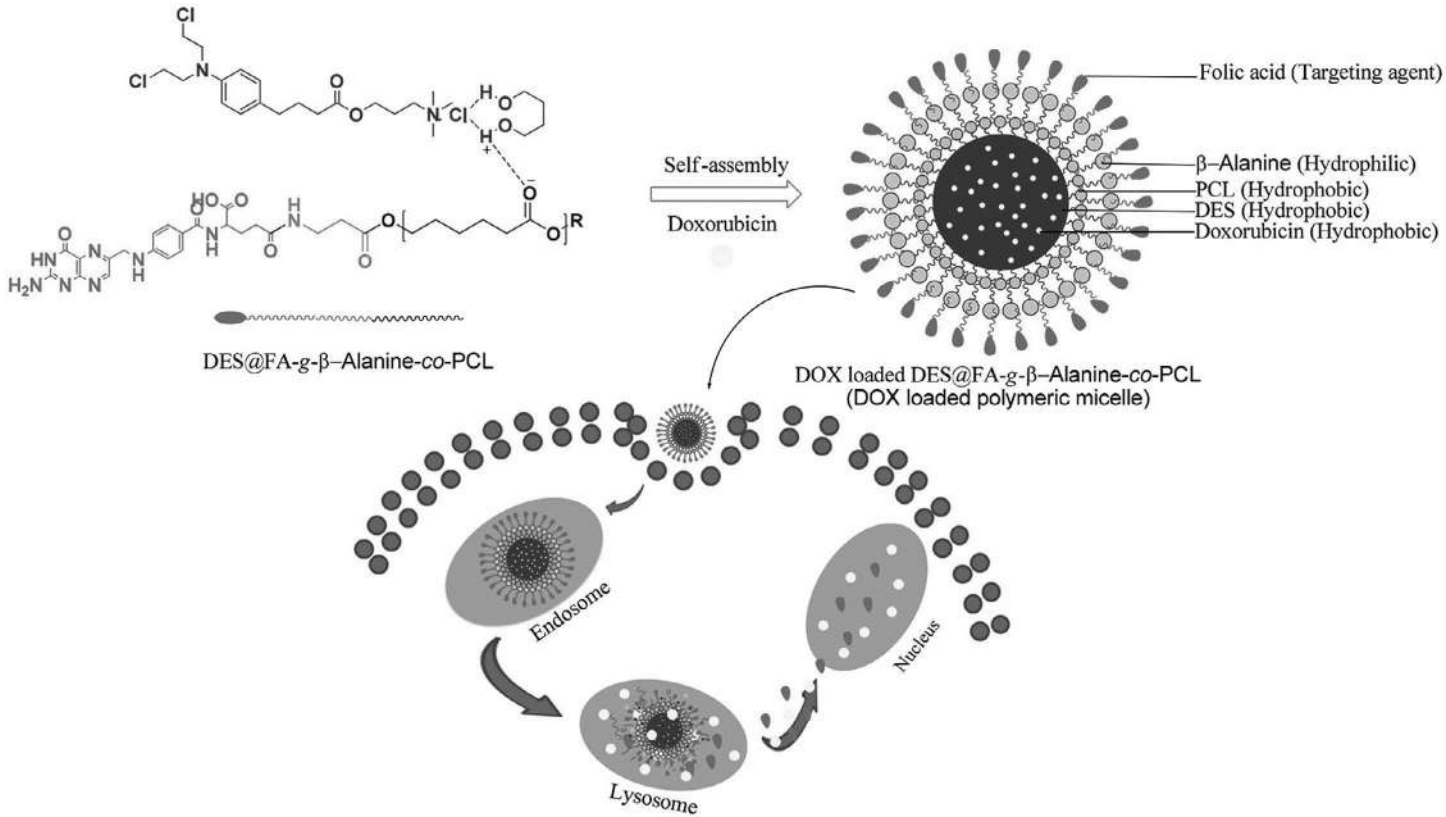

FIGURE 5.11 Schematic representation self-assembly of DOX-loaded polymeric micelle (DOX-loaded DES@FA-g-β-alanine-co-PCL).

Source: Reprinted (adapted) with permission from Pradeepkumar, P., et al., Deep eutectic solvent-mediated FA-g-β-alanine-co-PCL drug carrier for sustainable and site-specific drug delivery. *ACS Applied Bio Materials*, 2018. 1(6): p. 2094–2109. Copyright (2018) American Chemical Society [106].

physical properties. For the treatment of postherpetic neuralgia, Ohzeki et al. [114] developed an anesthetic cream based on a lidocaine–tetracaine eutectic mixture, which they used in clinical trials. A cellulose ester membrane was used to investigate the rate at which lidocaine was released from the prepared creams. Their research implies that creams can be used as a local anesthetic for therapeutic usage in the same way as injections, whether in an easy-to-use formulation or a low-cost formulation.

Additionally, DESs have lately demonstrated encouraging medicinal properties as antimicrobial (antiviral, antibacterial, and antifungal) [115] and anticancer instruments [116] in addition to drug delivery applications. It has been suggested in this area, based on early-stage research, that eutectic mixtures inherently may be examined in greater depth in the future for the advancement of innovative bio-inspired medicinal medicines.

5.8 DESs AS SOLVENT AND CATALYST

Organic synthesis for quite some time is an area of fundamental relevance from both an academic and an industrial standpoint, and the quest of sustainable procedures in this field is a matter of paramount importance. The development of DESs as ideal solvents for environmentally benign reactions [19] has occurred in this context, particularly in comparison to the use of ILs, which have demonstrated significant toxicity as well as exceedingly arduous formulation and refinement methods in numerous circumstances. The use of DESs as reaction vehicles for a wide range of organic conversions has increased significantly over the last 15 years, including alkylation, condensation, and multicomponent reactions [117], and organometallic reactions [118], as well as sporadic bio- and transition metal-catalyzed processes [119].

DESs have additionally demonstrated their practicability as ways in a variety of practices, including polymerization reactions [120], delignification of biomass feedstocks [121], and chemical components from complicated matrices by means of extraction [122] and purification [123]. Moreover, DESs have demonstrated their practicability as catalysts in a variety of practices, including the delignification of biomass feedstocks [120]. When looking over the huge sum of research on the utilization of DESs in synthesizing organics [117], the ones with a situation in which, at minimum, one DES component performs a critical role, transformation appears to be the most tempting. The DES plays an active role in the technique that involves the interaction of molecules with the surrounding environment or by dynamically supporting the process, suggesting that the eutectic mixture has a negligible effect on the chemistry involved. To provide a synopsis of the most fascinating and fresh developments in this picture, which is constantly progressing, the purpose of this section is to highlight and demonstrate how these unconventional media can be used as true protagonists, rather than simply as observers in the aforementioned fields.

Because of the seminal work of García Álvarez and Hevia's groups, the utilization of highly responsive organometallic group, such as Grignard and organolithium (RLi) reagents, in water-loving protic DESs has been unraveled. Organomagnesium

and RLi species were first introduced into the DESs for usage in reactions involving ketones [124], nonactivated imines [125], and polymerization reactions to produce synthetically relevant polyolefins [126], with high yields achieved in some cases. All the reactions occurred at a rapid rate at 25–40°C in air, resulting in higher yields and selectivity in several cases compared to typical protocols carried out in an inert atmosphere. As a result, an organometallic component might effectively compete with the DES medium's rate of protonation, opening new responsiveness for the construction of a broad spectrum of molecular architectures with different physical attributes. The method developed by Mallardo and colleagues uses t-BuLi in the "greener" solvent cyclopentyl methyl ether (CPME) and incremental quenching with a slew of electrophiles in ChCl/Gly (1:2) at 0°C to form o-substitution products chemoselectively at one phenyl ring with yields up to 90% in 10 minutes [127].

The researchers discovered that the o-tolylTHF byproducts could experience unmatched alkylative ring-opening caused by directed lateral lithiation (DLL) in a mixture of CPME/DES (ChCl/Gly; 1:2) could undergo unprecedented alkylative ring-opening [128]. A significant amount of DESs containing acidic precursors have been used as vehicles and reagents in a variety of renovations, including esterification [129], polymerization processes [130], and biomass valorization via cleavage of lignin feedstocks' chalcogenide components [131]. Nejrotti et al. [132] have provided an example of DESs in which this has occurred. Using a screening procedure for several Bronsted acid–based DESs, the researchers identified three chlorination systems: ChCl/MA (malonic acid), ChCl/OA (oxalic acid), and ChCl/TsOH (p-toluenesulfonic acid) as being moderate circumstances are ideal for boosting the response and in a judicious amount of time (60°C, 16 hours). Despite the greater sustainability observed in numerous cases, it is difficult to discern a specific influence of the DES in comparison to traditional systems (e.g., increased catalytic activity) from the examples presented earlier. Cavallo et al. described originally the Ru-catalyzed transfer hydrogenation of carbonyl compounds and imines in the presence of triethylamine (TEA) as the base where, both the reaction media and supply of H_2 are provided by the DES at this step of the reduction procedure [133] (Figure 5.12). According to the results of an extensive screening of several Ru-complexes and DESs, the most favorable system was determined to be TBABr/HCOOH, with formic acid serving as the H_2-source and the diphosphane complex [$RuCl_2$ (p-cymene)]2-dppf serving as the pre-catalyst. The Meyer–Schuster rearrangement of propargylic alcohols, which was recently reported by

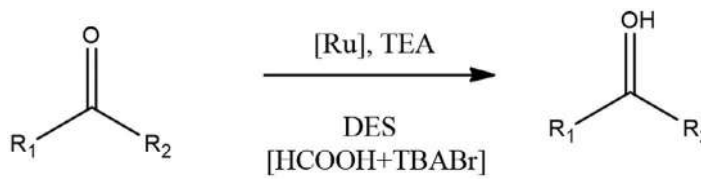

FIGURE 5.12 Ru-catalyzed transfer hydrogenation of carbonyl compounds promoted by DES (TBABr/HCOOH).

the González-Sabn and Garca-Alvarez groups [134], is an excellent example of a green transition–metal-catalyzed transformation.

5.9 DESs IN INNOVATIVE NANO-SORBENTS

As green chemistry and nanomaterial progress, a novel substitute for the customary volatile solvents is emerging as one of the many significant hot spots in the nanomaterial research and development discipline. ILs and DESs are great replacement solvents being used in the development of nano-sorbents, such as nanoparticles, nanogels, and nanofluids, among other applications. When it comes to extraction procedures, ILs and DESs are frequently utilized as carriers, modifiers, and dispersers of nano-sorbents in order to increase the adsorption and selectivity performance [135, 136]. Advantageous facts such as porous and cavity construction, broad specific surface area, high thermal stability, and ease of surface modification, multiwall carbon nanotubes (MWCNTs) offer a significant deal of potential for use in adsorption materials. MWCNTs, on the other hand, solution aggregation and matrix dispersion are both challenging for these compounds to achieve, resulting in a reduction in the specific surface area and adsorption capacity. It has been demonstrated that immobilizing green hydrophobic DESs on magnetic MWCNTs can effectively alleviate the difficulties listed earlier [137]. The employment of several DESs in the extraction process as nanoparticle transporters, modifiers, or dispersers can help to improve the affinity and selectivity between the nano-sorbents and the analyses in the extraction process.

As a result of their drawbacks, common nanoparticles as sorbents where the practical uses are limited, including single performance, difficulty in separation and recovery, among others. DESs combined with magnetic nanoparticles (MNPs), such as Fe_3O_4-DES [138] and $SiO_2@Fe_3O_4$-DES [139], have recently been confirmed to have a tiny particle size, a huge specific surface area, repeatability, and ecologically benign materials, making them ideal for use in the magnetic solid-phase extraction process, and the ease of solid–liquid separation. DESs based magnetic nano-sorbents have the ability to considerably enhance extraction efficiency when compared to ordinary nano-sorbents. Therefore, the creation and deployment of novel nano-sorbents customized with various solvents are the subject for future exploration. At present time, the majority of the research on MNPs including alternative solvents (DES) is being undertaken in the laboratory. For large-scale industrial applications, a more extensive examination of their viability and economic benefits is necessary. Solvents may be more effective when used in conjunction with one other, being versatile and uncomplicated; a bigger comparison, as well as an evaluation of their performance, is anticipated. It is envisaged that a series of commercial DES-based nano-sorbents will be released in the near future.

5.10 SUMMARY

The area of deep eutectic systems is an intriguing and impudent scientific province that has opened doors to a plethora of new viewpoints in the last few years. New scientific advancements are predicted as a result of the intensive research being

conducted on the subject, but there is unquestionably a need to systematize the efforts being done around the world in order to make the universal endeavors a tangible reality. If these systems are as promising as they are portrayed, society should reap the benefits of the investments being made in future, and sustainable processes such as metal processing, LLE, and biocatalysts should become a reality in the industrial sector. The creation of varieties of DESs was possible by the practically infinite number of eutectic combinations that could be made between HBAs and HBDs. This feature enables such systems to have superior physical qualities when compared to ILs. This resulted in extensive utilization of such systems in a wide range of research and applied fields, including a wide range of commercial and industrial applications. Several critical industrial fields of interest have been explored in this chapter. The top intensity of performance achieved in ionothermal synthesis by utilizing DESs as both solvents and shape-directing agents is astounding, and they pave the way for the synthesis of novel materials to come into existence. Furthermore, when such systems are used in VOC treatment devices, the environmental impact of such systems is extremely favorable. Furthermore, the widespread use of drug delivery systems (DESs) in the pharmacological domain has uncovered their tremendously encouraging means of enhancing the pharmacokinetic characteristics of pharmaceuticals of APIs and, in some cases, of acting as APIs themselves. However, the use of DESs is still at an early stage of development and will continue with greater possibilities as our understanding of their function at the molecular rank increases.

REFERENCES

1. Anastas, P. and N. Eghbali, *Green chemistry: Principles and practice*. Chemical Society Reviews, 2010. **39**(1): p. 301–312.
2. Bubalo, M.C., et al., *Green extraction of grape skin phenolics by using deep eutectic solvents*. Food Chemistry, 2016. **200**: p. 159–166.
3. Ahluwalia, V., *Green chemistry: Environmentally benign reactions*. 2021: Springer Nature.
4. Capello, C., U. Fischer, and K. Hungerbühler, *What is a green solvent? A comprehensive framework for the environmental assessment of solvents*. Green Chemistry, 2007. **9**(9): p. 927–934.
5. Dunn, P.J., *The importance of green chemistry in process research and development*. Chemical Society Reviews, 2012. **41**(4): p. 1452–1461.
6. Chemat, F., M.A. Vian, and G. Cravotto, *Green extraction of natural products: Concept and principles*. International Journal of Molecular Sciences, 2012. **13**(7): p. 8615–8627.
7. Andrew, C., et al., *Deep eutectic solvents: An overview of its application as a "green" extractant*. International Journal of Advanced Research in Chemical Science, 2017. **10**: p. 2349. 0403.0406003.
8. Abbott, A.P., et al., *Deep eutectic solvents formed between choline chloride and carboxylic acids: Versatile alternatives to ionic liquids*. Journal of the American Chemical Society, 2004. **126**(29): p. 9142–9147.
9. Abbott, A.P., et al., *Voltammetric and impedance studies of the electropolishing of type 316 stainless steel in a choline chloride based ionic liquid*. Electrochimica Acta, 2006. **51**(21): p. 4420–4425.
10. Dai, Y., et al., *Natural deep eutectic solvents as new potential media for green technology*. Analytica Chimica Acta, 2013. **766**: p. 61–68.

11. Yucui, H., Y. Congfei, and W. Weize, *Deep eutectic solvents: Green solvents for separation applications.* Acta Phys Chim Sin, 2018. **34**: p. 0001–0009.
12. Vanda, H., et al., *Green solvents from ionic liquids and deep eutectic solvents to natural deep eutectic solvents.* Comptes Rendus Chimie, 2018. **21**(6): p. 628–638.
13. Roda, A., et al., *Polymer science and engineering using deep eutectic solvents.* Polymers, 2019. **11**(5): p. 912.
14. Huang, Z.L., et al., *Deep eutectic solvents can be viable enzyme activators and stabilizers.* Journal of Chemical Technology & Biotechnology, 2014. **89**(12): p. 1975–1981.
15. Paiva, A., A.A. Matias, and A.R.C. Duarte, *How do we drive deep eutectic systems towards an industrial reality?* Current Opinion in Green and Sustainable Chemistry, 2018. **11**: p. 81–85.
16. Paiva, A., et al., *Natural deep eutectic solvents—solvents for the 21st century.* ACS Sustainable Chemistry & Engineering, 2014. **2**(5): p. 1063–1071.
17. Coutinho, J.A. and S.P. Pinho, *Special issue on deep eutectic solvents: A foreword.* Fluid Phase Equilibria, 2017. **448**(1).
18. Passos, H., et al., *Are aqueous biphasic systems composed of deep eutectic solvents ternary or quaternary systems?* ACS Sustainable Chemistry & Engineering, 2016. **4**(5): p. 2881–2886.
19. Smith, E.L., A.P. Abbott, and K.S. Ryder, *Deep eutectic solvents (DESs) and their applications.* Chemical Reviews, 2014. **114**(21): p. 11060–11082.
20. Smith, E., *Deep eutectic solvents (DESs) and the metal finishing industry: Where are they now?* Transactions of the IMF, 2013. **91**(5): p. 241–248.
21. Hansen, B.B., et al., *Deep eutectic solvents: A review of fundamentals and applications.* Chemical Reviews, 2020. **121**(3): p. 1232–1285.
22. Ali, E., S. Mulyono, and M. Hadj-Kali, *Scaling-up liquid-liquid extraction experiments with deep eutectic solvents.* New Developments in Biology, Biomedical Chemical Engineering and Materials Science, 2015.
23. Guajardo, N., et al., *Deep eutectic solvents for organocatalysis, biotransformations, and multistep organocatalyst/enzyme combinations.* ChemCatChem, 2016. **8**(6): p. 1020–1027.
24. Sheldon, R.A., *Biocatalysis and biomass conversion in alternative reaction media.* Chemistry—A European Journal, 2016. **22**(37): p. 12984–12999.
25. Xu, L., et al., *Deep eutectic solvents enable the enhanced production of n-3 PUFA-enriched triacylglycerols.* European Journal of Lipid Science and Technology, 2017. **119**(12): p. 1700300.
26. Abbott, A., et al., *Electrodeposition of nickel using eutectic based ionic liquids.* Transactions of the IMF, 2008. **86**(4): p. 234–240.
27. Oke, E.A. and S.P. Ijardar, *Advances in the application of deep eutectic solvents based aqueous biphasic systems: An up-to-date review.* Biochemical Engineering Journal, 2021. **176**: p. 108211.
28. Kuddushi, M., et al., *Understanding the peculiar effect of water on the physicochemical properties of choline chloride based deep eutectic solvents theoretically and experimentally.* Journal of Molecular Liquids, 2019. **278**: p. 607–615.
29. Francisco, M., A. van den Bruinhorst, and M.C. Kroon, *Low-transition-temperature mixtures (LTTMs): A new generation of designer solvents.* Angewandte Chemie International Edition, 2013. **52**(11): p. 3074–3085.
30. Pass, G. and H. Sutcliffe, *Chemistry in non-aqueous solvents*, in *Practical Inorganic Chemistry.* 1974, Springer. p. 122–132.
31. Shikov, A.N., et al., *Natural deep eutectic solvents for the extraction of phenyletanes and phenylpropanoids of Rhodiola rosea L.* Molecules, 2020. **25**(8): p. 1826.
32. Velásquez, P., et al., *Ultrasound-assisted extraction of anthocyanins using natural deep eutectic solvents and their incorporation in edible films.* Molecules, 2021. **26**(4): p. 984.

33. Altunay, N., A. Elik, and R. Gürkan, *Natural deep eutectic solvent-based ultrasound-assisted-microextraction for extraction, pre-concentration and analysis of methylmercury and total mercury in fish and environmental waters by spectrophotometry*. Food Additives & Contaminants: Part A, 2019. **36**(7): p. 1079–1097.
34. Islamčević Razboršek, M., et al., *Choline chloride based natural deep eutectic solvents as extraction media for extracting phenolic compounds from chokeberry (aronia melanocarpa)*. Molecules, 2020. **25**(7): p. 1619.
35. Tuntarawongsa, S. and T. Phaechamud. *Menthol, borneol, camphor and WS-3 eutectic mixture*. in *Advanced Materials Research*. 2012. Trans Tech Publ.
36. Silva, J.M., et al., *Design of functional therapeutic deep eutectic solvents based on choline chloride and ascorbic acid*. ACS Sustainable Chemistry & Engineering, 2018. **6**(8): p. 10355–10363.
37. Sekharan, T.R., et al., *Development of Ibuprofen-loaded emulsion from eutectic mixture and Eudragit RL 100*. Development, 2019. **7**: p. 0.
38. Gala, U., et al., *Characterization and comparison of lidocaine-tetracaine and lidocaine-camphor eutectic mixtures based on their crystallization and hydrogen-bonding abilities*. Aaps Pharmscitech, 2015. **16**(3): p. 528–536.
39. Tuntarawongsa, S. and T. Phaechamud, *Polymeric eutectic drug delivery system*. Journal of Metals, Materials and Minerals, 2012. **22**(2).
40. Lozowski, D., *Supercritical CO2: A green solvent*. Chemical Engineering, 2010. **117**(2): p. 15.
41. Ma, Y., Q. Wang, and T. Zhu, *Comparison of hydrophilic and hydrophobic deep eutectic solvents for pretreatment determination of sulfonamides from aqueous environments*. Analytical Methods, 2019. **11**(46): p. 5901–5909.
42. Van Osch, D.J., et al., *A search for natural hydrophobic deep eutectic solvents based on natural components*. ACS Sustainable Chemistry & Engineering, 2019. **7**(3): p. 2933–2942.
43. Dwamena, A.K., *Recent advances in hydrophobic deep eutectic solvents for extraction*. Separations, 2019. **6**(1): p. 9.
44. Qu, Q., et al., *Synthesis and characterization of deep eutectic solvents (five hydrophilic and three hydrophobic), and hydrophobic application for microextraction of environmental water samples*. Analytical and Bioanalytical Chemistry, 2019. **411**(28): p. 7489–7498.
45. Verma, R. and T. Banerjee, *Palmitic-acid-based hydrophobic deep eutectic solvents for the extraction of lower alcohols from Aqueous Media: Liquid—liquid equilibria measurements, validation and process economics*. Global Challenges, 2019. **3**(11): p. 1900024.
46. Verma, R. and T. Banerjee, *Liquid—liquid extraction of lower alcohols using menthol-based hydrophobic deep eutectic solvent: experiments and COSMO-SAC predictions*. Industrial & Engineering Chemistry Research, 2018. **57**(9): p. 3371–3381.
47. Lee, J., D. Jung, and K. Park, *Hydrophobic deep eutectic solvents for the extraction of organic and inorganic analytes from aqueous environments*. TrAC Trends in Analytical Chemistry, 2019. **118**: p. 853–868.
48. Florindo, C., L. Branco, and I. Marrucho, *Development of hydrophobic deep eutectic solvents for extraction of pesticides from aqueous environments*. Fluid Phase Equilibria, 2017. **448**: p. 135–142.
49. Yousefi, S.M., F. Shemirani, and S.A. Ghorbanian, *Hydrophobic deep eutectic solvents in developing microextraction methods based on solidification of floating drop: Application to the trace HPLC/FLD determination of PAHs*. Chromatographia, 2018. **81**(8): p. 1201–1211.
50. Tamilvanan, S., et al., *Candidiasis management: Current status of allopathic drugs and utility of corianderbased oil-less emulsions*. Letters in Applied NanoBioScience, 2019. **8**: p. 586–590.

51. Biswal, B., et al., *Formulation and evaluation of microemulsion based topical hydrogel containing lornoxicam*. Journal of Applied Pharmaceutical Science, 2014. **4**(12): p. 77–84.
52. Shen, Q., et al., *Enhanced intestinal absorption of daidzein by borneol/menthol eutectic mixture and microemulsion*. Aaps Pharmscitech, 2011. **12**(4): p. 1044–1049.
53. Cooper, E.R., et al., *Ionic liquids and eutectic mixtures as solvent and template in synthesis of zeolite analogues*. Nature, 2004. **430**(7003): p. 1012–1016.
54. Marcus, Y., *The variety of deep eutectic solvents*, in *Deep Eutectic Solvents*. 2019, Springer. p. 13–44.
55. Maschita, J., et al., *Ionothermal synthesis of imide-linked covalent organic frameworks*. Angewandte Chemie International Edition, 2020. **59**(36): p. 15750–15758.
56. Gao, Z., et al., *Ultrathin Mg-Al layered double hydroxide prepared by ionothermal synthesis in a deep eutectic solvent for highly effective boron removal*. Chemical Engineering Journal, 2017. **319**: p. 108–118.
57. Zheng, J., et al., *Industrial sector-based volatile organic compound (VOC) source profiles measured in manufacturing facilities in the Pearl River Delta, China*. Science of the Total Environment, 2013. **456**: p. 127–136.
58. Montero-Montoya, R., R. López-Vargas, and O. Arellano-Aguilar, *Volatile organic compounds in air: Sources, distribution, exposure and associated illnesses in children*. Annals of Global Health, 2018. **84**(2): p. 225.
59. Lin, C., et al., *Vertical stratification of volatile organic compounds and their photochemical product formation potential in an industrial urban area*. Journal of Environmental Management, 2018. **217**: p. 327–336.
60. Villanueva, F., et al., *Indoor and outdoor air concentrations of volatile organic compounds and NO2 in schools of urban, industrial and rural areas in Central-Southern Spain*. Science of the Total Environment, 2018. **622**: p. 222–235.
61. Settimo, G., M. Manigrasso, and P. Avino, *Indoor air quality: A focus on the European legislation and state-of-the-art research in Italy*. Atmosphere, 2020. **11**(4): p. 370.
62. Heymes, F., et al., *A new efficient absorption liquid to treat exhaust air loaded with toluene*. Chemical Engineering Journal, 2006. **115**(3): p. 225–231.
63. Darracq, G., et al., *Silicone oil: An effective absorbent for the removal of hydrophobic volatile organic compounds*. Journal of Chemical Technology & Biotechnology, 2010. **85**(3): p. 309–313.
64. Salar-García, M., et al., *Ionic liquid technology to recover volatile organic compounds (VOCs)*. Journal of Hazardous Materials, 2017. **321**: p. 484–499.
65. Kudłak, B., K. Owczarek, and J. Namieśnik, *Selected issues related to the toxicity of ionic liquids and deep eutectic solvents—a review*. Environmental Science and Pollution Research, 2015. **22**(16): p. 11975–11992.
66. Li, Z., et al., *Absorption of carbon dioxide using ethanolamine-based deep eutectic solvents*. ACS Sustainable Chemistry & Engineering, 2019. **7**(12): p. 10403–10414.
67. Mirza, N.R., et al., *Experiments and thermodynamic modeling of the solubility of carbon dioxide in three different deep eutectic solvents (DESs)*. Journal of Chemical & Engineering Data, 2015. **60**(11): p. 3246–3252.
68. Leron, R.B., A. Caparanga, and M.-H. Li, *Carbon dioxide solubility in a deep eutectic solvent based on choline chloride and urea at T= 303.15–343.15 K and moderate pressures*. Journal of the Taiwan Institute of Chemical Engineers, 2013. **44**(6): p. 879–885.
69. Lu, M., et al., *Solubilities of carbon dioxide in the eutectic mixture of levulinic acid (or furfuryl alcohol) and choline chloride*. The Journal of Chemical Thermodynamics, 2015. **88**: p. 72–77.
70. Moura, L., et al., *Deep eutectic solvents as green absorbents of volatile organic pollutants*. Environmental Chemistry Letters, 2017. **15**(4): p. 747–753.

71. Yang, D., et al., *Efficient SO 2 absorption by renewable choline chloride—glycerol deep eutectic solvents*. Green Chemistry, 2013. **15**(8): p. 2261–2265.
72. Deng, D., G. Han, and Y. Jiang, *Investigation of a deep eutectic solvent formed by levulinic acid with quaternary ammonium salt as an efficient SO 2 absorbent*. New Journal of Chemistry, 2015. **39**(10): p. 8158–8164.
73. Liu, X., B. Gao, and D. Deng, *SO2 absorption/desorption performance of renewable phenol-based deep eutectic solvents*. Separation Science and Technology, 2018. **53**(14): p. 2150–2158.
74. Liu, B., et al., *Characterization of amide—thiocyanates eutectic ionic liquids and their application in SO 2 absorption*. RSC Advances, 2013. **3**(7): p. 2470–2476.
75. Zhang, K., et al., *Efficient absorption of SO2 with low-partial pressures by environmentally benign functional deep eutectic solvents*. Journal of Hazardous Materials, 2017. **324**: p. 457–463.
76. Akhmetshina, A.I., et al., *Evaluation of methanesulfonate-based deep eutectic solvent for ammonia sorption*. Journal of Chemical & Engineering Data, 2018. **63**(6): p. 1896–1904.
77. Zhong, F.-Y., et al., *Phenol-based ternary deep eutectic solvents for highly efficient and reversible absorption of NH3*. ACS Sustainable Chemistry & Engineering, 2019. **7**(3): p. 3258–3266.
78. Zhong, F.-Y., K. Huang, and H.-L. Peng, *Solubilities of ammonia in choline chloride plus urea at (298.2–353.2) K and (0–300) kPa*. The Journal of Chemical Thermodynamics, 2019. **129**: p. 5–11.
79. Li, Y., et al., *Hybrid deep eutectic solvents with flexible hydrogen-bonded supramolecular networks for highly efficient uptake of NH3*. ChemSusChem, 2017. **10**(17): p. 3368–3377.
80. Deng, D., et al., *Investigation of protic NH4SCN-based deep eutectic solvents as highly efficient and reversible NH3 absorbents*. Chemical Engineering Journal, 2019. **358**: p. 936–943.
81. Di Pietro, M.E., et al., *Do cyclodextrins encapsulate volatiles in deep eutectic systems?* ACS Sustainable Chemistry & Engineering, 2019. **7**(20): p. 17397–17405.
82. Kalepu, S. and V. Nekkanti, *Insoluble drug delivery strategies: Review of recent advances and business prospects*. Acta Pharmaceutica Sinica B, 2015. **5**(5): p. 442–453.
83. Savjani, K.T., A.K. Gajjar, and J.K. Savjani, *Drug solubility: Importance and enhancement techniques*. International Scholarly Research Notices, 2012. **2012**.
84. Gala, U., H. Pham, and H. Chauhan, *Pharmaceutical applications of eutectic mixtures*. J. Dev. Drugs, 2013. **2**(2).
85. Cherukuvada, S. and A. Nangia, *Eutectics as improved pharmaceutical materials: Design, properties and characterization*. Chemical Communications, 2014. **50**(8): p. 906–923.
86. Zainal-Abidin, M.H., et al., *Emerging frontiers of deep eutectic solvents in drug discovery and drug delivery systems*. Journal of Controlled Release, 2019. **316**: p. 168–195.
87. Pedro, S.N., et al., *Deep eutectic solvents comprising active pharmaceutical ingredients in the development of drug delivery systems*. Expert Opinion on Drug Delivery, 2019. **16**(5): p. 497–506.
88. Lu, C., et al., *Significantly improving the solubility of non-steroidal anti-inflammatory drugs in deep eutectic solvents for potential non-aqueous liquid administration*. MedChemComm, 2016. **7**(5): p. 955–959.
89. Li, Z. and P.I. Lee, *Investigation on drug solubility enhancement using deep eutectic solvents and their derivatives*. International Journal of Pharmaceutics, 2016. **505**(1–2): p. 283–288.
90. Rahman, M.S., et al., *Formulation, structure, and applications of therapeutic and amino acid-based deep eutectic solvents: An overview*. Journal of Molecular Liquids, 2021. **321**: p. 114745.

91. Olivares, B., et al., *A natural deep eutectic solvent formulated to stabilize β-lactam antibiotics*. Scientific Reports, 2018. **8**(1): p. 1–12.
92. Sut, S., et al., *Natural deep eutectic solvents (NADES) to enhance berberine absorption: An in vivo pharmacokinetic study*. Molecules, 2017. **22**(11): p. 1921.
93. Aroso, I.M., et al., *Dissolution enhancement of active pharmaceutical ingredients by therapeutic deep eutectic systems*. European Journal of Pharmaceutics and Biopharmaceutics, 2016. **98**: p. 57–66.
94. Abbott, A.P., et al., *Liquid pharmaceuticals formulation by eutectic formation*. Fluid Phase Equilibria, 2017. **448**: p. 2–8.
95. Stott, P.W., A.C. Williams, and B.W. Barry, *Transdermal delivery from eutectic systems: Enhanced permeation of a model drug, ibuprofen*. Journal of Controlled Release, 1998. **50**(1–3): p. 297–308.
96. Nyqvist-Mayer, A.A., A.F. Brodin, and S.G. Frank, *Drug release studies on an oil—water emulsion based on a eutectic mixture of lidocaine and prilocaine as the dispersed phase*. Journal of Pharmaceutical Sciences, 1986. **75**(4): p. 365–373.
97. Park, C.-W., et al., *Phase behavior of itraconazole—phenol mixtures and its pharmaceutical applications*. International Journal of Pharmaceutics, 2012. **436**(1–2): p. 652–658.
98. Nazzal, S., et al., *Preparation and in vitro characterization of a eutectic based semisolid self-nanoemulsified drug delivery system (SNEDDS) of ubiquinone: Mechanism and progress of emulsion formation*. International Journal of Pharmaceutics, 2002. **235**(1–2): p. 247–265.
99. Wang, W., et al., *Microemulsions based on paeonol-menthol eutectic mixture for enhanced transdermal delivery: Formulation development and in vitro evaluation*. Artificial Cells, Nanomedicine, and Biotechnology, 2017. **45**(6): p. 1241–1246.
100. Duarte, A.R.C., et al., *A comparison between pure active pharmaceutical ingredients and therapeutic deep eutectic solvents: Solubility and permeability studies*. European Journal of Pharmaceutics and Biopharmaceutics, 2017. **114**: p. 296–304.
101. Woolfson, A., et al., *Rheological, mechanical and membrane penetration properties of novel dual drug systems for percutaneous delivery*. Journal of Controlled Release, 2000. **67**(2–3): p. 395–408.
102. Fiala, S., M.B. Brown, and S.A. Jones, *An investigation into the influence of binary drug solutions upon diffusion and partition processes in model membranes*. Journal of Pharmacy and Pharmacology, 2008. **60**(12): p. 1615–1623.
103. Wang, H., et al., *Simultaneous membrane transport of two active pharmaceutical ingredients by charge assisted hydrogen bond complex formation*. Chemical Science, 2014. **5**(9): p. 3449–3456.
104. Mota-Morales, J.D., et al., *Deep eutectic solvents as both active fillers and monomers for frontal polymerization*. Journal of Polymer Science Part A: Polymer Chemistry, 2013. **51**(8): p. 1767–1773.
105. Sánchez-Leija, R., et al., *Controlled release of lidocaine hydrochloride from polymerized drug-based deep-eutectic solvents*. Journal of Materials Chemistry B, 2014. **2**(43): p. 7495–7501.
106. Pradeepkumar, P., et al., *Deep eutectic solvent-mediated FA-g-β-alanine-co-PCL drug carrier for sustainable and site-specific drug delivery*. ACS Applied Bio Materials, 2018. **1**(6): p. 2094–2109.
107. Pradeepkumar, P., et al., *Folic acid conjugated polyglutamic acid drug vehicle synthesis through deep eutectic solvent for targeted release of paclitaxel*. ChemistrySelect, 2019. **4**(35): p. 10225–10235.
108. Aroso, I.M., et al., *Design of controlled release systems for THEDES—Therapeutic deep eutectic solvents, using supercritical fluid technology*. International Journal of Pharmaceutics, 2015. **492**(1–2): p. 73–79.

109. Chun, M.-K., et al., *Development of cataplasmic transdermal drug delivery system containing eutectic mixture of lidocaine and prilocaine*. Journal of Pharmaceutical Investigation, 2012. **42**(3): p. 139–146.
110. Serrano, M.C., et al., *Synthesis of novel lidocaine-releasing poly (diol-co-citrate) elastomers by using deep eutectic solvents*. Chemical Communications, 2012. **48**(4): p. 579–581.
111. Scherlund, M., A. Brodin, and M. Malmsten, *Nonionic cellulose ethers as potential drug delivery systems for periodontal anesthesia*. Journal of Colloid and Interface Science, 2000. **229**(2): p. 365–374.
112. Mano, F., et al., *Production of electrospun fast-dissolving drug delivery systems with therapeutic eutectic systems encapsulated in gelatin*. AAPS PharmSciTech, 2017. **18**(7): p. 2579–2585.
113. Zuń, M., et al., *The influence of the eutectic mixtures: Salicylic acid-menthol and benzocaine-menthol on physical properties of the creams with fluconazole*. Curr. Issues Pharm. Med. Sci, 2013. **26**(4): p. 457–460.
114. Ohzeki, K., et al., *Local anesthetic cream prepared from lidocaine-tetracaine eutectic mixture*. Yakugaku Zasshi, 2008. **128**(4): p. 611–616.
115. Zakrewsky, M., et al., *Choline and geranate deep eutectic solvent as a broad-spectrum antiseptic agent for preventive and therapeutic applications*. Advanced Healthcare Materials, 2016. **5**(11): p. 1282–1289.
116. Mbous, Y.P., et al., *Unraveling the cytotoxicity and metabolic pathways of binary natural deep eutectic solvent systems*. Scientific Reports, 2017. **7**(1): p. 1–14.
117. Alonso, D.A., et al., *Deep eutectic solvents: The organic reaction medium of the century*. 2016.
118. García-Álvarez, J., E. Hevia, and V. Capriati, *The future of polar organometallic chemistry written in bio-based solvents and water*. Chemistry-A European Journal, 2018.
119. Xu, P., et al., *Recent progress on deep eutectic solvents in biocatalysis*. Bioresources and Bioprocessing, 2017. **4**(1): p. 1–18.
120. Jablonský, M., A. Škulcová, and J. Šima, *Use of deep eutectic solvents in polymer chemistry—A review*. Molecules, 2019. **24**(21): p. 3978.
121. Grillo, G., et al., *Green deep eutectic solvents for microwave-assisted biomass delignification and valorisation*. Molecules, 2021. **26**(4): p. 798.
122. Chandran, D., et al., *Deep eutectic solvents for extraction-desulphurization: A review*. Journal of Molecular Liquids, 2019. **275**: p. 312–322.
123. Cai, T. and H. Qiu, *Application of deep eutectic solvents in chromatography: A review*. TrAC Trends in Analytical Chemistry, 2019. **120**: p. 115623.
124. Vidal, C., et al., *Introducing deep eutectic solvents to polar organometallic chemistry: Chemoselective addition of organolithium and grignard reagents to ketones in air*. Angewandte Chemie, 2014. **126**(23): p. 6079–6083.
125. Vidal, C., et al., *Exploiting deep eutectic solvents and organolithium reagent partnerships: Chemoselective ultrafast addition to imines and quinolines under aerobic ambient temperature conditions*. Angewandte Chemie International Edition, 2016. **55**(52): p. 16145–16148.
126. Sánchez-Condado, A., et al., *Organolithium-initiated polymerization of olefins in deep eutectic solvents under aerobic conditions*. ChemSusChem, 2019. **12**(13): p. 3134–3143.
127. Mallardo, V., et al., *Regioselective desymmetrization of diaryltetrahydrofurans via directed ortho-lithiation: An unexpected help from green chemistry*. Chemical Communications, 2014. **50**(63): p. 8655–8658.
128. Sassone, F.C., et al., *Unexpected lateral-lithiation-induced alkylative ring opening of tetrahydrofurans in deep eutectic solvents: Synthesis of functionalised primary alcohols*. Chemical Communications, 2015. **51**(46): p. 9459–9462.

129. De Santi, V., et al., *Novel Brønsted acidic deep eutectic solvent as reaction media for esterification of carboxylic acid with alcohols*. Tetrahedron Letters, 2012. **53**(38): p. 5151–5155.
130. Nahar, Y. and S.C. Thickett, *Greener, faster, stronger: The benefits of deep eutectic solvents in polymer and materials science*. Polymers, 2021. **13**(3): p. 447.
131. Kalhor, P. and K. Ghandi, *Deep eutectic solvents as catalysts for upgrading biomass*. Catalysts, 2021. **11**(2): p. 178.
132. Nejrotti, S., et al., *Natural deep eutectic solvents as an efficient and reusable active system for the Nazarov cyclization*. Green Chemistry, 2020. **22**(1): p. 110–117.
133. Cavallo, M., et al., *Deep eutectic solvents as H2-sources for Ru (II)-catalyzed transfer hydrogenation of carbonyl compounds under mild conditions*. Tetrahedron, 2021. **83**: p. 131997.
134. Ríos-Lombardía, N., et al., *Deep eutectic solvent-catalyzed Meyer—Schuster rearrangement of propargylic alcohols under mild and bench reaction conditions*. Chemical Communications, 2020. **56**(96): p. 15165–15168.
135. Zaib, Q., et al., *Deep eutectic solvent assisted dispersion of carbon nanotubes in water*. Frontiers in Chemistry, 2020. **8**.
136. Liu, H., et al., *Magnetic solid-phase extraction of pyrethroid pesticides from environmental water samples using deep eutectic solvent-type surfactant modified magnetic zeolitic imidazolate framework-8*. Molecules, 2019. **24**(22): p. 4038.
137. Tarigh, G.D., M. Bakhtiari, and F. Shemirani, *Green chemicals-assisted dispersive magnetic solid-phase extraction: A prospect for speciation of Cr (III)/Cr (VI) in environmental water samples*. International Journal of Environmental Analytical Chemistry, 2020: p. 1–17.
138. Liu, Q., X. Huang, and P. Liang, *Preconcentration of copper and lead using deep eutectic solvent modified magnetic nanoparticles and determination by inductively coupled plasma optical emission spectrometry*. Atomic Spectrosc, 2020. **41**: p. 36–42.
139. Majidi, S.M. and M.R. Hadjmohammadi, *Alcohol-based deep eutectic solvent as a carrier of SiO2@ Fe3O4 for the development of magnetic dispersive micro-solid-phase extraction method: Application for the preconcentration and determination of morin in apple and grape juices, diluted and acidic extract of dried onion and green tea infusion samples*. Journal of separation science, 2019. **42**(17): p. 2842–2850.

Appendix

1. SAMPLE CALCULATION FOR MOLE FRACTION FROM NUCLEAR MAGNETIC RESONANCE SPECTRA

In the following, a sample calculation has been illustrated for the quantification of the known composition of DES1, quinoline, and heptane in the mixture (Chapter 3). The peak position and its components are located in Figure A1.

Peak area equivalent to 1 Hydrogen of DES (Peaks of MTBP) = (6.09 + 24.58)/15 = 2.04
= 6.13/3 = 2.04

It is interesting to observe that the peak area of $-CH_2$ in ethylene glycol contributes an area of 33.07, or 33.07/4 = 8.267. This is exactly four times the contribution on hydrogen atom of methyltriphenyl phosphonium bromide (MTBP), that is, 2.04. This proves the fact that the mixture of MTBP and ethylene glycol is in the ratio of 1:4 and is a solution or solvent as a whole. Further continuing the calculation, we have the following:

Peak area equivalent to 1 hydrogen of toluene = (0.82 + 1.25)/5 = 0.41
Peak area equivalent to 1 hydrogen of heptane = 3.28/6 = 0.54
Now $\sum_{i=1}^{3} H_i$ = (2.04 + 0.41 + 0.54) = 2.99
Mole fraction of DES = 02.04/2.99 = 0.68
Mole fraction of toluene = 0.41/2.99 = 0.14
Mole fraction of heptane = 0.54/2.99 = 0.18

The reproducibility of the nuclear magnetic resonance (NMR)–derived mole fractions were checked on known mixtures of toluene–DES1 and quinoline–DES1, and it was found that the mole fractions lie within the uncertainty range of ±0.01. This was necessitated as all mixtures of DES–toluene/quinoline–heptane were found to lie in the heterogeneous region.

2. COSMO-SAC MODEL AND SOLUBILITY THERMODYNAMICS OF DESs

The Conductor-like Screening Model–Segment Activity Coefficient (COSMO-SAC) model was designed by Lin and Sandler [1]. Its purpose is to predict different phase equilibria thermodynamic properties using quantum and statistical mechanics. The model is based on the original work of Andreas Klamt [2] who developed COSMO for its ability to determine the screening charges around a

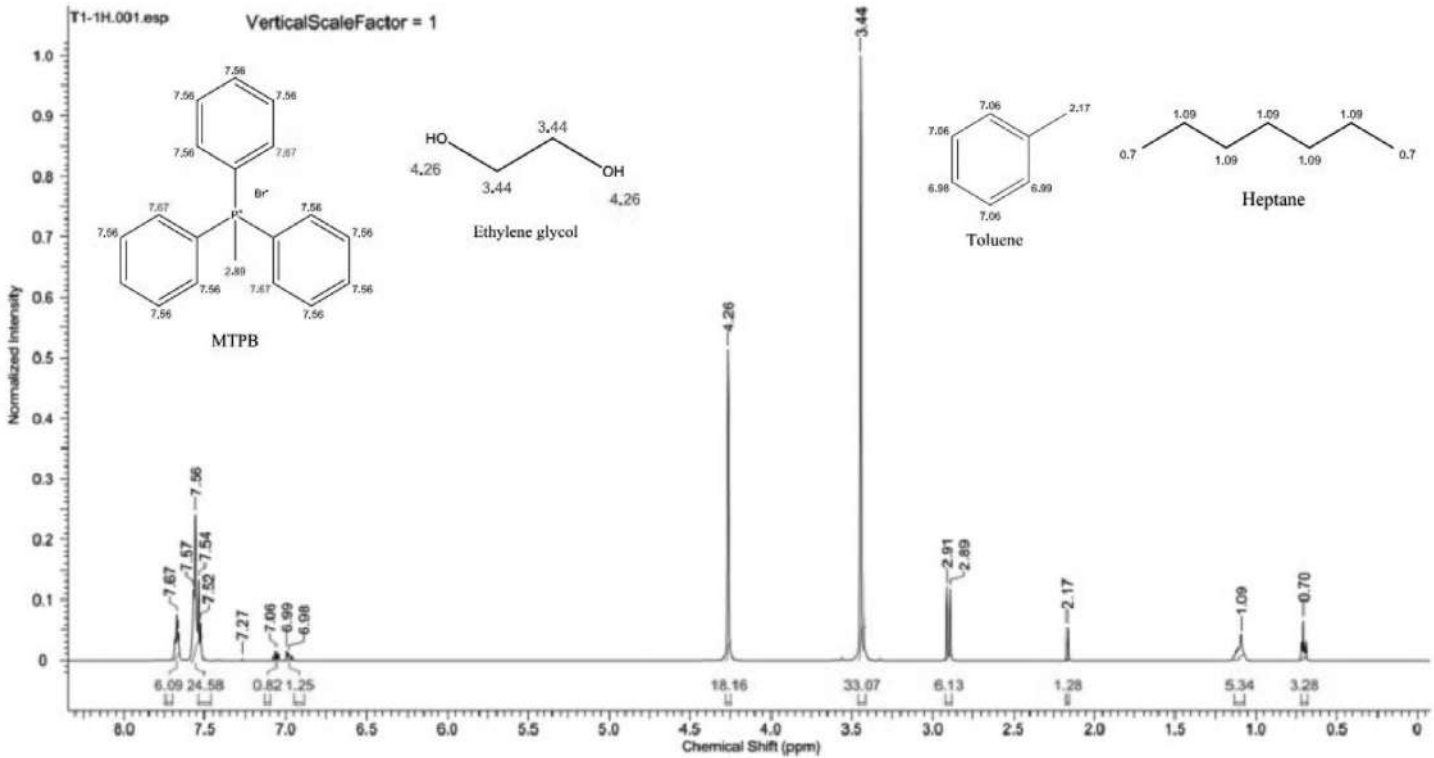

FIGURE A.1 Nuclear magnetic resonance spectra of extract phase of ternary system DES + heptane + toluene

solute in a conductor by using density functional theory (DFT) for real solvents (COSMO-RS). The COSMO-SAC allows the thermodynamic properties of molecules to be predicted from the activity coefficients of tiny segments. The COSMO-SAC model uses quantum chemical methods for the representation of the charge distribution of the molecules (σ-profiles), and statistical thermodynamics to get the molecular interactions for predicting the chemical potential of a molecule from its structure. To determine the activity coeffcient, only the σ-profiles and the van der Waals surface and volume are needed, which makes COSMO-SAC a fully predictive model.

The model gives an expression of the solvation free energy ΔG^{*solv}, which defines, at constant temperature and pressure, the energy difference between an ideal solution and the solute in the real solvent. The molecules are regarded as a collection of surface segments, and the chemical potential of each segment is determined. The difference in the segment activity coefficient between a mixture and a pure liquid gives the segment activity coefficients, and the activity coefficient of a molecule is obtained from the summation over the segment activity coefficients. The activity coefficient $\gamma_{i/s}$ of solute i in the solution s is derived from the following Equation A.1.

$$\ln \gamma_{i/s} = \frac{\Delta G_{i/s}^{*res} - \Delta G_{i/s}^{*res}}{RT} + \ln \gamma_{i/s}^{SG} \tag{A.1}$$

Here, ΔG^{*res} is the restoring solvation free energy, and superscript SG denotes the Staverman–Guggenheim combinatorial term (Table A.2). Finally, the activity coefficient is calculated and given as Equation A.2.

$$\ln\gamma_{i/s} = n_i \sum_{\sigma} P_i(\sigma_m)\left[\ln\Gamma_s(\sigma_m) - \Gamma_i(\sigma_m)\right] + \ln\gamma_{i/s}^{SG} \tag{A.2}$$

Here $\Gamma_s(\sigma_m)$ and $\Gamma_i(\sigma_m)$ are the activity coefficient of the segment in the mixture and in the component i, respectively. σ_m is the surface charge density of the segment mixture. The three-dimensional screening charge density distribution $p_i(\sigma_m)$ is quantified using the σ-profile, which is the probability of finding a surface segment with screening charge density σ; that is, $p(\sigma) = \{A_i(\sigma)\}/A_i$, where $A_i(\sigma)$ is the surface area with a charge density of value σ and A_i is total surface area of species i. The term, $n_i = A_i/a_{eff}$, here, a_{eff} is the effective area of the standard surface segment. The interactions, both electrostatic and hydrogen bonding are taken into account through a ΔW term (Equation A.3).

$$\Delta W(\sigma_m, \sigma_n) = \left(\frac{\alpha'}{2}\right)(\sigma_m + \sigma_n)^2 + c_{hb} \max[0, \sigma_{acc} - \sigma_{hb}] \min[0, \sigma_{don} + \sigma_{hb}], \tag{A.3}$$

where σ_m and σ_n are charge densities of the paired segments m and n in mixture, $\alpha'/2$ is a constant for the misfit energy, c_{hb} the hydrogen bonding parameter, and σ_{hb} a cutoff value for the hydrogen bonding interactions. Hydrogen bonds can occur between two segments. To express them, the segments are divided into two categories: acceptor

and donor. In fact, segments can be either neutral segments, acceptor segments (σ_{acc}), or donor segments (σ_{don}). The global adjustable parameters for generating the activity coeffcient via a statistical mechanical framework were the effective area of the standard surface segment (a_{eff} = 6.32 Å^2), the misfit energy interaction constant [α' = 8419 kcal Å^4/(mol e^2)], the cutoff for hydrogen-bonding interaction (σ_{hb} = 0.0084 e/Å^2), and the hydrogen-bonding interaction constant [c_{hb} = 75,006 kcal Å^4/(mol e^2)].

The DES has an interaction between the hydrogen bond donor (HBD) and hydrogen bond acceptor (HBA). This renders a new chemical entity with a melting point lower than those of the initial compounds that result in a eutectic point. Thus, the lowest temperature that needs to be computed in such a manner that a liquid phase of DES coexists. This can be initiated through quantum chemical calculations followed by a statistical-based approach. Hence, the COSMO-SAC model is adopted. COSMO-SAC applies the concept of mutual solubility as a function of temperature

TABLE A.1
Equations Used in the Nonrandom Two Liquid (NRTL) and Universal Quasi-Chemical (UNIQUAC) models

NRTL Model

$$\ln\gamma_i = \frac{\sum_{j=1}^{c}\tau_{ji}G_{ji}x_j}{\sum_{k=1}^{c}G_{ki}x_k} + \sum_{j=1}^{c}\left[\frac{G_{ij}x_j}{\sum_{k=1}^{c}G_{kj}x_k}\left(\tau_{ij} - \frac{\sum_{i=1}^{c}\tau_{ij}G_{ij}x_i}{\sum_{k=1}^{c}G_{kj}x_k}\right)\right]$$

$$G_{ij} = \exp\left(-\alpha_{ji}\tau_{ji}\right),\ \tau_{ji} = \left[\left(g_{ji} - g_{ii}\right)/RT\right] \text{ and } \alpha_{ji} = \alpha_{ij} = \alpha$$

UNIQUAC Model

$$\ln\gamma_i = \ln\left(\frac{\Phi_i}{x_i}\right) + \frac{z}{2}q_i\ln\left(\frac{\theta_i}{\Phi_i}\right) + l_i - \frac{\Phi_i}{x_i}\sum_{j=1}^{c}x_j l_j + q_i\left(1 - \ln\sum_{j=1}^{c}\theta_j\tau_{ji} - \sum_{j=1}^{c}\frac{\theta_j\tau_{ij}}{\sum_{k=1}^{c}\theta_k\tau_{kj}}\right)$$

$$\tau_{ji} = \frac{g_{ji} - g_{ii}}{RT} = \frac{A_{ji}}{T};\ \theta_i = \frac{q_i x_i}{q_T};\ q_T = \sum_k q_k x_k;\ \Phi_i = \frac{r_i x_i}{r_T}$$

$$r_T = \sum_k r_k x_k;\ l_i = \frac{z}{2}(r_k - q_k) + 1 - r_k$$

TABLE A.2
Equations Used in the COSMO-RS Calculations

Sigma profile of component and mixture	$P_s(\sigma) = \sum_{i \in S} x_i p^{x_i}(\sigma)$
Sigma profile averaging	$\sigma_m = \dfrac{\sum_n \sigma_n^* \dfrac{r_n^2 r_{eff}^2}{r_n^2 + r_{eff}^2} \exp\left(-\dfrac{d_{mn}^2}{r_n^2 + r_{eff}^2}\right)}{\sum_n \dfrac{r_n^2 r_{eff}^2}{r_n^2 + r_{eff}^2} \exp\left(-\dfrac{d_{mn}^2}{r_n^2 + r_{eff}^2}\right)}, \quad r_{eff} = \sqrt{a_{eff}/\pi}, \quad \mathrm{r}_n = \sqrt{a_n/\pi}$
Sigma potential (chemical potential of segment)	$\mu_s(\sigma) = -kT \ln\left\{\sum_{\sigma'} \exp\left[\dfrac{-E_{pair}(\sigma,\sigma') + \mu_s(\sigma')}{kT}\right]\right\} + kT \ln p_s(\sigma)$ (a)
	$p_s(\sigma)\Gamma_s(\sigma) = \exp\left(\dfrac{\mu_s(\sigma)}{kT}\right)$ (b)
Activity coefficient of segment	$\ln \Gamma_s(\sigma) = -\ln\left\{\sum_{\sigma'} p_s(\sigma)\Gamma_s(\sigma) \exp\left[\dfrac{-E(\sigma,\sigma')}{kT}\right]\right\}$
Solubility equation	$\ln\left(\gamma^L_{solute} x^L_{solute}\right) = \dfrac{-\Delta h_f}{R}\left(\dfrac{1}{T} - \dfrac{1}{T_m}\right) - \dfrac{\Delta c_p}{R}\left(\dfrac{T_m - T}{T}\right) + \dfrac{\Delta c_p}{R} \ln\left(\dfrac{T_m}{T}\right)$
Activity coefficient in mixture	$\ln\gamma_{i/s} = \mathrm{n_i} \sum_{\sigma} \mathrm{P_i}(\sigma)\left[\ln\Gamma_s(\sigma) - \Gamma_i(\sigma)\right] + \ln\gamma^{SG}_{i/s}$ (a)
	$\ln \gamma^{SG}_{i/s} = \ln \dfrac{\phi_i}{x_i} + \dfrac{z}{2} q_i \ln \dfrac{\theta_i}{\phi_i} + li - \dfrac{\phi_i}{x_i} \sum_j x_j l_j$ (b)
Staverman–Guggenheim term	Where $\theta_i = \dfrac{x_i q_i}{\sum_j x_j q_j}, \quad \phi_i = \dfrac{x_i r_i}{\sum_j x_j r_j}, \quad l_i = \dfrac{z}{2}\left(\left(r_i - q_i\right) - \left(r_i - 1\right)\right)$ (c)

and hence predicts the eutectic composition and temperature employing solid–liquid equilibrium theory [3]. The procedure starts with geometry optimization followed by COSMO-SAC predictions. The geometry optimization on all the structures was carried out using the density functional theory. Thereafter, the COSMO file was generated. Thereafter, the mole fraction was predicted for both the HBD and the HBA by the activity coeffcient in either phase at different temperatures (T) with the following Equation A.4.

$$\ln\left(\gamma_{solute} x_{solute}\right) = \frac{-\Delta H_f}{RT_m}\left(\frac{1}{T} - \frac{1}{T_m}\right), \tag{4}$$

where γ_{solute}, x_{solute}, ΔH_f, and T_m are the activity coeffcient, the mole fraction, the enthalpy of fusion, and the melting point, respectively. For the ideal situation, the activity coefficient of the solute in the liquid phase is unity, that is, $\gamma_{solute} = 1$. Then the ideal solubility equation is (Equation A.5):

$$\ln x_{solute} = \frac{-\Delta H_f}{RT_m}\left(\frac{1}{T} - \frac{1}{T_m}\right). \tag{5}$$

For the prediction of experimental mole fraction, the mole fraction at ideal solvation from Equation A.5 is predicted. This value is then used to obtain the activity coefficient of the component in the mixture using COSMO-SAC model in Equation A.2. Thereafter, the desired mole ratio for HBA:HDB can be found for the eutectic formation.

3. DESCRIPTION OF AMBER FORCE FIELD

$$E_{Total} = E_{Bonded} + E_{Nonbonded}$$

$$E_{Total} = \left(E_{Bond} + E_{Angle} + E_{Dihedral}\right) + \left(E_{vdW} + E_{Electrostatic}\right)$$

$$E_{Total} = \sum_{Bonds} K_b (r - r_0)^2 + \sum_{Angles} K_\theta (\theta - \theta_0)^2 + \sum_{Dihedrals} \frac{V_n}{2}[1 + \cos(n\phi - \gamma)]$$
$$+ \sum_{i=j}^{N-1} \sum_{i<j}^{N} \left\{ 4\varepsilon_{ij} \left[\left(\frac{\sigma_{ij}}{r_{ij}}\right)^{12} - \left(\frac{\sigma_{ij}}{r_{ij}}\right)^{6} \right] + \frac{q_i q_j}{4\pi\varepsilon_0 r_{ij}} \right\}$$

The total energy of the system includes both bonded and nonbonded terms. The first there bonded interactions are for bonds, angles, and torsions terms. The nonbonded interactions are described in the last term, which includes van der Waals (vdW) and electrostatic interactions of atom-centered point charges. Electrostatic and vdW interactions are calculated between only the atoms in different molecules or for the atoms in the same molecule separated by at least three bonds, where bond parameters K_b is the bond force constant (kcal·mol^{-1} Å^{-2}) and r_o is the equilibrium bond length in Å; angle parameters K_θ is the angle force constant (kcal·mol^{-1} radian^{-2}) and θ_o is the equilibrium angle (degree); dihedral parameters V_n is the dihedral force constant in kcal mol^{-1} and γ in degree; and nonbonded parameters ε in kcal·mol^{-1} and σ_{ij} in Å. The vdW energy is calculated with a standard 12–6 Lennard-Jones potential and the electrostatic energy with a Coulombic potential. In the Lennard–Jones potential earlier, the σ_{ij} is the distance between atoms i and j, at which the energy of the two atoms reaches zero.

4. A SAMPLE NAMD CONFIGURATION FILE

```
#############################################################
## JOB DESCRIPTION                                         ##
#############################################################
# Minimization of 400 DES, 400 heptane and 200 molecules #
# of quinoline                                             #
#############################################################
## ADJUSTABLE PARAMETERS                                   ##
#############################################################
ambercoor            ../common/ER4.inpcrd
set temperature      0
set outputname       ER4 _ min
set restart          0
# Continuing a job from the restart files
if {$restart} {
set inputname        $outputname
Coordinates          ../$inputname.restart.coor
Velocities           ../$inputname.restart.vel
extendedSystem       ../$inputname.xsc
}
firsttimestep 0
#############################################################
## SIMULATION PARAMETERS                                   ##
#############################################################
#Input
amber                on
parmfile             ../common/ER4.prmtop
if {$restart-1} {
temperature          $temperature
}
# Force-Field Parameters
dielectric           1.0     ;# Value of the dielectric
                             constant
exclude              scaled1-4
nonbondedScaling     1.0
1-4scaling           1.0
cutoff               12.0    ;#Angstorm
switching            on
switchdist           10.0    ;#Angstorm
pairlistdist         14.0    ;#Angstorm

# Integrator Parameters
timestep             1.0     ;# 1fs/step
rigidBonds           all
rigidTolerance       0.00001
```

```
rigidIterations      100       ;# Maximum number of SHAKE
                               iterations
nonbondedFreq        1
vdwGeometricSigma    yes
fullElectFrequency   2
stepspercycle        20
pairlistsperCycle    2

# Periodic Boundary Conditions
if {$restart-1} {
set X    150.00
set Y    75.00
set Z    75.00
set C    0.00
set C1   0.00
cellBasisVector1   $X    0.0    0.0    ;#Angstorm
cellBasisVector2   0.0    $Y    0.0    ;#Angstorm
cellBasisVector3   0.0    0.0    $Z    ;#Angstorm
cellOrigin         $C     $C1    $C1   ;#Angstorm

# PME (for full-system periodic electrostatics)
PME                  yes
PMEGridSpacing       1.0
PMETolerance         0.000001

#manual grid definition
#PMEGridSizeX        150
#PMEGridSizeY        75
#PMEGridSizeZ        75
}
wrapAll              on

# Constant Temperature Control
if {0} {
langevin             on        ;# do langevin dynamics
langevinDamping      1         ;# damping coefficient
                               (gamma) of 1/ps
langevinTemp         $temperature
langevinHydrogen     off       ;# don't couple langevin
                               bath to hydrogens
}

# Constant Pressure Control (variable volume)
if {0} {
useGroupPressure     yes       ;# needed for rigidBonds
useFlexibleCell      no
useConstantArea      no
```

```
langevinPiston         on
langevinPistonTarget   1.01325   ;# in bar -> 1 atm
langevinPistonPeriod   100.0
langevinPistonDecay    50.0
langevinPistonTemp     $temperature
}

# Fixed Atoms Constraint (set PDB beta-column to 1)
if {0} {
fixedAtoms                  on
fixedAtomsForces            on
fixedAtomsFile              myfixedatoms.pdb
fixedAtomsCol               B
}

# IMD Settings (can view sim in VMD)
if {0} {
IMDon            on
IMDport          3000    ;# port number (enter it
                         in VMD)
IMDfreq          1       ;# send every 1 frame
IMDwait          no      ;# wait for VMD to connect
                         before running?
}

# Output
outputName       $outputname
XSTfile          $outputname.xst

restartfreq      500     ;# 500steps = every 1ps
dcdfreq          2000
outputEnergies   100
outputPressure   100
binaryoutput     no
binaryrestart    no
#############################################################
## EXTRA PARAMETERS                                        ##
#############################################################

#############################################################
## EXECUTION SCRIPT                                        ##
#############################################################
# Minimization
minimization     on
seed             1536    ;# Random number
minimize         500000  ;# Number of integration
                         steps
```

REFERENCES

1. Lin, S.-T. and S.I. Sandler, *A priori phase equilibrium prediction from a segment contribution solvation model*. Industrial & Engineering Chemistry Research, 2002. **41**(5): p. 899–913.
2. Klamt, A., *Conductor-like screening model for real solvents: A new approach to the quantitative calculation of solvation phenomena*. The Journal of Physical Chemistry, 1995. **99**(7): p. 2224–2235.
3. Alkhatib, I.I., et al., *Perspectives and guidelines on thermodynamic modelling of deep eutectic solvents*. Journal of Molecular Liquids, 2019: p. 112183.

Index